



UNIVERSITAT ROVIRA I VIRGILI

NEW STRATEGIES FOR ENANTIOSELECTIVE CATALYSIS OF PHOTOCHEMICAL REACTIONS

Lukasz Wozniak

ADVERTIMENT. L'accés als continguts d'aquesta tesi doctoral i la seva utilització ha de respectar els drets de la persona autora. Pot ser utilitzada per a consulta o estudi personal, així com en activitats o materials d'investigació i docència en els termes establerts a l'art. 32 del Text Refós de la Llei de Propietat Intel·lectual (RDL 1/1996). Per altres utilitzacions es requereix l'autorització prèvia i expressa de la persona autora. En qualsevol cas, en la utilització dels seus continguts caldrà indicar de forma clara el nom i cognoms de la persona autora i el títol de la tesi doctoral. No s'autoritza la seva reproducció o altres formes d'explotació efectuades amb finalitats de lucre ni la seva comunicació pública des d'un lloc aliè al servei TDX. Tampoc s'autoritza la presentació del seu contingut en una finestra o marc aliè a TDX (framing). Aquesta reserva de drets afecta tant als continguts de la tesi com als seus resums i índexs.

ADVERTENCIA. El acceso a los contenidos de esta tesis doctoral y su utilización debe respetar los derechos de la persona autora. Puede ser utilizada para consulta o estudio personal, así como en actividades o materiales de investigación y docencia en los términos establecidos en el art. 32 del Texto Refundido de la Ley de Propiedad Intelectual (RDL 1/1996). Para otros usos se requiere la autorización previa y expresa de la persona autora. En cualquier caso, en la utilización de sus contenidos se deberá indicar de forma clara el nombre y apellidos de la persona autora y el título de la tesis doctoral. No se autoriza su reproducción u otras formas de explotación efectuadas con fines lucrativos ni su comunicación pública desde un sitio ajeno al servicio TDR. Tampoco se autoriza la presentación de su contenido en una ventana o marco ajeno a TDR (framing). Esta reserva de derechos afecta tanto al contenido de la tesis como a sus resúmenes e índices.

WARNING. Access to the contents of this doctoral thesis and its use must respect the rights of the author. It can be used for reference or private study, as well as research and learning activities or materials in the terms established by the 32nd article of the Spanish Consolidated Copyright Act (RDL 1/1996). Express and previous authorization of the author is required for any other uses. In any case, when using its content, full name of the author and title of the thesis must be clearly indicated. Reproduction or other forms of for profit use or public communication from outside TDX service is not allowed. Presentation of its content in a window or frame external to TDX (framing) is not authorized either. These rights affect both the content of the thesis and its abstracts and indexes.

UNIVERSITAT ROVIRA I VIRGILI
NEW STRATEGIES FOR ENANTIOSELECTIVE CATALYSIS OF PHOTOCHEMICAL REACTIONS
Lukasz Wozniak

UNIVERSITAT ROVIRA I VIRGILI
NEW STRATEGIES FOR ENANTIOSELECTIVE CATALYSIS OF PHOTOCHEMICAL REACTIONS
Lukasz Wozniak

Łukasz Woźniak

**New Strategies for Enantioselective Catalysis
of Photochemical Reactions**

Doctoral Thesis
Supervised by Prof. Paolo Melchiorre
ICIQ – Institut Català d'Investigació Química



UNIVERSITAT ROVIRA I VIRGILI

Tarragona

2017

UNIVERSITAT ROVIRA I VIRGILI
NEW STRATEGIES FOR ENANTIOSELECTIVE CATALYSIS OF PHOTOCHEMICAL REACTIONS
Lukasz Wozniak



UNIVERSITAT ROVIRA I VIRGILI

Prof. Paolo Melchiorre, ICREA Research Professor & ICIQ Group Leader

I STATE that the present study, entitled “New Strategies for Enantioselective Catalysis of Photochemical Reactions.” presented by ŁUKASZ WOŹNIAK for the award of the degree of Doctor, has been carried out under my supervision at the Institut Català d'Investigació Química (ICIQ).

Tarragona, August the 10th 2017

Doctoral Thesis Supervisor

Prof. Paolo Melchiorre

UNIVERSITAT ROVIRA I VIRGILI
NEW STRATEGIES FOR ENANTIOSELECTIVE CATALYSIS OF PHOTOCHEMICAL REACTIONS
Lukasz Wozniak

Acknowledgements

This thesis would have never come into existence without very important people who I came across. First, I would like to genuinely thank my supervisor Professor Paolo Melchiorre, who gave me the unforgettable opportunity to enter this stimulating scientific environment and this fascinating area of organic chemistry. I could always count on his support from the very first day of my studies at ICIQ. I am very grateful for all the knowledge that he shared with me, constant motivation and a big dose of trust in giving me a lot of freedom to explore different aspects of enantioselective catalysis.

Thanks to all the people that are, and have been, part of the group. Especially to Dr. John Murphy, with whom I was very fortunate to work on the first project of this thesis. Approaching a difficult target with this extraordinary chemist was a pleasure and a very important lesson for me during my first years in ICIQ. Thanks to Giandomenico Magagnano for continuing to explore photo-organo cascade chemistry while I was abroad and writing this manuscript. Many thanks to David Bastida, Ana Bahamonde, Luca Buzetti as well as John and Giandomenico for being great companions over several years in Tarragona. I am also very grateful to Dr. Catherine Holden for her contribution to this manuscript, for proofreading, and many useful suggestions and discussions. Thanks to Lorna Piazzini and María Checa for administrative support and Dr. Eva Raluy for making the laboratory work easier.

Thanks to ICIQ research support area for help on many occasions.

During these years, I had also a chance to spend a time in two different research groups. I would like to thank Professor Melanie Sanford for the possibility to spend 10 weeks in her laboratory at the University of Michigan where I was exposed to many interesting aspects of transition metal catalysis and all my colleges from Ann Arbor for memorable times. I am also very grateful to Professor Takashi Ooi for giving me the opportunity to work in his laboratory at the Institute of Transformative Bio-Molecules at Nagoya University for 4 months. The time spent in Japan was very important scientific and personal experience.

Thanks to my family, who have always supported me and have made me feel like I have never left home.

I would also like to acknowledge the financial support from the Institute of Chemical Research of Catalonia (ICIQ) from the European Research Council for the ERC starting grant (278541-ORGA-NAUT) and ERC consolidator grant (681840-CATA-LUX).

Additionally, I am personally grateful to:

- ICIQ Foundation for the predoctoral fellowship (ref. 02/13-17)
- UM-ICIQ Global Engagement Program
- JSPS (Japan Society for Promotion of Science) Fellowship



Publication:

Some of the results presented in this thesis have been published:

Łukasz Woźniak, John J. Murphy, Paolo Melchiorre, Photo-organocatalytic Enantioselective Perfluoroalkylation of β -Ketoesters, *J. Am. Chem. Soc.*, **2015**, *137*, 5678-5681.

UNIVERSITAT ROVIRA I VIRGILI
NEW STRATEGIES FOR ENANTIOSELECTIVE CATALYSIS OF PHOTOCHEMICAL REACTIONS
Lukasz Wozniak

UNIVERSITAT ROVIRA I VIRGILI
NEW STRATEGIES FOR ENANTIOSELECTIVE CATALYSIS OF PHOTOCHEMICAL REACTIONS
Lukasz Wozniak

Rodzicom i Bratu

UNIVERSITAT ROVIRA I VIRGILI
NEW STRATEGIES FOR ENANTIOSELECTIVE CATALYSIS OF PHOTOCHEMICAL REACTIONS
Lukasz Wozniak

Table of Contents

1. General Overview.....	1
1.1 Strategies in Enantioselective Organocatalysis	2
1.1.1 Enantioselective Phase Transfer Catalysis	3
1.1.2 Enantioselective Aminocatalysis	5
1.1.2.1 Enantioselective Organo-Cascade Catalysis.....	6
1.2 Photochemistry and Enantioselective Organocatalysis	7
1.2.1 Photochemical Activity of Electron Donor Acceptor (EDA) Complexes	10
1.2.2 Photoexcitation of Chiral Iminium Ions and Enamines	11
1.3 Objectives and Summary of The Thesis	12
1.3.1 The Photochemistry of Electron Donor–acceptor (EDA) Complexes Derived from Chiral Enolates	12
1.3.2 Enantioselective Photochemical Organocascade Catalysis	13
2. Enantioselective Photochemical Reactions.....	15
2.1 Asymmetric Induction by Chiral Templates	16
2.2 Enantioselective Catalysis of Photochemical Reactions	19
2.2.1 Chiral Photocatalysts	20
2.2.2 Chiral Catalysts in Cooperation with Achiral Photocatalysts	24
2.2.3 Chiral Photoactive Catalytic Intermediates	31
3. Photo-Organocatalytic Enantioselective Perfluoroalkylation of β-Ketoesters....	39
3.1 Introduction.....	39
3.2 Reactions of Enolates Proceeding by Electron Transfer Mechanism	42
3.3 Target of the Project	48
3.4 Results and Discussion	50
3.4.1 Optimization Studies	53
3.4.2 Reaction Scope	61
3.4.3 Reaction Mechanism	62
3.5 Conclusions and Remarks	65
3.6 Experimental Section	65
4. Enantioselective Photochemical Organo-cascade Catalysis	97
4.1 Introduction.....	97

4.2 Ground-state Enantioselective Iminium Ion Catalysis	97
4.3 Enantioselective Organocascade Catalysis	101
4.4 Enantioselective Iminium Ion Catalysis in the Excited-State	107
4.5 Target of the Project	108
4.6 Results and Discussion	109
4.6.1 Design Plan	109
4.6.2 Initial Results.....	111
4.6.3 Synthesis of Cyclopropanol 49.....	113
4.6.4 Optimization Studies of the Photochemical Organocascade	115
4.6.5 Reaction Scope.....	122
4.6.6 Reaction Mechanism	123
4.7 Conclusions and Remarks.....	129
4.8 Experimental Section	130
5. General Conclusions	179

UNIVERSITAT ROVIRA I VIRGILI
NEW STRATEGIES FOR ENANTIOSELECTIVE CATALYSIS OF PHOTOCHEMICAL REACTIONS
Lukasz Wozniak

UNIVERSITAT ROVIRA I VIRGILI
NEW STRATEGIES FOR ENANTIOSELECTIVE CATALYSIS OF PHOTOCHEMICAL REACTIONS
Lukasz Wozniak

Chapter I

General Overview

The main aim of this research thesis is to develop enantioselective, photochemical organocatalytic reactions that can provide new strategies for the synthesis of enantio-enriched chiral compounds. There is an obvious need for the synthesis of single enantiomers, since any molecule created by humankind to interact with nature has to act within a chiral environment. The crucial role of stereochemistry has direct implications in pharmaceutical chemistry. Chiral drugs have to be produced in an enantiomerically pure form to eliminate risks of possible harmful activity of the opposite enantiomer.¹ The history of drugs has taught that, while one enantiomer of a drug can have beneficial effects, the other can be very toxic and even teratogenic.² The growing demand for chiral, enantiomerically pure compounds and drugs in the pharmaceutical industry has created a formidable synthetic challenge for chemists to find cost-effective and highly stereoselective means to assemble these molecules. Besides these considerations, stereoselective synthesis constitutes an intrinsically interesting research field in its own right. The ability to combine the fields of geometry and topology with the understanding of organic molecule reactivity has always fascinated synthetic chemists.

Enantioselective catalysis is one of the most efficient chemical approaches for targeting useful chiral compounds with high optical purity in an economical, energy-saving and environmentally benign way.³ Developments in this area had an enormous impact on organic syntheses,⁴ as testified by the Nobel Prize for chemistry awarded in 2001 to Knowles, Noyori, and Sharpless for their work on ‘chirally catalyzed hydrogenation reactions’ and ‘chirally catalyzed oxidation reactions’.⁵

One effective strategy in enantioselective catalysis relies on the use of small chiral organic molecules as catalysts, a field which is termed “asymmetric organocatalysis”.⁶ The roots of this field date back to the beginning of the 20th century, when Bredig reported his -

¹<https://www.fda.gov/Drugs/GuidanceComplianceRegulatoryInformation/Guidances/ucm122883.htm>-date accessed 13.07.2017.

² N. Vargesson, Thalidomide-Induced Teratogenesis: History and Mechanisms, *Birth Defects Research Part C: Embryo Today: Reviews*, **2015**, 105, 2, 140.

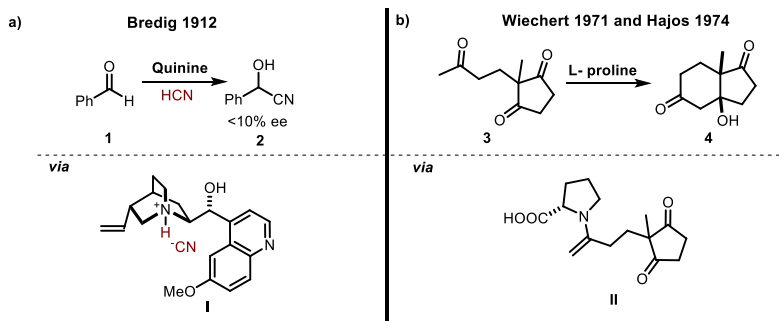
³ R. Noyori, Synthesizing our future, *Nat. Chem.*, **2009**, 1, 5.

⁴ H. U. Blaser, H. J. Federsel, *Asymmetric Catalysis on Industrial Scale*, 2nd edition, Wiley, **2010**.

⁵ R. Noyori, Asymmetric Catalysis: Science and Opportunities (Nobel Lecture), *Angew. Chem. Int. Ed.*, **2002**, 41, 2008, b) W. S. Knowles, Asymmetric Hydrogenations (Nobel Lecture), *Angew. Chem. Int. Ed.* **2002**, 41, 1998. c) K. B. Sharpless, Searching for New Reactivity (Nobel Lecture), *Angew. Chem. Int. Ed.* **2002**, 41, 2024.

⁶ D. W. C. MacMillan, The Advent and Development of Organocatalysis, *Nature*, **2008**, 455, 304.

now legendary - study on the use of natural cinchona alkaloids as chiral catalysts (Scheme 1.1).⁷ Another remarkable example, reported by Hajos and Wiechert in the 1970s, was the enantioselective aldol reaction catalyzed by a simple proteinogenic amino acid: proline.⁸



Scheme 1.1 Early examples of enantioselective organocatalysis a) Bredig's asymmetric hydrocyanation of aldehydes, b) enantioselective aldol reaction developed by Wiechert and Hajos.

Because of a poor understanding of their activation mechanisms, those early examples of enantioselective organocatalysis were considered as rather exotic and the synthetic potential of enantioselective organocatalysis was not fully recognized. However, over the last 20 years, the progress in organocatalysis has been breathtaking and this field has grown to become an established and independent field of asymmetric catalysis, complementing metal and bio-catalysis.⁹

1.1 Strategies in Enantioselective Organocatalysis

On a mechanistic basis, organocatalytic transformations can be divided into covalent and noncovalent catalysis, depending on the type of interactions the organic catalyst has with the substrate. In the former case, a catalyst forms a covalent adduct with a substrate within a catalytic cycle (Scheme 1.1 - intermediate **II**)¹⁰. Noncovalent catalysis¹¹ is governed by

⁷ G. Bredig, P. S. Fiske. Asymmetric Synthesis Caused by Catalysts, *Biochem., Z.* **1912**, 46, 7.

⁸ a) U. Eder, G. Sauer, R. Wiechert. New Type of Asymmetric Cyclization to Optically Active Steroid CD Partial Structures, *Angew. Chem. Int. Ed. Engl.*, **1971**, 10, 496, b) Z. G. Hajos, D. R. Parrish, Asymmetric Synthesis of Bicyclic Intermediates of Natural Product Chemistry, *J. Org. Chem.*, **1974**, 39, 1615.

⁹ P. Melchiorre, M. Marigo, A. Carlone, G. Bartoli, Asymmetric Aminocatalysis - Gold Rush in Organic Chemistry, *Angew. Chem. Int. Ed.*, **2008**, 47, 6138.

¹⁰ K. L. Brown, L. Damm, J. D. Dunitz, A. Eschenmoser, R. Hobi, C. Kratky, Structural Studies of Crystalline Enamines, *Helv. Chim. Acta*, **1978**, 61, 3108.

¹¹ R. R. Knowles, E. N. Jacobsen, Attractive Noncovalent Interactions in Asymmetric Catalysis: Links Between Enzymes and Small Molecule Catalysts, *Proc. Natl. Acad. Sci. U.S.A.* **2010**, 107, 20678.

weak electrostatic interactions or hydrogen bonds between substrates and a catalyst. The quinine-catalyzed addition of cyanide, reported by Bredig (Scheme 1.1a), is an example of noncovalent catalysis, which most likely involves the formation of a chiral salt **I**.

1.1.1 Enantioselective Phase Transfer Catalysis

Noncovalent catalysis has been successfully applied to control the reactivity and the enantioselectivity of processes involving organic and inorganic anions. The stereochemical control is provided by weak electrostatic interactions between the reactive anion and a cationic chiral catalyst. In many reactions, generation of the reactive anion requires the use of a stoichiometric amount of base, which complicates the development of a catalytic variant. This limitation can be overcome by employing phase transfer catalysis (PTC).¹²

The foundations of PTC were laid in the mid-1960s by Stark and Mąkosza.¹³ The pioneering studies demonstrated that reactions between substances located in two immiscible phases can be catalyzed by tetraalkyl ammonium or phosphonium salts (Q^+X^-) (Figure 1.1). The key element of this process is the formation of an onium salt (Q^+R^-) of the catalyst (Q^+) with an organic or an inorganic anionic substrate (R^-), which can undergo further reaction in the organic phase. The pathway by which the onium salt is generated is often a topic of discussion, centered on the Stark's extraction or Mąkosza's interfacial models (Figure 1.1). The Stark's extraction mechanism implies that a phase transfer catalyst (Q^+X^-) can move across both phases and extract a hydroxide ion from the aqueous, basic solution, into the organic phase. While present in the organic solvent, the resulting hydroxide anion (Q^+OH^-) can deprotonate an acidic organic substrate (RH) and form the reactive species (Q^+R^-). In the Mąkosza's mechanism, deprotonation of an acidic substrate (RH) takes place at the interface of organic and aqueous phases. Then, the phase transfer catalyst (Q^+X^-) equilibrates with the anionic substrate and transfers the reactive species (Q^+R^-) from the interphase to the organic solvent. Chiral phase transfer catalysts usually contain highly lipophilic organic scaffold that makes them practically insoluble in water. In these cases, the interfacial Mąkosza's mechanism is more plausible.

¹² S. Shirakawa, K. Maruoka, Recent Developments in Asymmetric Phase-Transfer Reactions, *Angew. Chem. Int. Ed.*, **2013**, 52, 4312.

¹³ a) C. M. Starks, Phase-Transfer Catalysis. I. Heterogeneous Reactions Involving Anion Transfer by Quaternary Ammonium and Phosphonium, Salts, *J. Am. Chem. Soc.*, **1971**, 93, 195, b) M. Mąkosza, Reactions of Organic Anions. XI. Catalytic Alkylation of Indene, *Tetrahedron Lett.*, **1966**, 4621, c) M. Mąkosza, Reactions of Organic Anions. XII. Vinylation of Phenylacetonitrile Derivatives, *Tetrahedron Lett.*, **1966**, 5489.

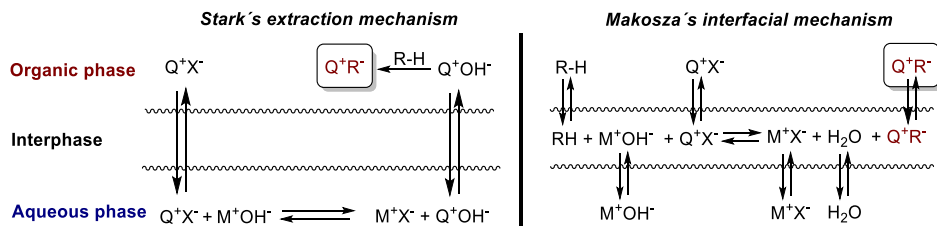
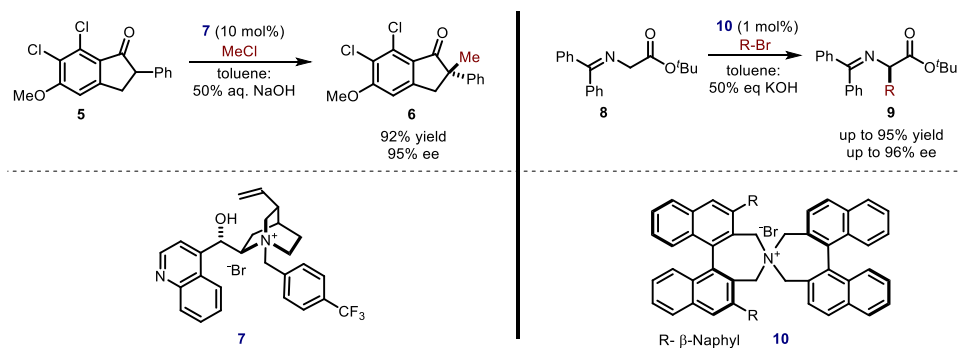


Figure 1.1 Mechanisms of generation of reactive onium carbanion species Q^+R^- .

The first meaningful discovery in enantioselective PTC was reported in 1984 by researchers from Merck (Scheme 1.2). The *N*-(*p*-(trifluoromethyl)benzyl)cinchonidinium bromide **7** was found to catalyze the S_N2 -type methylation reaction of indanone derivative **5** and methyl chloride with high stereoselectivity (up to 92% ee).¹⁴ Following this breakthrough, many other cinchona alkaloid-based phase transfer catalysts were developed for different enantioselective transformations.¹⁵ In 1999, a new rational approach to the design of efficient phase transfer catalysts was introduced by Maruoka (Scheme 1.2). C2-symmetric chiral quaternary ammonium salts **10** were successfully applied as highly efficient catalysts for enantioselective alkylation of a *tert*-butyl glycinate-benzophenone Schiff base **8**.¹⁶ Nowadays, these two catalyst types are common tools in enantioselective PTC.



Scheme 1.2 Enantioselective alkylation of carbonyls under phase transfer conditions.

¹⁴ U. H. Dolling, P. Davis, E. J. J. Grabowski, Efficient Catalytic Asymmetric Alkylations. 1. Enantioselective Synthesis of (+) Indacrinone via Chiral Phase-Transfer Catalysis, *J. Am. Chem. Soc.*, **1984**, 106, 446.

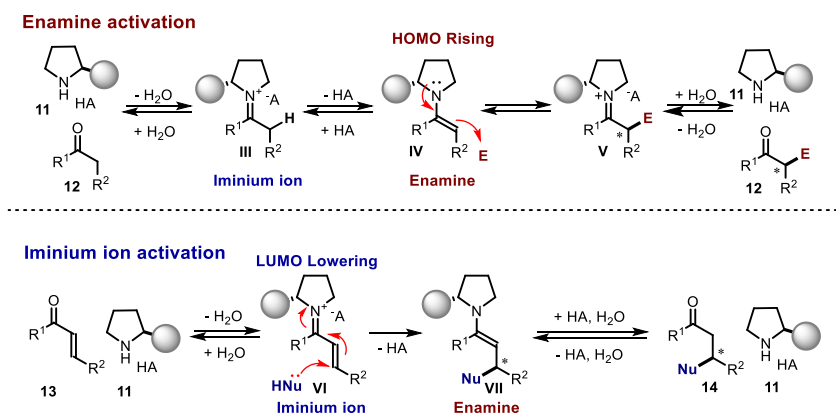
¹⁵ Keiji Maruoka, *Asymmetric Phase Transfer Catalysis*, Chapter II-IV, p. 9-68, Wiley, **2008**.

¹⁶ T. Ooi, M. Kameda, K. Maruoka, Molecular Design of a C2-Symmetric Chiral Phase-Transfer Catalyst for Practical Asymmetric Synthesis of α -Amino Acids, *J. Am. Chem. Soc.*, **1999**, 121, 6519.

1.1.2 Enantioselective Aminocatalysis

Catalysis with chiral primary or secondary amines (asymmetric aminocatalysis)⁹ has become a powerful strategy for enantioselective functionalization of carbonyl compounds (Scheme 1.3). Condensation of the amine catalyst **11** with the carbonyl compound **12** produces a covalent intermediate, the iminium ion **III**, which can be deprotonated to give the corresponding enamine **IV**. The 4- π electron enamine species exhibits a high electron density at the α -carbon. This can be attributed to the overlap of the nitrogen lone pair with the π system of the enamine, which leads to an increase in the energy of the highest occupied molecular orbital (HOMO).¹⁷ Chiral enamines can selectively trap a variety of electrophiles to form α -functionalized products **12**.

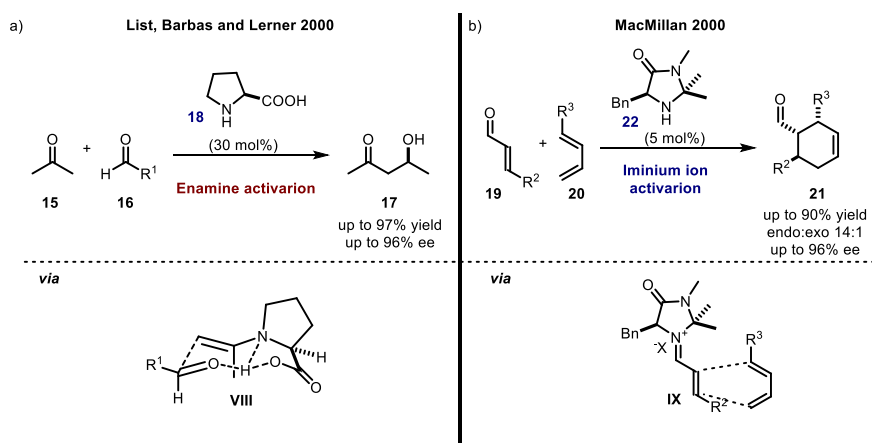
Conjugated iminium ions, formed upon condensation of an amine catalyst **11** with the carbonyl substrate **13**, on the other side, resemble a classical Lewis acid activation of unsaturated carbonyl compounds. Coordination of the Lewis acid to the carbonyl group displaces an electronic distribution in a π -system toward the positively charged metal center, which leads to the lowering of the energy of the lowest unoccupied molecular orbital (LUMO). The same effect is responsible for the LUMO lowering within the positively charged iminium ions intermediates **VI**, which facilitates the conjugate addition of soft nucleophiles and pericyclic reactions.



Scheme 1.3 Enamine and iminium ion activation modes. E: electrophile, Nu: nucleophile, HA: acid, the filled grey circle represents a bulky substituent on the chiral amine catalyst.

¹⁵ I. Fleming, *Molecular Orbitals and Organic Chemical Reactions: Reference Edition*, Chapter 2 p. 84-85 Wiley, 2010.

These modes of organocatalytic reactivity are well understood. In particular, the nucleophilic reactivity of stoichiometric enamines has been extensively explored by Gilbert Stork in the 1960s.¹⁸ Despite a few isolated examples (see Scheme 1.1), enantioselective aminocatalysis was conceptualized as a field of research only in 2000. Inspired by the mechanism of Class I aldolases¹⁹, which utilizes an enamine-based mechanism, Barbas III, Lerner, and List developed an enantioselective aldol reaction employing L-proline as the chiral organocatalyst (Scheme 1.4).²⁰ Almost simultaneously, MacMillan reported a new organocatalytic strategy for an enantioselective Diels-Alder reaction employing chiral iminium ions **IX**.²¹ Since then, the use of chiral aminocatalysts to functionalize carbonyl compounds has grown exponentially and features broad scope and high enantioselectivities.



Scheme 1.4 a) Enamine-mediated asymmetric organocatalytic aldol reaction developed by List, Barbas, and Lerner. b) Iminium ion-mediated asymmetric organocatalytic Diels-Alder reaction developed by MacMillan.

1.1.2.1 Enantioselective Organo-Cascade Catalysis

One step forward in the evolution of the field of aminocatalysis involved the combination of the iminium ion and enamine activation modes in a cascade sequence (Scheme 1.5).

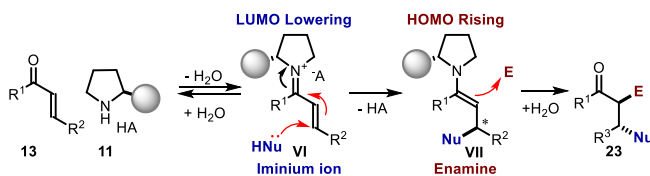
¹⁸ G. Stork, A. Brizzolara, H. Landesman, J. Szmuszkovicz, R. Terrell, The Enamine Alkylation and Acylation of Carbonyl Compounds, *J. Am. Chem. Soc.*, **1963**, 85, 207.

¹⁹ A. J. Morris, D. R. Tolan, Lysine-146 of Rabbit Muscle Aldolase Is Essential for Cleavage and Condensation of the C3-C4 Bond of Fructose 1,6-Bis(phosphate), *Biochemistry*, **1994**, 33, 12291.

²⁰ B. List, R. A. Lerner, C. F. Barbas III. Proline-Catalyzed Direct Asymmetric Aldol Reactions, *J. Am. Chem. Soc.*, **2000**, 122, 2395.

²¹ K. A. Ahrendt, C. J. Borths, D. W. C. MacMillan, New Strategies for Organic Catalysis: The First Highly Enantioselective Organocatalytic Diels-Alder Reaction, *J. Am. Chem. Soc.*, **2000**, 122, 4243.

The ability of chiral amine catalyst **11** to control distinct consecutive steps allows the design of elegant cascade reactions leading to complex, stereochemically dense molecules in a single operation. Development of such transformations, which offer rapidly increasing structural and stereochemical complexity, remains a constant goal for chemical sciences.²² Additionally, by combining multiple asymmetric, catalytic transformations in a cascade sequence, chemists can impart increased enantiomeric excess to the final product when compared to the corresponding discrete transformations.²³ Various cascade sequences have been developed following a variety of mechanistic pathways. Among them, the iminium ion-enamine sequence has been recognized as the most effective (Scheme 1.5).²⁴ First, an enantioselective, nucleophilic conjugate addition is triggered by the formation of an iminium ion intermediate **VI**. Next, the resulting enamine **VII** undergoes reaction with an electrophile to forge a second stereogenic center while affording the double-substituted product **23**. Enantioselective cascade processes and the reasons for the intrinsic asymmetric amplification will be further discussed in Chapter IV of this thesis.



Scheme 1.5 Iminium Ion/Enamine Cascade. E: electrophile, Nu: nucleophile, HA: acid, the filled grey circle represents a bulky substituent on the chiral amine catalyst.

1.2 Photochemistry and Enantioselective Organocatalysis

Recently it was found that the synthetic potential of organocatalytic intermediates is not limited to the ground-state domain, but can be expanded by exploiting their *photochemical activity*. By bringing an organocatalytic intermediate to an electronically excited-state, light excitation unlocks reaction manifolds that are unavailable to

²² C. Grondal, M. Jeanty, D. Enders, Organocatalytic Cascade Reactions as a New Tool in Total Synthesis, *Nat. Chem.*, **2010**, 2, 167.

²³ The Horeau principle provides the mathematical foundation for the rationalization of the enantio-enrichment observed in successive catalytic asymmetric cycles. The first statistical asymmetric amplifications were observed and quantified in dimerization reactions, see: F. J. P. Vigneron, M. Dhaenens, A. Horeau, Nouvelle Methode pour Porter au Maximum la Purete Optique d'un Produit Partiellement Dedouble Sans l'Aide d'Acune Substance Chirale, *Tetrahedron*, **1973**, 29, 1055.

²⁴ D. Enders, C. Grondal, M. R. M. Hüttl, Asymmetric Organocatalytic Cascade Reactions, *Angew. Chem. Int. Ed.*, **2007**, 46, 1570.

conventional ground-state organocatalytic pathways. The reactions of organic molecules initiated by the absorption of light has always played an important role in synthetic methodology. Photochemical retrosynthesis provides unique disconnections that are mostly not available to thermal processes.²⁵ Additionally, recent progress of visible light-mediated reactivity has provided mild and efficient routes for realizing previously difficult transformations.²⁶ Therefore, it is very alluring and widely sought to control stereochemical outcome of light induced processes.

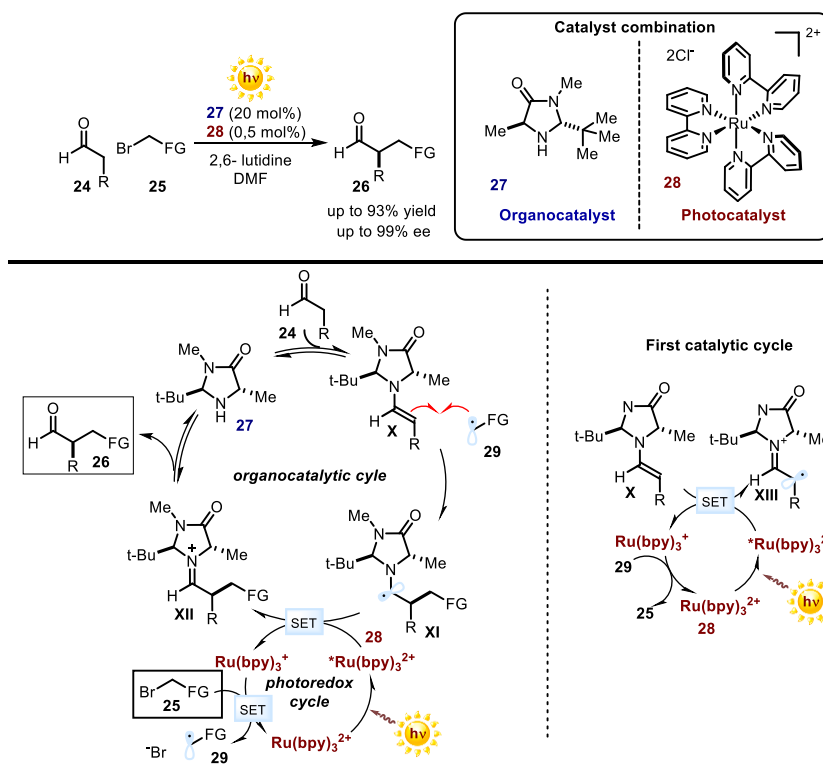
Photochemistry and enantioselective organocatalysis represent two powerful fields of molecule activation. Merging these two strategies brought new perspectives and solutions for longstanding synthetic problems in asymmetric catalysis. In 2008, MacMillan demonstrated that the combination of enamine and photoredox activations had the potential to perform an enantioselective catalytic intermolecular alkylation of aldehydes, a widely sought yet elusive transformation (Scheme 1.6).²⁷ Despite the great interest for this transformation, an enamine-mediated enantioselective catalytic approach was not accessible before. The main obstacle for achieving the polar S_N2 reaction pathway is mainly ascribable to the modest reactivity of alkyl halides, which complicates the ionic alkylation step while favouring side processes, *e.g.* N-alkylation of the Lewis basic amine catalysts with the alkyl halides and self-aldol condensation. Realizing that the main hurdle to overcome was intrinsic to the ionic S_N2 path, MacMillan envisioned the use of alkyl bromides not as electrophiles but as precursors for generating radicals. The underlying idea was to exploit the innate tendency of electron-deficient radicals to rapidly react with π -rich olefins, including enamines, thus allowing the formation of difficult-to-make carbon-carbon bonds.

A ruthenium-based polypyridyl photocatalyst **28** (Ru(bpy)₃²⁺ where bpy is 2,2'-bipyridine) was used to easily generate open-shell reactive species from organic bromides **25**.

²⁵ P. Klán, J. Wirz, *Photochemistry of Organic Compounds*, Chapter 7, p 455-466, Wiley, Chichester, **2009**.

²⁶ M. H. Shaw, J. Twilton, D. W. C. MacMillan, *Organic Photoredox Catalysis*, *J. Org. Chem.*, **2016**, *81*, 16, 6898.

²⁷ D. A. Nicewicz, D. W. C. MacMillan, *Merging Photoredox Catalysis with Organocatalysis: The Direct Asymmetric Alkylation of Aldehydes*, *Science*, **2008**, *322*, 77.



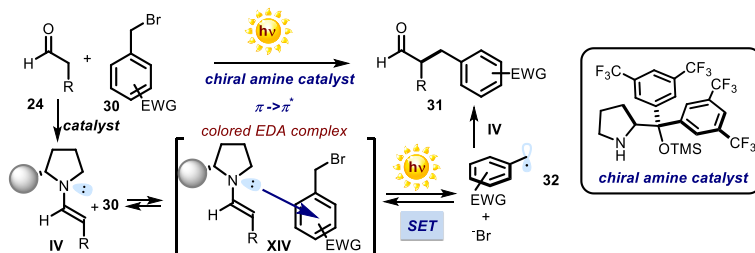
Scheme 1.6 MacMillan's photochemical alkylation of enamines with alkyl halides;
 SET: single-electron transfer, FG: functional group, DMF: dimethyl formamide,
 Ru(bpy)₃²⁺: photocatalyst.

The proposed photoredox process is initiated by the photoexcitation of the Ru(bpy)₃²⁺ catalyst to form an electronically excited-state intermediate *Ru(bpy)₃²⁺ which can remove one electron from the enamine **X** (acting as a sacrificial compound in the first cycle of the photoredox catalytic manifold) to provide the electron-rich intermediate Ru(bpy)₃⁺. This Ru(I) complex is a potent reductant that can transfer an electron to the organic bromide **25** to regenerate Ru(bpy)₃²⁺ while furnishing the active radical species **29**, upon reductive cleavage of the carbon-bromide bond. The electron-deficient radical **29** rapidly combines with the chiral electron-rich enamine **X** to forge the new carbon-carbon bond and generate the stereogenic center within the α -aminoradical **XI**. This electron-rich intermediate can undergo single-electron transfer (SET) oxidation by *Ru(bpy)₃²⁺ to form the iminium ion intermediate **XII** while restarting the photoredox cycle. Hydrolysis of **XII** returns the chiral amine catalyst **27** and delivers the enantioenriched alkylation product **26**.

This report was a milestone for the enantioselective organocatalysis field, since it uncovered the potential of visible-light-driven reactions employing classical organocatalytic tools. Besides providing a general solution for the asymmetric catalytic α -alkylation of unmodified aldehydes, the main synthetic impact was the demonstration that radical intermediates could be generated from readily available, bench-stable precursors and at ambient temperature when using a photocatalyst activated by weak light. This stands in sharp contrast with classical radical generation strategies, which often requires hazardous radical initiators, toxic reagents, and in many cases, high temperatures. The combination with a light-activated catalysts meant that the tools and the mechanisms of stereocontrol inherent to enantioselective organocatalysis, which require mild conditions for optimal efficiency, could be successfully applied within radical reactivity patterns.

1.2.1 Photochemical Activity of Electron Donor Acceptor (EDA) Complexes

In 2013, our research group demonstrated that the visible-light-promoted, enantioselective alkylation of aldehydes, originally developed by MacMillan, could be achieved without the addition of an external photocatalyst (Scheme 1.7).²⁸ This intriguing result is a consequence of light-induced generation of radical **32** by direct excitation of the EDA complex **XIV**, a ground-state association between the chiral enamine **IV** and the alkyl bromide **30**. The reductive cleavage of **30**, triggered by photo-induced SET within the EDA complex **XIV**, provided access to the key carbon-centered radical **32**.



Scheme 1.7 The EDA complex activation strategy for the enantioselective α -alkylation of aldehydes.

SET: single-electron transfer, EWG: electron-withdrawing group, the filled grey circle represents a bulky substituent on the chiral amine catalyst.

²⁸ E. Arceo, I. D. Jurberg, A. Álvarez-Fernández, P. Melchiorre, Photochemical Activity of a Key Donor-acceptor Complex Can Drive Stereoselective Catalytic α -alkylation of Aldehydes, *Nat. Chem.*, **2013**, 5, 750.

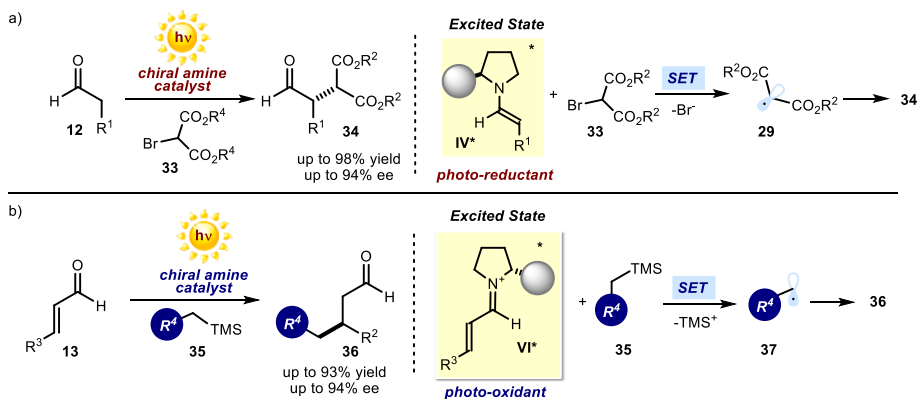
In this system, the chiral amine catalyst allows the photo-activation of substrates by inducing the formation of a light-absorbing enamine-based EDA complex **XIV**. At the same time, it ensures effective stereochemical control over the following radical trapping event. This mechanistically peculiar approach demonstrates the potential of organocatalytic intermediates to participate in photochemical activation pathways. The characteristics and uses of EDA complexes will be further discussed in the second and third chapters of this thesis.

1.2.2 Photoexcitation of Chiral Iminium Ions and Enamines

The photochemical activity of aminocatalytic intermediates is not limited to the formation of ground-state EDA complexes. It was found in our laboratories that the direct photoexcitation of chiral enamines and iminium ions enables unique enantioselective redox processes, which are not achievable under thermal conditions (Scheme 1.8). Enamines in the excited state (**IV***) become strong reductants. They can be used to reduce α -bromo malonates **33** by SET to generate electron-deficient radicals **29**, which then can be trapped by the ground-state enamine intermediate **IV**.²⁹ On the other side, excited iminium ions **VI*** serve as strong photo-oxidants, which can generate reactive open-shell species **37** upon SET oxidation of electron-rich silanes.³⁰ The mechanisms of actions of these photo-excited chiral organocatalytic intermediates will be further discussed in more details in the second and fourth chapter of this thesis.

²⁹ M. Silvi, E. Arceo, I. D. Jurberg, C. Cassani, P. Melchiorre, Enantioselective Organocatalytic Alkylation of Aldehydes and Enals Driven by the Direct Photoexcitation of Enamines, *J. Am. Chem. Soc.*, **2015**, *137*, 6120.

³⁰ M. Silvi, C. Verrier, Y.P. Rey, L. Buzzetti, P. Melchiorre, Visible-light Excitation of Iminium Ions Enables the Enantioselective Catalytic β -alkylation of Enals, *Nat. Chem.*, **2017**, DOI: 10.1038/nchem.2748.



Scheme 1.8 a) Direct photo-excitation of enamines enables enantioselective α -alkylation of aldehydes; b) direct photo-excitation of iminium ions enables enantioselective β -alkylation of enals, SET: single-electron transfer, TMS: trimethylsilyl.

These photo-organocatalytic approaches provide unique strategies for the enantioselective functionalization of carbonyl compounds, which until very recently has been hidden in the dark.

1.3 Objectives and Summary of The Thesis

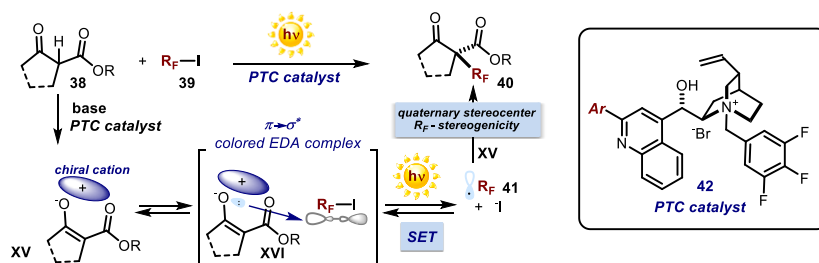
The main objective of this research thesis was to develop new enantioselective photo-organocatalytic transformations capitalizing upon the unique reactivities unlocked by the direct excitation of common chiral organocatalytic intermediates.

1.3.1 The Photochemistry of Electron Donor–acceptor (EDA) Complexes Derived from Chiral Enolates

The first objective of the thesis was to further advance the EDA complex activation strategy to include electron-rich chiral organocatalytic intermediates other than enamines, namely enolates. The ability of achiral enolates to form EDA complexes with perfluoroalkyl iodides was previously demonstrated by our group. Specifically, a light-driven aryl perfluoroalkylation of α -cyano arylacetates was developed, which demonstrated the ability of non-chiral enolates to form an EDA complex.³¹ Building upon this precedent, the goal of my studies was to develop an enantioselective

³¹ M. Nappi, G. Bergonzini, P. Melchiorre, Metal-Free Photochemical Aromatic Perfluoroalkylation of α -Cyano Arylacetates, *Angew. Chem. Int. Ed.*, **2014**, *53*, 4921.

perfluoroalkylation of β -ketoesters **38**, promoted by visible light excitation of chiral enolate-based EDA complexes (Scheme 1.9). Enantiocontrol of this process relies on a phase transfer catalyst **42**, which provided a suitable chiral environment for the enantioselective trapping of the reactive perfluoroalkyl radical **41**. This work represents the first implementation of chiral enolates **XV** as partners in photo-organocatalytic EDA complex activation for the construction of chiral stereocenters.



Scheme 1.9 EDA complex activation strategy employing chiral enolates as donors and perfluoroalkyl iodides (R_F-I) as acceptors. SET: single-electron transfer, PTC: phase transfer catalysis.

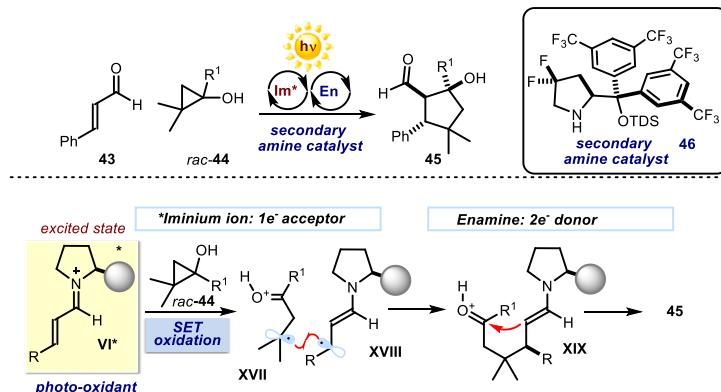
The work was undertaken in collaboration with Dr. John Joseph Murphy, who was involved in the initial optimization studies and greatly contributed to the discussion and experimental design.³²

1.3.2 Enantioselective Photochemical Organocascade Catalysis

The second goal of my doctoral research was to uncover the reactivity of photo-excited iminium ion intermediates **VI** to design enantioselective catalytic cascade reactions. In Chapter IV, I will describe the realization of this goal: a new photo-organocatalytic cascade process, which proceeds through a photochemical iminium ion-mediated step followed by a polar enamine-mediated process, is discussed (Scheme 1.10). This reaction sequence has been accomplished employing racemic cyclopropanols **44** that, upon SET oxidation by the photo-excited iminium ion **VI***, undergo ring-opening of the cyclopropane ring to form the β -ketoradical **XVII** along with the chiral 5π -electron β -enaminy radical intermediate **XVIII**. The subsequent radical coupling generates compound **XIX**, bearing a carbonyl moiety which is amenable to further reacts through a polar enamine-mediated intramolecular aldol process. Overall, this photo-iminium

³² Ł. Woźniak, J. J. Murphy, P. Melchiorre, Photo-organocatalytic Enantioselective Perfluoroalkylation of β -Ketoesters, *J. Am. Chem. Soc.*, **2015**, *137*, 5678.

ion/enamine cascade sequence affords highly enantioenriched, stereochemically dense cyclopentenes **45** from readily available starting materials in one step while consuming only photons.



Scheme 1.10 Enantioselective photochemical organo-cascade catalysis to afford chiral cyclopentenes.

SET: single-electron transfer, Im^* : photo-excited iminium ion, En: enamine

This work demonstrates that the reactivity of two chiral catalytic intermediates, one in the excited-state and the other in the ground-state, can be combined to implement an enantioselective, photochemical cascade process.

The project was conducted in collaboration with Giandomenico Magagnano, who contributed to the final stage of the optimization process and developed most of the scope of this transformation.

Chapter II

Enantioselective Photochemical Reactions

The purpose of this chapter is to provide the readers with a general overview of enantioselective photochemistry, a field which pervades the whole research work developed during this thesis. Specifically, I will detail the general strategies and concepts underlying the implementation of catalytic enantioselective light-mediated processes in solution. IUPAC provides the following definition of a photochemical reaction: *'a chemical reaction caused by absorption of ultraviolet, visible or infrared radiation. There are many ground-state reactions, which have photochemical counterparts. Among these are photochemical nitrogen extrusions, photocycloadditions, photodecarbonylations, photodecarboxylations, photoenolizations, photo-Fries rearrangement, photoisomerizations, photooxidations, photorearrangements, photoreductions, photosubstitutions, etc.'*

From this definition, it is important to distinguish between processes where the key bond-forming or bond-fragmenting event takes place in the electronically excited-state and transformations where photochemically generated reactive species undergo a subsequent ground-state reaction. This distinction is especially important when discussing enantioselective transformations. The control of the stereochemical outcome is a difficult task for both processes, but it requires different approaches.

Excited-state photochemical processes have great synthetic potential, but developing enantioselective variants have proven particularly difficult. The reasons for this are related to the challenge of a thorough mechanistic understanding of the photochemical process. Indeed, chemistry that evolves from excited states is more complex than ground-state reactivity. Reactions and conformational analysis of the electronic ground state of a molecule can be represented by a single energy surface.¹ Upon excitation, each electronically excited state of the molecule possesses its own energy surface placed at higher energy than the ground state. Figure 2.1 shows the Jablonski diagram, which represents three energy surfaces (represented by Morse potentials) and the key photophysical processes that must be considered when irradiating molecules.² It is very common that the chemical and structural properties of molecules are different in the

¹ E. V. Anslyn, D. A. Dougherty, Energy Surfaces and Kinetic Analyses, Chapter 7, p. 355-419 in *Modern Physical Organic Chemistry*, 2006.

² E. V. Anslyn, D. A. Dougherty, Photochemistry, Chapter 16, p. 937-939 in *Modern Physical Organic Chemistry*, 2006.

various surfaces. In this respect, careful and often very sophisticated design of a chiral catalyst is required to channel the photochemical reaction through an enantioselective path. The catalyst has to ensure that the substrate molecule already resides in a chiral environment during the excitation step, thus securing a selective irradiation of the catalyst-substrate aggregate, and that the catalyst-substrate interactions are maintained in the excited-states.³

Controlling the stereochemistry of photochemical reactions in which the enantioselective bond-formation takes place in the ground state offers a less severe problem, since it can be often controlled by classical strategies of asymmetric catalysis. This approach generally relies on the light-triggered generation of reactive intermediates, such as open-shell species, that can be intercepted using traditional tools of ground-state asymmetric catalysis (including organocatalysis). This raises interesting possibilities of developing new enantioselective photoinduced reactions, employing established tools of asymmetric synthesis.

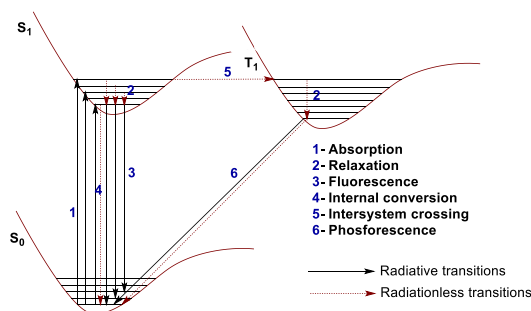


Figure 2.1 General Jablonski diagram.

2.1 Asymmetric Induction by Chiral Templates

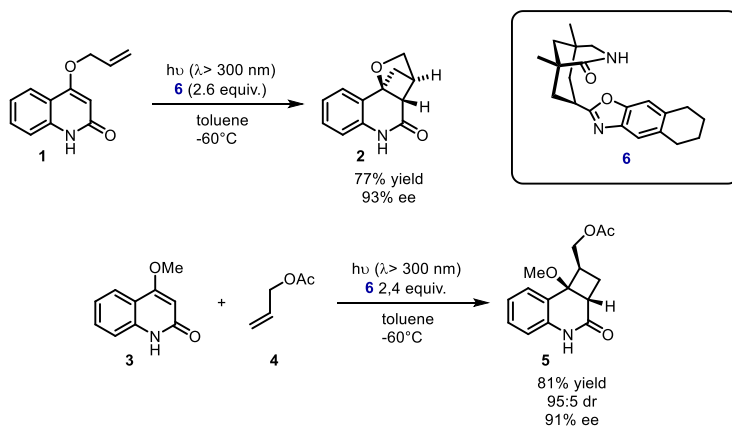
Early approaches to control enantioselectivity of photochemical reactions used stoichiometric amounts of chiral templates, which can bind to the substrates before of their photoexcitation.⁴ A molecule that can absorb light, upon excitation, possesses an energy that is sufficient to undergo fast, low-energy-barrier steps without additional activation. Therefore, the controlled formation of a new stereogenic center is facilitated when the achiral substrate is pre-assembled within a chiral environment during the

³ R. Brimiouille, D. Lenhart, M. M. Maturi, T. Bach, *Enantioselective Catalysis of Photochemical Reactions*, *Angew. Chem. Int. Ed.*, **2015**, *54*, 3872.

⁴ C. Müller, T. Bach, *Chirality Control in Photochemical Reactions: Enantioselective Formation of Complex Photoproducts in Solution*, *Aust. J. Chem.*, **2008**, *61*, 557.

excitation. The chiral complexing agent secures this condition. Multiple weak non-covalent interactions between the substrate and the chiral template can lead to chirality transfer in photochemical process. Both supramolecular and small molecule templates have been employed to transfer stereochemical information in photoinduced processes. To date, few highly enantioselective transformations have been achieved applying stoichiometric or super stoichiometric amount of chiral templates.

In 2000, Bach reported highly enantioselective intramolecular⁵ and intermolecular⁶ [2+2] photocycloaddition reactions of 2-quinolones **1** using chiral amides **6** derived from the Kemp's triacid (1,3,5-trimethylcyclohexan-1,3,5-tricarboxylic acid) as the chiral templates (Scheme 2.1). The success of this transformation is attributed to the formation of well-organized association between the chiral template and the prochiral lactam **1**, which can aggregate through a network of hydrogen bonding interactions. This chiral host-guest complex, when excited, can successfully undergo a highly stereoselective [2+2] photocycloaddition. This approach requires low temperatures to avoid any racemic background reaction while favoring the complete association of all substrate molecules with the chiral template.



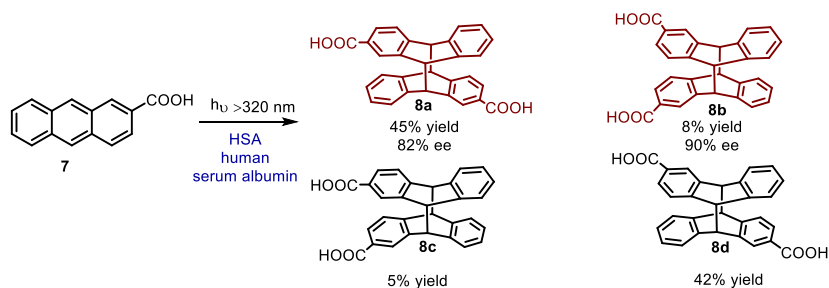
Scheme 2.1 Enantioselective [2+2] photocycloadditions mediated by a chiral template.

With regard to supramolecular templates, a major achievement was accomplished in 2007. Inoue and Bohne demonstrated that human serum albumin (HSA), acting as a

⁵ T. Bach, H. Bergmann, K. Harms, Enantioselective Intramolecular [2+2]-Photocycloaddition Reactions in Solution, *Angew. Chem. Int. Ed.* **2000**, *39*, 2302.

⁶ T. Bach, H. Bergmann Enantioselective Intermolecular [2+2]-Photocycloaddition Reactions of Alkenes and a 2-Quinolone in Solution, *J. Am. Chem. Soc.* **2000**, *122*, 11525.

natural supramolecular chiral host, can effectively transfer micro-environmental chirality to the prochiral 2-anthracenecarboxylate **7** (Scheme 2.2).⁷ The protein was tested for the [4+4] cycloaddition of **7**, which is a popular model system to study template-mediated enantioselective photochemical reactions. In this transformation, four dimeric products can be formed, two of which are chiral. HSA provides a good photo-chirogenic environment for photo-cyclodimerization to give both chiral products **8a** and **8b** with high enantiomeric excess (ee). Other supramolecular templates tested in this transformation, such as cyclodextrins, produced the chiral products only with low ee.⁸



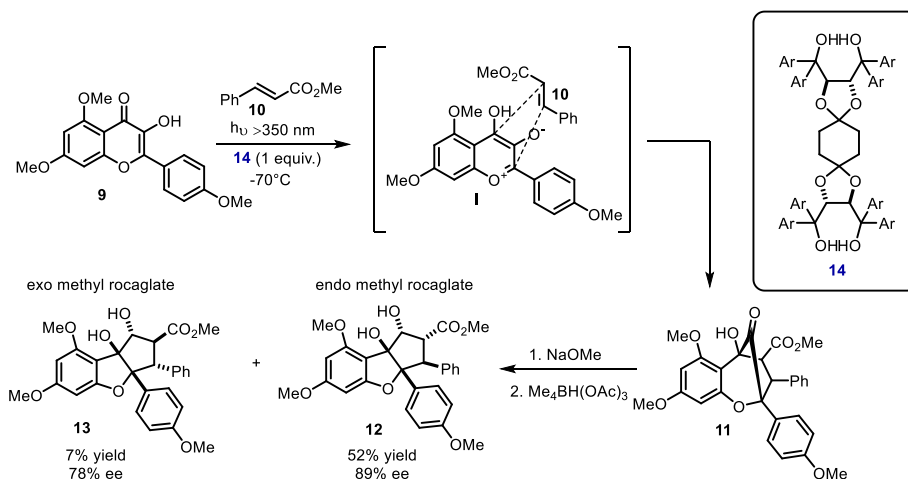
Scheme 2.2 Enantioselective [4+4] photocycloadditions mediated by biological template.

The chiral template strategy was also applied in the synthesis of enantiopure Rocaglamides **12** and **13** (Scheme 2.3).⁹ Intramolecular excited-state proton transfer (ESPT) within **9** leads to the formation of the intermediate **I**, which undergoes a [3+2] cycloaddition with **10** as controlled by the chiral TADDOL derivative **14**. A hydrogen bond assembly between the oxidopyrylium **I** with the chiral alcohol **14** was proposed to explain the observed enantioselectivity.

⁷ M. Nishijima, T. Wada, T. Mori, T. C. S. Pace, C. Bohne, Y. Inoue, Highly Enantiomeric Supramolecular [4 + 4] Photocyclodimerization of 2-Anthracenecarboxylate Mediated by Human Serum Albumin, *J. Am. Chem. Soc.*, **2007**, 129, 3478.

⁸ A. Nakamura, Y. Inoue, Electrostatic Manipulation of Enantiodifferentiating Photocyclodimerization of 2-Anthracenecarboxylate within γ -Cyclodextrin Cavity through Chemical Modification. Inverted Product Distribution and Enhanced Enantioselectivity, *J. Am. Chem. Soc.*, **2005**, 127, 15, 5338.

⁹ B. Gerard, S. Sangji, D. J. O'Leary, J. A. Porco Jr, Enantioselective Photocycloaddition Mediated by Chiral Brønsted Acids: Asymmetric Synthesis of the Rocaglamides, *J. Am. Chem. Soc.*, **2006**, 128, 7754.



Scheme 2.3 Enantioselective [3+2] photocycloadditions mediated by chiral template.

2.2 Enantioselective Catalysis of Photochemical Reactions

The fundamental idea of catalysis is to decrease the activation barrier of the reaction under study by means of a catalyst, which secures a lower energy pathway (Figure 2.2a). Indeed, prohibitive energy activation barriers often faced in common organic transformations can be overcome employing suitable catalysts. When a chiral catalyst is used, it is possible to direct the reaction through an enantioselective pathway. This scenario, however, is more difficult to achieve for photochemical processes. After excitation, the molecule gains sufficient energy to overcome an activation barrier - as such, it does not need any catalyst to undergo a productive process (Figure 2.2b). This creates a central issue in developing enantioselective photochemical processes, namely the difficult control of racemic, background photoreactions.¹⁰ Additionally, the short lifetime of the excited-state intermediates limits the ability of a chiral catalyst to guide the selectivity of these highly reactive species. In photochemical reactions proceeding through excited-state energy surfaces, the main role of a chiral catalyst is not to lower the activation barrier, but instead to interact with the substrates during the excitation event. This may ensure that a strong binding could be maintained also in the excited state, thus allowing the reaction to proceed through a stereocontrolled manifold.

¹⁰ Tehshik P. Yoon, Photochemical Stereocontrol Using Tandem Photoredox-Chiral Lewis Acid Catalysis, *Acc. Chem. Res.*, **2016**, *49*, 2307.

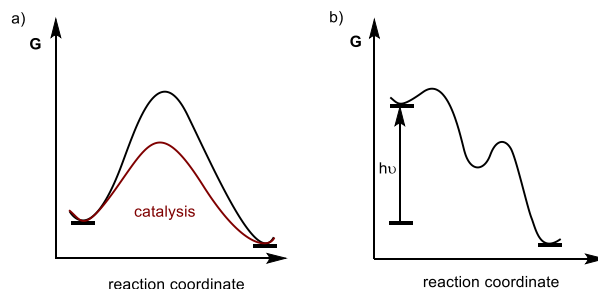


Figure 2.2 Enthalpy diagrams of a) thermal and b) photochemical reactions.

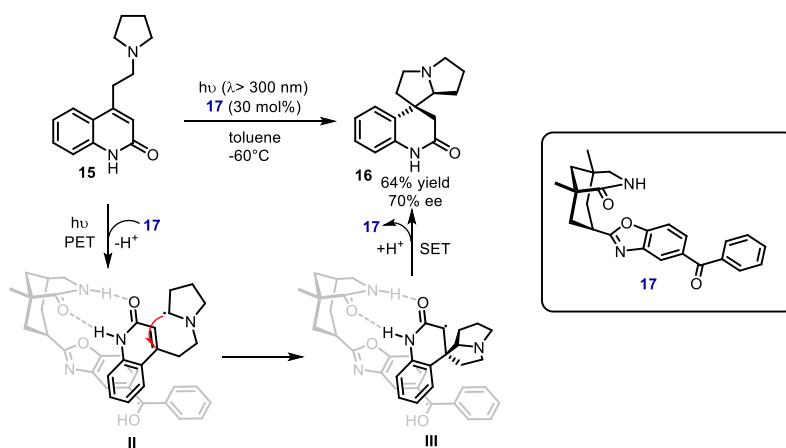
Processes where the photochemical step is separated from the enantioselective bond-forming event offers a completely different scenario. In this case, an external visible-light-absorbing photocatalyst is responsible for the generation of reactive species, which can be successively trapped by a ground-state chiral catalytic intermediate in an enantioselective fashion. The photochemical generation of reactive species does not always require an external photosensitizer. For example, our group demonstrated that chiral organocatalytic intermediates can directly serve as photoactive species to generate radicals upon light absorption (section 2.2.3). At the same time, the chiral organocatalyst ensures effective stereochemical control in the ensuing radical trapping event. In these cases, however, the stereo-defining event happens in the ground state.

Catalytic enantioselective photochemical reactions will be logically discussed in terms of the mechanistic frameworks underpinning these main strategies. The first part is dedicated to transformations in which the chiral catalysts absorb light and undergo energy or electron transfer with the substrates. This chemistry happens in the excited state. The second part will describe reactions in which the chiral catalysts do not undergo light excitation but work cooperatively with an achiral external photocatalyst. The last section focuses on transformations which employ chiral catalysts that do not absorb light but, when interacting with substrates, form a photoactive intermediates inducing enantioselective photochemical reactions. The processes discussed in the last two sections mainly rely on stereo-defining steps in the ground-state.

2.2.1 Chiral Photocatalysts

Chiral photoactive catalysts often transfer the chirality to the substrates through weak interactions that are maintained in the short-lived excited state. This secures the formation of enantiomerically enriched products. Efficient photosensitized enantio-differentiation is a difficult process to achieve. Despite considerable efforts over several decades, Bach

accomplished a major breakthrough in this field in 2005,¹¹ when he developed an enantioselective photocatalytic intramolecular conjugate addition of α -amino alkyl radicals to enones (Scheme 2.4). A significant enantiomeric excess was obtained by using the designed electron-accepting chiral organocatalyst **17**, which secured a chiral environment around the substrate through hydrogen bonding interactions. The high rigidity of the linker was key to secure a strong association with the substrate. The reaction is believed to proceed through photo-induced single-electron transfer (SET) to form the radical pair **II**. Next, a fast cyclization takes place before of possible competing back-electron transfer. The catalytic cycle is presumably closed by SET reduction of the α -ketoradical by the reduced form of the catalyst (intermediate **III**), and subsequent protonation of the resulting enolate.



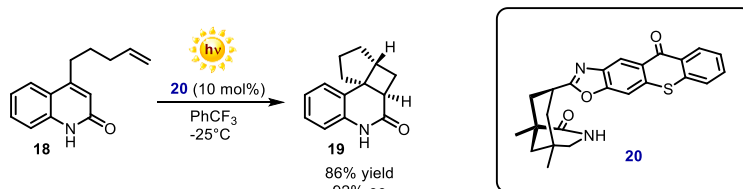
Scheme 2.4 Catalytic enantioselective photochemical cyclization of **15**.

A bridge between aromatic rings was installed in the next generation of chiral photocatalysts, which resulted in a completely flat structure of the photoactive unit (thioxantane catalyst **20** in Scheme 2.5). The planarity of the xantone or thioxantone motifs was found to be essential to control the enantioselectivity of the [2+2] cycloaddition.¹² It is believed that any distortion from the planar structure of the excited benzophenone (catalyst **17**) can facilitate dissociation of the substrate, which results in a racemic pathway. Additionally, the thioxantone catalyst **20** exhibits a significant

¹¹ A. Bauer, F. Westkämper, S. Grimme, T. Bach, Catalytic Enantioselective Reactions Driven by Photoinduced Electron Transfer, *Nature*, **2005**, 436, 1139.

¹² R. Alonso, T. Bach, A Chiral Thioxanthone as an Organocatalyst for Enantioselective [2+2] Photocycloaddition Reactions Induced by Visible Light, *Angew. Chem. Int. Ed.*, **2014**, 53, 4368.

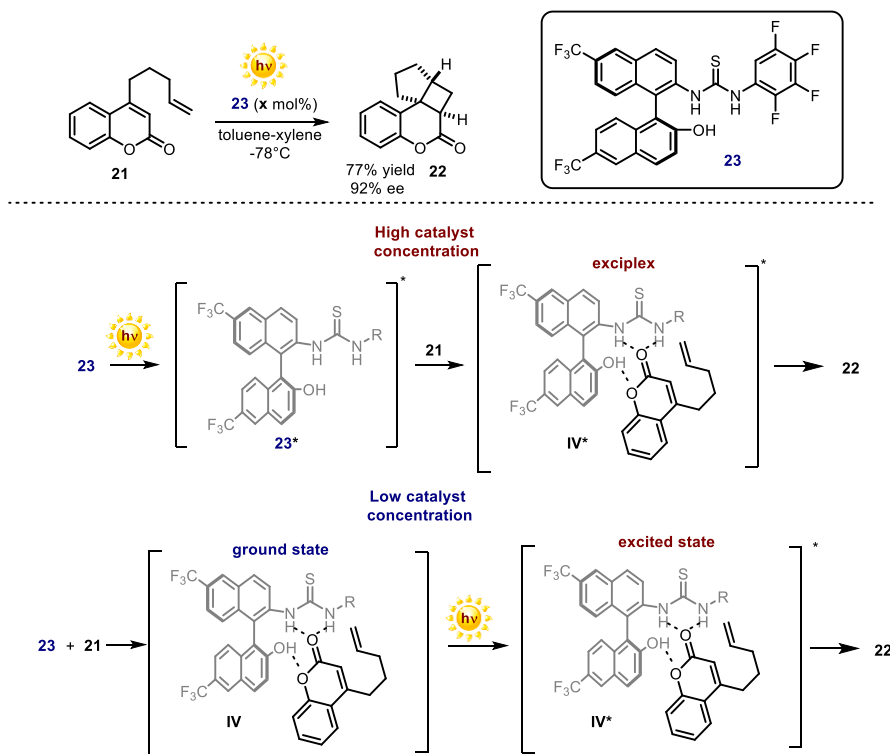
absorption in the visible light region, which provides a catalyst system activated by low energy, visible light irradiation. This chemistry follows energy transfer pathway from the photoexcited chiral catalyst **20** to substrate **18**.



Scheme 2.5 Catalytic enantioselective [2+2] photocycloaddition.

A different organocatalytic system, enabling a highly enantioselective [2+2] cycloaddition, was developed by Sibi and Sivaguru.¹³ The chiral thiourea catalyst **23** was employed to transfer stereochemical information to the excited states of coumarins **21** (Scheme 2.6). Interestingly, two mechanisms were proposed depending on the concentration of the catalyst. When using a high concentration, the catalyst possesses higher optical density than other reaction components. In this case, a direct excitation of the catalyst takes place. Aggregation of the catalyst excited state with the substrate **21** leads to the formation of an exciplex **IV*** (a noncovalent electronically excited complex of a molecule in an excited state with a different molecule in a ground state that acts together to emit a photon). However, when a low catalyst loading is used, the major species absorbing light is a ground-state complex between the catalyst and the substrate, leading to intermediate **IV**. Direct photoexcitation of **IV** triggers the stereocontrolled formation of the product **22**. In both cases, the stereo-differentiation arises from the atropisomeric binaphthyl motif of the catalyst, which interacts with the substrate through hydrogen bonding.

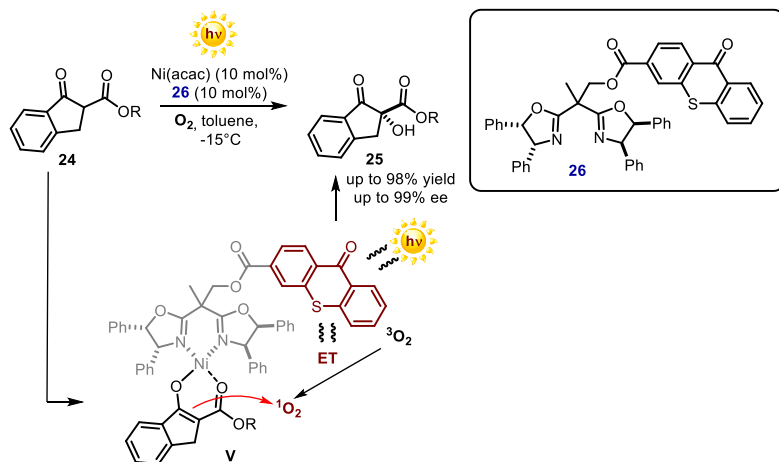
¹³ N. Vallavoju, S. Selvakumar, S. Jockusch, M. P. Sibi, J. Sivaguru, Enantioselective Organo-Photocatalysis Mediated by Atropisomeric Thiourea Derivatives, *Angew. Chem. Int. Ed.*, **2014**, *53*, 5604.



Scheme 2.6 Enantioselective [2+2] cycloaddition catalyzed by chiral thiourea derivative.

More recently, Xiao reported visible-light-responsive chiral ligands by grafting chiral bisoxazoline with thioxantone **26**.¹⁴ These new ligands were successfully applied in visible-light-promoted Lewis acid-catalyzed hydroxylation of β -ketoesters **24** by molecular oxygen (Scheme 2.7). The thioxantone photosensitizer is responsible for the generation of an electrophilic singlet oxygen, which is next trapped by the chiral Ni-enolate **V**. The bifunctional catalyst **26** is crucial to form product **25** with high efficiency and selectivity. Both the yield and enantioselectivity of the product decreased significantly when the photooxygenation reaction was performed with the chiral bisoxazoline ligand and thioxantone separately.

¹⁴ W. Ding, L.-Q. Lu, Q.-Q. Zhou, Y. Wei, J.-R. Chen, W.-J. Xiao, Bifunctional Photocatalysts for Enantioselective Aerobic Oxidation of β -Ketoesters, *J. Am. Chem. Soc.*, **2017**, *139*, 63.



Scheme 2.7 Enantioselective photochemical oxidation of β -ketoesters. ET: energy transfer, acac: acetylacetonate.

2.2.2 Chiral Catalysts in Cooperation with Achiral Photocatalysts

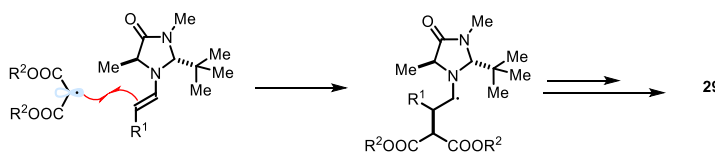
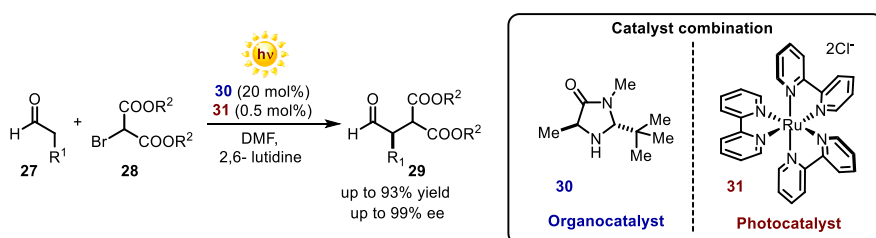
Dual catalytic approaches, which merge the redox activity of a visible-light-absorbing photocatalyst with the ground-state reactivity of a chiral intermediate, have emerged as powerful strategies to control the stereochemistry of light-induced reactions. This approach, by exploiting the unique reactivity of photocatalytically generated open-shell intermediates, allows to expand the successful tools of classical enantioselective catalysis from a *polar* to a *radical* reactivity domain. In this scenario, the role of the achiral photocatalyst is to generate a reactive, often radical, species which then undergoes subsequent bond-forming step in the ground state controlled by the second chiral catalyst. MacMillan introduced this strategy in 2008¹⁵ in the field of organocatalysis. Specifically, an enamine-mediated enantioselective α -alkylation of aldehydes with alkyl halides was developed, which could not be accomplished through a traditional S_N2 -type ionic pathway (Scheme 2.8). The reaction, as already discussed in Chapter I, section 1.2 of this thesis, combined asymmetric organocatalysis with a photoredox catalytic cycle. Later, the same group expanded this methodology to the enantioselective α -trifluoromethylation¹⁶ and α -benzylation¹⁷ of aldehydes. These studies, along with others

¹⁵ D. A. Nicewicz, D. W. C. MacMillan, Merging Photoredox Catalysis with Organocatalysis: The Direct Asymmetric Alkylation of Aldehydes, *Science*, **2008**, 322, 77.

¹⁶ D. A. Nagib, M. E. Scott, D. W. C. MacMillan, Enantioselective α -Trifluoromethylation of Aldehydes via Photoredox Organocatalysis, *J. Am. Chem. Soc.*, **2009**, 131, 10875.

¹⁷ H.-W. Shih, M. N. Vander Wal, R. L. Grange, D. W. C. MacMillan, Enantioselective α -Benzylation of Aldehydes via Photoredox Organocatalysis, *J. Am. Chem. Soc.*, **2010**, 132, 13600.

published almost at the same time but not dealing with stereoselective chemistry,¹⁸ provided the impetus for the conceptualization and development of the rapidly growing field of light-mediated photoredox catalysis.¹⁹ The use of a photoredox catalyst offers an effective way of generating radical intermediates from readily available, bench-stable precursors under very mild conditions. This means that enantioselective organocatalysis, which requires mild conditions for optimal efficiency and stereocontrol, could be successfully applied within radical reactivity patterns.



Scheme 2.8 Cooperation of photoredox catalysis with enamine-mediated catalysis. DMF: dimethyl formamide.

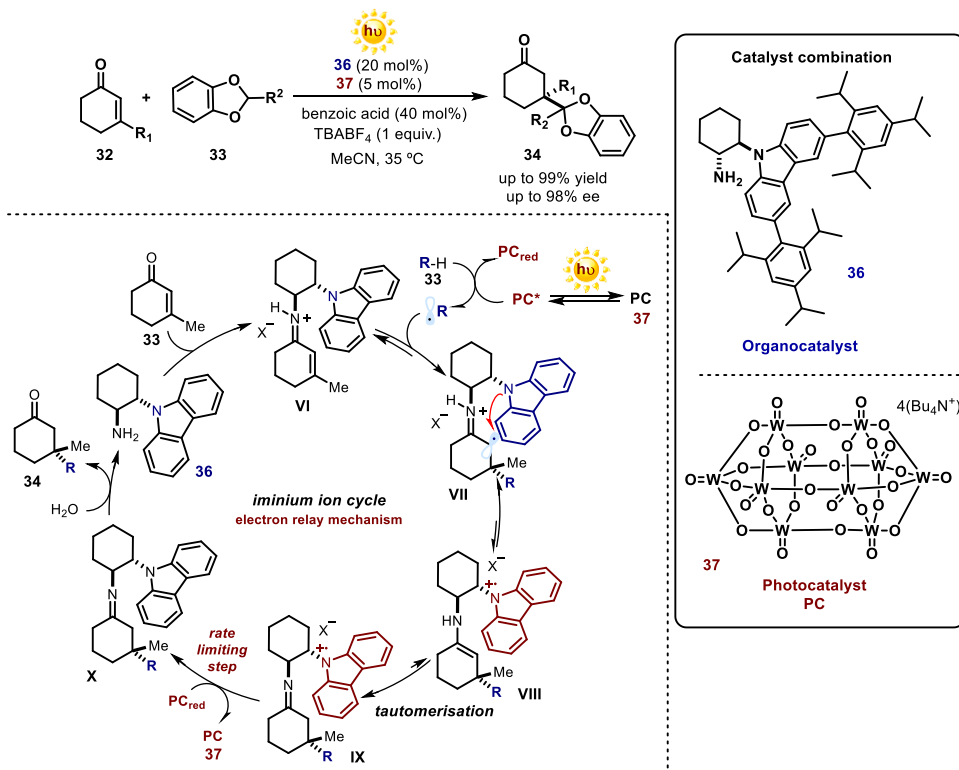
Despite this progress, it was difficult to expand redox-active photocatalysts in synergy with the ground-state reactivity of well-established chiral organocatalytic intermediates other than enamines. Particularly difficult was the development of catalytic enantioselective addition of photochemically generated radicals to chiral iminium ions, a problem that was only recently addressed (Scheme 2.9).²⁰ The key issue stems from the nature of the radical intermediate **VII**, generated upon radical conjugate addition and carbon-carbon bond formation. The short-lived, highly reactive α -iminyl radical cation **VII** tends to undergo reverse reaction (so-called β -scission) to regenerate the more stable

¹⁸ a) M. A. Ischay, M. E. Anzovino, J. Du, T. P. Yoon, Efficient Visible Light Photocatalysis of [2+2] Enone Cycloadditions, *J. Am. Chem. Soc.*, **2008**, 130, 12886, b) J. M. R. Narayanam, J. W. Tucker, C. R. J. Stephenson, Electron-Transfer Photoredox Catalysis: Development of a Tin-Free Reductive Dehalogenation Reaction, *J. Am. Chem. Soc.*, **2009**, 131, 8756.

¹⁹ M. H. Shaw, J. Twilton, D. W. C. MacMillan, Photoredox Catalysis in Organic Chemistry, *J. Org. Chem.*, **2016**, 81, 16, 6898.

²⁰ J. J. Murphy, D. Bastida, S. Paria, M. Fagnoni, P. Melchiorre, Asymmetric Catalytic Formation of Quaternary Carbons by Iminium Ion Trapping of Radicals, *Nature* **2016**, 532, 218.

iminium ion precursor **VI**. The solution came with the design of a redox-active organocatalyst, amine **36**, which secured a fast, intramolecular SET reduction of the unstable radical intermediate **VII**.

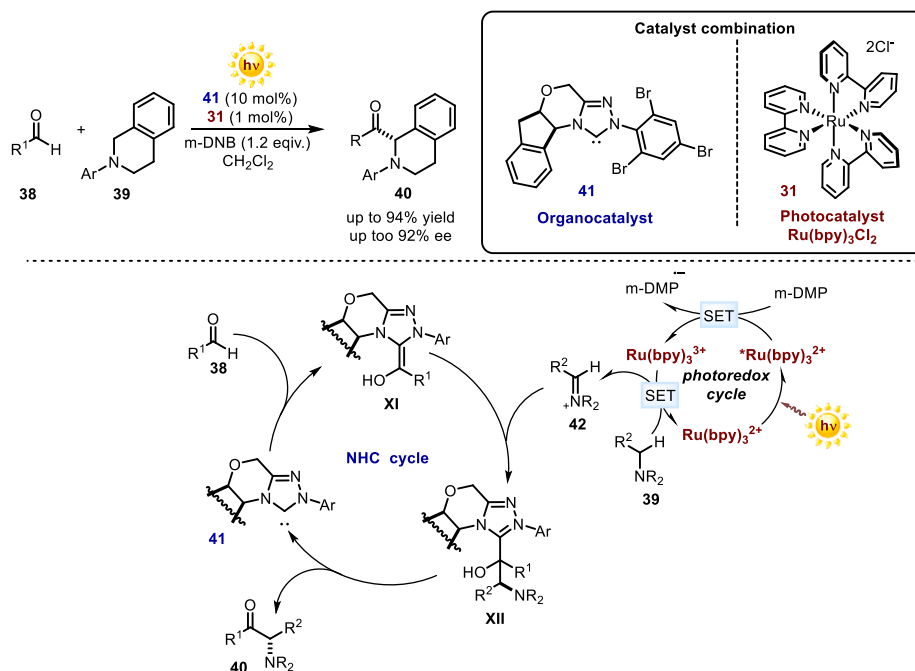


Scheme 2.9 Cooperation of photoredox catalysis with the iminium ion activation mode to realize the enantioselective radical conjugate addition to enone **32**. PC: photocatalyst, PC_{red}: reduced photocatalyst, TBABF₄: tetrabutylammonium tetrafluoroborate.

Upon radical conjugate addition to the iminium ion **VI**, an electron-relay mechanism, by shuttling electrons from the redox-active carbazole moiety, bypasses the unstable radical cation **VII** producing a carbazoliumyl radical cation **VIII**, which is prevented from undergoing back-electron transfer by tautomerization of the secondary enamine to the corresponding imine **IX**. Regeneration of the photocatalyst is achieved by reduction of the carbazoliumyl radical cation in **IX**, while the aminocatalyst **36** is liberated upon hydrolysis of imine **X**. Detailed mechanistic investigations uncovered an unanticipated turnover-limiting step of this reaction, which is the reduction of the carbazole radical

cation within intermediate **IX** and the regeneration of the photocatalyst (PC).²¹ This knowledge allows rational tuning of the redox properties of the chiral organocatalyst **36** to improve the catalytic activity.

Photoredox catalysis was also combined with another chiral organocatalytic intermediate, the Breslow intermediate (Scheme 2.10).²² In 2012, Rovis reported the enantioselective nucleophilic addition of acyl anion equivalents **XI** to the photochemically generated iminium ions **42** employing chiral N-heterocyclic carbene catalyst **41**.



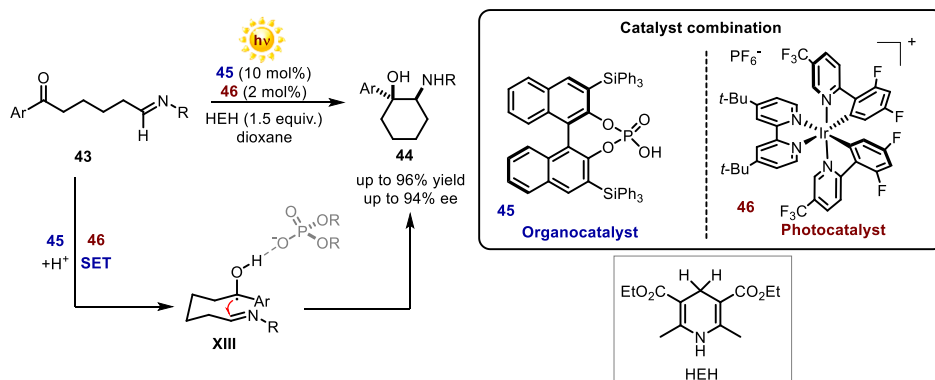
Scheme 2.10 Cooperation of photoredox and N-heterocyclic carbene catalysis; m-DNB: meta-dinitrobenzene.

In addition to covalent catalysis, organocatalytic strategies employing noncovalent catalyst-substrate interactions were successfully coupled with photoredox systems. A novel approach was demonstrated by Knowles, who used chiral phosphoric acids to

²¹ A. Bahamonde, J. J. Murphy, M. Savarese, É. Brémond, A. Cavalli, P. Melchiorre, Studies on the Enantioselective Iminium Ion Trapping of Radicals Triggered by an Electron-Relay Mechanism, *J. Am. Chem. Soc.*, **2017**, *139*, 4559.

²² M. N. Hopkinson, C. Richter, M. Schedler, F. Glorius, An Overview of N-Heterocyclic Carbenes, *Nature*, **2014**, *510*, 485.

promote stereocontrolled intramolecular aza-pinacol reactions (Scheme 2.11).²³ In this process, SET from the light-activated iridium catalyst **46** to the ketone **43** occurs in concert with proton transfer, as aided by the presence of the chiral phosphoric acid **45**. During the course of SET, the position of the proton within the H-bond shifts from the phosphoric acid to the more basic ketyl radical. The hydrogen bond complex **XIII** between the ketyl radical and phosphate anion persists on the time-scale of the carbon-carbon bond forming step, thus allowing an effective chirality transfer from the catalyst.

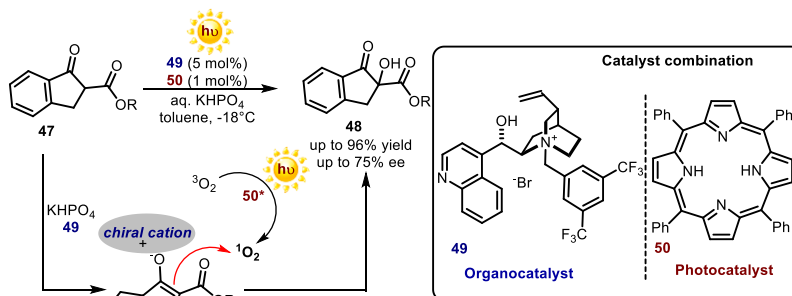


Scheme 2.11 Cooperation of photoredox and chiral Brønstad acid catalysis. HEH: Hantzsch ester, SET: single-electron transfer.

Chiral cationic catalysts can also be employed to dictate the enantioselectivity of photochemical reactions. Meng reported the enantioselective photo-oxygenation of β -ketoesters under phase-transfer conditions (Scheme 2.12).²⁴ In this reaction, a chiral enolate reacted with photochemically generated, electrophilic singlet oxygen affording hydroxylated product **48** with moderate enantioselectivities.

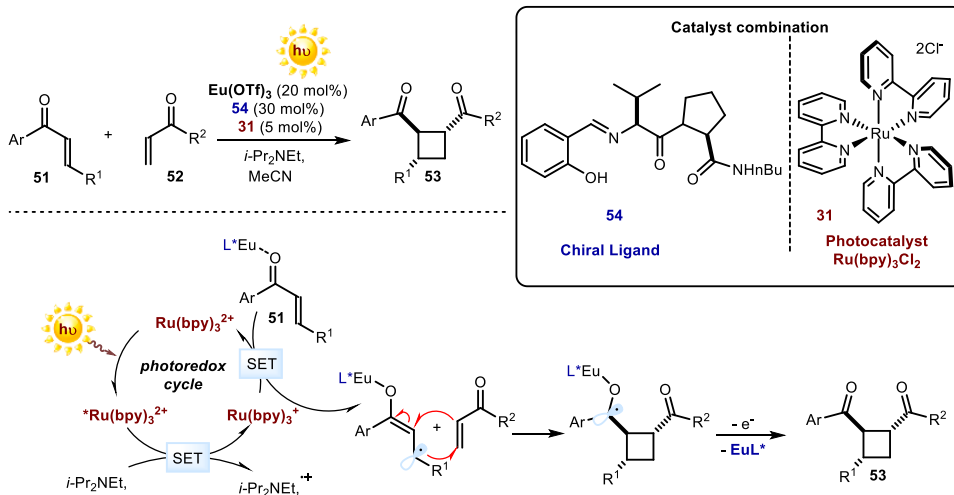
²³ L. J. Rono, H. G. Yayla, D. Y. Wang, M. F. Armstrong, R. R. Knowles, Enantioselective Photoredox Catalysis Enabled by Proton-Coupled Electron Transfer: Development of an Asymmetric Aza-Pinacol Cyclization, *J. Am. Chem. Soc.*, **2013**, 135, 17735.

²⁴ M. Lian, Z. Li, Y. Cai, Q. Meng, Z. Gao, Enantioselective Photooxygenation of β -Keto Esters by Chiral Phase Transfer Catalysis Using Molecular Oxygen, *Chem. Asian J.*, **2012**, 7, 2019.



Scheme 2.12 Enantioselective photo-oxygenation of β -ketoesters in phase transfer conditions.

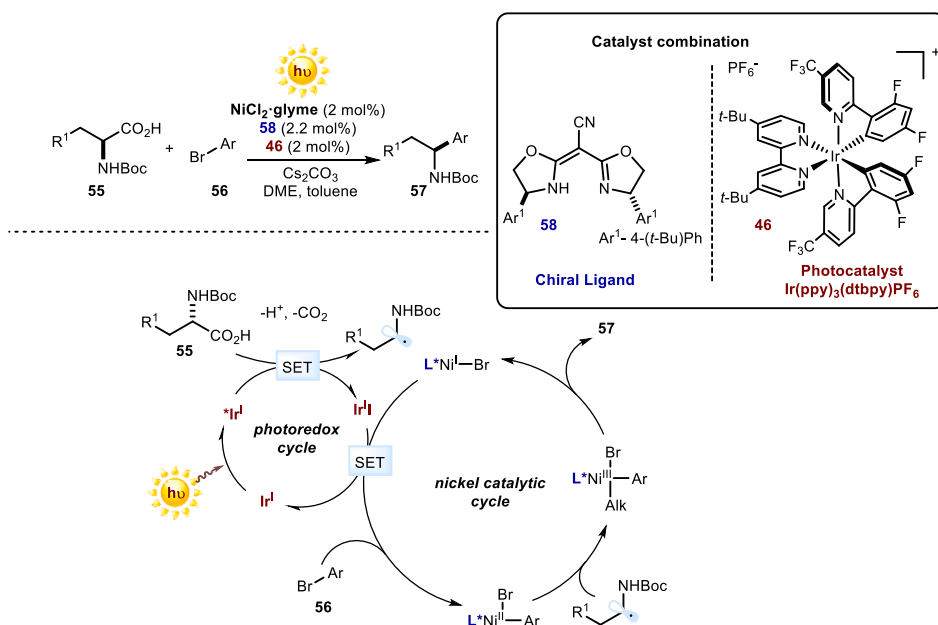
Combining chiral Lewis acid catalysis with photoredox catalysis was also a successful stereoselective strategy, as nicely demonstrated by Yoon to perform highly enantioselective intramolecular [2+2] cycloaddition of enones **51** (Scheme 2.13).²⁵ Coordination of a chiral europium complex to the substrate facilitated the SET reduction of enone **51** from the ruthenium-based photocatalyst **31** while, at the same time, securing a suitable chiral environment for the subsequent radical cyclization with **52**.



Scheme 2.13 Cooperation of photoredox and Lewis acid catalysis. SET: single-electron transfer, L*: chiral ligand, Tf: trifluoromethane sulfonate.

²⁵ J. Du, K. L. Skubi, D. M. Schultz, T. P. Yoon, A Dual-Catalysis Approach to Enantioselective [2+2] Photocycloadditions Using Visible Light, *Science*, **2014**, 344, 392.

The marriage of transition metal and photoredox catalysis has also been a successful strategy for the synthesis of valuable enantioenriched chiral compounds. The MacMillan and Fu research groups combined their efforts to develop an enantioselective sp^2 - sp^3 coupling by means of nickel/photoredox synergistic catalysis (Scheme 2.14).^{26,27} The proposed reaction mechanism starts with an oxidative addition of Ni(0) into the aryl halide **56** to produce a Ni(II) intermediate. Concurrently with this process, the SET oxidation of a carboxylate, formed upon deprotonation of the carboxylic acid substrate **55** by cesium carbonate, by the photoexcited catalyst **46** and subsequent decarboxylation generates an α -amino radical, which is intercepted by the Ni(II) complex to give the organometallic Ni(III) adduct. Carbon-carbon bond forming reductive elimination forms the enantioenriched benzyl amine product **57**. The resulting Ni(I) complex is returned into the original Ni(0) species by SET from the reduced form of the iridium photocatalyst, closing both the photoredox and nickel catalytic cycles. The stereochemical information is dictated by the chiral ligand **58**.



Scheme 2.14 Cooperation of photoredox and nickel acid catalysis. SET: single-electron transfer, DME: 1,2-dimethoxyethane.

²⁶ Z. Zuo, H. Cong, W. Li, J. Choi, G. C. Fu, D. W. C. MacMillan, Enantioselective Decarboxylative Arylation of α -Amino Acids via the Merger of Photoredox and Nickel Catalysis, *J. Am. Chem. Soc.*, **2016**, *138*, 1832.

²⁷ J. Twilton, C. C. Le, P. Zhang, M. H. Shaw, R. W. Evans, D. W. C. MacMillan, The Merger of Transition Metal and Photocatalysis, *Nature Reviews Chemistry*, **2017**, *1*, 0052.

The selected examples of the combination of photoredox catalysis with various substrate activation modes available to asymmetric catalysis highlight the generality and utility of these strategies as new powerful tools for making chiral molecules.

2.2.3 Chiral Photoactive Catalytic Intermediates

In 2013, our research group identified a different strategy to promote enantioselective photochemical reactions based on the photochemical activity of chiral organocatalytic intermediates. Specifically, chiral enamines **XV** could aggregate in the ground state with electron-poor alkyl halides of type **60** to afford visible-light absorbing electron donor-acceptor complexes (EDA complex **XVI** in Figure 2.3).²⁸ These aggregates, upon light excitation, could provide access to reactive open-shell intermediates, which could then be trapped stereoselectively by the ground-state chiral enamines. This strategy opened a new research line in our group dedicated to the development of new enantioselective reactions initiated by direct visible-light excitation of chiral catalytic intermediates, without the need of an external photocatalyst.

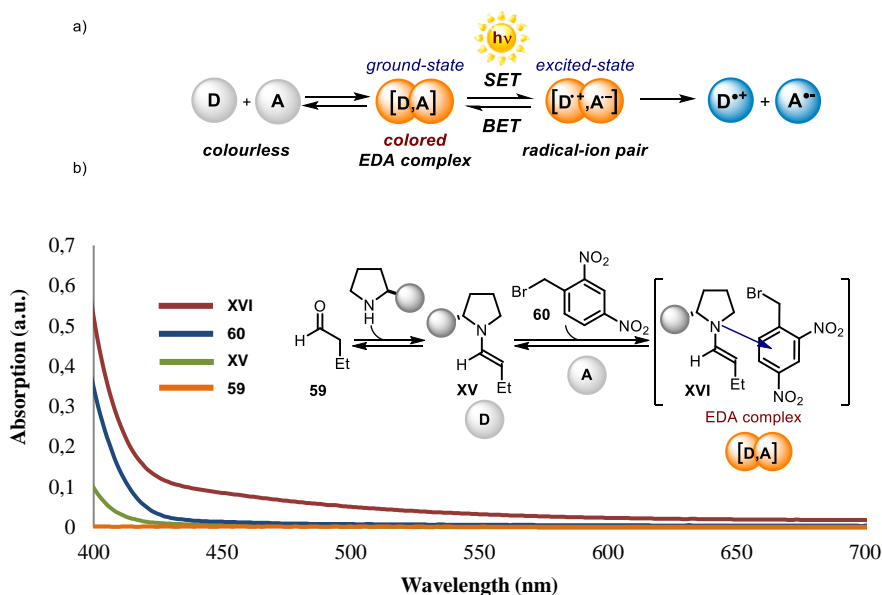
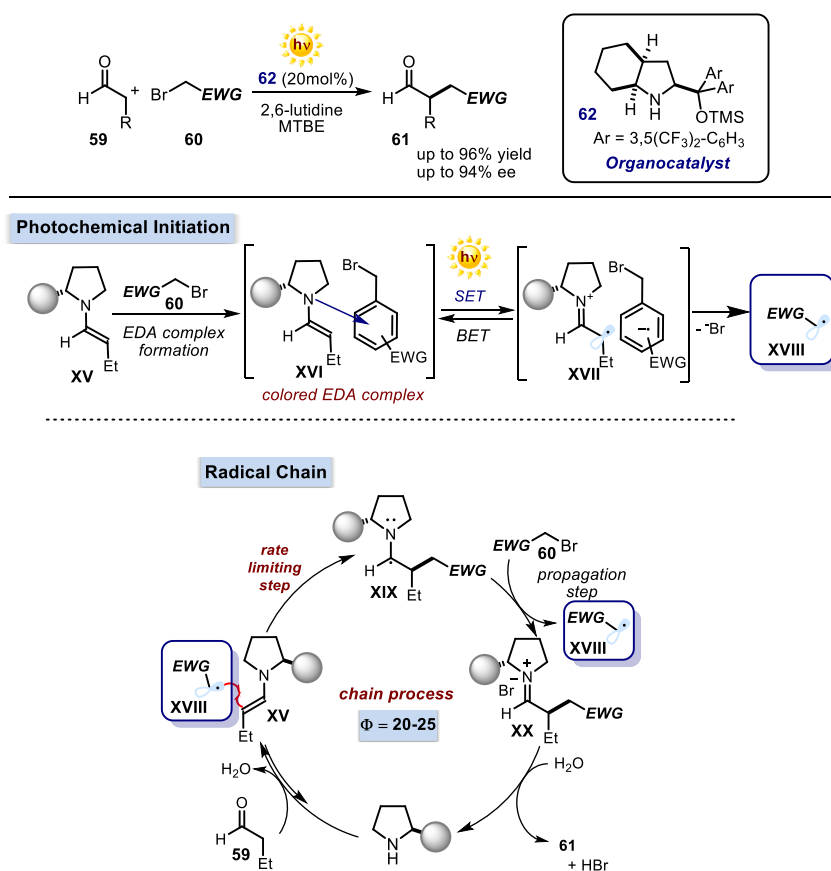


Figure 2.3 a) Formation and excitation of an EDA complex. D: donor, A: acceptor, SET: single-electron transfer, BET: back-electron transfer. b) Optical absorption spectra of reaction components²⁸, the filled grey circle represents a bulky substituent on the chiral amine catalyst.

²⁸ E. Arceo, I.D. Jurberg, A. Álvarez-Fernández, P. Melchiorre, Photochemical Activity of a Key Donor-acceptor Complex Can Drive Stereoselective Catalytic α -alkylation of Aldehydes, *Nat. Chem.*, **2013**, 5, 750.

Applying EDA complex strategy, the enantioselective, enamine-mediated α -alkylation of aldehydes was accomplished by simple irradiation of the reaction mixture with visible light (Scheme 2.15).²⁸ The key initiation step, promoted by visible light excitation of the EDA complex **XVI**, leads to a radical ion pair **XVII** and subsequent formation of benzyl radical **XVIII** upon carbon-bromide bond fragmentation. The resulting electron-poor benzyl radical can be trapped in enantioselective fashion by another molecule of chiral enamine **XV**. The newly formed electron-rich α -amino radical **XIX** can reduce, by SET, a new molecule of benzyl bromide to reform the propagating benzyl radical. The resulting iminium salt **XX** undergoes hydrolysis to release the product and the catalyst.



Scheme 2.15 Proposed mechanism of photoinitiation and the catalytic cycle of the enantioselective α -alkylation of aldehydes. Φ : quantum yield of the reaction. The filled grey circle represents a bulky substituent on the chiral amine catalyst, SET: single-electron transfer, BET: back-electron transfer

Overall, the process proceeds through a radical self-propagating chain process. Measurements of the quantum yield of this process, which defines the amount of product formed per photon absorbed by the reaction, revealed that a radical chain mechanism is operative ($\Phi=25$ for the reaction between butanal and benzyl bromide **60**, which implies that at least 25 molecules of product **61** are formed upon absorption of one photon by **XVI**).²⁹ The reaction-profile analysis and rate-order assessment indicated the trapping of the carbon-centered radical by the enamine, to form the carbon-carbon bond, as rate-determining. This work demonstrated the use of chiral EDA complexes to connect two powerful fields of molecule activation: asymmetric organocatalysis and photochemistry. This study constituted the first use of the EDA complex strategy in asymmetric catalysis. However, chemists have been fascinated by the features of EDA complexes since the past century, and their photophysical properties have been investigated for almost 70 years.³⁰ EDA complexes are ground-state associations between donors, having low ionization potentials, and acceptor molecules, with high electron affinities. The main peculiarity of EDA complexes is that their formation is accompanied by the appearance of a new absorption band, the charge-transfer band, associated with a charge transition from donor to acceptor. The new band is shifted from the individual absorbances and is often in the visible range of the spectrum (Figure 2.3), which results in the appearance of a new color of the reaction mixture. Elucidation of this phenomenon was a subject of studies for many chemists. The concept of an electron donor-acceptor interactions was introduced by Benesi and Hildebrand in 1949³¹ and soon after had been related to the molecular orbital theory by Mulliken.³⁰ Formation of these complexes was explained by an energetically and geometrically favored overlap of accessible molecular orbitals of donor and acceptor molecules.

The EDA complexes feature charge distribution between donor and acceptor molecules in the ground state. The electron mobility within the complex depends on two key factors: resonance stabilization (H_{DA}) of donor-acceptor assembly [D,A] and the reorganization energy penalty (λ_T) required for the interconversion into the charge-transfer state [D^+ , A^-] (Figure 2.1).³²

²⁹ A. Bahamonde, P. Melchiorre, Mechanism of the Stereoselective α -Alkylation of Aldehydes Driven by the Photochemical Activity of Enamines, *J. Am. Chem. Soc.*, **2016**, *138*, 8019.

³⁰ R. S. Mulliken, Structures of Complexes Formed by Halogen Molecules with Aromatic and with Oxygenated Solvents *J. Am. Chem. Soc.*, **1950**, *72*, 600.

³¹ H. A. Benesi, J. H. A. Hildebrand, Spectrophotometric Investigation of the Interaction of Iodine with Aromatic Hydrocarbons, *J. Am. Chem. Soc.*, **1949**, *71*, 2703.

³² S. V. Rosokha, J. K. Kochi, Fresh Look at Electron-transfer Mechanisms via the Donor/acceptor Bindings in the Critical Encounter Complex, *Acc. Chem. Res.*, **2008**, *41*, 641.



Figure 2.4 Formation and excitation of an EDA complex. D: donor, A: acceptor, H_{DA} : resonance stabilization, λ_{T} : reorganization energy.

Those two variables give a factor $Q = 2H_{\text{DA}}/\lambda_{\text{T}}$ that represents a quantitative measure of the inner sphere/outer sphere interactions that are possible between the precursor complexes. Two extreme situations can be described: when $Q \ll 1$ and $Q \geq 1$.

In the first scenario ($Q \ll 1$), a high intrinsic activation barrier (reorganization energy penalty) λ_{T} and a low stabilization energy H_{DA} of the encounter complex leads to slow electron transfer rates (Figure 2.5a). These SET characteristics resemble the classical Marcus outer-sphere SET mechanism.³³ In this situation, the formation of the new charge-transfer band is usually insufficient for experimental observation. The other extreme ($Q \geq 1$) is represented by an overwhelming dominance of the resonance stabilization H_{DA} , which predicts that the SET within the EDA occurs without any barrier, such as it is just in coincidence with the diffusional association of donor and acceptor (Figure 2.5c). The new absorption band formed upon mixing a donor with an acceptor is most likely associated with the absorption of the resulting donor radical cation or acceptor radical anion after immediate barrier-less SET. In these cases, experimental observation of a charge-transfer band might be possible, but mainly at low temperatures.³⁴ In between of these two extremes lies a continuum set of states where $0 < Q < 1$ (Figure 2.5b). These charge transfer complexes are characterized by a significant resonance stabilization H_{DA} and SET possesses some activation barrier. In this scenario, the charge transfer band is usually easily observable in solution.

The energy needed for SET might be delivered by heat or direct excitation of the EDA complex. The latter produces an excited-state with electrons equally distributed between the donor–acceptor $[\text{D}^+\cdots\text{A}^-]$ irrespective of the ground-state charge distribution.

³³ Marcus, R. A. Electron-transfer Reactions in Chemistry: Theory and Experiment (Nobel Lecture), *Angew. Chem., Int. Ed.*, **1993**, *32*, 1111.

³⁴ S. V. Rosokha, S. M. Dibrov, T. Y. Rosokha, J. K. Kochi, Electronic Structures of Intermolecular Charge-transfer States in Fast Electron Transfers with Tetrathiafulvalene Donor. Thermal and Photoactivation of [2 + 4] Cycloaddition to o-chloranil Acceptor, *Photochem. Photobiol. Sci.*, **2006**, *5*, 914.

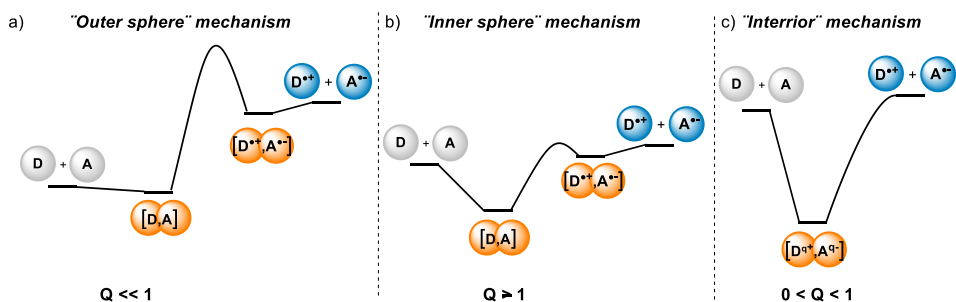
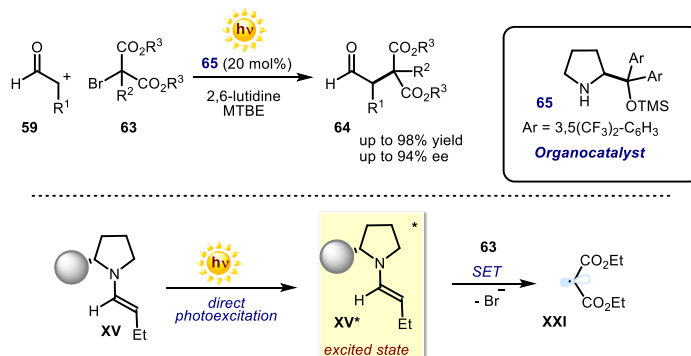


Figure 2.5 Three distinctive mechanisms for bimolecular electron transfer, as progressively modulated by the donor/acceptor binding within the encounter complex. D: donor, A: acceptor, Q: a quantitative measure of inner sphere/outer sphere interactions between precursor complexes.

From a synthetic point of view, the key requirement to achieve productive pathway is often an efficient dissociation of the resulting radical pair, which can be accelerated by the presence of a suitable leaving group within the EDA complex. Fast, irreversible bond fragmentation within the radical ion pair is crucial to avoid unproductive BET (back-electron transfer), which would lead to the regeneration of the starting materials. This strategy was crucial for the development of the enantioselective α -alkylation of aldehydes discussed in Scheme 2.15.

Our research group has identified that a mechanistically different scenario takes place when α -bromomalonates are employed as reaction partners with chiral enamines (Scheme 2.16).³⁵ The reaction proceeds with high yields and enantiomeric excesses and requires light illumination (at about 400 nm). However, no EDA complex formation was detected on bringing together the chiral enamine with the substrate **63**. This intriguing observation suggested that a different mechanism of photoinitiation was involved in this process. Mechanistic investigations demonstrated that the direct photoexcitation of chiral enamines **XV**, which could barely absorb light until 420 nm, induces the formation of an electron-poor radical, which further reacted with the ground-state enamines in a similar mechanism as depicted in Scheme 2.18 ($\Phi = 20$).

³⁵ M. Silvi, E. Arceo, I. D. Jurberg, C. Cassani, P. Melchiorre, Enantioselective Organocatalytic Alkylation of Aldehydes and Enals Driven by the Direct Photoexcitation of Enamines, *J. Am. Chem. Soc.*, **2015**, *137*, 6120.



Scheme 2.16 Proposed mechanism of the photoinitiation of α -alkylation of aldehydes with α -bromomalonates. The filled grey circle represents a bulky substituent on the chiral amine catalyst. SET: single-electron transfer, MTBE: tert-butyl methyl ether, TMS: trimethylsilyl.

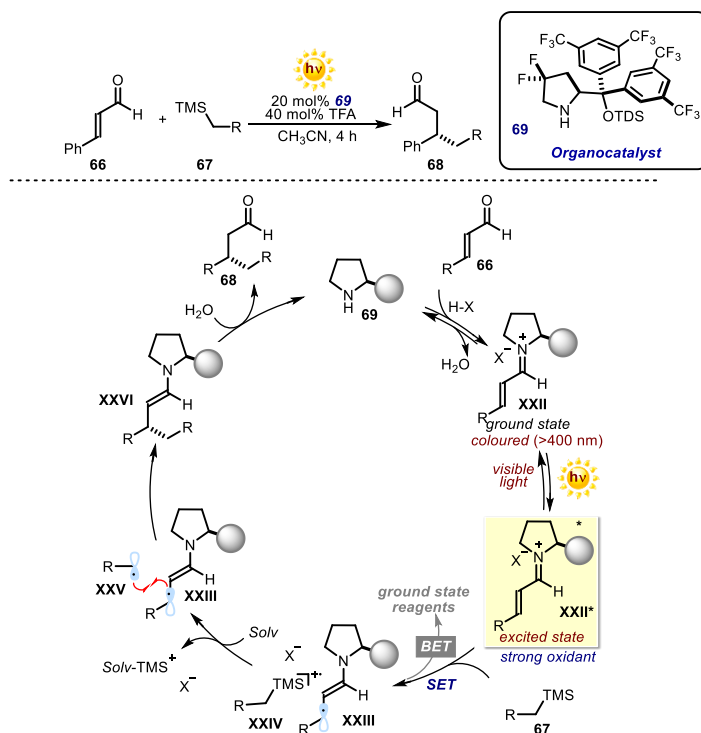
This study demonstrated that electron-rich enamines, which are primarily understood as nucleophiles in their ground state, could become strong reductants upon light excitation and trigger the formation of radicals through the SET reduction of electron-poor organic halides. At the same time, the ground-state chiral enamines provided effective stereochemical control over the enantioselective radical trapping process. That strategy, where stereinduction and photoactivation merged in a sole chiral organocatalytic intermediate, enabled light-driven enantioselective transformations that could not be realized using the thermal reactivity of enamines. Recently, our group expanded this methodology to achieve the formal enantioselective α -methylation of aldehydes.³⁶

An important step forward in the development new photochemical activation pathways has been the direct photoexcitation of other chiral aminocatalytic intermediates, such as iminium ions. Recently, our group demonstrated that exposure to visible light brings the electron-poor iminium ion **XXII** to an electronically excited state **XXII***, thus unlocking reactivities not available to iminium ion ground-state chemistry. Since an excited state possesses much higher electronic affinity³⁷ (that is, it is a better electron acceptor) than the ground state, the photoexcited iminium ion **XXII*** function as a strong oxidant, affording reactive open-shell intermediates upon SET oxidation from electron-rich substrates. This strategy allowed enantioselective β -alkylation of enals with substrates

³⁶ G. Filippini, M. Silvi, P. Melchiorre, Enantioselective Formal α -Methylation and α -Benzylation of Aldehydes by Means of Photo-Organocatalysis, *Angew. Chem., Intl. Ed.*, **2017**, 56, 4447.

³⁷ E. V. Anslyn, D. A. Dougherty, Photochemistry, Chapter 16, p. 955-956 in *Modern Physical Organic Chemistry*, **2006**.

that are recalcitrant to polar conjugate addition manifolds (Scheme 2.17).³⁸ Mechanistically, SET oxidation of the electron-rich alkyl trimethylsilane **67** by the photoexcited iminium ion **XXII*** furnishes the 5 π -electron β -enaminy radical intermediate **XXIII** along with the silyl radical cation **XXIV**. Irreversible fragmentation of the carbon-silicon bond in **XXIV** triggers the generation of neutral radical intermediates **XXV**, along with a formal trimethylsilyl cation (TMS⁺). At this juncture, a stereocontrolled intermolecular coupling of the chiral β -enaminy radical **XXIII** with **XXV** forms a new carbon-carbon bond while forging the stereogenic center. The resulting enamine intermediate **XXVI**, upon hydrolysis, regenerates the catalyst **69** whilst liberating the β -functionalized aldehyde **68**.



Scheme 2.17 Proposed mechanism of the enantioselective β -alkylation of enals driven by photoexcited iminium ion **VII***. SET: single-electron transfer, TFA: trifluoroacetic acid, BET: back-electron transfer, TMS: trimethylsilyl, the filled grey circle represents a bulky substituent on the chiral amine catalyst.

³⁸ M. Silvi, C. Verrier, Y.P. Rey, L. Buzzetti, P. Melchiorre, Visible-light Excitation of Iminium Ions Enables the Enantioselective Catalytic β -alkylation of Enals, *Nat. Chem.*, **2017**, DOI: 10.1038/nchem.2748.

In addition to these studies, there are a few reports in which metal complexes form photoactive chiral catalytic intermediates upon binding with a substrate and promote enantioselective photochemical reactions.³⁹

The photo-organocatalytic strategies described above provided the conceptual roots and the synthetic tools for the chemistry developed in this doctoral thesis and form the conceptual basis for the discussion in the following chapters.

³⁹ For selected examples a) R. Brimiouille, T. Bach, Enantioselective Lewis Acid Catalysis of Intramolecular Enone [2+2] Photocycloaddition Reactions, *Science* **2013**, 342, 840, b) H. Huo, X. Shen, C. Wang, L. Zhang, P. Rçse, L.-A. Chen, K. Harms, M. Marsch, G. Hilt, E. Meggers, Asymmetric Photoredox Transition-metal Catalysis Activated by Visible Light, *Nature*, **2014**, 515, 100, c) Q. M. Kainz, C. D. Matier, A. Bartoszewicz, S. L. Zultanski, J. C. Peters, G. C. Fu, Asymmetric Copper-catalyzed C–N Cross-couplings Induced by Visible Light, *Science*, **2016**, 351, 681.

Chapter III

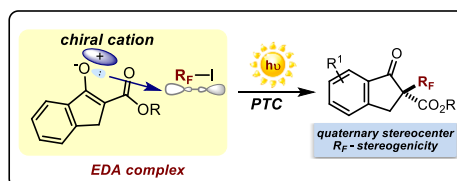
Photo-Organocatalytic Enantioselective Perfluoroalkylation of β -Ketoesters

Target

Developing a visible-light-driven, phase-transfer-catalyzed, enantioselective perfluoroalkylation and trifluoromethylation of cyclic β -ketoesters to forge quaternary carbon stereocenters.¹

Tool

Photochemical activity of *in situ* generated electron donor-acceptor (EDA) complexes, arising from the association of chiral enolates and perfluoroalkyl iodides.



3.1 Introduction

The chemistry of chiral enolates has a rich history in stereoselective synthesis. The diverse portfolio of possible bond-forming processes, offered by the reactivity of enolates, makes this branch of asymmetric synthesis particularly interesting. Generally, enolates are generated upon deprotonation of carbonyl substrates. The first strategies to forge new stereogenic centers using enolates relied on the extant asymmetry of chiral substrates to provide suitable stereochemical control for bond-forming events (Scheme 3.1a).² Later, the use of removable chiral auxiliaries provided a robust and highly predictable tool for the stereoselective α -functionalization of carbonyls (Scheme 3.1b).³ Interestingly enough, such traditional asymmetric approaches, despite the great advances in catalytic enantioselective strategies, remain often the methods of choice, both in academia and industry.⁴ Still, enantioselective catalysis provides a vast array of methods to control the stereochemical outcome of enolate-mediated processes. Both metal catalysis and organocatalysis are widely applied to channel those reactions through enantioselective pathways. A broad scope of electrophiles can be employed to achieve

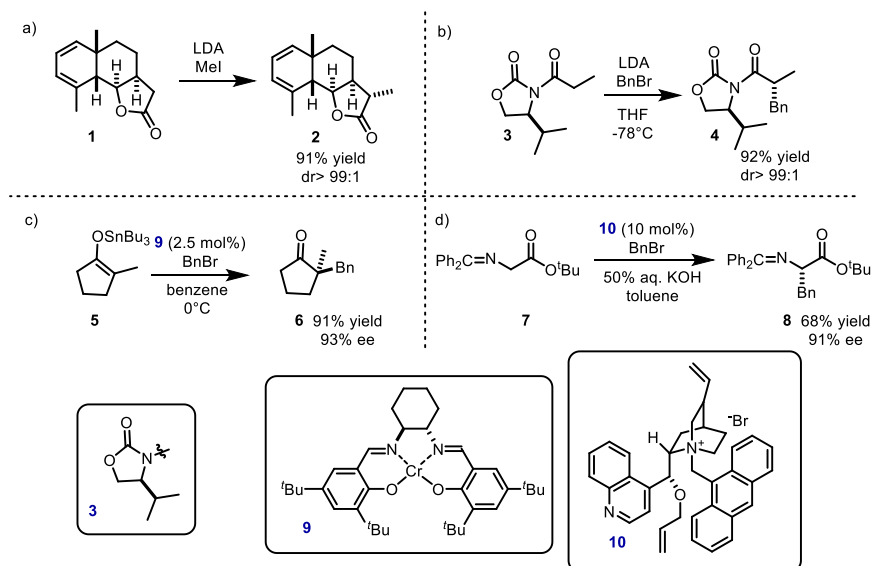
¹ The work discussed in this chapter has been published: Ł. Woźniak, J. J. Murphy, P. Melchiorre, Photo-organocatalytic Enantioselective Perfluoroalkylation of β -Ketoesters, *J. Am. Chem. Soc.*, **2015**, 137, 5678.

² J. A. Marshall, P. G. M. Wuts, Stereoselective Total synthesis of The Marine Diterpene Dictyolene and its C-11 Epimer *J. Am. Chem. Soc.*, **1978**, 100, 1627.

³ D. A. Evans, M. D. Ennis, D. J. Mathre, Asymmetric Alkylation Reactions of Chiral Imide Enolates. A Practical Approach to the Enantioselective Synthesis of α -Substituted Carboxylic Acid Derivatives, *J. Am. Chem. Soc.*, **1982**, 104, 1737.

⁴ M. M. Heravi, V. Zadsirjan, B. Farajpour, Applications of oxazolidinones as chiral auxiliaries in the asymmetric alkylation reaction applied to total synthesis, *RSC Adv.*, **2016**, 6, 30498.

enantioselective functionalizations of carbonyls, for example S_N2 -type alkylations with organic halides,⁵ arylations,⁶ conjugate additions,⁷ aldol reaction,⁸ or oxidations.⁹ Selected examples of stereoselective alkylations of enolates are presented in Scheme 3.1.¹⁰



Scheme 3.1 Examples of stereoselective alkylation of enolates controlled by: a) extant asymmetry of chiral substrates. b) Chiral auxiliary. c) A chiral chromium salen catalyst. d) A chiral phase transfer catalyst. LDA: lithium diisopropylamide.

⁵ B. Lygo, P. G. Wainwright, A New Class of Asymmetric Phase-transfer Catalysts Derived from Cinchona Alkaloids - Application in the Enantioselective Synthesis of α -amino Acids, *Tetrahedron Lett.*, **1997**, 38, 49, 8595.

⁶ J. Åhman, J. P. Wolfe, M. V. Troutman, M. Palucki, S. L. Buchwald, Asymmetric Arylation of Ketone Enolates, *J. Am. Chem. Soc.*, **1998**, 120, 8, 1918.

⁷ D. Uraguchi, K. Yoshioka, Y. Ueki, T. Ooi, Highly Regio-, Diastereo-, and Enantioselective 1,6- and 1,8-Additions of Azlactones to Di- and Trienyl N-Acylpyrroles, *J. Am. Chem. Soc.*, **2012**, 134, 19370.

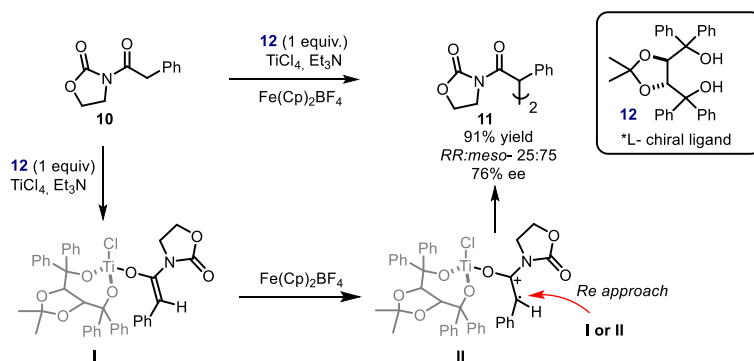
⁸ N. Yoshikawa, Y. M. A. Yamada, J. Das, H. Sasai, M. Shibasaki, Direct Catalytic Asymmetric Aldol Reaction, *J. Am. Chem. Soc.*, **1999**, 121, 4168.

⁹ M. Lian, Z. Li, Y. Cai, Q. Meng, Z. Gao, Enantioselective Photooxygenation of β -Keto Esters by Chiral Phase Transfer Catalysis Using Molecular Oxygen, *Chem. Asian J.*, **2012**, 7, 2019.

¹⁰ A. G. Doyle, E. N. Jacobsen, Enantioselective Alkylations of Tributyltin Enolates Catalyzed by Cr(salen)Cl: Access to Enantiomerically Enriched All-Carbon Quaternary Centers, *J. Am. Chem. Soc.*, **2005**, 127, 62.

Generally, enantioselective enolate chemistry has been used within polar reactivity domains. In sharp contrast, few examples of radical trap from enolates have been reported.¹¹

In 2001, Schäfer reported an enantioselective oxidative coupling of titanium enolate **I** employing the chiral ligand **12** in stoichiometric quantity (Scheme 3.2).^{11a} The titanium enolate **I**, upon treatment with ferrocenium cation, undergoes a single-electron transfer (SET) oxidation to form the radical cation **II**. This species can undergo a radical coupling with another molecule of **II** or radical addition to the enolate **I**¹² to form the product **11**.



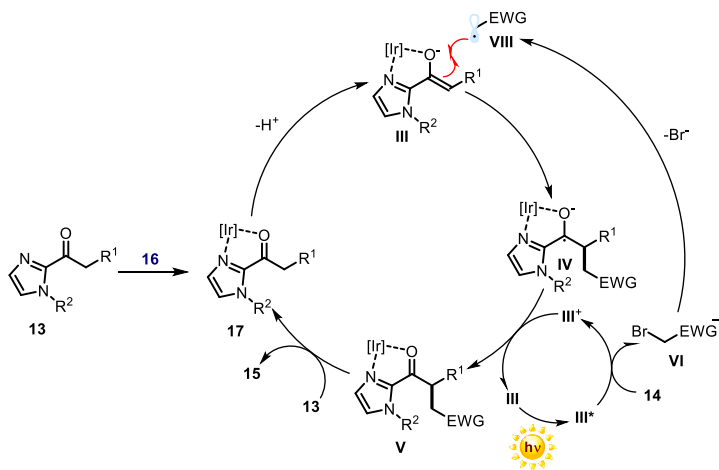
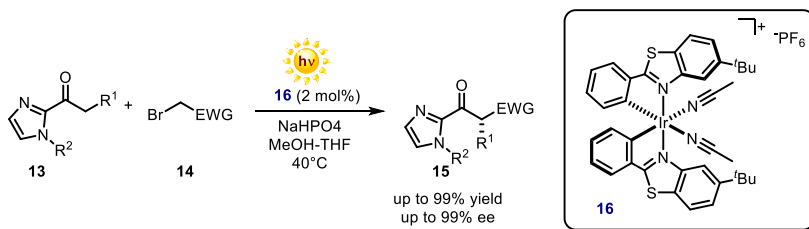
Scheme 3.2 Enantioselective oxidative coupling of the titanium enolate. Cp: cyclopentadien.

A catalytic enantioselective radical transformation of enolates was reported by Meggers in 2014 (Scheme 3.3).^{11b} A chiral-at-metal iridium complex **16** was employed to achieve a photochemical, enantioselective alkylation of ketones. The reaction is initiated by the coordination of 2-acyl imidazole **13** to the iridium catalyst **16** to form complex **17**. The nucleophilic iridium enolate complex **III**, formed upon deprotonation of **17**, serves as a chiral photocatalyst, which upon photoexcitation reduces the electron-poor alkyl bromide **14** via a SET manifold. Carbon-bromide bond cleavage within the radical anion **VI** lead to the formation of the alkyl radical **VII**, which can be trapped by the chiral iridium enolate **III**. Oxidation of the resulting ketyl intermediate **IV** to a ketone by SET

¹¹ a) P. Q. Nguyen, H. J. Schäfer, Enantioselective Oxidative Coupling of the Titanium Enolate of 3-Phenylacetyl-2-oxazolidinone, *Org. Lett.*, **2001**, 3, 2993, b) H. Huo, X. Shen, C. Wang, L. Zhang, P. Rçse, L.A. Chen, K. Harms, M. Marsch, G. Hilt, E. Meggers, Asymmetric Photoredox Transition-metal Catalysis Activated by Visible Light, *Nature*, **2014**, 515, 100.

¹² J. Ullrich, Highly Efficient Generation of Radicals from Ester Enolates by the Ferrocenium Ion. Application to Selective α -Oxygenation and Dimerization Reactions of Esters, *J. Org. Chem.*, **1998**, 63, 7130.

regenerates the iridium photosensitizer and provides the iridium coordinated product **V**, which is released upon exchange with the unreacted starting material **13**.



Scheme 3.3 Enantioselective alkylation of ketones by asymmetric photoredox transition-metal catalysis. THF: tetrahydrofuran, EWG: electron-withdrawing group.

We envisioned that the strategy developed in our research group, which is based on the photochemical activity of EDA complexes generated from chiral enamines (discussed in Chapter 2), could be translated to the chemistry of enolates. This would allow the development of light-triggered enantioselective radical transformations of enolates that might not be possible through classical polar reactivity.

3.2 Reactions of Enolates Proceeding by Electron Transfer Mechanism

Despite the high nucleophilicity of enolates, many substitution reactions with alkyl halides have been shown to proceed slowly or be not possible under traditional ionic pathways. The lack of reactivity is usually due to strain, steric and electronic factors or a combination of them. For example, secondary and tertiary halides are unreactive in $\text{S}_{\text{N}}2$

pathways mainly because of the steric bulk generated by neighboring substituents. Electronic factors have a strong influence on the reactivity of perfluoroalkyl iodides, which are completely recalcitrant to the nucleophilic displacement of iodide under S_N2 or S_N1 conditions. The shielding of the carbon by the surrounding lone electron pairs on fluorine atoms destabilize and repel the approaching carbonanion.¹³

In these cases, when classical ionic pathways are precluded, nucleophilic substitution can be accomplished by $S_{RN}1$ mechanisms that involve open-shell intermediates, generated by SET events, as originally demonstrated by Kornblum¹⁴ and Russell¹⁵ in 1966. Scheme 3.4b shows the $S_{RN}1$ mechanism of the reaction reported by Kornblum between β -ketoester **17** and the electron-poor alkyl halide **18**. The process is initiated by SET¹⁶ from the enolate **I** to **18**, which leads to the formation of the neutral radical **X** and the radical anion **XI**. Carbon-chlorine bond fragmentation within **XI** affords the benzyl radical **XII**, which can be trapped by the enolate **IX**. The resulting intermediate **XIII** can reduce, via an SET, another molecule of **18** to form the product **19** and the propagating benzyl radical **XII**. Overall, this process proceeds through a self-propagating radical chain mechanism. Even though the S_N2 pathway is feasible, Kornblum proposed the $S_{RN}1$ mechanism based on the observed suppression of the alkylation process when adding a catalytic amount of one-electron acceptor, such as *p*-dinitrobenzene, which can interfere with the SET event underlying the radical chain manifold. Additionally, a markedly different product distribution between C and O alkylation adducts (**19** and **20**, respectively, with **20** being associated to a purely ionic path) was observed when adding a small amount of cupric chloride (Scheme 3.2a), which was proposed to suppress the radical-anion reaction while allowing the displacement through an S_N2 process. One year later, Kornblum reported a remarkable example of $S_{RN}1$ process employing tertiary benzyl chloride **22**, a substrate which definitely cannot undergo a classical S_N2 reaction (Scheme 3.4c).¹⁷

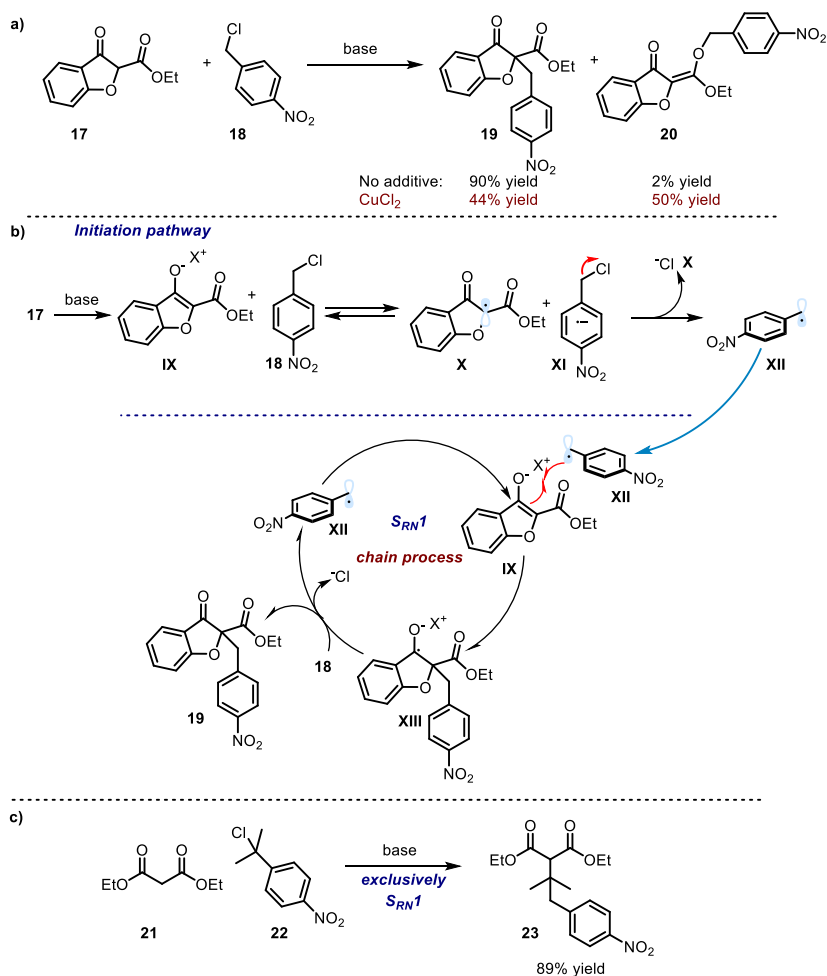
¹³ P. Kirsch, *Modern Fluoroorganic Chemistry Synthesis, Reactivity, Applications*, Chapter 2, p. 91-92, Wiley **2004**.

¹⁴ N. Kornblum, R. E. Michel, R. C. Kerber, Chain Reactions in Substitution Processes Which Proceed via Radical-Anion Intermediates, *J. Am. Chem. Soc.*, **1966**, *88*, 5662.

¹⁵ G. Russell, W. C. Danen, Coupling Reactions of the 2-Nitro-2-propyl Anion¹, *J. Am. Chem. Soc.*, **1966**, *88*, 5663.

¹⁶ R. C. Kerber, G. W. Urry, N. Kornblum, Radical Anions as Intermediates in Substitution Reactions. The Mechanism of Carbon Alkylation of Nitroparaffin Salts, *J. Am. Chem. Soc.*, **1965**, *87*, 4520.

¹⁷ N. Kornblum, G. W. Earl, N. L. Holy, J. W. Manthey, M. T. Musser, D. H. Snow, R. T. Swiger, New and Facile Substitution Reactions at Tertiary Carbon. The Use of Oxygen as a Mechanistic Probe, *J. Am. Chem. Soc.*, **1968**, *90*, 6221.

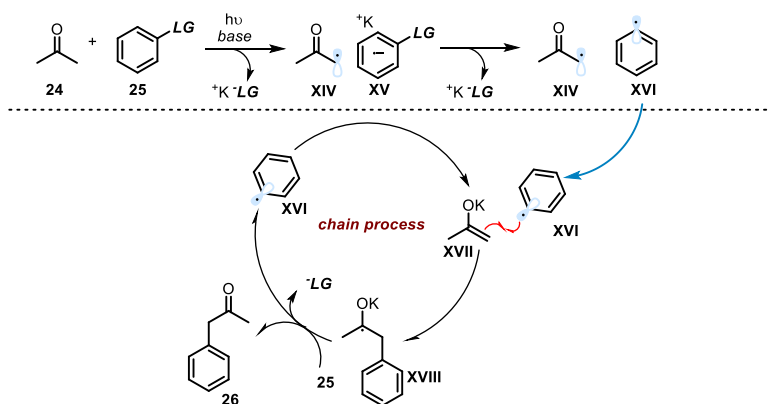


Scheme 3.4 a) Alkylation of enolates through an $\text{S}_{\text{RN}}1$ pathway employing primary electron-poor benzyl chlorides. b) The proposed reaction mechanism. c) Alkylation of enolates through an $\text{S}_{\text{RN}}1$ pathway employing a tertiary electron-poor benzyl chloride.

The distinction between an $\text{S}_{\text{N}}2$ and an SET process is related to bonding interactions between the enolate and the electrophile in the transition state. In an $\text{S}_{\text{N}}2$ process, the transfer of electrons is accompanied with significant bond reorganization within the reaction complex and is favored in terms of energy by the bonding interactions. However, $\text{S}_{\text{N}}2$ transition states have a strict requirement for the relative alignment of the nucleophile and the carbon-halide bond within the electrophile. On the other side, the transition state in the electron transfer mechanism has a looser structure with no substantial bond

formation.¹⁸ This makes the SET pathways rather insensitive to steric hindrance, thus explaining why $S_{RN}1$ mechanisms are favored over S_N2 for sterically encumbered substrates.

In general, the electron transfer event can be spontaneous or may require thermal or photochemical activation. Photochemical $S_{RN}1$ α -arylation of ketone **24** was reported in 1973 by Bunnett (Scheme 3.5).¹⁹ Photochemically induced SET from enolate to the aromatic partner **25** results in the formation of aryl radical anion **XV**, which after fragmentation of a leaving group, produces an aryl radical **XVI**. Trapping of this resulting radical by the enolate **XIV** generates the ketyl radical intermediate **XVIII**, which can reduce another molecule of the aromatic substrate **25** to propagate a chain reaction and release the product **26**. Although Bunnett did not provide mechanistic details of the initiation step, this reaction was later studied by Fox who proposed the involvement of charge transfer complexes in this transformation.²⁰



Scheme 3.5 $S_{RN}1$ α -arylation of enolates initiated by photoexcitation of EDA complexes. LG: leaving group.

¹⁸ R. A. Rossi, A. B. Pierini, A. B. Peñeñory, Nucleophilic Substitution Reactions by Electron Transfer, *Chem. Rev.*, **2003**, *103*, 71.

¹⁹ R. A. Rossi, J. F. Bunnett, Photostimulated Aromatic $S_{RN}1$ Reactions, *J. Org. Chem.*, **1973**, *38*, 1407.

²⁰ M. A. Fox, J. Younathan, G. E. Fryxell, Photoinitiation of the Sml Reaction by Excitation of Charge-Transfer Complexes, *J. Org. Chem.*, **1983**, *48*, *18*, 3109.

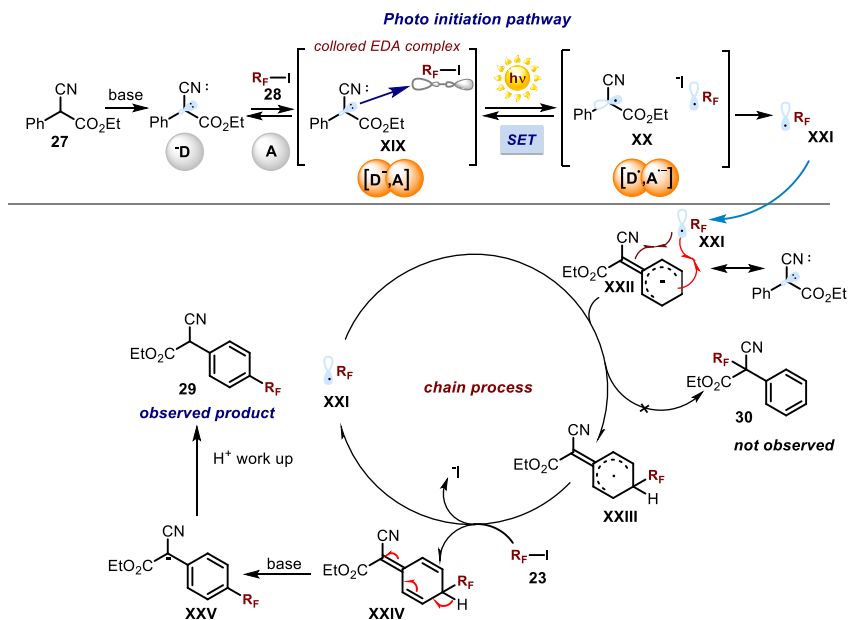
Due to the low ionization potentials, enolates can be considered as suitable donors for the formation of EDA complexes. Based on our group previous studies on EDA complex activation involving enamines²¹, and their electronic similarities with enolates, our group developed an enolate-based EDA complex activation strategy to access synthetically appealing photochemical transformation.²² Perfluoroalkyl iodides **28** were selected as reaction partners, because sparse literature precedents²³ qualify them as potential acceptors for facilitating associations of EDA complexes. This study focused on the reactivity of ethyl α -cyano phenylacetate **27** with perfluorohexyl iodide **28** under visible light irradiation (Scheme 3.6). In analogy to our group previous work involving enamines, the radical trap by the enolate **XXII** was anticipated to form the α -perfluoroalkylated product **30** with a new quaternary stereogenic center. The arene perfluoroalkylation product **29** was generated instead. Mechanistically, the reaction is initiated by photo-induced SET within the EDA complex **XIX**. A rapid carbon-iodine bond fragmentation renders the perfluoroalkyl radical **XXI** under mild conditions. **XXI** further reacts with the aromatic system of the deprotonated substrate **XXII**, through a classical homolytic aromatic substitution (HAS) pathway.²⁴ Upon C-C bond formation, the resulting cyclohexadienyl radical intermediate **XXIII** most likely reduces another molecule of perfluoroalkyl iodide **28** to propagate the reaction chain and release the product **29**.

²¹ E. Arceo, I. D. Jurberg, A. Álvarez-Fernández, P. Melchiorre, Photochemical Activity of a Key Donor-acceptor Complex Can Drive Stereoselective Catalytic α -alkylation of Aldehydes, *Nat. Chem.*, **2013**, *5*, 750.

²² M. Nappi, G. Bergonzini, P. Melchiorre, Metal-Free Photochemical Aromatic Perfluoroalkylation of α -Cyano Arylacetates, *Angew. Chem. Int. Ed.*, **2014**, *53*, 4921.

²³ D. Cantacuzene, C. Wakselman, R. Dorme, Condensation of Perfluoroalkyl Iodides with Unsaturated Nitrogen Compounds, *J. Chem. Soc., Perkin Trans. 1*, **1977**, 1365.

²⁴ D. H. R. Barton, W. Doering, Homolytic Aromatic Substitution, *International Series of Monographs on Organic Chemistry*, **1960**, vol. 4.



Scheme 3.6 Photochemical aromatic perfluoroalkylation of α -cyano arylacetates driven by the photochemical activity of EDA complexes. SET: single-electron transfer, R_F: perfluoroalkyl.

This method provides an easy access to valuable perfluoroalkylated aromatic compounds **29**. Nevertheless, the initial idea of this studies was to apply EDA complex strategy to initiate the enantioselective transformation of enolates and trapping the resulting perfluoroalkyl radical **XXI** at the α -position to the carbonyl group to forge a new stereogenic center. However, the α -perfluoroalkylation product **30** was never observed employing α -cyano arylacetates **27**. The overall reaction mechanism and the origin of the regioselectivity, with the exclusive aromatic perfluoroalkylation, was studied by DFT (density functional theory) calculations.²⁵ This work indicated that the highest occupied molecular orbital (HOMO) of **XXII** has a significant component in the phenyl ring, which favors the HAS manifold. The key factor precluding the radical attack at the α -carbonyl position is the large cost for the distortion of the anionic fragment **XXII** associated with this pathway.

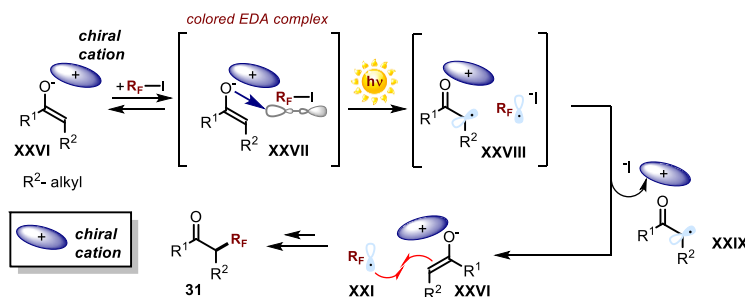
We hypothesized that the desired α -regioselectivity could be achieved employing an enolate possessing different electronic and structural features. This would allow the use

²⁵ V. M. Fernández-Álvarez, M. Nappi, P. Melchiorre, F. Maseras, Computational Study with DFT and Kinetic Models on the Mechanism of Photoinitiated Aromatic Perfluoroalkylations, *Org. Lett.*, **2015**, *17*, 2676.

of the EDA complex activation strategy to enable a photochemical enantioselective α -perfluoroalkylation of carbonyls.

3.3 Target of the Project

The aim of the research project described in this chapter is to investigate the photochemical reactivity of EDA complexes transiently generated from chiral enolates. The synthetic target is to develop efficient methods for the enantioselective catalytic production of perfluoroalkyl-containing stereogenicity, which would not be possible via classical ionic pathways. Based on our group's previous studies,¹⁶ we identified perfluoroalkyl iodides as suitable radical precursors for an enantioselective transformation initiated by the photoexcitation of chiral EDA complexes (Scheme 3.7). Specifically, we envisioned that photochemically generated perfluoroalkyl radicals **XXI** could be trapped by chiral enolates of type **XXVI** to achieve enantioselective electrophilic α -perfluoroalkylation of carbonyls, a functionalization which is largely underdeveloped. One effective strategy to provide a chiral environment for reactive enolates relies on phase transfer catalysis,²⁶ where chiral quaternary ammonium salts serve as chiral cations. We envisioned that this strategy may serve as a suitable platform for developing an enantioselective photochemical radical perfluoroalkylation of enolates (Scheme 3.7).

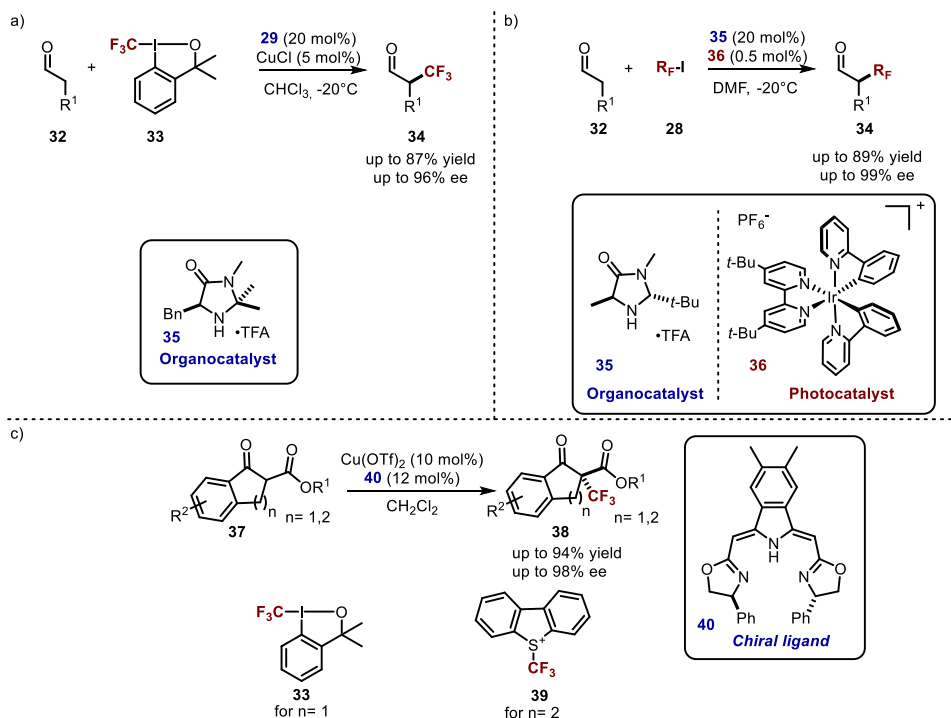


Scheme 3.7 Design plan for the enantioselective perfluoroalkylation of enolates promoted by the photoexcitation of chiral enolate-based EDA complexes. R_F: perfluoroalkyl.

There are only two existing highly enantioselective approaches for α -perfluoroalkylation of carbonyls. One of them relies on the reactivity of chiral enamines, which can selectively forge perfluoroalkyl stereogenicity reacting with Togni's reagent **33**, which is

²⁶ S. Shirakawa, K. Maruoka, Recent Developments in Asymmetric Phase-Transfer Reactions, *Angew. Chem. Int. Ed.*, **2013**, 52, 4312.

an electrophilic source of the trifluoromethyl group allowing ionic trifluoromethylation (Scheme 3.8a).²⁷ Chiral enamines can also intercept photochemically generated perfluoroalkyl radicals, as demonstrated by MacMillan (Scheme 3.8b).²⁸ In a distinct approach, Gade used a copper catalyst with a chiral pincer ligand **40** to perform a highly enantioselective trifluoromethylation of β -ketoesters **37**, using both Togni's **33** and Umemoto's reagents **39** (Scheme 3.8c).²⁹



Scheme 3.8 Enantioselective electrophilic perfluoroalkylation of carbonyls. a) Enantioselective anionic trifluoromethylation of aldehydes using chiral secondary amine catalyst **35**. b) Enantioselective radical trifluoromethylation of aldehydes; R_F : perfluoroalkyl. c) Enantioselective anionic trifluoromethylation of β -ketoesters employing chiral copper complex. Tf: trifluoromethyl sulfonate.

²⁷ A. E. Allen, D. W. C. MacMillan, The Productive Merger of Iodonium Salts and Organocatalysis: A Non-photolytic Approach to the Enantioselective α -Trifluoromethylation of Aldehydes, *J. Am. Chem. Soc.*, **2010**, *132*, 4986.

²⁸ D. A. Nagib, M. E. Scott, D. W. C. MacMillan, Enantioselective α -Trifluoromethylation of Aldehydes via Photoredox Organocatalysis, *J. Am. Chem. Soc.*, **2009**, *131*, 10875.

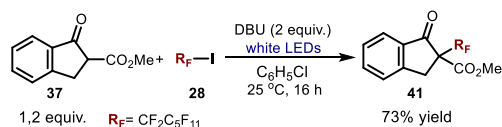
²⁹ Q.-H. Deng, H. Wadepohl, L. H. Gade, Highly Enantioselective Copper-Catalyzed Electrophilic Trifluoromethylation of β -Ketoesters, *J. Am. Chem. Soc.*, **2012**, *134*, 10769.

Gade's method features a broad scope of β -ketoesters, but is limited to the installation of trifluoromethyl group, which is an intrinsic limitation of the ionic pathway. The electrophilic reagents available as a source of trifluoromethyl group are expensive, and access to other perfluoroalkyl fragments is rather limited.

Other attempts to achieve enantioselective electrophilic perfluoroalkylation using chiral bases or phase transfer catalysts feature only low to moderate enantioselectivities (19–70% ee).³⁰

3.4 Results and Discussion

We choose a β -ketoester bearing an indanone scaffold **37** as a model substrate and tested the feasibility of charge transfer interactions between the resulting enolate **XXVI** and perfluorohexyl iodide **28** (Scheme 3.9). Enolate **XXVI** was formed upon deprotonation of the β -ketoester **37** with an excess of base (DBU, 1,8-diazabicyclo[5.4.0]undec-7-ene). Subsequent addition of perfluorohexyl iodide **28** to the colorless solution of **XXVI** resulted in the immediate appearance of a yellow color, which suggests the formation of a light-absorbing EDA complex **XXVII**. The confirmation was obtained from the absorption spectra of separate reaction components and their mixtures (Figure 3.1). The formation of a new absorption band indicated the generation of the charge transfer complex, and its absorption until 480 nm explains the appearance of the yellow coloration. Direct, visible light irradiation of this mixture resulted in the formation of the desired product **41** in 73% yield. Importantly, no reaction was observed in the dark (Scheme 3.9).



Scheme 3.9 Racemic perfluoroalkylation of **35** using 2 eq. of DBU-1,8-diazabicyclo[5.4.0]undec-7-ene.

³⁰ a) S. Noritake, N. Shibata, Y. Nomura, Y. Huang, A. Matsnev, S. Nakamura, T. Torua, D. Cahard, Enantioselective Electrophilic Trifluoromethylation of β -keto Esters with Umemoto Reagents Induced by Chiral Nonracemic Guanidines, *Org. Biomol. Chem.*, **2009**, 7, 3599, b) J.-A. Ma, D. Cahard, Strategies for Nucleophilic, Electrophilic, and Radical Trifluoromethylations, *J. Fluor. Chem.* **2007**, 128, 975.

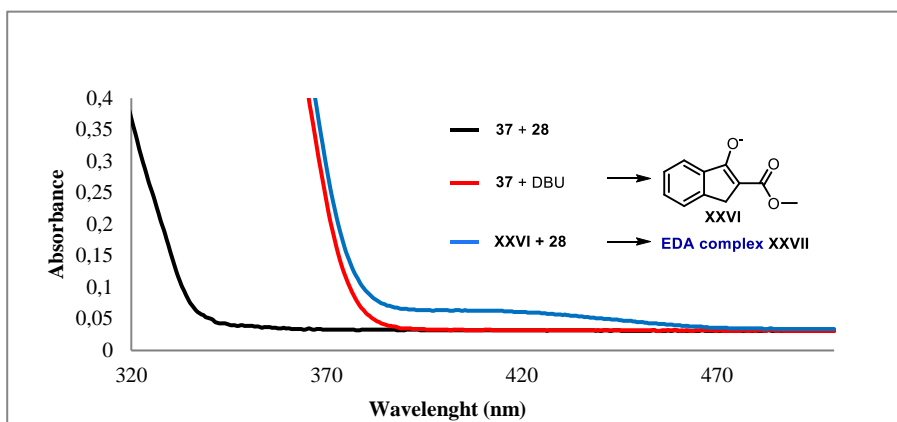


Figure 3.1 Optical absorption spectra recorded in chlorobenzene in a 1 cm path quartz cuvettes using a Shimadzu 2401PC UV-visible spectrophotometer, $[37] = 15 \mu\text{M}$, $[28] = 15 \mu\text{M}$, $[\text{DBU}] = 30 \mu\text{M}$. While the substrates **37** and **28** are achromatic, the resulting enolate **xxvi** (formed upon mixing **37** with 2 equiv. of DBU) showed a weak absorption at about 380 nm (red line), its combination with perfluorohexyl iodide **28** determines a strong bathochromic shift (blue line).

Next, we evaluated the formation of the EDA complex **XXVII** and its reactivity under phase transfer conditions. We observed that, upon addition of perfluorohexyl iodide **28** to the heterogeneous mixture of **37** and cesium carbonate in chlorobenzene, yellowish spots appeared on the surface of the white solid on the bottom of the Schlenk tube (the insoluble cesium carbonate), while the solution remained colorless (Figure 3.3b). This indicates the formation of the EDA complex **XXVII** between the enolate, which is formed after deprotonation of **37** by cesium carbonate and is adsorbed on its surface, with perfluorohexyl iodide **28**. Next, upon addition of the cinchona alkaloid-based phase transfer catalyst **42**, the colorless solution became yellow as well. This visual observation showed that the catalyst **42** can transfer the EDA complex **XXVII** from the surface of the insoluble inorganic base into the solution. Direct, visible light excitation of this mixture by a simple compact fluorescent light bulb (CFL) resulted in the formation of the product **41** in low yield and low enantioselectivity (Figure 3.3a). The absorption spectrum of the yellow mixture, measured upon filtration of Cs_2CO_3 , featured a charge transfer band which overlays with the absorption band observed when using DBU (Figure 3.2).

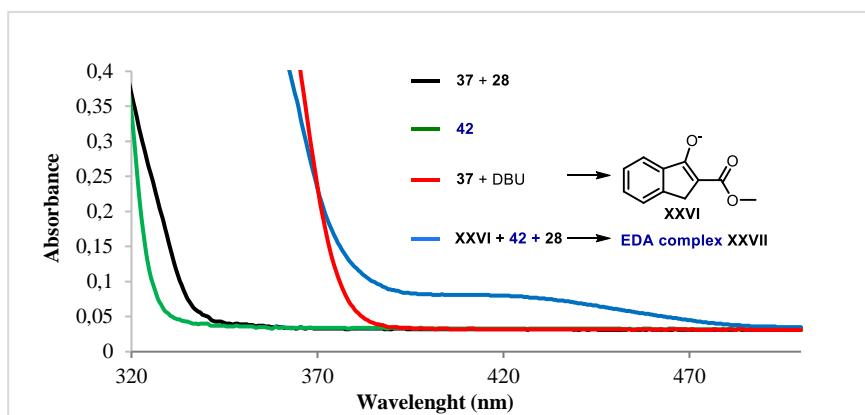


Figure 3.2 Optical absorption spectra recorded in chlorobenzene in a 1 cm path quartz cuvettes using a Shimadzu 2401PC UV-visible spectrophotometer, [37] = 15 μM , [28] = 15 μM , [DBU] = 30 μM , [42] = 3 μM . While the substrates **37** and **28** are achromatic, the resulting enolate **XXVI** showed a weak absorption at about 380 nm (red line), the optical absorption spectrum of the reaction mixture under PTC conditions (recorded upon filtration of Cs_2CO_3) determines a strong bathochromic shift (blue line), DBU-1,8-diazabicyclo[5.4.0]undec-7-ene.

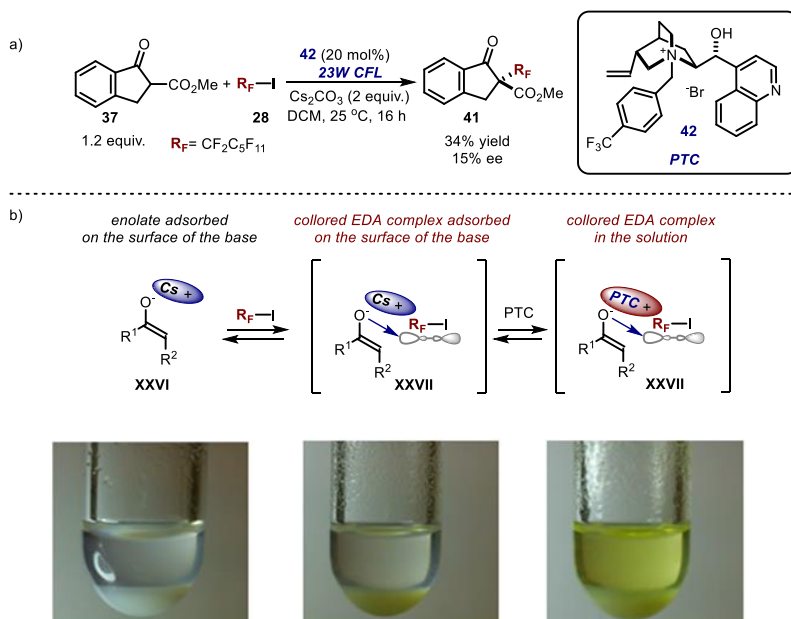
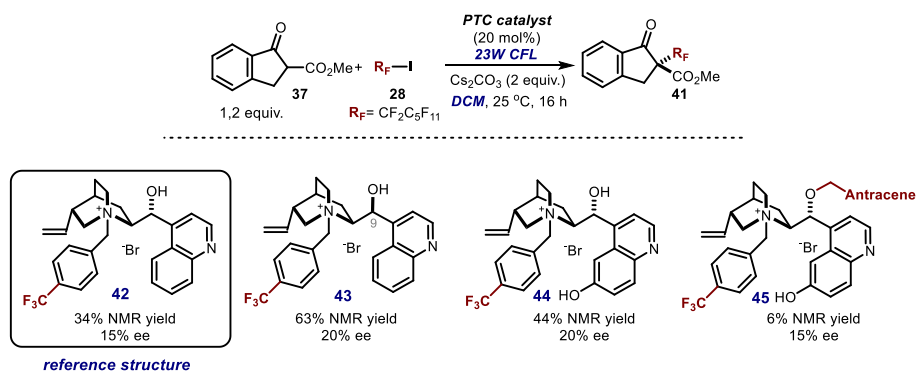


Figure 3.3 a) Enantioselective perfluoroalkylation in phase transfer conditions. b) Images showing the formation of the EDA complex (yellow) on the surface of Cs_2CO_3 (white solid) and its subsequent dispersion into the organic phase (chlorobenzene) upon addition of the PTC catalyst **42**.

3.4.1 Optimization Studies

Next, we focused on identifying a chiral PTC organocatalyst that could infer high stereocontrol on the photochemical perfluoroalkylation of **37**. The commercially available cinchonidine derivative catalyst **42** yielded the desired product with low efficiency³¹ and enantioselectivity. We decided to modify the structure of the cinchona-based catalysts to study their structure-activity and selectivity relationship.

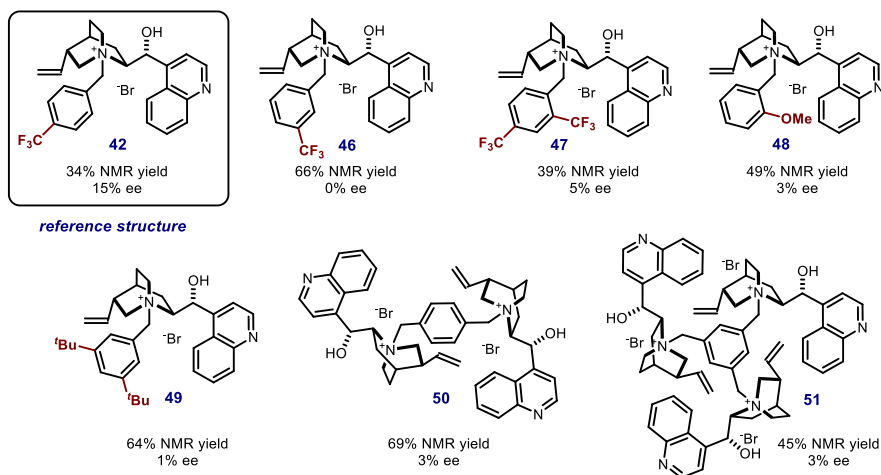
Various structural modifications of the core of the cinchona alkaloid scaffold did not significantly influence the enantio-induction (Scheme 3.10). Higher reaction yields were obtained employing epimer **43**, where the hydroxyl moiety at C9 position has been inverted, and cupreidine derivative **44**, but the stereocontrol remained low.



Scheme 3.10 Initial catalyst screening. CFL: compact fluorescent light.

Next, we evaluated some structural modifications of the benzyl substituent, used to quaternarize the nitrogen within the quinuclidine, while keeping the core of the cinchonidine structure unaltered (Scheme 3.11). Here, the situation became more interesting because every modification of the structure of the benzyl substituent led to an almost racemic product.

³¹ NMR yield: determined by ¹⁹F NMR analysis of crude reaction mixtures employing 1-fluoro-2-nitrobenzene as the internal standard.



Scheme 3.11 Optimization of the catalyst structure - modification of the benzyl substituent.

This seemingly unfortunate situation brought a new hypothesis for our optimization strategy. We questioned why this specific substitution pattern (4- CF_3PhCH_2 -) in the catalyst structure **42** had a unique ability in inferring stereocontrol and what kind of possible secondary interactions might be involved between the substrate and catalyst **42** that is not present with other catalysts **46-51**.

We hypothesized that the role of the benzyl substituent was not only to provide steric shielding and shaping the catalyst pocket, as proposed by Corey for a similar system.³² The specific substitution pattern might also provide a suitable handle for attractive weak interactions between the benzyl substituent and substrates. One possible interaction that can be considered is a π - π interaction between the benzyl substituent and the substrate. However, it is rather difficult to relate the observed selectivity trend with π - π stacking. Next, we considered the benzyl substituent as acting as a hydrogen bond donor. The importance of such an interaction has been observed and discussed in other transformations employing cinchona alkaloid-derived PTC catalyst³³ and binaphthyl-modified chiral PTC catalyst.³⁴ Since the ability of an aromatic C-H group to serve as hydrogen bond donor increases with the number and strength of electron-withdrawing

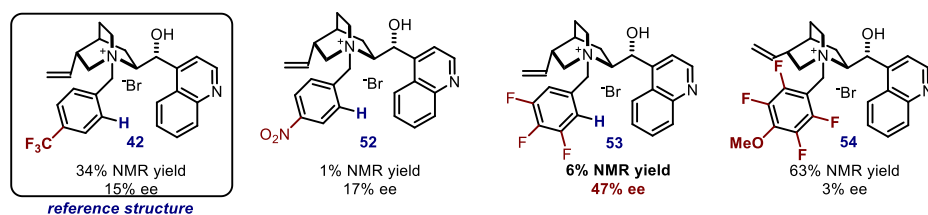
³² a) E. J. Corey, Feng Xu, Mark C. Noe, A Rational Approach to Catalytic Enantioselective Enolate Alkylation Using a Structurally Rigidified and Defined Chiral Quaternary Ammonium Salt under Phase Transfer Conditions, *J. Am. Chem. Soc.*, **1997**, 119, 12414, b) T. C. Cook, M. B. Andrus, D. H. Ess, Quantum Mechanical Transition-State Analysis Reveals the Precise Origin of Stereoselectivity in Chiral Quaternary Cinchonidinium Phase-Transfer Catalyzed Enolate Alkylation, *Org. Lett.* **2012**, 14, 23, 5836.

³³ E. F. Martins, J. Rodriguez Pliego, Unraveling the Mechanism of the Cinchoninium Ion Asymmetric Phase-Transfer-Catalyzed Alkylation Reaction Jr, *ACS Catal.*, **2013**, 3, 613.

³⁴ T. Kamachi, K. Yoshizawa, Enantioselective Alkylation by Binaphthyl Chiral Phase-Transfer Catalysts: A DFT-Based Conformational Analysis, *Org. Lett.*, **2014**, 16, 472.

groups on the aromatic ring,³⁵ the particular substitution pattern of the benzyl group (4-CF₃PhCH₂-) might be crucial to allow hydrogen-bond interactions between the benzyl substituent and the substrate (the ester group in **37** may act as a hydrogen bond acceptor). In consonance with this hypothesis, moving the CF₃ group from the para **42** to the meta position **46** led to a racemic product formation, which might be attributed to the change of the geometry of the benzyl group affecting the hydrogen-bond interaction. Other catalysts possessing electron-donating (**48**) or bulky substituents (**49**, **50**, **51**) on the benzyl group, which may decrease or blocks a hydrogen bond donor ability, led to product with a negligible levels of enantioselectivity.

To further evaluate this hypothesis, we introduced different small electron-withdrawing groups at strategic positions of the benzyl substituent so to leave hydrogen atoms in 2,6 positions available (Scheme 3.12). Employing catalyst **52**, only traces of product **41** were observed, but the enantiomeric excess remained similar to the product obtained with the so-far-best catalyst **42**. Gratifyingly, the introduction of three fluorine substituents in 3, 4, 5 positions of the benzyl group (catalyst **53**) brought about a significant improvement of the enantioselectivity of the model reaction (from 15% to 47% ee). In order to further test the viability of our hypothesis, we prepared catalyst **54** with fully substituted phenyl ring to suppress the proposed hydrogen bond interactions. In line with our mechanistic hypothesis, the product **41** was obtained in almost racemic form.

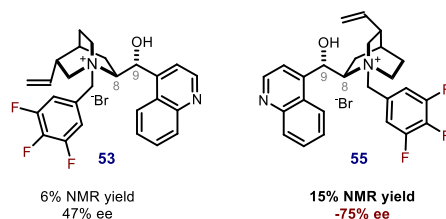


Scheme 3.12 Optimization of the catalyst structure - rational design of the benzyl substitution pattern.

After identification of the best substitution pattern of the benzyl group, we found that the diastereoisomeric catalyst **55**, derived from cinchonine, inferred a higher level of stereocontrol generating the opposite enantiomer of the product (Scheme 3.13). Cinchonine and cinchonidine (the same for quinine and quinidine) are diastereoisomers with different absolute configurations at C8 and C9 stereogenic centers (absolute configuration of cinchonine: 1S,3R,4S,8R,9S and cinchonidine: 1S,3R,4S,8S,9R). This

³⁵ A. Allerhand, P. R. Schleyer, A Survey of C-H Groups as Proton Donors in Hydrogen Bonding, *J. Am. Chem. Soc.*, **1963**, *85*, 1715.

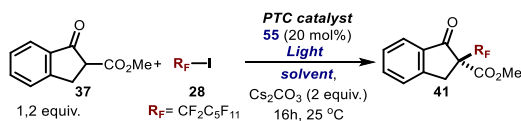
diastereomeric pairs of natural alkaloids are commonly referred as “pseudoenantiomers” because often behave like enantiomers when catalyzing and enantioselective reaction. When used as chiral catalysts, cinchonine often yields one enantiomer while cinchonidine yields the opposite enantiomer of a product.³⁶ However, the diastereomeric relation of those molecules means that they can impart a slightly different reactivity and selectivity when catalyzing the same reaction, a situation which (likely) was magnified in our system.



Scheme 3.13 Optimization of the catalyst structure: comparison of the pseudo-enantiomeric cinchonidine- and cinchonine-derived catalysts.

We observed that changing the solvent from dichloromethane to chlorobenzene provided the product **41** with higher enantiomeric excess, albeit with a very low yield (Table 3.1). Replacing the original source of irradiation (CFL: compact light fluoresce bulb) with a white light-emitting-diode (LED) strip containing 240 diodes (maximum emissions at about 450 nm and 560 nm, see experimental section) resulted in a small increase of the reaction yield. This might be attributed to the higher number of photons provided to the reaction mixture by 240 LED diodes as compared to single CFL bulb.

Table 3.1 Optimization studies: influence of the solvent and the light source.



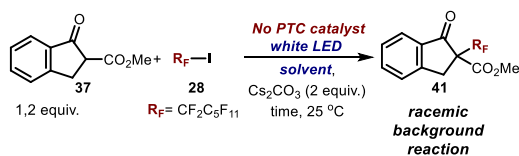
entry	solvent	light	yield [%]	ee [%]
1	DCM	CFL	15	75
2	C_6H_5Cl	CFL	4	86
3	C_6H_5Cl	White LED	12	86

Yields determined by ^{19}F NMR analysis of crude reaction mixtures employing 1-fluoro-2-nitrobenzene as the internal standard, DCM: dichloromethane, CFL: compact fluorescent light, LED: light emitting diode.

³⁶ E. M. O. Yeboah, S. O. Yeboah, G. S. Singh, Recent Applications of Cinchona Alkaloids and their Derivatives as Catalysts in Metal-free Asymmetric Synthesis, *Tetrahedron*, **2011** 67, 1725.

We were intrigued by the increase of the enantiomeric excess upon changing the solvent from DCM (dichloromethane) to chlorobenzene and tried to rationalize this effect. One possible explanation might be related to different conformation adopted by the chiral enolate in different solvents. In addition to that, the enantioselectivity change can be attributed to a different contribution of the racemic, background reaction in different solvents. We performed control experiments without the PTC catalyst in both solvents (Table 3.2). In DCM, we observed the formation of 7% of the product after 16 hours. This result suggests that the inorganic base (cesium carbonate) might be slightly soluble in DCM. This would result in a small quantity of cesium enolate in the organic phase that triggers a background, racemic transformation by forming an achiral enolate. On the other hand, no background reaction was observed in chlorobenzene, even after prolonged reaction time. The lack of background reaction in this case might explain the higher enantiomeric excess of the final product.

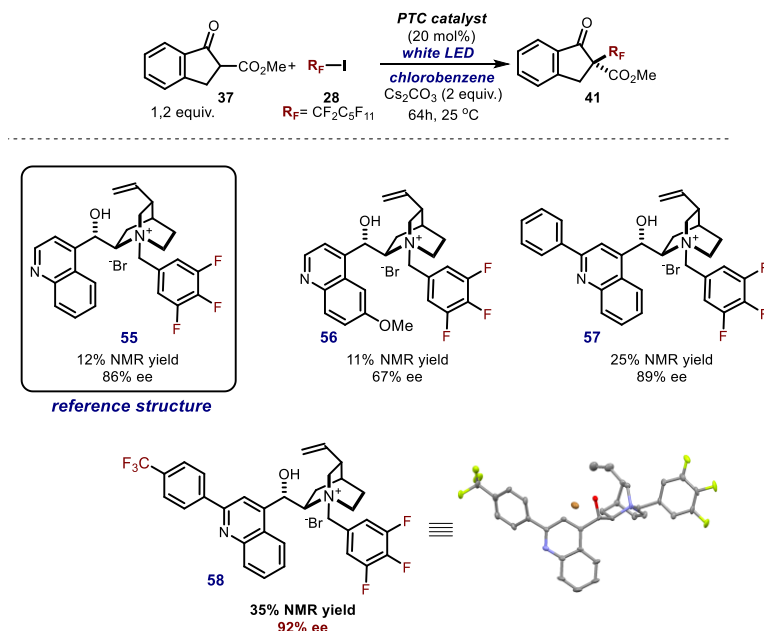
Table 3.2 Examination of the racemic, background reaction in different solvents.



entry	solvent	time [hours]	yield [%]
1	DCM	16	7
2	C ₆ H ₅ Cl	64	0

Yields determined by ¹⁹F NMR analysis of crude reaction mixtures employing 1-fluoro-2-nitrobenzene as the internal standard. DCM: dichloromethane

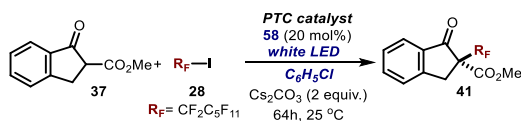
Next, we focused on further optimization of the catalyst structure (Scheme 3.14). We tested the effects of subtle changes of the catalyst scaffold with the hope to increase the reaction yield without affecting the stereocontrol. We first evaluated different substitution patterns of the quinoline ring. The quinidine-derived catalyst **56** gave the reaction product **41** in similar yield as catalyst **55**, but with lower enantiomeric excess. The introduction of the phenyl substituent at the C2 position of the quinoline ring (catalyst **57**) turns out to be beneficial for both yield and enantioselectivity. In order to avoid the presence of an electron-rich aromatic ring in the catalyst structure, which might be exposed to the attack of perfluoroalkyl radical, we introduced an electron-poor aromatic substituent (catalyst **58**). This catalyst gave access to product **41** with 35% yield and 92% ee.



Scheme 3.14 Optimization of the catalyst structure- functionalization of the quinoline ring. The X-ray structure of catalyst **54** is shown.

This result was a turning point of our optimization studies, since we could obtain for the first time the reaction product **41** with a reasonable yield and high enantioselectivity. However, careful analysis of the reaction mixture indicated that the starting materials were completely consumed regardless of the stoichiometry of the reaction (Table 3.3).

Table 3.3 Examination of the stoichiometry of the reaction.

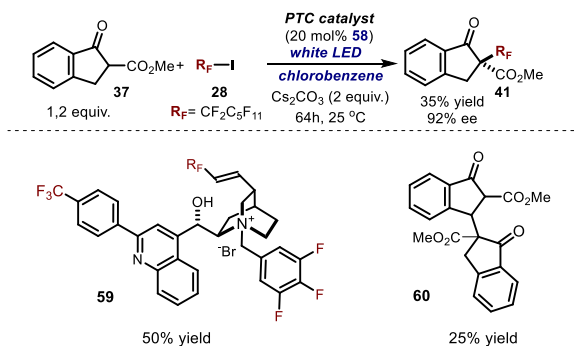


entry	37 [equiv.]	28 [equiv.]	conv.	yield [%]	ee [%]
1	1,2	1	Full	35	92
2	1	3	Full	41	92

Yields are of isolated products; conv.: conversion of the limiting reagent.

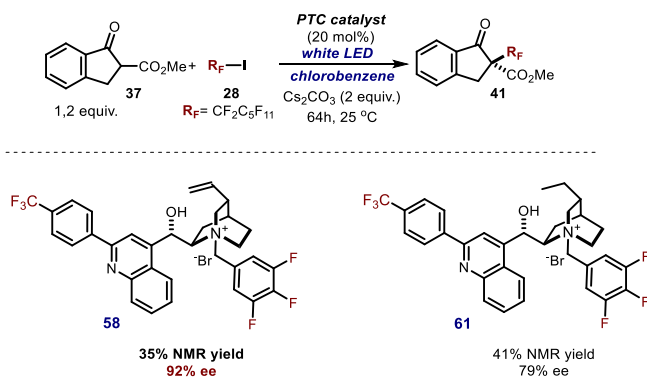
We wondered what kind of side reactions could hamper the productive pathway. Therefore, we aimed to isolate and identify the reaction byproducts. The two main

isolated side products **59** and **60**, shown in Scheme 3.15, indicated that both substrates can undergo undesired reactions.



Scheme 3.15 Identification of main byproducts.

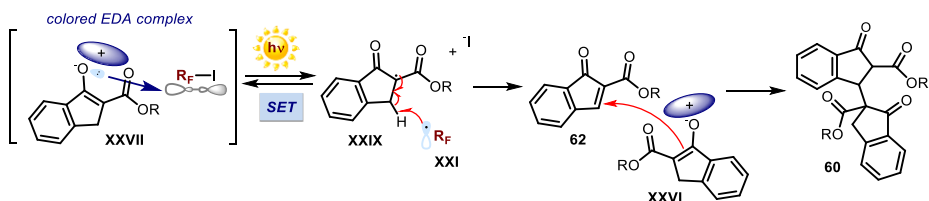
We found that the catalyst was partially converted into the perfluoroalkyl derivative **59**, most likely due to atom transfer radical addition of **28** onto the olefinic catalyst moiety followed by a net HI elimination. In order to avoid this side reaction, we prepared catalyst **61** and tested it in the same conditions (Scheme 3.16). The product **41** was obtained with slightly higher yield, but with lower stereo-control indicating that the double bond is beneficial for the enantioselectivity of this reaction. The activity of the in situ generated catalyst **59** was evaluated later (Scheme 3.18).



Scheme 3.16 Optimization of the catalyst structure- presence of the double bond.

The other identified byproduct (compound **60**) was a dimer of the ketoester substrate. We hypothesized that **60** was formed by the nucleophilic addition of enolate **XXVI** to the α,β -unsaturated β -ketoester **62**. Compound **62** could be formed by a hydrogen atom

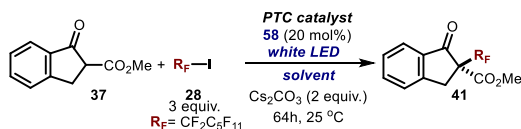
abstraction from the benzylic position of the α -keto radical **XXIX** by the perfluoroalkyl radical **XXI**, but the exact mechanism of the formation of **60** is unclear (Scheme 3.17).



Scheme 3.17 A possible mechanism of for the formation of byproduct **60**. SET: single-electron transfer.

Following this mechanistic hypothesis, we tried to channel the reactivity of perfluoroalkyl radicals exclusively toward the desired reaction manifold while avoiding the formation of **60**. Specifically, we hypothesized that decreasing the concentration of the free perfluoroalkyl radicals **XXI** in the organic phase might improve the selectivity toward the reaction with the enolate **XXVI**. We decided to introduce a perfluoroalkyl phase to our reaction mixture. The idea was that the radicals **XXI** could accumulate in the perfluorinated medium and be slowly extracted by the organic solvent. This could ensure a constantly low concentration of perfluoroalkyl radicals **XXI** in the organic phase, which could selectively react with the most nucleophilic species: the chiral enolate **XXVI**.

Table 3.4 Influence of the perfluorinated medium.

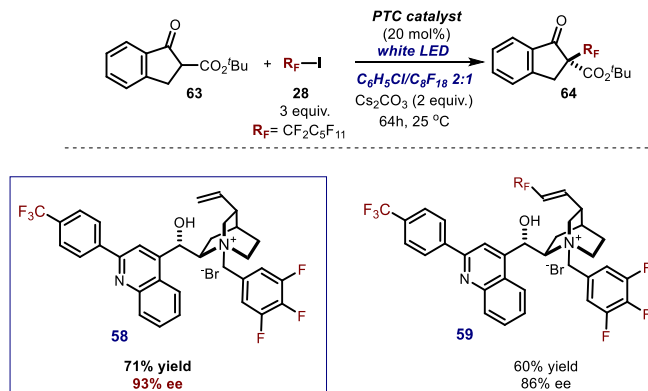


entry	solvent	yield [%]	ee [%]
1	C ₆ H ₅ Cl	41	92
2	C ₆ H ₅ Cl/C ₆ F ₁₄ 1:1	58	89
3	C ₆ H ₅ Cl/C ₆ F ₁₄ 2:1	49	92
4	C ₆ H ₅ Cl/C ₁₀ F ₂₂ 2:1	56	92
5	C₆H₅Cl/C₈F₁₈ 2:1	59	93

Yields are of isolated products.

We were pleased to see that the addition of a perfluoroalkyl phase (C₈F₁₈) positively influenced the reactivity, without affecting the stereoselectivity of the process (Table 3.4). By employing the three phase system (solid: Cs₂CO₃, organic: C₆H₅Cl and perfluorooctane: C₈F₁₈), we obtained the desired product **41** with 59% isolated yield and 93% ee.

The last improvement of the reaction conditions was achieved employing the *tert*-butyl ketoester **63**, which afforded the corresponding adduct **64** with 71% yield and 93% ee (Scheme 3.18).

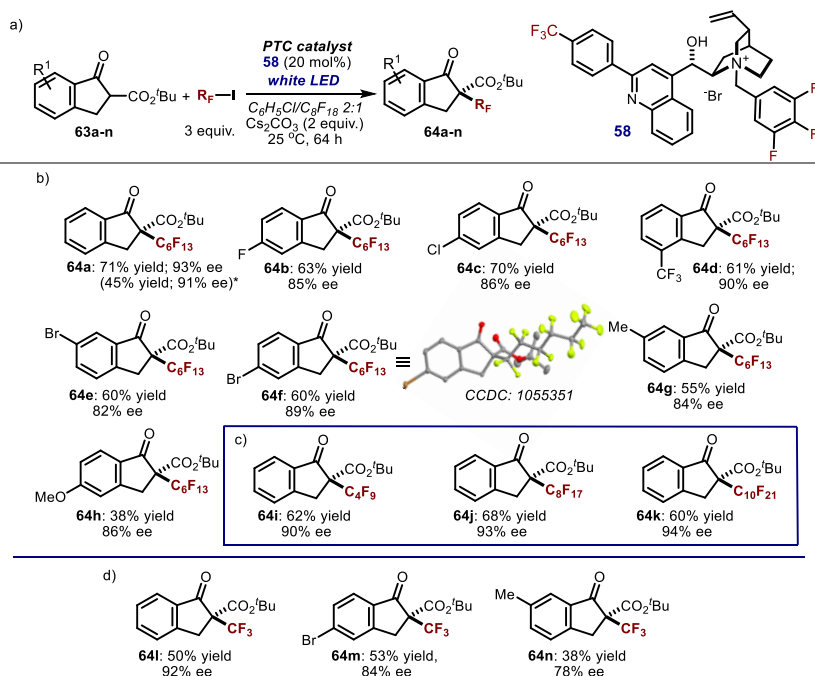


Scheme 3.18 Evaluation of the catalytic activity generated in situ catalyst **59**.

We also evaluated the catalytic activity of the in situ generated perfluoroalkylated catalyst **59**. The isolated **59** was tested it in the final catalytic conditions and provided only slightly inferior results than the progenitor **58**. In contrast, catalyst **61**, which does not bear the alkene moiety, provided markedly lower stereoselectivity, as previously shown in scheme 3.16. This experiment concluded our optimization studies indicating **58** as the catalyst of choice.

3.4.2 Reaction Scope

With the optimized conditions in hand, we evaluated the synthetic potential of the photo-organocatalytic enantioselective perfluoroalkylation strategy. We tested differently substituted indanone-derived β -ketoesters with perfluoroalkyl iodides employing catalyst **58** (Scheme 3.19). A variety of electron-withdrawing substituents were well tolerated, independently of their position on the aromatic ring, giving products **64b-64f** with good yields and high enantioselectivities. The presence of electron-donating substituents lowered the reactivity, however, the enantioselectivity remained high (**64g** and **64h**). Both shorter and longer perfluorinated chains could be also installed in **63** in a good yields and with a high stereocontrol (ee ranging from 90% to 94%, products **64i-64k**). Additionally, trifluoromethyl-containing quaternary stereocenters could be forged, with high fidelity, when reacting β -ketoesters with CF_3I (products **64l-64n**).



Scheme 3.19 Photochemical enantioselective perfluoroalkylation of indanone-derived β -ketoesters under PTC conditions. (a) Reactions performed using the optimized conditions. Yields are of isolated products. The X-ray structure of **64f** is shown. (b) The scope of the β -ketoesters using perfluorohexyl iodide **28**. (c) The scope of perfluoroalkylating agents. (d) Enantioselective trifluoromethylation.

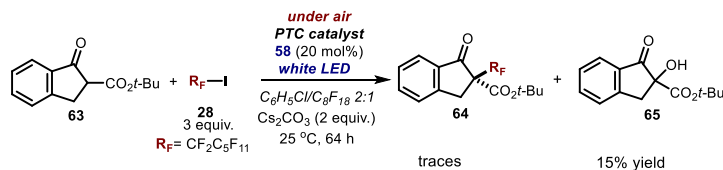
*1 mmol scale reaction.

The process is amenable to scale up to 1 mmol, (**64a**: 45% yield, 91% ee), but with a slightly reduced yield. This might be a consequence of a lower amount of photons per mole of reagents delivered to the reaction at higher scale employing the same light source. Crystals of compound **64f** were suitable for X-ray crystallographic analysis, which established the stereochemical outcome of the photo-organocatalytic process.

3.4.3 Reaction Mechanism

Control experiment revealed that the exclusion of light or of the PTC catalyst completely suppressed the process. Inhibition of the reactivity also occurred in the presence of TEMPO (1 equiv.), which is indicative of a radical mechanism. Under an aerobic atmosphere only traces of the desired product **64** were observed together with byproduct **65**, which was most likely formed in the reaction of enolate with oxygen³⁷ (Scheme 3.20).

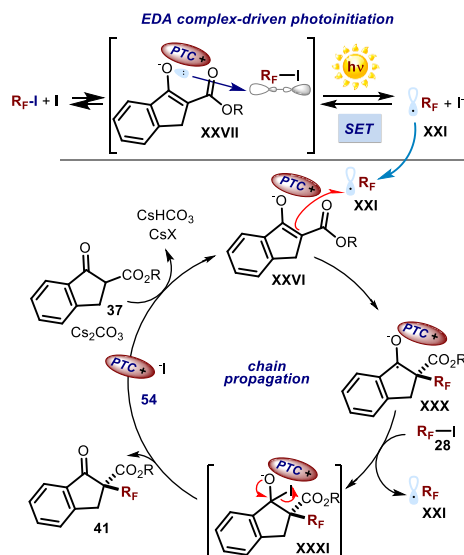
³⁷ H. H. Wasserman, B. H. Lipshutz, Reactions of Lithium Enolates with Molecular Oxygen α -Hydroxylation of Amides and Other Carboxylate Derivatives, *Tetrahedron Lett.*, **1975**, 21, 1731.



Scheme 3.20 Model reaction under an aerobic atmosphere.

Additionally, an experiment using a 300 W xenon lamp, equipped with a band-pass filter at 400 nm so to exclude high-energy photons, did not significantly alter the reaction efficiency (53% yield, 13% ee: conditions from Figure 3.2a). This result is mechanistically relevant since it excluded both possible homolytic cleavage of the carbon- iodine bond in **36** and direct photoexcitation of the enolate **XXVI** (which is unable to absorb at 400 nm, red line on Figure 3.1 and Figure 3.2) as pathways for the generation of perfluoroalkyl radical **XXI**. All of these observations, together with the optical absorption spectra presented in Figure 3.1 and Figure 3.3, are consonant with the EDA complex-driven photochemical initiation of the perfluoroalkylation process.

As for the mechanism of this asymmetric photochemical perfluoroalkylation, we propose a radical chain propagation pathway, as depicted on Scheme 3.21. The chain reaction is initiated by the photochemical activity of the EDA complex of type **XXVII**, formed upon aggregation of the chiral enolate **XXVI** with **28**. A visible-light-promoted electron transfer leads to the formation of the electron-deficient perfluoroalkyl radical **XXI** through the reductive cleavage of the carbon- iodine bond within **28**. The electrophilic perfluoroalkyl radical is next trapped by the chiral enolate **XXVI** in a stereocontrolled fashion. The resulting ketyl intermediate **XXX** would then abstract an iodine atom from **28**, thereby regenerating radical **XXI**. The adduct **XXXI** is not stable and collapses to release the product **41** and the PTC catalyst **58**. At the present level of investigation, an alternative electron transfer process, where the ketyl intermediate **XXX** reduces **28** to directly afford the final product **41**, cannot be excluded.



Scheme 3.21 Proposed mechanism: initiation, triggered by the photo-activity of the EDA complex **XXVII**, and radical chain propagation.

The chain mechanism is supported by a quantum yield (Φ) of 1.2 ($\lambda = 400$ nm), which was determined for the model reaction (β -ketoester **37**) promoted by DBU (2 equiv.). DBU is a competent promoter of the photochemical perfluoroalkylation, providing the corresponding product **41** in 73% yield (

Scheme 3.9 Racemic perfluoroalkylation of **35** using 2 eq. of DBU-1,8-diazabicyclo[5.4.0]undec-7-ene.

3.9). Our attempts to determine the quantum yield under PTC conditions were frustrated by the heterogeneity of the reaction mixture, which precluded a homogeneous illumination, a crucial requirement for a reliable quantum yield determination. Quantum yield is an indicator of how efficient a particular photochemical process is and indicates a number of defined events occurring per photon absorbed by the system.

$$(\Phi) = \frac{\text{amount of product formed}}{\text{amount of photon absorbed}}$$

The obtained number of quantum yield [$\Phi = 1.2$] indicates that more than one molecule of the product is generated upon absorption of one photon. It is important to point out that, upon excitation, organic molecules can release the excitation energy in many different non-productive processes, such as phosphorescence, internal conversion, or back electron transfer, that can only decrease the observed quantum yield. The small

quantum yield (Φ) = 1,2 does not provide a definitive conclusion; it is however consonant with a chain mechanism being operative.

3.5 Conclusions and Remarks

In conclusion, we have developed a photochemical enantioselective perfluoroalkylation of cyclic β -ketoesters. The photoorganocatalytic process occurs at ambient temperature under visible light illumination. This study establishes the ability of chiral enolates, generated under PTC conditions, to be suitable donors in photoactive EDA complex while providing effective asymmetric induction in the trapping of the resulting radical species. Preliminary mechanistic studies indicated that the reaction is promoted by a visible light excitation of the key EDA complex and a chain propagation mechanism is operative.

3.6 Experimental Section

The NMR spectra were recorded at 400 MHz and 500 MHz for ^1H and 100 or 125 MHz for ^{13}C . The chemical shift (δ) for ^1H and ^{13}C are given in ppm relative to residual signals of the solvents (CHCl_3 @ 7.26 ppm ^1H NMR and 77.16 ppm ^{13}C NMR). Coupling constants are given in Hertz. The following abbreviations are used to indicate the multiplicity: s, singlet; d, doublet; q, quartet; m, multiplet; bs, broad signal.

High resolution mass spectra (HRMS) were obtained from the ICIQ HRMS unit on Waters GCT gas chromatograph coupled time-of-flight mass spectrometer (GC/MS-TOF) with electrospray ionization (ESI). X-ray data were obtained from the ICIQ X-Ray unit using a Bruker-Nonius diffractometer equipped with an APPEX 2 4K CCD area detector. Optical rotations are reported as follows: $[\alpha]_D^{25}$ (c in g per 100 mL, solvent).

UV-vis measurements were carried out on a Shimadzu UV-2401PC spectrophotometer equipped with photomultiplier detector, double beam optics and D₂ and W light sources. Cut off and band-pass photochemical experiments have been performed using a 300 W xenon lamp (*Asashi Spectra Co., Ltd.*) to irradiate the reaction mixture.

General Procedures.

All reactions were set up under an argon atmosphere in oven-dried glassware using standard Schlenk techniques, unless otherwise stated. Synthesis grade solvents were used as purchased and the reaction mixtures were degassed by three cycles of freeze-pump-thaw. Chromatographic purification of products was accomplished using force-flow chromatography (FC) on silica gel (35-70 mesh). For thin layer chromatography (TLC) analysis throughout this work, Merck precoated TLC plates (silica gel 60 GF₂₅₄, 0.25 mm) were employed, using UV light as the visualizing agent and basic aqueous potassium permanganate (KMnO₄) stain solutions, and heat as developing agents. Organic solutions were concentrated under reduced pressure on a Büchi rotatory evaporator.

The light source used for illuminating the reaction vessel consisted of white LED light strips (19.2 W/m, 240 LEDs per meter) purchased from Farnell (<http://www.farnell.com/>). A picture of the utilized white LED light strip is portrayed on the Figure 3.4.



Figure 3.4 White LED strip used to irradiate the reaction

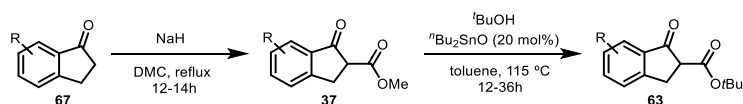
Determination of Enantiomeric Purity: HPLC analysis on chiral stationary phase was performed on an Agilent 1200-series instrumentation using a Daicel Chiralpak AD-H column and hexane, *i*Pr-OH and/or DCM as the eluents. GC analysis was performed using a chiral Alphadex column. HPLC and GC traces were compared to racemic samples prepared using a superstoichiometric amount of DBU (1,8-diazabicyclo[5.4.0]undec-7-ene, 2 equiv.) as the promoter of the photochemical perfluoroalkylation.

Materials. Commercial grade reagents and solvents were purchased from Sigma-Aldrich, Fluka, Alfa Aesar, Fluorochem, SynQuest and used as received, without further purifications.

The ¹H NMR, ¹⁹F NMR, ¹³C NMR spectra and HPLC traces are available in literature and are not reported in the present dissertation.¹

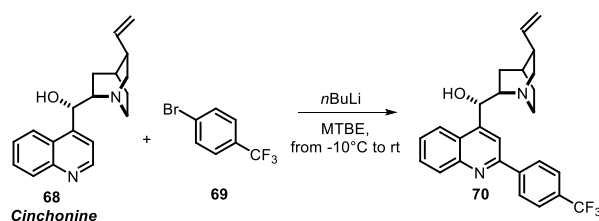
Representative Procedure for the Synthesis of the Cyclic *tert*-Butyl-Ketoesters **63**.

NaH (5.2 mmol, 210 mg, 2.2 eq., 60% dispersion in mineral oil) and anhydrous dimethyl carbonate (**DMC**, 10 mL) were added sequentially to a dry three-necked flask equipped with a septum, condenser, argon inlet, and a large stirring egg. The indan-1-one derivative **67** (2.37 mmol, 1 eq), partially solubilized in anhydrous dimethyl carbonate (10 mL), was added via a syringe pump over the course of 30 minutes. The heterogeneous mixture was brought to reflux (80 °C), and heated overnight at this temperature. The reaction was allowed to cool and cautiously quenched at 0°C under an argon atmosphere with H₂O (10 mL). The mixture was transferred to a separative funnel with EtOAc while adding additional 50 mL of 1M HCl. The reaction was extracted with EtOAc (50 mL x 3) and the combined organic layers washed with a saturated brine solution before being dried over solid anhydrous magnesium sulfate and concentrated. The crude material was then dissolved in toluene (20 mL), and *t*BuOH (30 eq, 71.1 mmol, 6.5 mL), and dibutyl-tin oxide (0.2 eq, 118 mg) was added. The flask was fitted with an air condenser and the heterogeneous mixture was heated at 115°C until the starting methyl ester **37** was fully consumed (12-36h), as judged by TLC. The mixture was allowed to cool to room temperature and concentrated under reduced pressure and the residue was purified by column chromatography on silica gel (eluent Et₂O/Hexane 1:9 to 2:8) to yield the pure keto-ester **63**.



Scheme 3.22 Synthesis of cyclic *tert*-butyl-ketoesters **63**

Synthesis of the PTC Catalyst **58**.



Scheme 3.23 Synthesis of cinchonine derivative **70**

Based on the procedure reported by Hintermann³⁸. Cinchonine (1.5 g, 5.1 mmol) was suspended in 25 ml of dry MTBE (dried over molecular sieves) and cooled to -10°C (ice/EtOH bath) under an argon atmosphere. The organo-lithium compound was prepared in a separate flask by adding *n*BuLi (5.1 mL, 12.75 mmol, 2.5 M) to a 5 mL MTBE solution of 4-bromobenzotrifluoride **69** (1.785 mL, 2.869 g, 12.75 mmol). The organo-lithium compound was added at once to the vigorously stirred MTBE solution of cinchonine and stirred at -10°C for 20 min. Then the mixture was warmed to ambient temperature and stirred over 2 h. The reaction was quenched by dropwise addition of HOAc (2.5 mL) with rapid stirring and cooling, followed by the addition of water (30 mL) and EtOAc (30 mL).

Solid iodine (1.25 g) was added in several portions and the mixture shaken vigorously after each addition until all the solids had dissolved. A solution of sodium metabisulfite (Na₂S₂O₅; 0.500 g) in water (10 mL) was added to quench the excess of iodine. The mixture was made basic with the addition of aqueous ammonia (concentrated, 28%) and shaken thoroughly. The aqueous phase was extracted with AcOEt twice and the collected organic phases were washed with brine and dried over sodium sulfate. After evaporation of the solvent, the crude product was purified by column chromatography on silica gel (30% MeOH-EtOAc) to give the reaction product **70** as an orange solid in 51% yield (1.129 g, 2.57 mmol). $[\alpha]_D^{25} = +70.0$ (c= 0.55 DMSO).

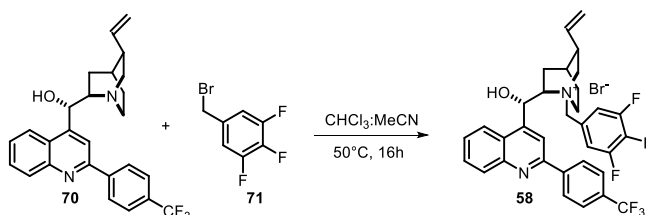
¹H NMR (400 MHz, CDCl₃) δ 8.28 (d, *J* = 8.0 Hz, 2H), 8.24 – 8.17 (m, 1H), 8.08 (s, 1H), 8.01 (d, *J* = 7.9 Hz, 1H), 7.80 – 7.75 (m, 2H), 7.75 – 7.70 (m, 1H), 7.54 (ddd, *J* = 8.3, 6.9, 1.3 Hz, 1H), 5.99 (ddd, *J* = 17.1, 10.5, 7.4 Hz, 1H), 5.72 (d, *J* = 4.8 Hz, 1H), 5.07 – 4.97 (m, 2H), 3.26 – 3.12 (m, 2H), 2.92 (dd, *J* = 13.9, 9.7 Hz, 2H), 2.84 – 2.71 (m, 1H), 2.24 (q, *J* = 8.4 Hz, 1H), 2.07 – 1.96 (m, 1H), 1.82 – 1.75 (m, 1H), 1.58 – 1.48 (m, 2H), 1.35 – 1.27 (m, 1H).

¹⁹F NMR decoupled ¹H (376 MHz, CDCl₃+ TFA) δ -62.68 (s, 3F).

¹³C NMR (101 MHz, chloroform-*d*) δ 162.2 (q, *J* = 37.2 Hz, C=O, TFA), 154.5, 149.8, 144.9, 139.8, 135.7, 132.3 (q, *J* = 32.7 Hz), 131.2, 128.6, 128.4, 128.0, 126.0 (q, *J* = 3.7 Hz), 123.9 (q, *J* = 272.5 Hz, CF₃), 123.5, 122.2, 118.1, 117.2, 116.20 (q, *J* = 290.7 Hz, CF₃, TFA), 66.9, 60.7, 49.5, 48.7, 37.3, 27.3, 23.2, 18.0.

HRMS calculated for C₂₆H₂₆F₃N₂O (M+H): 439.1992, found: 439.1996.

³⁸ L. Hintermann, M. Schmitz, U. Englert, Nucleophilic Addition of Organometallic Reagents to Cinchona Alkaloids: Simple Access to Diverse Architectures, *Angew. Chem. Int. Ed.* **2007**, *46*, 5164.

Scheme 3.24 Synthesis of catalyst **58**

5-(Bromomethyl)-1,2,3-trifluorobenzene **71** (0,27 mL, 457 mg, 2,03 mmol) was added to a MeCN-CHCl₃ (1:1, 34 mL) suspension of cinchonine derivative **70** (742 mg, 1,69 mmol). The reaction mixture was stirred for 16 h at 50 °C under an argon atmosphere. After complete consumption of **70** (inferred by TLC analysis) the solvent was evaporated under reduced pressure. DCM was added to the resulting orange solid followed by a small amount of MeOH in order to completely dissolve the crude product. Next Et₂O was added and the mixture was slowly concentrated under reduced pressure. When precipitation of a solid began, more Et₂O was added and the mixture was concentrated again. This procedure was repeated twice in order to remove traces of methanol and dichloromethane and the mixture was placed in a freezer. The precipitated yellow solid was filtrated and washed with cold Et₂O to give the product **58** in 70% yield (789 mg, 1.19 mmol). [α]_D²⁵ = +131.8 (c= 0.52 DMSO).

¹H NMR (400 MHz, DMSO-*d*₆) δ 8.52 (d, *J* = 8.2 Hz, 2H), 8.47 – 8.38 (m, 2H), 8.22 (d, *J* = 8.3 Hz, 1H), 8.04 – 7.87 (m, 5H), 7.84 – 7.75 (m, 1H), 6.92 (d, *J* = 3.6 Hz, 1H), 6.55 (s, 1H), 6.10 (ddd, *J* = 17.4, 10.0, 7.2 Hz, 1H), 5.31 – 5.17 (m, 3H), 4.98 (d, *J* = 12.4 Hz, 1H), 4.29 – 4.18 (m, 1H), 4.07 – 3.86 (m, 2H), 3.59 (t, *J* = 11.4 Hz, 1H), 3.14 – 2.99 (m, 1H), 2.62 (q, *J* = 8.3 Hz, 1H), 2.42 (t, *J* = 11.8 Hz, 1H), 1.87 (s, 1H), 1.82 – 1.71 (m, 2H), 1.22 – 1.08 (m, 1H).

¹⁹F NMR decoupled ¹H (376 MHz, DMSO-*d*₆) δ -61.18 (s, 3F), -134.68 (d, *J* = 21.7 Hz, 2F), -159.61 (t, *J* = 21.7 Hz, 1F).

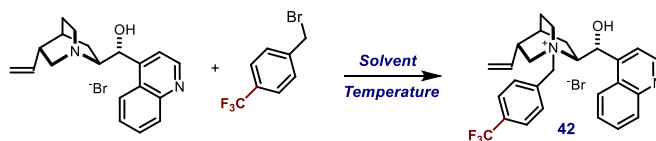
¹³C NMR (101 MHz, DMSO-*d*₆) δ 154.6, 152.0 – 151.6 (m), 149.5 – 149.2 (m), 148.1, 147.1, 142.9, 139.3, 137.7, 130.7, 130.2 (q, *J* = 31.8 Hz), 128.56, 128.2, 126.4 (q, *J* = 3.9 Hz), 125.8 – 125.1 (m), 124.3 (q, *J* = 272.1 Hz), 124.3, 124.3, 119.4, 119.4 (d, *J* = 21.7 Hz), 119.3, 117.7, 117.6, 68.2, 65.7, 61.1, 56.4, 54.6, 37.6, 26.8, 23.5, 21.0

HRMS calculated for C₃₃H₂₉F₆N₂O (M^{*}): 583.2179, found: 583.2176

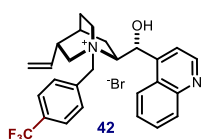
The relative and absolute configuration for **58** was unambiguously inferred by anomalous dispersion X-ray crystallographic analysis, see X-ray Crystallographic Data section.

General Procedure A for Synthesis of other PTC Catalysts Employed in the Optimization Studies 42-57 and 61.

To a flame-dried flask equipped with a magnetic stirring bar and a reflux condenser was added cinchona alkaloid, solvent, and desired benzyl bromide derivative. The mixture was heated to the indicated temperature until judged to be complete by TLC-analysis and then cooled to room temperature. The crude product was purified by crystallization or flash column chromatography.



Scheme 3.25 Synthesis of PTC catalysts Employed in the Optimization Studies

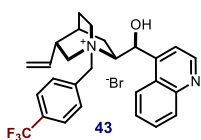


Prepared according to general procedure A using cinchonidine (1.00 g, 3.4 mmol) and 1-(bromomethyl)-4-(trifluoromethyl)benzene (3.4 mmol, 812 mg). The mixture was stirred in THF (50 mL) at reflux until complete consumption of cinchonidine. The mixture was cooled to room temperature and poured onto Et₂O with stirring. The resulting suspension was stirred for 1 h and the precipitated solids were isolated by filtration and recrystallized from MeOH/Et₂O to afford the product **42** (1.404 g, 77% yield).

¹H NMR (400 MHz, CDCl₃) δ 8.79 (d, *J* = 4.5 Hz, 1H), 8.20 – 8.12 (m, 1H), 7.88 (d, *J* = 7.8 Hz, 2H), 7.78 (d, *J* = 4.5 Hz, 1H), 7.59 – 7.51 (m, 1H), 7.41 (d, *J* = 7.9 Hz, 2H), 7.06 – 6.98 (m, 2H), 6.57 – 6.44 (m, 2H), 6.35 (d, *J* = 11.9 Hz, 1H), 5.56 (d, *J* = 11.8 Hz, 1H), 5.45 – 5.27 (m, 2H), 4.95 – 4.87 (m, 1H), 4.71 – 4.58 (m, 1H), 4.28 – 4.17 (m, 1H), 4.05 – 3.94 (m, 1H), 3.08 – 2.88 (m, 2H), 2.54 – 2.43 (m, 1H), 2.07 (dt, *J* = 3.9, 2.0 Hz, 0H), 1.99 (s, 1H), 1.92 (t, *J* = 3.6 Hz, 1H), 1.89 – 1.78 (m, 1H), 1.60 (d, *J* = 7.4 Hz, 1H), 1.07 – 0.93 (m, 1H).

¹⁹F NMR (376 MHz, CDCl₃) δ -63.20 (s, 3F).

¹³C NMR (101 MHz, CDCl₃) δ 149.3, 146.9, 144.0, 135.6, 134.5, 132.3, 132.0, 131.06, 129.6, 128.3, 127.2, 125.4, 125.3, 125.3, 124.7, 123.3, 122.6, 122.0, 119.6, 118.0, 67.2, 65.2, 60.9, 60.0, 50.5, 37.7, 26.2, 25.1, 22.5.

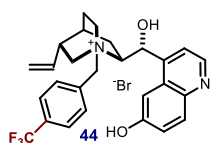


Prepared according to general procedure A using corresponding cinchonidine derivative (0.187 mmol, 55 mg) and 1-(bromomethyl)-4-(trifluoromethyl)benzene (0.206 mmol, 49 mg). The mixture was stirred in THF (2.5 mL) at reflux until complete consumption of

cinchonidine. The mixture was cooled to room temperature and poured onto Et₂O with stirring. The resulting suspension was stirred for 1 h and the precipitated solids were isolated by filtration and recrystallized from DCM/hexane to afford **43** as a yellow solid (48 mg, 48% yield).

¹H NMR (500 MHz, CDCl₃) δ 8.76 (d, J = 4.4 Hz, 1H), 8.56 (d, J = 8.4 Hz, 1H), 8.07 (d, J = 8.4 Hz, 1H), 7.95 (d, J = 7.9 Hz, 2H), 7.67 (t, J = 7.6 Hz, 1H), 7.62 (m, 1H), 7.58 – 7.50 (m, 3H), 6.72 (s, 1H), 6.49 – 6.40 (m, 1H), 5.70 (m, 1H), 5.65 – 5.54 (m, 2H), 5.16 – 5.06 (m, 2H), 4.95 (t, J = 12.5 Hz, 1H), 4.61 – 4.51 (m, 1H), 3.92 – 3.83 (m, 1H), 3.83 – 3.74 (m, 1H), 3.31 (t, J = 10.2 Hz, 1H), 2.75 – 2.65 (m, 1H), 2.18 – 2.06 (m, 1H), 2.03 – 1.86 (m, 2H), 1.83 (s, 1H), 1.62 (d, J = 12.6 Hz, 1H), 1.05 (d, J = 14.5 Hz, 1H).

¹³C NMR (75 MHz, CDCl₃) δ 150.2, 148.6, 145.5, 135.1, 134.3, 132.6, 132.2, 131.8, 130.5, 129.7, 127.9, 126.1, 125.9, 125.8, 125.3, 123.7, 120.0, 118.6, 118.6, 67.7, 65.04, 60.7, 50.8, 37.4, 26.6, 25.0, 25.0.



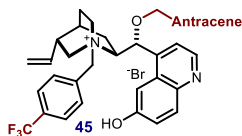
Prepared according to the procedure reported in literature.³⁹

¹H NMR (400 MHz, DMSO-*d*₆) δ 10.17 (s, 1H), 8.74 (d, J = 4.5 Hz, 1H), 8.04 – 7.91 (m, 5H), 7.69 (d, J = 4.5 Hz, 1H), 7.48 (d, J = 2.5 Hz, 1H), 7.38 (dd, J = 9.1, 2.4 Hz, 1H), 6.59 (d, J = 4.1 Hz, 1H), 6.39 (d, J = 4.2 Hz, 1H), 5.73 (ddd, J = 17.2, 10.5, 6.5 Hz, 1H), 5.37 (d, J = 12.2 Hz, 1H), 5.19 (dt, J = 17.3, 1.3 Hz, 1H), 5.08 – 4.96 (m, 2H), 4.33 – 4.19 (m, 1H), 3.93 (t, J = 8.8 Hz, 1H), 3.84 – 3.73 (m, 1H), 3.30 – 3.17 (m, 1H), 2.74 – 2.62 (m, 1H), 2.26 – 2.06 (m, 2H), 2.01 (d, J = 3.7 Hz, 1H), 1.87 – 1.74 (m, 1H), 1.44 – 1.32 (m, 1H).

¹⁹F NMR (376 MHz, DMSO-*d*₆) δ -61.38 (s, 3F).

¹³C NMR (101 MHz, DMSO) δ 156.4, 147.1, 143.5, 143.4, 138.4, 135.2, 133.1, 132.0, 131.3, 131.0, 130.7, 130.7, 130.4, 126.2, 126.2, 126.1, 122.2, 120.4, 117.0, 104.7, 68.6, 64.4, 62.5, 59.5, 51.1, 37.4, 26.4, 24.6, 20.9.

Spectral data match with the ones reported in literature.³⁹



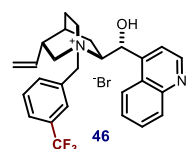
Prepared according to general procedure A using corresponding cinchonidine derivative (0.3 mmol, 150 mg) and 1-(bromomethyl)-4-(trifluoromethyl)benzene (0.36 mmol, 86 mg). The mixture was stirred in toluene (5 mL) at 80°C until

³⁹ K. C. Nicolaou, G. Liu, K. Beabout, M. D. McCurry, Y. Shamoo, Asymmetric Alkylation of Anthrones, Enantioselective Total Synthesis of (-) and (+)-Viridicatumtoxins B and Analogues Thereof: Absolute Configuration and Potent Antibacterial Agents, *J. Am. Chem. Soc.*, **2017**, *139*, 3736.

complete consumption of cinchonidine derivative. Product was crystallized from toluene/MTBE to afford **45** as a yellow solid (29 mg, 13% yield).

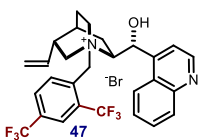
$^1\text{H NMR}$ (400 MHz, CDCl_3) δ 9.12 (s, 1H), 9.00 (d, $J = 4.4$ Hz, 1H), 8.54 (s, 1H), 8.21 – 8.07 (m, 5H), 7.93 (d, $J = 2.5$ Hz, 1H), 7.88 (d, $J = 4.4$ Hz, 1H), 7.60 (m, 2H), 7.56 – 7.47 (m, 3H), 7.43 – 7.36 (m, 2H), 6.64 (d, $J = 7.9$ Hz, 2H), 6.07 (d, $J = 2.7$ Hz, 1H), 6.00 – 5.85 (m, 2H), 5.63 (d, $J = 13.4$ Hz, 1H), 5.46 (d, $J = 11.5$ Hz, 1H), 5.36 – 5.27 (m, 2H), 5.12 (dt, $J = 17.2, 1.0$ Hz, 1H), 4.92 (t, $J = 11.5$ Hz, 1H), 4.34 (t, $J = 9.9$ Hz, 1H), 3.90 (ddd, $J = 11.9, 8.6, 2.7$ Hz, 1H), 2.97 (d, $J = 11.5$ Hz, 1H), 2.80 – 2.70 (m, 1H), 2.48 (m, 2H), 2.34 – 2.23 (m, 1H), 1.99 (t, 1H), 1.97 (t, $J = 4.8$ Hz, 1H), 1.95 – 1.80 (m, 1H).

$^{19}\text{F NMR}$ (376 MHz, CDCl_3) δ -63.16 (s, 3F).



Prepared according to general procedure A using cinchonidine (0.34 mmol, 100 mg) and 1-(bromomethyl)-3-(trifluoromethyl)benzene (0.37 mmol, 89 mg). The mixture was stirred in THF (5 mL) at reflux until complete consumption of cinchonidine. The mixture was cooled to room temperature and poured onto Et_2O with stirring. The resulting suspension was stirred for 1 h and the precipitated solids were isolated by filtration and recrystallized from $\text{MeOH}/\text{Et}_2\text{O}$ to afford **46** as a white solid (122 mg, 80% yield).

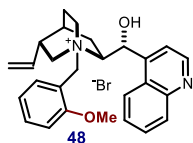
$^1\text{H NMR}$ (300 MHz, CD_3OD) δ 8.95 (d, $J = 4.6$ Hz, 1H), 8.30 (d, $J = 8.1$ Hz, 1H), 8.18 – 8.08 (m, 2H), 8.04 (d, $J = 7.8$ Hz, 1H), 8.00 – 7.75 (m, 5H), 6.66 (s, 1H), 5.69 (m, 1H), 5.29 (d, $J = 12.5$ Hz, 1H), 5.14 (m, 2H), 5.01 (d, $J = 10.5$ Hz, 1H), 4.62 – 4.42 (m, 1H), 4.02 (t, $J = 9.4$ Hz, 1H), 3.70 (d, $J = 12.7$ Hz, 1H), 3.54 – 3.34 (m, 2H), 2.77 – 2.17 (m, 2H), 2.09 (d, $J = 4.7$ Hz, 1H), 1.89 (s, 1H), 1.43 (t, $J = 11.9$ Hz, 1H).



Prepared according to general procedure A using cinchonidine (0.34 mmol, 100 mg) and 1-(bromomethyl)-2,4-bis(trifluoromethyl)benzene (0.37 mmol, 115 mg). The mixture was stirred in THF (5 mL) at reflux until complete consumption of cinchonidine. The mixture was cooled to room temperature and poured onto Et_2O with stirring. The resulting suspension was stirred for 1 h and the precipitated solids were isolated by filtration and recrystallized from toluene/MTBE to afford **47** as a white solid (145 mg, 60% yield).

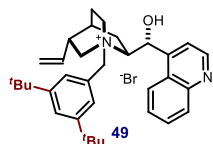
$^1\text{H NMR}$ (300 MHz, OD) δ 8.97 (d, $J = 4.5$ Hz, 1H), 8.40 (dd, $J = 16.0, 7.9$ Hz, 2H), 8.30 – 8.17 (m, 2H), 8.13 (d, $J = 8.3$ Hz, 1H), 8.03 – 7.93 (m, 1H), 7.93 – 7.76 (m, 2H), 6.63 (s, 1H), 6.01 (ddd, $J = 17.3, 10.5, 7.0$ Hz, 1H), 5.69 – 5.41 (m, 2H), 5.33 – 5.15 (m, 2H), 4.47 (t, $J = 10.3$ Hz, 1H), 4.34 – 4.08 (m, 2H), 3.56 – 3.35 (m, 1H), 2.63 (dd, $J = 16.7,$

8.5 Hz, 1H), 2.44 (dd, $J = 24.3, 12.7$ Hz, 1H), 2.05 – 1.84 (m, 3H), 1.23 – 0.97 (m, 2H).
 ^{13}C NMR (75 MHz, CD_3OD) δ 149.7, 147.4, 145.7, 137.8, 136.0, 133.1, 132.69, 132.3,
 129.9, 129.3, 128.9, 127.9, 124.9, 124.8, 123.1, 119.8, 116.5, 68.2, 65.8, 58.0, 57.5, 55.9,
 37.4, 26.6, 23.4, 21.1, 10.2.



Prepared according to general procedure A using cinchonidine (0.68 mmol, 200 mg) and 1-(bromomethyl)-2-methoxybenzene (0.88 mmol, 178 mg). The mixture was stirred in THF (5 mL) at reflux until complete consumption of cinchonidine. Product was purified by flash column chromatography to afford ($\text{CHCl}_3/\text{MeOH}$ 10%) **48** (300 mg, 89% yield).

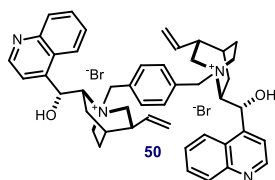
^1H NMR (400 MHz, CDCl_3) δ 8.91 (d, $J = 4.5$ Hz, 1H), 8.12 – 8.04 (m, 2H), 8.01 (dd, $J = 8.3, 1.4$ Hz, 1H), 7.87 (d, $J = 4.5$ Hz, 1H), 7.60 – 7.54 (m, 1H), 7.54 – 7.47 (m, 1H), 7.41 (ddd, $J = 8.2, 7.4, 1.7$ Hz, 1H), 7.03 (td, $J = 7.5, 1.1$ Hz, 1H), 6.88 (d, $J = 8.0$ Hz, 1H), 6.78 (d, $J = 5.7$ Hz, 1H), 6.66 (d, $J = 6.6$ Hz, 1H), 5.96 (d, $J = 11.8$ Hz, 1H), 5.58 – 5.47 (m, 1H), 5.11 (dd, $J = 17.2, 0.9$ Hz, 1H), 5.06 – 4.90 (m, 3H), 3.86 (s, $J = 4.5$ Hz, 3H), 3.80 (t, $J = 9.0$ Hz, 1H), 3.45 – 3.35 (m, 1H), 3.24 (dd, $J = 13.2, 10.6$ Hz, 1H), 3.10 (td, $J = 11.9, 5.7$ Hz, 1H), 2.58 – 2.47 (m, 1H), 2.37 – 2.25 (m, 1H), 2.25 – 2.14 (m, 1H), 1.99 (dd, $J = 6.4, 3.2$ Hz, 1H), 1.76 – 1.64 (m, $J = 14.7, 8.6$ Hz, 1H), 1.36 – 1.26 (m, 1H).
 ^{13}C NMR (101 MHz, CDCl_3) δ 158.6, 150.1, 147.8, 145.6, 136.5, 136.23, 132.4, 130.5, 128.9, 127.3, 124.4, 122.4, 121.4, 120.3, 117.7, 115.5, 111.2, 77.4, 77.2, 77.0, 76.7, 69.7, 63.8, 60.6, 58.1, 55.8, 50.9, 38.1, 26.4, 25.0, 21.6.



Prepared according to general procedure A using cinchonidine (0.34 mmol, 100 mg) and 1-(bromomethyl)-3,5-di-tert-butylbenzene (0.41 mmol, 115 mg). The mixture was stirred in THF (5 mL) and MeCN (1mL) at reflux until complete consumption of cinchonidine. Product was purified by flash column chromatography (AcOEt/MeOH 5-20%) to afford **49** (189 mg, 96% yield).

^1H NMR (300 MHz, CDCl_3) δ 8.78 – 8.70 (m, 1H), 8.07 – 7.99 (m, 1H), 7.92 – 7.81 (m, 1H), 7.76 (d, $J = 4.5$ Hz, 1H), 7.62 (dd, $J = 8.0, 1.5$ Hz, 2H), 7.47 – 7.41 (m, 1H), 7.41 – 7.30 (m, 2H), 6.85 – 6.72 (m, 1H), 6.48 (s, 1H), 5.93 – 5.74 (m, 1H), 5.43 – 5.29 (m, 2H), 5.14 – 5.03 (m, 2H), 4.54 – 4.40 (m, 1H), 4.32 (t, $J = 10.6$ Hz, 1H), 4.04 – 3.90 (m, 1H), 3.43 (t, $J = 11.4$ Hz, 1H), 2.93 – 2.77 (m, 1H), 2.35 (dd, $J = 17.2, 8.7$ Hz, 1H), 2.27 – 2.11 (m, 1H), 1.78 – 1.48 (m, 3H), 1.34 – 1.21 (m, 18H), 0.74 – 0.62 (m, 1H).

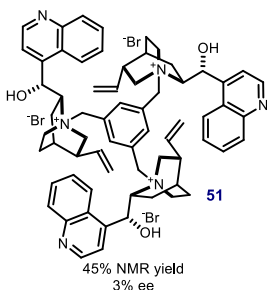
^{13}C NMR (75 MHz, CDCl_3) δ 151.7, 151.7, 149.7, 147.5, 144.9, 135.7, 129.6, 129.1, 128.5, 127.8, 126.5, 124.3, 124.0, 123.6, 120.1, 117.9, 67.1, 65.0, 63.4, 56.3, 54.3, 38.2, 35.0, 31.5, 27.2, 24.0, 21.4, 11.3.



Prepared according to general procedure A using cinchonidine (0.83 mmol, 245 mg) and 1,4-bis(bromomethyl)benzene (0.38 mmol, 100 mg). The mixture was stirred in the mixture of EtOH, DMF, CHCl₃ (2.5 mL, 3 mL, 1 mL) at 100°C until complete consumption of cinchonidine. Product was crystallized from MeOH/Et₂O to afford **50** (312 mg, 97% yield).

¹H NMR (400 MHz, DMSO) δ 9.01 (d, *J* = 4.4 Hz, 2H), 8.34 (d, *J* = 8.4 Hz, 2H), 8.13 (dd, *J* = 8.3, 1.0 Hz, 2H), 7.93 – 7.82 (m, 8H), 7.82 – 7.73 (m, 2H), 6.75 (d, *J* = 4.2 Hz, 2H), 6.59 (d, *J* = 2.7 Hz, 2H), 5.71 (ddd, *J* = 17.1, 10.5, 6.4 Hz, 2H), 5.26 – 5.06 (m, 6H), 4.97 (d, *J* = 10.5 Hz, 2H), 4.33 – 4.20 (m, 2H), 3.94 (t, *J* = 8.7 Hz, 2H), 3.84 – 3.66 (m, 4H), 3.57 – 3.43 (m, 2H), 2.88 – 2.76 (m, 2H), 2.20 – 2.10 (m, 2H), 2.08 – 1.88 (m, 6H), 1.37 – 1.25 (m, 2H).

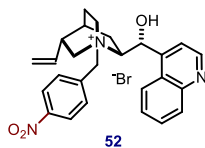
¹³C NMR (101 MHz, DMSO) δ 150.7, 148.1, 145.7, 138.8, 134.5, 130.4, 130.2, 129.90, 127.7, 124.8, 124.1, 120.6, 116.7, 79.7, 68.1, 64.6, 62.6, 59.6, 51.0, 37.2, 36.3, 26.4, 24.6, 21.6.



Prepared according to general procedure A using cinchonidine (0.93 mmol, 272 mg) and 1,3,5-tris(bromomethyl)benzene (0.28 mmol, 100 mg). The mixture was stirred in the mixture of EtOH, DMF, CHCl₃ (2.5 mL, 3 mL, 1 mL) at 100°C until complete consumption of cinchonidine. Product was crystallized from MeOH/Et₂O to afford **51** (271 mg, 78% yield).

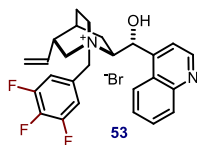
¹H NMR (400 MHz, DMSO) δ 9.03 (d, *J* = 4.5 Hz, 3H), 8.37 (d, *J* = 8.2 Hz, 3H), 8.26 (s, 3H), 8.16 (dd, *J* = 8.4, 1.4 Hz, 3H), 7.98 – 7.71 (m, 9H), 6.84 – 6.55 (m, 6H), 5.73 (ddd, *J* = 17.1, 10.6, 6.5 Hz, 3H), 5.23 (s, 6H), 5.13 (d, *J* = 17.2 Hz, 3H), 4.96 (d, *J* = 10.5 Hz, 3H), 4.34 – 4.11 (m, 6H), 3.95 (t, *J* = 7.9 Hz, 3H), 3.75 (d, *J* = 11.0 Hz, 3H), 3.70 – 3.55 (m, 3H), 3.01 – 2.84 (m, 3H), 2.21 – 2.11 (m, 3H), 2.04 (dt, *J* = 10.9, 5.2 Hz, 3H), 1.93 (dd, *J* = 19.3, 11.6 Hz, 6H), 1.47 – 1.25 (m, 3H).

¹³C NMR (101 MHz, DMSO) δ 162.8, 150.7, 148.1, 145.5, 140.5, 138.8, 130.4, 130.0, 129.9, 127.7, 124.8, 124.1, 120.6, 116.6, 68.3, 65.0, 62.8, 59.8, 50.9, 37.2, 36.3, 26.1, 24.6, 21.8.



Prepared according to general procedure A using cinchonidine (0.34 mmol, 100 mg) and 1-(bromomethyl)-4-nitrobenzene (0.41 mmol, 88 mg). The mixture was stirred in the mixture of THF, EtOH, CHCl_3 (1.5 mL, 1.25 mL, 0.5 mL) at 100°C until complete consumption of cinchonidine. Product was purified by flash column chromatography ($\text{CHCl}_3/\text{MeOH}$ 10%) to afford **52** (97 mg, 56% yield).

$^1\text{H NMR}$ (300 MHz, DMSO) δ 8.99 (d, $J = 4.5$ Hz, 1H), 8.47 – 8.37 (m, 2H), 8.30 (d, $J = 8.0$ Hz, 1H), 8.12 (dd, $J = 8.4, 1.1$ Hz, 1H), 8.08 – 8.02 (m, 2H), 7.92 – 7.70 (m, 3H), 6.84 (d, $J = 4.3$ Hz, 1H), 6.55 (d, $J = 4.5$ Hz, 1H), 5.69 (ddd, $J = 17.1, 11.7, 6.5$ Hz, 1H), 5.33 (d, $J = 12.2$ Hz, 1H), 5.20 – 5.10 (m, 2H), 4.96 (dt, $J = 10.5, 1.2$ Hz, 1H), 4.40 – 4.24 (m, 1H), 3.94 (t, $J = 9.0$ Hz, 1H), 3.85 – 3.71 (m, 1H), 3.30 – 3.18 (m, 2H), 2.64 (s, 1H), 2.20 – 1.95 (m, 3H), 1.87 – 1.70 (m, 1H), 1.38 – 1.24 (m, 1H).

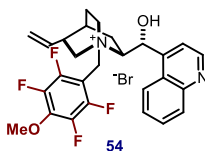


Prepared according to general procedure A using cinchonidine (0.34 mmol, 100 mg) and 5-(bromomethyl)-1,2,3-trifluorobenzene (0.37 mmol, 84 mg). The mixture was stirred in the mixture of EtOH, DMF, CHCl_3 (1.25 mL, 1.5 mL, 0.5 mL) at 100°C until complete consumption of cinchonidine. Product was crystallized from MeOH/Et₂O to afford **53** (127 mg, 72% yield).

$^1\text{H NMR}$ (300 MHz, DMSO) δ 8.98 (d, $J = 4.4$ Hz, 1H), 8.30 (d, $J = 8.4$ Hz, 1H), 8.11 (d, $J = 8.1$ Hz, 1H), 7.95 – 7.79 (m, 4H), 7.79 – 7.68 (m, 1H), 6.69 (d, $J = 4.3$ Hz, 1H), 6.53 – 6.42 (m, 1H), 5.67 (ddd, $J = 17.0, 10.5, 6.2$ Hz, 1H), 5.28 – 5.03 (m, 3H), 4.95 (d, $J = 10.5$ Hz, 1H), 4.38 – 4.19 (m, 1H), 3.88 (t, $J = 8.5$ Hz, 1H), 3.82 – 3.70 (m, 1H), 3.48 – 3.35 (m, 1H), 2.71 – 2.59 (m, 1H), 2.21 – 1.97 (m, 3H), 1.88 – 1.69 (m, 1H), 1.35 – 1.17 (m, 1H).

$^{19}\text{F NMR}$ (376 MHz, DMSO) δ -127.10 (d, $J = 21.8$ Hz, 2F), -152.03 (t, $J = 21.8$ Hz, 1F).

$^{13}\text{C NMR}$ (101 MHz, DMSO) δ 150.6, 148.1, 145.5, 138.5, 130.4, 129.9, 127.7, 124.7, 123.9, 120.5, 119.4, 119.1, 116.9, 68.5, 64.7, 61.8, 59.8, 51.3, 37.5, 26.2, 24.7, 21.4.



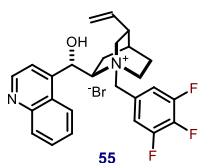
Prepared according to general procedure A using cinchonidine (0.34 mmol, 100 mg) and 1-(bromomethyl)-2,3,5,6-tetrafluoro-4-methoxybenzene (0.34 mmol, 102 mg). The mixture was stirred in THF (5 mL) at reflux until complete consumption of cinchonidine. The mixture was cooled to room temperature and poured onto Et₂O with stirring. The resulting suspension was stirred for 1 h and the precipitated solids were isolated by

filtration, purified by flash column chromatography ($\text{CHCl}_3/\text{MeOH}$ 10%) and crystallized from $\text{MTBE}/\text{DCM}/\text{Et}_2\text{O}$ to afford **54** (97 mg, 50% yield).

$^1\text{H NMR}$ (400 MHz, CD_3OD) δ 8.96 (d, $J = 4.6$ Hz, 1H), 8.31 (d, $J = 7.9$ Hz, 1H), 8.17 – 8.09 (m, 1H), 7.97 (d, $J = 4.5$ Hz, 1H), 7.87 (ddd, $J = 8.4, 6.9, 1.4$ Hz, 1H), 7.81 (ddd, $J = 8.3, 7.0, 1.4$ Hz, 1H), 7.25 – 7.07 (m, 1H), 6.69 – 6.62 (m, 1H), 5.71 (ddd, $J = 17.3, 10.4, 7.0$ Hz, 1H), 5.36 (d, $J = 13.4$ Hz, 1H), 5.13 (dt, $J = 17.2, 1.2$ Hz, 1H), 5.07 – 4.93 (m, 2H), 4.54 – 4.41 (m, 1H), 4.17 – 4.07 (m, 1H), 3.73 (t, $J = 11.5$ Hz, 1H), 3.66 – 3.56 (m, 1H), 3.46 – 3.34 (m, 1H), 2.85 – 2.74 (m, 1H), 2.31 – 2.20 (m, 2H), 2.15 – 2.05 (m, 1H), 2.02 – 1.85 (m, 1H), 1.50 – 1.37 (m, 1H).

$^{13}\text{C NMR}$ (101 MHz, CD_3OD) δ 149.7, 147.4, 146.0, 137.22, 129.9, 129.0, 128.6, 127.9, 127.78, 125.0, 124.8, 122.7, 120.1, 116.4, 99.9, 68.6, 65.2, 61.6, 61.1, 51.9, 51.6, 38.1, 26.2, 2.7, 21.2.

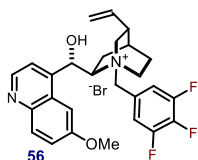
$^{19}\text{F NMR}$ (376 MHz, CD_3OD) δ -139.11 (d, $J = 19.2$ Hz, 2F), -158.58 (dd, $J = 20.9, 8.3$ Hz, 2F).



Prepared according to general procedure A using cinchonine (1.38 mmol, 405 mg) and 5-(bromomethyl)-1,2,3-trifluorobenzene (1.38 mmol, 310 mg). The mixture was stirred in the mixture of EtOH/DMF, CHCl_3 (2.5 mL, 3 mL, 1 mL) at 100°C until complete consumption of cinchonine. Product was crystallized from $\text{MeOH}/\text{Et}_2\text{O}$ to afford **55** (374 mg, 52% yield).

$^1\text{H NMR}$ (400 MHz, DMSO) δ 8.99 (d, $J = 4.5$ Hz, 1H), 8.35 – 8.24 (m, 1H), 8.12 (dd, $J = 8.4, 0.9$ Hz, 1H), 7.92 – 7.79 (m, 4H), 7.79 – 7.69 (m, 1H), 6.79 (d, $J = 3.4$ Hz, 1H), 6.50 – 6.37 (m, 1H), 6.06 – 5.88 (m, 1H), 5.31 – 5.19 (m, 2H), 5.09 (d, $J = 12.5$ Hz, 1H), 4.85 (d, $J = 12.6$ Hz, 1H), 4.30 – 4.17 (m, 1H), 4.12 (s, 1H), 3.93 – 3.74 (m, 2H), 3.09 – 2.90 (m, 1H), 2.66 – 2.52 (m, 1H), 2.34 – 2.21 (m, 1H), 1.94 – 1.85 (m, 1H), 1.80 – 1.70 (m, 2H), 1.13 – 0.97 (m, 1H).

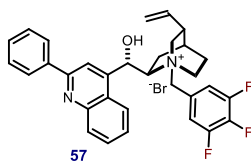
$^{19}\text{F NMR}$ (376 MHz, DMSO) δ -134.51 (d, $J = 21.8$ Hz), -159.41 (t, $J = 21.8$ Hz).



Prepared according to general procedure A using quinidine (0.46 mmol, 150 mg) and 5-(bromomethyl)-1,2,3-trifluorobenzene (0.51 mmol, 140 mg). The mixture was stirred in the mixture of EtOH/DMF, CHCl_3 (1.25 mL, 1.5 mL, 0.5 mL) at 100°C until complete consumption of cinchonine. Product was purified by flash column chromatography ($\text{CHCl}_3/\text{MeOH}$ 10%) and crystallized from DCM/MTBE to afford **56** (195 mg, 77% yield).

$^1\text{H NMR}$ (400 MHz, CDCl_3) δ 8.45 (d, $J = 4.5$ Hz, 1H), 7.76 – 7.69 (m, 2H), 7.58 (d, $J = 2.6$ Hz, 1H), 7.50 (t, $J = 6.8$ Hz, 2H), 6.94 (dd, $J = 9.3$, 2.5 Hz, 1H), 6.44 (d, $J = 5.8$ Hz, 1H), 6.41 – 6.30 (m, 1H), 6.14 (d, $J = 12.2$ Hz, 1H), 5.84 (ddd, $J = 17.3$, 10.5, 6.9 Hz, 1H), 5.67 (d, $J = 12.3$ Hz, 1H), 5.30 – 5.16 (m, 2H), 4.59 – 4.46 (m, 1H), 4.40 – 4.26 (m, 1H), 4.19 (t, $J = 10.4$ Hz, 1H), 3.67 (s, 3H), 3.25 (t, $J = 11.5$ Hz, 1H), 2.90 – 2.75 (m, 1H), 2.38 (dd, $J = 17.1$, 8.6 Hz, 1H), 2.27 – 2.16 (m, 1H), 1.90 – 1.68 (m, 3H), 0.94 – 0.79 (m, 1H).

$^{19}\text{F NMR}$ (376 MHz, CDCl_3) δ -131.56 (d, $J = 20.4$ Hz, 2F), -156.58 (t, $J = 20.4$ Hz, 1F).



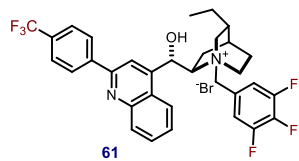
Prepared according to general procedure A using cinchonine derivative (0.27 mmol, 100 mg) and 5-(bromomethyl)-1,2,3-trifluorobenzene (0.30 mmol, 64 mg). The mixture was stirred in the mixture of EtOH DMF, CHCl_3 (1.25 mL, 1.5 mL, 0.5 mL) at 100°C until complete consumption of cinchonine.

Product was purified by flash column chromatography (MeOH-AcOEt 5- 40%) and recrystallized from DCM/MTBE to give **57** (58 mg, 36% yield).

$^1\text{H NMR}$ (400 MHz, CDCl_3) δ 8.26 – 8.14 (m, 4H), 7.66 – 7.55 (m, 3H), 7.55 – 7.43 (m, 3H), 7.03 – 6.95 (m, 1H), 6.96 – 6.87 (m, 1H), 6.60 (s, 1H), 6.52 – 6.44 (m, 1H), 6.30 (d, $J = 12.0$ Hz, 1H), 5.86 (ddd, $J = 17.4$, 10.4, 7.3 Hz, 1H), 5.60 (d, $J = 12.3$ Hz, 1H), 5.35 – 5.12 (m, 2H), 4.62 – 4.46 (m, 1H), 4.23 – 3.98 (m, 2H), 3.30 – 3.19 (m, 1H), 2.89 – 2.73 (m, 1H), 2.35 (dd, $J = 17.5$, 8.8 Hz, 1H), 2.23 – 2.07 (m, 1H), 1.91 – 1.69 (m, 3H).

$^{19}\text{F NMR}$ (376 MHz, CDCl_3) δ -131.32 (d, $J = 20.3$ Hz, 2F), -156.46 (t, $J = 20.3$ Hz, 1F).

$^{13}\text{C NMR}$ (101 MHz, CDCl_3) δ 156.3, 147.2, 144.1, 139.8, 134.7, 130.0, 129.7, 129.3, 128.9, 128.0, 127.7, 127.0, 123.2, 122.4, 122.2, 118.9, 118.6, 118.4, 117.3, 67.5, 65.8, 59.7, 56.5, 54.1, 49.4, 38.1, 29.7, 27.0, 23.7, 21.7.



Prepared according to general procedure A using corresponding cinchonine derivative (2.27 mmol, 1 g) and 5-(bromomethyl)-1,2,3-trifluorobenzene (2.50, mmol, 532 mg). The mixture was stirred in the mixture of *i*-PrOH and DMF, (2 mL, 12 mL) at 70°C until complete consumption

of cinchonine derivative. Product was crystallized from MeOH/ Et_2O to afford **61** (226 mg, 15% yield).

$^1\text{H NMR}$ (400 MHz, $\text{DMSO}-d_6$) δ 8.53 (d, $J = 8.1$ Hz, 2H), 8.42 (s, 1H), 8.38 (d, $J = 8.4$ Hz, 1H), 8.21 (d, $J = 8.2$ Hz, 1H), 7.97 (d, $J = 8.2$ Hz, 2H), 7.95 – 7.86 (m, 3H), 7.78 (t, $J = 7.6$ Hz, 1H), 6.94 (s, 1H), 6.51 (s, 1H), 5.12 (d, $J = 12.3$ Hz, 1H), 4.92 (d, $J = 12.4$ Hz, 1H), 4.03 – 3.82 (m, 3H), 3.53 (t, $J = 11.2$ Hz, 1H), 3.00 (q, $J = 10.2$ Hz, 1H), 2.37

(t, $J = 11.8$ Hz, 1H), 1.83 (s, 1H), 1.80 – 1.63 (m, 3H), 1.64 – 1.46 (m, 2H), 1.17 – 1.06 (m, 1H), 0.88 (t, $J = 7.3$ Hz, 3H).

^{19}F NMR (376 MHz, $\text{DMSO-}d_6$) δ -61.16 (s, 3F), -134.64 (d, $J = 21.7$ Hz, 2F), -159.60 (t, $J = 21.7$ Hz, 1F).

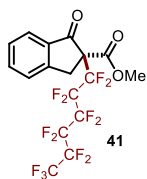
^{13}C NMR (101 MHz, $\text{DMSO-}d_6$) δ 154.6, 148.1, 147.2, 142.8, 130.7, 130.4, 130.1, 128.6, 128.2, 126.58 – 126.17 (m), 126.1, 125.5, 124.3, 124.2, 123.4, 119.4, 119.4, 119.2, 117.8, 68.4, 65.6, 61.1, 56.5, 35.4, 29.4, 24.7, 24.2, 24.1, 20.7, 11.9.

General Procedures B for the Photochemical Enantioselective Perfluoroalkylation of β -Ketoesters under PTC Conditions.

A 15 mL Schlenk tube was charged with β -ketoester **63** (0.1 mmol), the PTC catalyst **58** (0.02 mmol), chlorobenzene (0.25 mL), perfluorooctane (0.125 mL), the perfluoroalkyl iodide (0.3 mmol, 3 equiv.) and cesium carbonate (0.2 mmol). The reaction mixture was degassed via freeze pump thaw (x3), and the vessel refilled with argon. After the reaction mixture was thoroughly degassed, the Schlenk tube was sealed and positioned in the middle of a 250 mL evaporation bath surrounded by 1 m strip containing white LEDs. A small fan was installed directly above the Schlenk tube so as to keep the temperature constant. After stirring (1000 rpm) for 64 hours, reaction was quenched by adding an aqueous 1M HCl solution and extracted 3 times with DCM. The organic phase was dried over Na_2SO_4 , the solvent was removed under reduced pressure and the crude mixture was purified by column chromatography to give the product **63** in the stated yield and optical purity.



Figure 3.5 Reaction set up under irradiation of white LEDs



Methyl (S)-1-oxo-2-(perfluorohexyl)-2,3-dihydro-1H-indene-2-carboxylate (41). Prepared according to general procedure B using methyl 1-oxo-2,3-dihydro-1H-indene-2-carboxylate (0.1 mmol, 19 mg), perfluorohexyl iodide (0.3 mmol, 134 mg, 0.065 mL), the phase transfer catalyst **58** (0.002 mmol, 13 mg) and cesium carbonate (0.2

mmol, 65 mg). Time of irradiation: 64 hours. The crude mixture was purified by flash column chromatography (hexane, EtOAc:hex 5:95) to afford the product as a white solid (21 mg, 41% yield, **92%** ee). The enantiomeric excess was determined by HPLC analysis on a Daicel Chiralpak AD-H column, 99:1 hexane:iPrOH, flow rate 0.50 mL/min, $\lambda =$

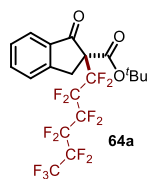
254 nm: $\tau_{\text{minor}} = 9.8$ min, $\tau_{\text{major}} = 10.8$ min (90% ee); $[\alpha]_{\text{D}}^{25} = +38.9$ (c = 0.83, CHCl_3 , 92% ee).

$^1\text{H NMR}$ (400 MHz, CDCl_3) δ 7.82 (d, $J = 7.7$ Hz, 1H), 7.69 (td, $J = 7.6, 1.2$ Hz, 1H), 7.53 (d, $J = 7.7$ Hz, 0H), 7.44 (t, $J = 7.1$ Hz, 1H), 3.94 (d, $J = 17.9$ Hz, 1H), 3.80 (s, 3H), 3.61 (d, $J = 17.6$ Hz, 1H).

$^{19}\text{F NMR}$ decoupled ^1H (376 MHz, CDCl_3) δ -80.77 – -81.06 (m, 3F), -109.21 – -111.91 (m, 2F), -116.22 – -116.74 (m, 2F), -122.16 (m, 2F), -122.59 (m, 2F), -126.09 – -126. (m, 2F).

$^{13}\text{C NMR}$ (126 MHz, CDCl_3) δ 192.1, 164.8 (d, $J = 8.7$ Hz), 151.7, 136.3, 133.9, 128.4, 126.2, 125.5, 63.1 (dd, $J = 24.2, 18.5$ Hz), 53.9, 33.4 – 33.2 (m).

HRMS calculated for $\text{C}_{17}\text{H}_9\text{F}_{13}\text{NaO}_3$ (M+Na): 531.0236, found: 531.0222



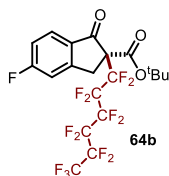
tert-Butyl (S)-1-oxo-2-(perfluorohexyl)-2,3-dihydro-1H-indene-2-carboxylate (64a) Prepared according to general procedure B using *tert*-butyl 1-oxo-2,3-dihydro-1H-indene-2-carboxylate (0.1 mmol, 23 mg), perfluorohexyl iodide (0.3 mmol, 134 mg, 0.065 mL), phase transfer catalyst **58** (0.002 mmol, 13 mg) and cesium carbonate (0.2 mmol, 65 mg). Time of irradiation: 64 hours. The crude mixture was purified by flash column chromatography (hexane, EtOAc:hex 5:95) to give the product as a white solid (39 mg, 71% yield, 93% ee). The enantiomeric excess was determined by HPLC analysis on a Daicel Chiralpak AD-H column, 99.5:0.5 hexane:iPrOH, flow rate 0.60 mL/min, $\lambda = 254$ nm: $\tau_{\text{minor}} = 6.7$ min, $\tau_{\text{major}} = 7.6$ min (94% ee); $[\alpha]_{\text{D}}^{25} = +28.2$ (c = 1.08 CHCl_3 , 93% ee).

$^1\text{H NMR}$ (400 MHz, CDCl_3) δ 7.81 (d, $J = 7.2$ Hz, 1H), 7.71 – 7.62 (m, 1H), 7.56 – 7.48 (m, 1H), 7.48 – 7.40 (m, 1H), 3.85 (d, $J = 17.5$ Hz, 1H), 3.55 (d, $J = 17.5$ Hz, 1H), 1.44 (s, 9H).

$^{19}\text{F NMR}$ decoupled ^1H (376 MHz, Chloroform-*d*) δ -80.88 (t, $J = 10.0$ Hz, 3F), -108.19 – -111.48 (m, 2F), -115.68 – -115.89 (m, 2F), -122.08 – -122.38 (m, 2F), -122.41 – -122.73 (m, 2F), -126.11 – -126.33 (m, 2F).

$^{13}\text{C NMR}$ (75 MHz, CDCl_3) δ 192.7, 163.0 (d, $J = 8.9$ Hz), 151.9, 136.0, 134.1, 128.2, 126.1, 125.3, 84.6, 64.4 – 63.6 (m), 33.9 – 32.1 (m), 27.5.

HRMS calculated for $\text{C}_{20}\text{H}_{15}\text{F}_{13}\text{NaO}_3$ (M+Na): 573.0706, found: 573.0697



***tert*-Butyl (S)-5-fluoro-1-oxo-2-(perfluorohexyl)-2,3-dihydro-1H-indene-2-carboxylate (64b)**

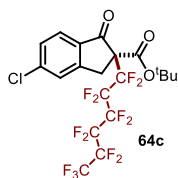
Prepared according to general procedure B using *tert*-butyl 5-fluoro-1-oxo-2,3-dihydro-1H-indene-2-carboxylate (0.1 mmol, 25 mg), perfluorohexyl iodide (0.3 mmol, 134 mg, 0.065 mL), phase transfer catalyst **58** (0.002 mmol, 13 mg) and cesium carbonate (0.2 mmol, 65 mg). Time of irradiation: 64 hours. The crude mixture was purified by flash column chromatography (hexane, EtOAc:hex 5:95) to give the product as a yellow solid (36 mg, 63% yield, 87% ee). The enantiomeric excess was determined by HPLC analysis on a Daicel Chiralpak AD-H column, 99.5:0.5 hexane:iPrOH, flow rate 0.60 mL/min, $\lambda = 254$ nm: $\tau_{\text{minor}} = 7.1$ min, $\tau_{\text{major}} = 11.3$ min (87% ee); $[\alpha]_{\text{D}}^{28} = +29.71$ ($c = 1.00$, CHCl_3 , 87% ee).

$^1\text{H NMR}$ (400 MHz, CDCl_3) δ 7.82 (dd, $J = 8.5, 5.2$ Hz, 1H), 7.21 – 7.10 (m, 2H), 3.85 (d, $J = 17.6$ Hz, 1H), 3.52 (d, $J = 17.6$ Hz, 1H), 1.44 (s, 9H).

$^{19}\text{F NMR}$ decoupled ^1H (376 MHz, CDCl_3) δ -80.89 (tt, $J = 10.3, 2.8$ Hz, 3F), -99.85 (s, 1F), -108.11 – -111.75 (m, 2F), -115.71 – -115.94 (m, 2F), -122.08 – -122.42 (m, 2F), -122.42 – -122.71 (m, 2F), -126.12 – -126.34 (m, 2F).

$^{13}\text{C NMR}$ (101 MHz, CDCl_3) δ 190.8, 167.8 (d, $J = 259.3$ Hz), 162.8 (d, $J = 9.1$ Hz), 154.9 (d, $J = 10.5$ Hz), 130.3, 127.8 (d, $J = 10.8$ Hz), 116.8 (d, $J = 24.0$ Hz), 113.0 (d, $J = 23.0$ Hz), 84.9, 64.0, 33.1, 27.5.

HRMS calculated for $\text{C}_{20}\text{H}_{14}\text{F}_{14}\text{NaO}_3$ (M+Na): 591.0612, found: 591.0604



***tert*-butyl (S)-5-chloro-1-oxo-2-(perfluorohexyl)-2,3-dihydro-1H-indene-2-carboxylate (64c)**

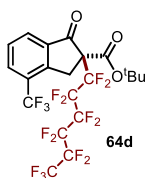
Prepared according to general procedure B using *tert*-butyl 5-chloro-1-oxo-2,3-dihydro-1H-indene-2-carboxylate (0.1 mmol, 27 mg), perfluorohexyl iodide (0.3 mmol, 134 mg, 0.065 mL), phase transfer catalyst **58** (0.002 mmol, 13 mg) and cesium carbonate (0.2 mmol, 65 mg). Time of irradiation: 64 hours. The crude mixture was purified by flash column chromatography (hexane, EtOAc:hex 5:95) to give the product as a yellow solid (41 mg, 70% yield, 86% ee). The enantiomeric excess was determined by HPLC analysis on a Daicel Chiralpak AD-H column, 99.5:0.5 hexane:iPrOH, flow rate 0.60 mL/min, $\lambda = 254$ nm: $\tau_{\text{minor}} = 8.1$ min, $\tau_{\text{major}} = 12.4$ min (86% ee); $[\alpha]_{\text{D}}^{28} = +46.74$ ($c = 0.88$, CHCl_3 , 86% ee).

$^1\text{H NMR}$ (400 MHz, CDCl_3) δ 7.74 (d, $J = 8.3$ Hz, 1H), 7.52 (d, $J = 1.0$ Hz, 1H), 7.41 (dd, $J = 8.3, 1.8$ Hz, 1H), 3.83 (d, $J = 17.5$ Hz, 1H), 3.51 (d, $J = 17.6$ Hz, 1H), 1.44 (s, 9H).

^{19}F NMR decoupled ^1H (376 MHz, CDCl_3) δ -80.89 (t, J = 10.0 Hz, 3F), -108.16 – -111.52 (m, 2F), -115.70 – -115.97 (m, 2F), -122.05 – -122.41 (m, 2F), -122.42 – -122.72 (m, 2F), -126.10 – -126.41 (m, 2F).

^{13}C NMR (101 MHz, CDCl_3) δ 191.3, 162.7 (d, J = 8.7 Hz), 153.3, 142.8, 132.5, 129.2, 126.4, 126.34, 85.0, 64.5 – 63.9 (m), 33.3 – 32.8 (m), 27.5.

HRMS calculated for $\text{C}_{20}\text{H}_{14}\text{ClF}_{13}\text{NaO}_3$ (M+Na): 607.0316, found: 607.0331



***tert*-Butyl (S)-1-oxo-2-(perfluorohexyl)-4-(trifluoromethyl)-2,3-**

dihydro-1H-indene-2-carboxylate (64d) Prepared according to general

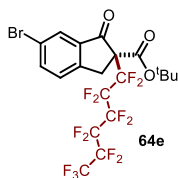
procedure B using *tert*-butyl 1-oxo-4-(trifluoromethyl)-2,3-dihydro-1H-indene-2-carboxylate (0.1 mmol, 30 mg), perfluorohexyl iodide (0.3 mmol, 134 mg, 0.065 mL), phase transfer catalyst **58** (0.002 mmol, 13 mg) and cesium carbonate (0.2 mmol, 65 mg). Time of irradiation: 64 hours. The crude mixture was purified by flash column chromatography (hexane, EtOAc:hex 3:97) to give the product as a yellow oil (38 mg, 61% yield, 94% ee) The enantiomeric excess was determined by GC analysis on an Alphadex column (120 30x0.25mm, 0.25 μm , Tinj/aux 280 Flow 1.5mL/min split 50:1 (1 μL) Isotherm 80 $^\circ\text{C}$, FID detector) τ_{minor} = 486.0, 1 min, τ_{major} = 495.9 min (94% ee). $[\alpha]_{\text{D}}^{25}$ = +22.6 (c = 0.40, CHCl_3 , 94% ee).

^1H NMR (400 MHz, CDCl_3) δ 8.00 (d, J = 8.2 Hz, 1H), 7.96 – 7.92 (m, 1H), 7.64 – 7.24 (m, 1H), 4.03 (d, J = 18.2 Hz, 1H), 3.67 (d, J = 18.2 Hz, 1H), 1.44 (s, 9H).

^{19}F NMR decoupled ^1H (376 MHz, CDCl_3) δ -62.45 (s, 3F), -80.88 (tt, J = 9.9, 2.5 Hz, 3F), -107.99 – -111.60 (m, 2F), -115.63 – -115.88 (m, 2F), -122.05 – -122.39 (m, 2F), -122.42 – -122.71 (m, 2F), -126.11 – -126.36 (m, 2F).

^{13}C NMR (101 MHz, CDCl_3) δ 191.6, 162.3 (d, J = 8.4 Hz), 149.1, 135.6, 132.6 (q, J = 4.6 Hz), 128.8, 128.7, 128.3 (d, J = 33.0 Hz), 123.4 (q, J = 273.3 Hz), 85.2, 64.2 – 63.4 (m), 32.3, 27.5.

HRMS calculated for $\text{C}_{21}\text{H}_{14}\text{F}_{16}\text{NaO}_3$ (M+Na): 641.0580, found: 641.0572



***tert*-Butyl 6-bromo-1-oxo-2-(perfluorohexyl)-2,3-dihydro-1H-**

indene-2-carboxylate (64e) Prepared according to general procedure

B using *tert*-butyl 6-bromo-1-oxo-2,3-dihydro-1H-indene-2-carboxylate (0.1 mmol, 31 mg), perfluorohexyl iodide (0.3 mmol, 134 mg, 0.065 mL), phase transfer catalyst **58** (0.002 mmol, 13 mg) and cesium carbonate (0.2 mmol, 65 mg). Time of irradiation: 64 hours. The crude mixture was purified by flash column chromatography (hexane, EtOAc:hex 5:95) to give the

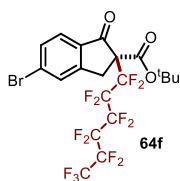
product as a yellow solid (38 mg, 60% yield, 82% ee). The enantiomeric excess was determined by HPLC analysis on a Daicel Chiralpak AD-H column, 99.5:0.5 hexane:iPrOH, flow rate 0.60 mL/min, $\lambda = 254$ nm: $\tau_{\text{minor}} = 6.2$ min, $\tau_{\text{major}} = 7.4$ min (82% ee); $[\alpha]_{\text{D}}^{28} = +11.53$ ($c = 1.00$, CHCl_3 , 82% ee).

^1H NMR (400 MHz, CDCl_3) δ 7.93 (d, $J = 1.8$ Hz, 1H), 7.77 (dd, $J = 8.2, 1.9$ Hz, 1H), 7.41 (d, $J = 8.2$ Hz, 1H), 3.80 (d, $J = 17.5$ Hz, 1H), 3.48 (d, $J = 17.6$ Hz, 1H), 1.44 (s, 9H).

^{19}F NMR decoupled ^1H (376 MHz, CDCl_3) δ -80.86 (t, $J = 10.0$ Hz, 3F), -108.03 – -111.50 (m, 2F), -115.72 – -115.94 (m, 2F), -122.07 – -122.39 (m, 2F), -122.41 – -122.71 (m, 2F), -126.10 – -126.33 (m, 2F).

^{13}C NMR (75 MHz, CDCl_3) δ 191.3, 162.5 (d, $J = 8.7$ Hz), 150.4, 138.8, 135.8, 128.1, 127.6, 122.4, 85.0, 65.1 – 63.6 (m), 33.3 – 32.7 (m), 27.5.

HRMS calculated for $\text{C}_{20}\text{H}_{14}\text{BrF}_{13}\text{NaO}_3$ ($\text{M}+\text{Na}$): 650.9811, found: 650.9799



***tert*-Butyl (*S*)-5-bromo-1-oxo-2-(perfluorohexyl)-2,3-dihydro-1H-indene-2-carboxylate (**64f**)** Prepared according to general procedure B using *tert*-butyl 5-bromo-1-oxo-2,3-dihydro-1H-indene-2-carboxylate (0.1 mmol, 31 mg), perfluorohexyl iodide (0.3 mmol, 134 mg, 0.065 mL), phase transfer catalyst **58** (0.002 mmol, 13 mg) and cesium carbonate (0.2 mmol, 65 mg). Time of irradiation: 64 hours. The crude mixture was purified by flash column chromatography (hexane, EtOAc:hex 5:95) to give the product as a yellow solid (38 mg, 60% yield, 88% ee). The enantiomeric excess was determined by HPLC analysis on a Daicel Chiralpak AD-H column, 99.5:0.5 hexane:iPrOH, flow rate 0.60 mL/min, $\lambda = 254$ nm: $\tau_{\text{minor}} = 6.5$ min, $\tau_{\text{major}} = 8.9$ min (88% ee); $[\alpha]_{\text{D}}^{28} = +45.52$ ($c = 0.41$, CHCl_3 , 88% ee).

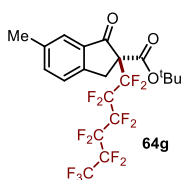
^1H NMR (400 MHz, CDCl_3) δ 7.74 – 7.67 (m, 1H), 7.66 (d, $J = 8.2$ Hz, 1H), 7.61 – 7.54 (m, 1H), 3.84 (d, $J = 17.6$ Hz, 1H), 3.52 (d, $J = 17.7$ Hz, 1H), 1.44 (s, 9H).

^{19}F NMR decoupled ^1H (376 MHz, CDCl_3) δ -80.88 (t, $J = 9.9$ Hz, 3F), -109.02 (m, 2F), -115.70 – -115.93 (m, 2F), -122.07 – -122.40 (m, 2F), -122.41 – -122.71 (m, 2F), -126.10 – -126.35 (m, 2F).

^{13}C NMR (101 MHz, CDCl_3) δ 191.5, 162.6 (d, $J = 8.9$ Hz), 153.3, 132.8, 132.0, 131.72, 129.4, 126.3, 84.9, 64.4 – 63.6 (m), 33.0 – 32.8 (m), 27.5.

HRMS calculated for $\text{C}_{20}\text{H}_{14}\text{BrF}_{13}\text{NaO}_3$ ($\text{M}+\text{Na}$): 650.9811, found: 650.9811

The absolute configuration for **64f** was unambiguously inferred by anomalous dispersion X-ray crystallographic analysis, see X-ray Crystallographic Data section.



tert-Butyl (S)-6-methyl-1-oxo-2-(perfluorohexyl)-2,3-dihydro-1H-indene-2-carboxylate (64g) Prepared according to general procedure B using *tert*-butyl 6-methyl-1-oxo-2,3-dihydro-1H-indene-2-carboxylate (0.1 mmol, 25 mg), perfluorohexyl iodide (0.3 mmol, 134 mg, 0.065 mL), phase transfer catalyst **58** (0.002 mmol,

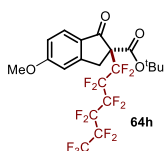
13 mg) and cesium carbonate (0.2 mmol, 65 mg). Time of irradiation: 64 hours. The crude mixture was purified by flash column chromatography (hexane, EtOAc:hex 5:95) to give the product as a yellow oil (31 mg, 55% yield, 83% ee). The enantiomeric excess was determined by HPLC analysis on a Daicel Chiralpak AD-H column, 99.5:0.5 hexane:iPrOH, flow rate 0.60 mL/min, $\lambda = 254$ nm: $\tau_{\text{minor}} = 6.2$ min, $\tau_{\text{major}} = 6.8$ min (83% ee); $[\alpha]_{\text{D}}^{28} = +22.98$ ($c = 0.95$, CHCl_3 , 83% ee).

$^1\text{H NMR}$ (400 MHz, CDCl_3) δ 7.60 (s, 1H), 7.48 (dd, $J = 7.6, 1.5$ Hz, 1H), 7.40 (d, $J = 7.9$ Hz, 1H), 3.78 (d, $J = 17.4$ Hz, 1H), 3.49 (d, $J = 17.4$ Hz, 1H), 2.41 (s, 3H), 1.43 (s, 9H).

$^{19}\text{F NMR}$ decoupled ^1H (376 MHz, CDCl_3) δ -80.90 (t, $J = 9.8$ Hz, 3F), -108.25 – -111.39 (m, 2F), -115.66 – -115.94 (m, 2F), -122.04 – -122.40 (m, 2F), -122.41 – -122.72 (m, 2F), -126.11 – -126.36 (m, 2F).

$^{13}\text{C NMR}$ (101 MHz, CDCl_3) δ 192.8, 163.2 (d, $J = 8.8$ Hz), 149.4, 138.4, 137.3, 134.3, 125.7, 125.1, 84.5, 64.7 – 63.9 (m), 33.2 – 32.8 (m), 27.5, 21.0.

HRMS calculated for $\text{C}_{21}\text{H}_{17}\text{F}_{13}\text{NaO}_3$ ($\text{M}+\text{Na}$): 587.0862, found: 587.0855



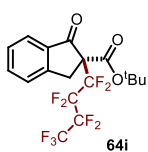
tert-Butyl (S)-5-methoxy-1-oxo-2-(perfluorohexyl)-2,3-dihydro-1H-indene-2-carboxylate (64h) Prepared according to general procedure B using *tert*-butyl 5-methoxy-1-oxo-2,3-dihydro-1H-indene-2-carboxylate (0.1 mmol, 26 mg), perfluorohexyl iodide (0.3 mmol, 134 mg, 0.065 mL), phase transfer catalyst **58** (0.002 mmol, 13 mg) and cesium carbonate (0.2 mmol, 65 mg). Time of irradiation: 64 hours. The crude mixture was purified by flash column chromatography (hexane, EtOAc:hex 5:95) to give the product as a yellow solid (22 mg, 38% yield, 86% ee). The enantiomeric excess was determined by HPLC analysis on a Daicel Chiralpak AD-H column, 99.5:0.5 hexane:iPrOH, flow rate 0.60 mL/min, $\lambda = 254$ nm: $\tau_{\text{minor}} = 7.7$ min, $\tau_{\text{major}} = 8.5$ min (86% ee); $[\alpha]_{\text{D}}^{28} = +57.76$ ($c = 0.52$, CHCl_3 , 86% ee).

$^1\text{H NMR}$ (400 MHz, CDCl_3) δ 7.73 (d, $J = 8.5$ Hz, 1H), 6.97 – 6.91 (m, 2H), 3.91 (s, 3H), 3.79 (d, $J = 17.5$ Hz, 1H), 3.46 (d, $J = 17.5$ Hz, 1H), 1.44 (s, 9H).

^{19}F NMR decoupled ^1H (376 MHz, CDCl_3) δ -80.88 (t, $J = 10.0$ Hz, 3F), -108.29 – -111.88 (m, 2F), -115.71 – -115.93 (m, 2F), -122.08 – -122.40 (m, 2F), -122.41 – -122.69 (m, 2F), -126.10 – -126.35 (m, 2F).

^{13}C NMR (101 MHz, CDCl_3) δ 190.6, 166.3, 163.3 (d, $J = 9.4$ Hz), 155.1, 127.1, 127.1, 116.5, 109.1, 84.4, 65.0 – 63.2 (m), 55.82, 33.4 – 33.1 (m), 27.56.

HRMS calculated for $\text{C}_{21}\text{H}_{17}\text{F}_{13}\text{NaO}_4$ (M+Na): 603.0811, found: 603.0827



tert-Butyl (S)-1-oxo-2-(perfluorobutyl)-2,3-dihydro-1H-indene-2-carboxylate (64i) Prepared according to general procedure B using tert-butyl 1-oxo-2,3-dihydro-1H-indene-2-carboxylate (0.1 mmol, 23 mg), perfluorobutyl iodide (0.3 mmol, 104 mg, 0.052 mL), phase transfer catalyst **58** (0.002 mmol, 13 mg) and cesium carbonate (0.2 mmol, 65 mg).

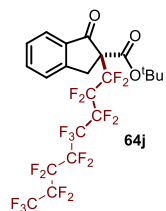
Time of irradiation: 64 hours. The crude mixture was purified by flash column chromatography (hexane, EtOAc:hex 5:95) to give the product as a yellow solid (28 mg, 62% yield, 90% ee). The enantiomeric excess was determined by HPLC analysis on a Daicel Chiralpak AD-H column, 99.5:0.5 hexane:iPrOH, flow rate 0.60 mL/min, $\lambda = 254$ nm: $\tau_{\text{minor}} = 7.8$ min, $\tau_{\text{major}} = 9.0$ min (90% ee); $[\alpha]_{\text{D}}^{28} = +32.23$ ($c = 0.40$, CHCl_3 , 90% ee).

^1H NMR (400 MHz, CDCl_3) δ 7.81 (d, $J = 7.7$ Hz, 1H), 7.67 (td, $J = 7.6, 1.2$ Hz, 1H), 7.52 (dt, $J = 7.7, 0.9$ Hz, 1H), 7.48 – 7.39 (m, 1H), 3.85 (d, $J = 17.5$ Hz, 1H), 3.55 (d, $J = 17.5$ Hz, 1H), 1.44 (s, 9H).

^{19}F NMR decoupled ^1H (376 MHz, CDCl_3) δ -80.75 (tt, $J = 10.4, 3.1$ Hz, 3F), -108.46 – -111.60 (m, 2F), -116.56 – -116.87 (m, 2F), -126.49 (m, 2F).

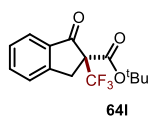
^{13}C NMR (101 MHz, CDCl_3) δ 192.7, 163.0 (d, $J = 8.7$ Hz), 151.9, 136.0, 134.1, 128.2, 126.1, 125.3, 84.6, 64.2 – 63.6 (m) 33.5 – 33.2 (m), 27.5.

HRMS calculated for $\text{C}_{18}\text{H}_{15}\text{F}_9\text{NaO}_3$ (M+Na): 473.0770, found: 473.0761



tert-Butyl (S)-1-oxo-2-(perfluorooctyl)-2,3-dihydro-1H-indene-2-carboxylate (64j) Prepared according to general procedure B using tert-butyl 1-oxo-2,3-dihydro-1H-indene-2-carboxylate (0.1 mmol, 23 mg), perfluorooctyl iodide (0.3 mmol, 164 mg, 0.079 mL), phase transfer catalyst **58** (0.002 mmol, 13 mg) and cesium carbonate (0.2 mmol, 65 mg).

Time of irradiation: 64 hours. The crude mixture was purified by flash column chromatography (hexane, EtOAc:hex 5:95) to give the product as a yellow solid (44 mg, 68% yield, 93% ee). The enantiomeric excess was determined by HPLC analysis on a Daicel Chiralpak AD-H column, 99.5:0.5 hexane:iPrOH, flow



tert-Butyl (S)-1-oxo-2-(trifluoromethyl)-2,3-dihydro-1H-indene-2-carboxylate (64l). Prepared according to general procedure B using *tert*-butyl 1-oxo-2,3-dihydro-1H-indene-2-carboxylate (0.1 mmol, 23 mg), phase transfer catalyst **58** (0.002 mmol, 13 mg) and cesium carbonate

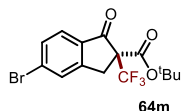
(0,2 mmol, 65 mg). Trifluoroiodomethane (0.3 mmol, 7.5 mL, gas) was added after the 3 cycles of freeze pump thaw via gas syringe at $-196\text{ }^{\circ}\text{C}$ (nitrogen bath). Time of irradiation: 64 hours. The crude mixture was purified by flash column chromatography (hexane, EtOAc:hex 4:96) to give the product as a white solid (15 mg, 50% yield, 96% ee). The enantiomeric excess was determined by HPLC analysis on a Daicel Chiralpak AD-H column, 99.5:0.5 hexane:iPrOH, flow rate 0.60 mL/min, $\lambda = 254\text{ nm}$: $\tau_{\text{minor}} = 9.4\text{ min}$, $\tau_{\text{major}} = 10.7\text{ min}$ (96% ee); $[\alpha]_{\text{D}}^{28} = +27.2$ ($c = 0.25$, CHCl_3 , 96% ee)

$^1\text{H NMR}$ (400 MHz, CDCl_3) δ 7.83 (d, $J = 7.6\text{ Hz}$, 1H), 7.72 – 7.63 (m, 1H), 7.52 (dt, $J = 7.7, 0.9\text{ Hz}$, 1H), 7.49 – 7.40 (m, 1H), 3.68 (d, $J = 17.6\text{ Hz}$, 1H), 3.56 (d, $J = 17.6\text{ Hz}$, 1H), 1.43 (s, 9H).

$^{19}\text{F NMR}$ decoupled ^1H (376 MHz, CDCl_3) δ -69.19 (s, 3F).

$^{13}\text{C NMR}$ (101 MHz, CDCl_3) δ 193.4, 164.1 (q, $J = 2.0\text{ Hz}$), 151.7, 136.0, 134.7 – 134.5 (m), 128.3, 126.2, 125.4, 123.6 (q, $J = 281.3\text{ Hz}$), 84.3, 63.9 (q, $J = 25.8\text{ Hz}$), 34.3 (q, $J = 1.9\text{ Hz}$), 27.7.

Spectral data match with the ones reported in literature.⁴⁰



tert-Butyl (S)-5-bromo-1-oxo-2-(trifluoromethyl)-2,3-dihydro-1H-indene-2-carboxylate (64m) Prepared according to general procedure B using *tert*-butyl 6-bromo-1-oxo-2,3-dihydro-1H-indene-2-carboxylate (0.1 mmol, 31 mg), phase transfer catalyst **58** (0.002

mmol, 13 mg) and cesium carbonate (0,2 mmol, 65 mg). Trifluoroiodomethane (0.3 mmol, 7.5 mL, gas) was added after the 3 cycles of freeze pump thaw via gas syringe at $-196\text{ }^{\circ}\text{C}$ (nitrogen bath). Time of irradiation: 64 hours. The crude mixture was purified by flash column chromatography (hexane, DCM:hex 4:6) to give the product as a white solid (20 mg, 53% yield, 84% ee). The enantiomeric excess was determined by HPLC analysis on a Daicel Chiralpak AD-H column, 99.5:0.5 hexane:iPrOH, flow rate 0.60 mL/min, $\lambda = 254\text{ nm}$: $\tau_{\text{minor}} = 15.3\text{ min}$, $\tau_{\text{major}} = 22.6\text{ min}$ (84% ee); $[\alpha]_{\text{D}}^{25} = +47.8$ ($c = 0.83$, CHCl_3 , 84% ee).

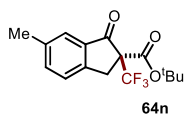
⁴⁰ Q-H. Deng, H. Wadepohl, L. H. Gade, Highly Enantioselective Copper-Catalyzed Electrophilic Trifluoromethylation of β -Ketoesters *J. Am. Chem. Soc.*, **2012**, 134, 10769.

$^1\text{H NMR}$ (400 MHz, CDCl_3) δ 7.73 – 7.66 (m, 2H), 7.62 – 7.56 (m, 1H), 3.67 (d, $J = 17.8$ Hz, 1H), 3.53 (d, $J = 17.8$ Hz, 1H), 1.44 (s, 9H).

$^{19}\text{F NMR}$ decoupled ^1H (376 MHz, Chloroform- d) δ -69.20 (s, 3F).

$^{13}\text{C NMR}$ (101 MHz, CDCl_3) δ 192.1, 163.6 (q, $J = 2.2$ Hz), 153.1, 133.5 (t, $J = 1.8$ Hz), 132.1, 131.6, 129.6, 126.5, 123.4 (q, $J = 281.5$ Hz), 84.6, 63.94 (q, $J = 26.0$ Hz), 33.9 – 33.7 (m), 27.7.

Spectral data match with the ones reported in literature.⁴⁰



tert-Butyl (S)-6-methyl-1-oxo-2-(trifluoromethyl)-2,3-dihydro-1H-indene-2-carboxylate (64n) Prepared according to general procedure B using *tert*-butyl 6-methyl-1-oxo-2,3-dihydro-1H-indene-2-carboxylate (0.1 mmol, 25 mg), phase transfer catalyst **58**

(0.002 mmol, 13 mg) and cesium carbonate (0.2 mmol, 65 mg). Trifluoroiodomethane (0.3 mmol, 7.5 mL, gas) was added after the 3 cycles of freeze pump thaw via gas syringe at -196 °C (nitrogen bath). Time of irradiation: 64 hours. The crude mixture was purified by flash column chromatography (hexane, DCM:hex 4:6) to give the product as a white solid (12 mg, 38% yield, 78% ee). The enantiomeric excess was determined by HPLC analysis on a Daicel Chiralpak AD-H column, 99.5:0.5 hexane:iPrOH, flow rate 0.60 mL/min, $\lambda = 254$ nm: $\tau_{\text{minor}} = 12.7$ min, $\tau_{\text{major}} = 13.9$ min (78% ee); $[\alpha]_{\text{D}}^{25} = +12.7$ ($c = 1.05$, CHCl_3 , 78% ee).

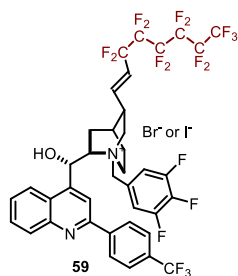
$^1\text{H NMR}$ (400 MHz, Chloroform- d) δ 7.62 (s, 1H), 7.48 (dd, $J = 7.9, 1.1$ Hz, 1H), 7.39 (d, $J = 7.8$ Hz, 1H), 3.62 (d, $J = 17.5$ Hz, 1H), 3.50 (d, $J = 17.4$ Hz, 1H), 2.42 (s, 1H), 1.43 (s, 9H).

$^{19}\text{F NMR}$ decoupled ^1H (376 MHz, Chloroform- d) δ -69.23 (s, 3F).

$^{13}\text{C NMR}$ (101 MHz, Chloroform- d) δ 193.4, 164.2 (d, $J = 2.4$ Hz), 149.1, 138.5, 137.3, 134.8 (d, $J = 1.7$ Hz), 125.9, 125.2, 123.7 (q, $J = 281.3$ Hz), 64.2 (d, $J = 25.8$ Hz), 34.0 – 33.8 (m), 27.7, 21.0.

Spectral data match with the ones reported in literature.⁴⁰

Byproducts.



59 was purified by column chromatography (AcOEt, 30% MeOH-AcOEt) from reaction mixture (general procedure B) as violet solid (11 mg, 54% yield). $[\alpha]_{\text{D}}^{25} = +64.0$ ($c = 0.80$ DMSO).

$^1\text{H NMR}$ (400 MHz, $\text{DMSO}-d_6$) δ 8.42 – 8.34 (m, 3H), 8.27 – 8.19 (m, 2H), 7.96 – 7.87 (m, 5H), 7.78 (ddd, $J = 8.4, 6.9, 1.3$ Hz, 1H), 7.21 (d, $J = 3.8$ Hz, 1H), 6.76 – 6.66 (m, 1H), 6.57 – 6.51 (m, 1H), 6.26 (q, $J = 14.0, 13.4$ Hz, 1H), 5.19 (d, $J = 12.5$

Hz, 1H), 5.09 (d, $J = 12.5$ Hz, 1H), 4.48 – 4.37 (m, 1H), 3.94 (t, $J = 10.0$ Hz, 2H), 3.66 (t, $J = 11.6$ Hz, 1H), 3.09 (q, $J = 10.2$ Hz, 1H), 2.96 – 2.84 (m, 1H), 2.17 (t, $J = 11.6$ Hz, 1H), 2.12 – 2.04 (m, 1H), 1.90 – 1.73 (m, 2H), 1.23 – 1.17 (m, 1H).

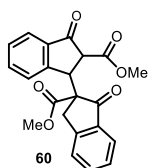
^1H { ^{19}F } NMR (400 MHz, $\text{DMSO-}d_6$) δ 8.42 – 8.34 (m, 3H), 8.27 – 8.19 (m, 2H), 7.96 – 7.87 (m, 5H), 7.78 (ddd, $J = 8.4, 6.9, 1.3$ Hz, 1H), 7.21 (d, $J = 3.8$ Hz, 1H), 6.71 (dd, $J = 16.1, 5.4$ Hz, 1H), 6.57 – 6.51 (m, 1H), 6.26 (dd, $J = 16.1, 1.7$ Hz, 1H), 5.19 (d, $J = 12.5$ Hz, 1H), 5.09 (d, $J = 12.5$ Hz, 1H), 4.48 – 4.37 (m, 1H), 3.94 (t, $J = 10.0$ Hz, 2H), 3.66 (t, $J = 11.6$ Hz, 1H), 3.09 (q, $J = 10.2$ Hz, 1H), 2.96 – 2.84 (m, 1H), 2.17 (t, $J = 11.6$ Hz, 1H), 2.12 – 2.04 (m, 1H), 1.90 – 1.73 (m, 2H), 1.23 – 1.17 (m, 1H).

^{19}F NMR decoupled ^1H (376 MHz, $\text{DMSO-}d_6$) δ -61.63 (s, 3F), -80.47 (t, $J = 9.9$ Hz, 3F), -108.67 – -112.29 (m, 2F), -121.23 – -121.62 (m, 2F), -122.28 – -122.95 (m, 4F), -125.74 – -126.18 (m, 2F), -134.67 (d, $J = 21.8$ Hz, 2F), -159.54 (t, $J = 21.8$ Hz, 1F).

^{19}F NMR (376 MHz, $\text{DMSO-}d_6$) δ -61.62 (s, 3F), -80.47 (t, $J = 9.6$ Hz, 3F), -108.63 – -112.29 (m, 2F), -121.20 – -121.64 (m, 2F), -122.23 – -123.10 (m, 4F), -125.72 – -126.18 (m, 2F), -134.67 (dd, $J = 21.6, 9.1$ Hz, 2F), -159.54 (tt, $J = 21.7, 6.9$ Hz, 1F).

^{13}C NMR (126 MHz, $\text{DMSO-}d_6$) δ 154.7, 151.7 – 151.4 (m), 149.7 – 149.2 (m), 148.2, 147.1, 143.7 (t, $J = 9.6$ Hz), 143.1, 139.5, 130.7, 130.6, 130.2 (q, $J = 31.9$ Hz), 128.3, 128.2, 126.2 – 126.0 (m), 125.51 – 125.1 (m), 124.6 (q, $J = 272.0$ Hz), 124.3, 124.2, 119.4, 119.4 (d, $J = 20.9$ Hz), 119.3, 117.9, 117.7, 79.6, 68.0, 65.4, 61.2, 56.5, 53.8, 35.5, 31.4, 26.1, 23.1, 22.5, 21.0, 14.4.

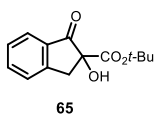
HRMS calculated for $\text{C}_{39}\text{H}_{28}\text{F}_{19}\text{N}_2\text{O}$ (M^*): 901.1893, found: 901.1883



60 was purified by column chromatography (DCM-hexane 40%, AcOEt) from reaction mixture (general procedure B) as a mixture of two diastereoisomers 1:2.5 dr (5 mg, 25%).

^1H NMR (400 MHz, CDCl_3) δ 7.88 (d, $J = 7.8$ Hz, 1H), 7.84 – 7.73 (m, 2H), 7.65 (tt, $J = 7.4, 1.1$ Hz, 1H), 7.58 (td, $J = 7.5, 1.3$ Hz, 1H), 7.52 – 7.39 (m, 3H), 7.39 – 7.30 (m, 3H), 7.21 – 7.11 (m, 1H) - aromatic protons of both diastereoisomers, 5.15 (d, $J = 3.8$ Hz, 0.4H, minor), 5.03 (d, $J = 3.5$ Hz, 1H, major), 3.87 (s, 1.2H, minor), 3.84 (s, 3H, major), 3.78 (s, 1.2H, minor), 3.71 (s, 3H, major), 3.68 – 3.57 (m, 2.8H, both diastereoisomers), 3.07 (d, $J = 3.9$ Hz, 0.4H, minor), 2.63 – 1.56 (m, 1.4H, both diastereoisomers).

MS (ES^+) 378 $\text{C}_{22}\text{H}_{18}\text{O}_6$ ($M + \text{Na}$) $^+$



65 was purified by column chromatography (AcOEt-hexane 5-20%) from reaction performed under air (see Scheme 3.20), (7 mg, 15% yield).

$^1\text{H NMR}$ (400 MHz, CDCl_3) δ 7.79 (d, $J = 7.4$ Hz, 1H), 7.68 – 7.56 (m, 1H), 7.50 – 7.36 (m, 2H), 3.98 (s, 1H), 3.65 (d, $J = 17.2$ Hz, 1H), 3.22

(d, $J = 17.1$ Hz, 1H), 1.36 (s, 9H).

$^{13}\text{C NMR}$ (101 MHz, CDCl_3) δ 201.3, 170.5, 152.3, 135.8, 133.9, 127.9, 126.3, 125.1, 84.0, 80.5, 39.4, 27.9.

Spectral data match with the ones reported in literature.⁴¹

Quantum Yield Measurement.

A ferrioxalate actinometry solution was prepared by following the Hammond variation of the Hatchard and Parker procedure outlined in *Handbook of Photochemistry*⁴². Ferrioxalate actinometer solution measures the decomposition of ferric ions to ferrous ions, which are complexed by 1,10-phenanthroline and monitored by UV/Vis absorbance at 510 nm. The moles of iron-phenanthroline complex formed are related to moles of photons absorbed.

The solutions were prepared and stored in the dark (red light):

1. Potassium ferrioxalate solution: 589,5 mg of potassium ferrioxalate (commercially available from Alfa Aesar) and 278 μL of sulfuric acid (96%) were added to a 100 mL volumetric flask, and filled to the mark with water (HPLC grade).
2. Phenanthroline solution: 0,2% by weight of 1,10-phenanthroline in water (200 mg in 100 mL volumetric flask).
3. Buffer solution: to a 100 mL volumetric flask 4,94 g of NaOAc and 1 mL of sulfuric acid (96%) were added and filled to the mark with water (HPLC grade).
4. Model reaction solution: tert-butyl 1-oxo-2,3-dihydro-1H-indene-2-carboxylate **1b** (0,2 mmol, 46 mg), perfluorohexyl iodide **28** (0.6 mmol, 0,130 ml) tetradecane (0,1 mmol, 0,026ml) and 1,8-Diazabicyclo[5.4.0]undec-7-ene (0,4 mmol, 0,06 mL) were added to a 5 mL volumetric flask 442 μL and filled to the mark with chlorobenzene.

⁴¹ M. Lu, D. Zhu, Y. Lu, X. Zeng, B. Tan, Z. Xu, G. Zhong, Chiral Brønsted Acid-Catalyzed Enantioselective α -Hydroxylation of β -Dicarbonyl Compounds, *J. Am. Chem. Soc.*, **2009**, 131, 4562.

⁴² S. Murov, L., *Handbook of Photochemistry*, Marcel Dekker, New York, **1973**.

The actinometry measurements were done as follows:

1. 1 mL of the actinometer solution was added to a quartz cuvette ($l = 10$ mm). The cuvette was placed along with a sample solution (1 mL in a similar cuvette) whose quantum yield has to be measured (our model reaction). The sample and actinometry solutions (placed 10 cm away from the lamp) were irradiated with 300 W Xenon Lamp (50% of light intensity, 400 ± 5 nm bandpass filter high transmittance) *for specified time intervals* (5, 7.5, 10, 12.5) min.
2. After irradiation all the actinometer solution was removed and placed in a 10 mL volumetric flask. 0.5 mL of 1,10-phenanthroline solution and 2 mL of buffer solution was added to this flask and filled to the mark with water (HPLC grade).
3. The UV-Vis spectra of actinometry samples were recorded for each time interval. The absorbance of the actinometry solution was monitored at 510 nm.
4. The moles of Fe^{2+} formed for each sample is determined according to the Beers' Law:

$$\text{moles } \text{Fe}^{+2} = \frac{V_1 \cdot V_3 \cdot \Delta A(510 \text{ nm})}{10^3 \cdot V_2 \cdot l \cdot \varepsilon(510 \text{ nm})}$$

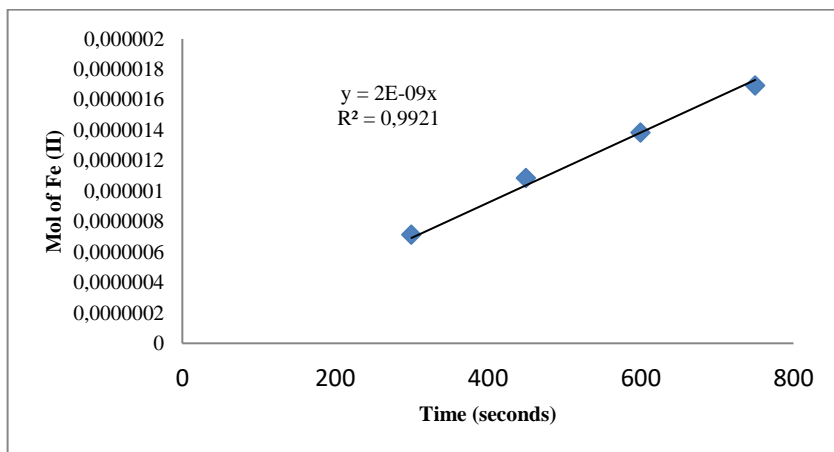
where V_1 is the irradiated volume (1 mL), V_2 is the aliquot of the irradiated solution taken for the determination of the ferrous ions (1 mL), V_3 is the final volume after complexation with phenanthroline (10 mL), l is the optical path-length of the irradiation cell (1 cm), $\Delta A(510 \text{ nm})$ the optical difference in absorbance between the irradiated solution and the one stored in the dark, $\varepsilon(510 \text{ nm})$ is that of the complex $\text{Fe}(\text{phen})_3^{2+}$ ($11100 \text{ L mol}^{-1} \text{ cm}^{-1}$).

5. The moles of Fe^{2+} formed (dx) are plotted as a function of time (dt). The slope of this line was correlated to the moles of incident photons by unit of time ($q_{n,p}^0$) by the use of the following equation (6):

$$\Phi(\lambda) = \frac{dx/dt}{q_{n,p}^0 [1 - 10^{-A(\lambda)}]} \quad (6)$$

where dx/dt is the rate of change of a measurable quantity (spectral or any other property), the quantum yield (Φ) for Fe^{2+} at 400 nm is $1,13^{42}$ and $A(\lambda)$ is the absorbance at the excitation wavelength (400 nm). The absorbance at this wavelength, $A^{(400)}$, was measured using a Shimadzu 2401PC UV-Vis spectrophotometer in 1 mm path quartz cuvettes in the presence of the bandpass

filter of 400 nm employed to carry out the measurements, obtaining an absorbance of 0,256. $q_{n,p}^0$ was determined to be $5,25 \cdot 10^{-9}$ einstein s^{-1} .

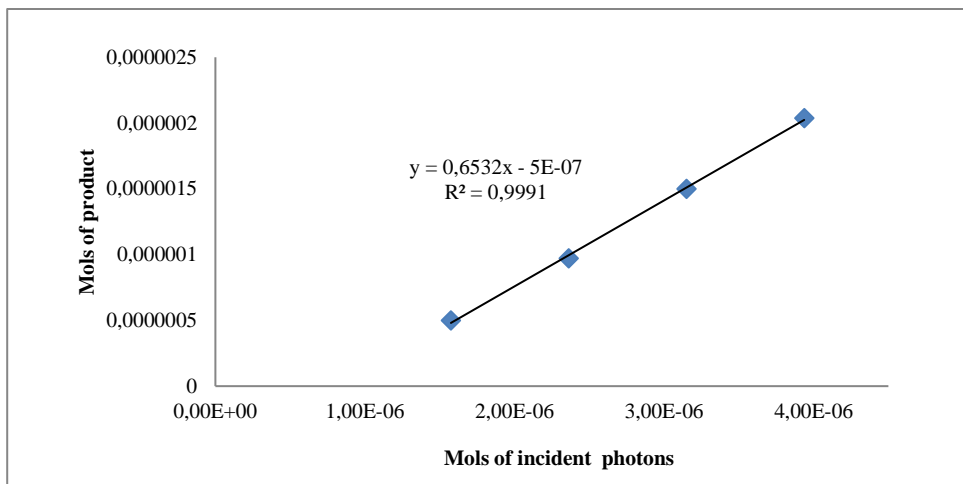


The moles of products formed for the reaction of interest (performed by irradiating the sample alongside with the actinometer solution) are described below.

- The moles of products formed were determined by GC measurement (FID detector) using tetradecane as reference standard. The number of moles of product per unit time is related to the number of photons absorbed. The number of photons absorbed is correlated to the number of incident photons by the use of the equation displayed in the previous point.

According to the equation the slope (dx/dt) is equal to: $\Phi \cdot (1 - 10^{-A(400 \text{ nm})}) \cdot q_{n,p}^0$,

where $(1 - 10^{-A(400 \text{ nm})})$ was measured using a Shimadzu 2401PC UV-Vis spectrophotometer in 1 mm path quartz cuvettes in the presence of the bandpass filter of 400 nm employed to carry out the measurements, obtaining an absorbance of 0,302. The calculation yields the quantum yield (Φ) of the photoreaction = **1,2**.



X-ray Crystallographic Data

Single Crystal X-ray Diffraction Data for Compound **64f**

X-ray structure determinations: Crystals of compound **64f** were obtained by slow diffusion of hexane into a saturated ethyl acetate solution. *Data Collection.* Measurements were made on a Bruker-Nonius diffractometer equipped with an APPEX 2 4K CCD area detector, a FR591 rotating anode with $\text{MoK}\alpha$ radiation, Montel mirrors and a Cryostream Plus low temperature device ($T = 100\text{K}$). Full-sphere data collection was used with ω and φ scans.

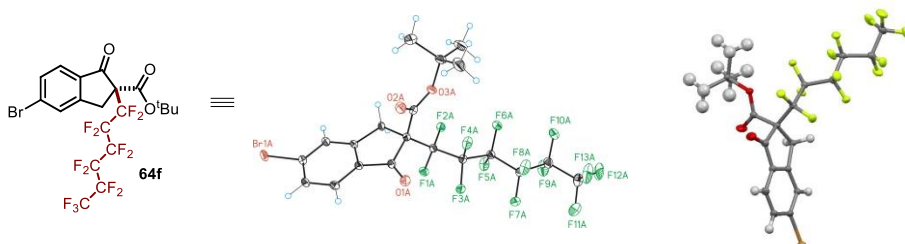


Table S2. Crystal data and structure refinement for **64f** at 100 K: **CCDC 1055351**

Identification code	mo_LW3021_0m
Empirical formula	C20 H14 Br1 F13 O3
Formula weight	629.22
Temperature	100(2) K
Wavelength	0.71073 Å
Crystal system	Triclinic
Space group	P1
Unit cell dimensions	a = 6.7268(7)Å, α = 75.871(2)°. b = 12.1525(10)Å, β = 85.192(4)°. c = 14.3989(15)Å, γ = 89.437(3)°.
Volume	1137.38(19) Å ³
Z	2
Density (calculated)	1.837 Mg/m ³
Absorption coefficient	1.935 mm ⁻¹
F(000)	620
Crystal size	0.40 x 0.10 x 0.10 mm ³
Theta range for data collection	1.463 to 31.632°.
Index ranges	-9 <= h <= 9, -17 <= k <= 17, -
Reflections collected	14059
Independent reflections	8670[R(int) = 0.0208]
Completeness to theta = 31.632°	91.1%
Absorption correction	Empirical
Max. and min. transmission	0.830 and 0.625
Refinement method	Full-matrix least-squares on F ²
Data / restraints / parameters	8670 / 3 / 673
Goodness-of-fit on F ²	1.087
Final R indices [I > 2sigma(I)]	R1 = 0.0285, wR2 = 0.0778
R indices (all data)	R1 = 0.0307, wR2 = 0.0869
Flack parameter	x = 0.000(4)
Largest diff. peak and hole	0.915 and -0.549 e.Å ⁻³

Single Crystal X-ray Diffraction Data for compound **58**

X-ray structure determinations: Crystals of compound **58** were obtained by slow diffusion of hexane into a saturated methanol, diethyl ether solution. Measurements were made on a Rigaku XtaLab P200 diffractometer equipped with a Pilatus 200K area detector, a Microfocus-HF007 rotating anode with $\text{MoK}\alpha$ radiation, Confocal Max Flux optic and a Cryostream Plus low temperature device ($T = 100\text{K}$). Full-sphere data collection was used with ω and φ scans.

For the absolute configuration determination of the light-atom molecule **58** the methodology described in the following work has been followed:

The use of Mo K α radiation in the assignment of the absolute configuration of light-atom molecules; the importance of high-resolution data

E. C. Escudero-Adán, J. Benet-Buchholz, P. Ballester *Acta Cryst. B*, **2014**, *70*, 660-668

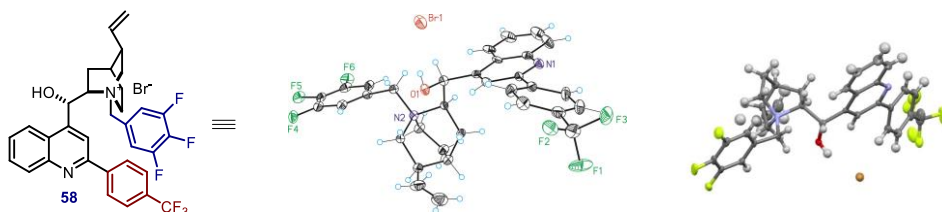


Table S3. Crystal data and structure refinement for **58** at 100 K: **CCDC 1056560**

Identification code	mo_LWCN13_0m
Empirical formula	C ₃₅ H ₃₄ Br F ₆ N ₂ O _{1.50}
Formula weight	700.55
Temperature	100(2) K
Wavelength	0.71073 Å
Crystal system	Monoclinic
Space group	P2(1)

Unit cell dimensions	a= 12.0338(6)Å, α = 90°. b= 8.9481(6)Å, β = 100.6910(17)°. c= 15.3554(9)Å, γ = 90°.
Volume	1624.76(17) Å ³
Z	2
Density (calculated)	1.432 Mg/m ³
Absorption coefficient	1.332 mm ⁻¹
F(000)	718
Crystal size	0.20 x 0.05 x 0.01 mm ³
Theta range for data collection	1.722 to 28.095°.
Index ranges	-13<=h<=15,-11<=k<=11,-
19<=l<=14	
Reflections collected	13252
Independent reflections	6279[R(int) = 0.0338]
Completeness to theta =28.095°	87.5%
Absorption correction	Empirical
Max. and min. transmission	0.987 and 0.651
Refinement method	Full-matrix least-squares on F ²
Data / restraints / parameters	6279/ 220/ 525
Goodness-of-fit on F ²	1.064
Final R indices [I>2sigma(I)]	R1 = 0.0564, wR2 = 0.1612
R indices (all data)	R1 = 0.0699, wR2 = 0.1746
Flack parameter	x =0.015(7)
Largest diff. peak and hole	1.118 and -0.523 e.Å ⁻³

Chapter IV

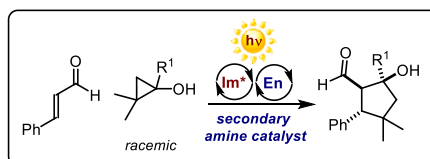
Enantioselective Photochemical Organocascade Catalysis

Target

Development of visible-light-promoted enantioselective photo-organocatalytic cascade transformations to uncover new strategies in domino processes.

Tool

Photochemical reactivity of excited-state chiral iminium ions and ground-state reactivity of chiral enamines combined in a cascade process.



4.1 Introduction

Enantioselective organocascade catalysis has been extensively explored over the last 10 years.¹ A great number of novel concepts and chemical transformations has been developed at an impressive pace. Nowadays, it is remarkably hard to bring further innovation to the field, which has been growing exponentially and reached a high level of maturity and sophistication. We believe that an important step for the evolution of organocascade processes would be merging classical ground-state aminocatalytic transformations with the recently uncovered excited-state reactivity of chiral organocatalytic intermediates.^{2,3} This would open new avenues for the design of cascade processes. In this chapter, I will describe how this idea was reduced to practice.

4.2 Ground-state Enantioselective Iminium Ion Catalysis

In 2000, MacMillan's laboratory introduced a new strategy for asymmetric synthesis based on the ability of chiral amines to function as LUMO (lowest unoccupied molecular orbital) lowering catalyst through iminium ion activation of unsaturated carbonyl

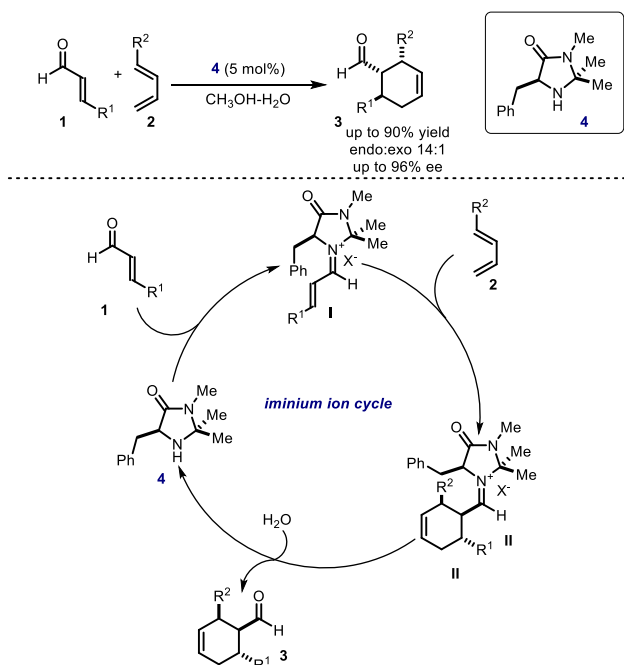
¹ C. Grondal, M. Jeanty, D Enders, Organocatalytic Cascade reactions as a New Tool in Total Synthesis, *Nat. Chem.*, **2010**, 2, 167.

² M. Silvi, C. Verrier, Y.P. Rey, L. Buzzetti, P. Melchiorre, Visible-light Excitation of Iminium Ions Enables the Enantioselective Catalytic β -alkylation of Enals, *Nat. Chem.*, **2017**, DOI: 10.1038/nchem.2748.

³ M. Silvi, E. Arceo, I. D. Jurberg, C. Cassani, P. Melchiorre, Enantioselective Organocatalytic Alkylation of Aldehydes and Enals Driven by the Direct Photoexcitation of Enamines, *J. Am. Chem. Soc.*, **2015**, 137, 6120.

substrates (Scheme 4.1, see also Chapter I, section 1.1.2).⁴ A range of stereocontrolled transformations, which traditionally employed Lewis acids, has been achieved using chiral secondary amine catalysts. This strategy is founded on the mechanistic postulate that the LUMO of iminium ion possesses significantly lower energy than the corresponding carbonyl substrate precursor. The reversible condensation of chiral amines to α,β -unsaturated ketones and aldehydes enables turnover of the catalyst. Additionally, the amine catalyst is generally able to infer a high level of iminium ion geometry control and selective differentiation of the olefin π face, which are essential elements for inducing high enantioselectivity to the reaction.

The iminium ion strategy was originally implemented to perform the enantioselective Diels-Alder reaction of enals **1** and dienes **2** using the imidazolidinone catalyst **4**, providing an alternative to the existing Lewis acid-catalyzed reactions (Scheme 4.1).⁵ The control of the iminium ion geometry **I**, by means of steric constraints on the catalyst architecture **4**, was crucial to provide high levels of enantioselectivity.



Scheme 4.1 Iminium ion activation for enantioselective Diels-Alder reaction of α,β -unsaturated aldehydes.

⁴ K. A. Ahrendt, C. J. Borths, D. W. C. MacMillan, New Strategies for Organic Catalysis: The First Highly Enantioselective Organocatalytic Diels-Alder Reaction, *J. Am. Chem. Soc.*, **2000**, 122, 4243.

⁵ L. C. Dias, Chiral Lewis Acid Catalysts in Diels-Alder Cycloadditions: Mechanistic Aspects and Synthetic Applications of Recent Systems, *J. Braz. Chem. Soc.*, **1997**, 8, 4, 289.

The same catalyst **4** could also successfully promote the stereocontrolled iminium ion-mediated enantioselective Friedel-Crafts reaction of pyrroles **7** and enals **1** (Scheme 4.2b).⁶ However, employing indoles **9**, which are less activated substrates toward electrophilic aromatic substitution, resulted in significantly lower enantioselectivities and yields when using catalyst **4** (Scheme 4.2c - result in the box).⁷ This highlighted the need for a new, more reactive, and versatile amine catalyst (Scheme 4.2a). Since both the formation of iminium ion and the carbon-carbon bond forming step influence the reaction rate, it was theorized that replacement of the methyl group, in a *trans* geometry with respect to the benzyl substituent, with a hydrogen atom would lower the steric hindrance and allow the faster formation of the iminium ions, increasing the overall reaction rate. Additionally, introduction of a bigger *tert*-butyl group in the place of the remaining methyl would provide better control of iminium ion geometry while effectively shielding the *si*-face of the activated olefin, leaving the *re*-face exposed to indole addition. The new catalyst design was essential to obtain high enantioselectivities and yields in the alkylation of indoles (Scheme 4.2c),⁷ as well as in other mechanistically related processes, including Mukayama aldol reaction,⁸ amination,⁹ and hydrogenation.¹⁰

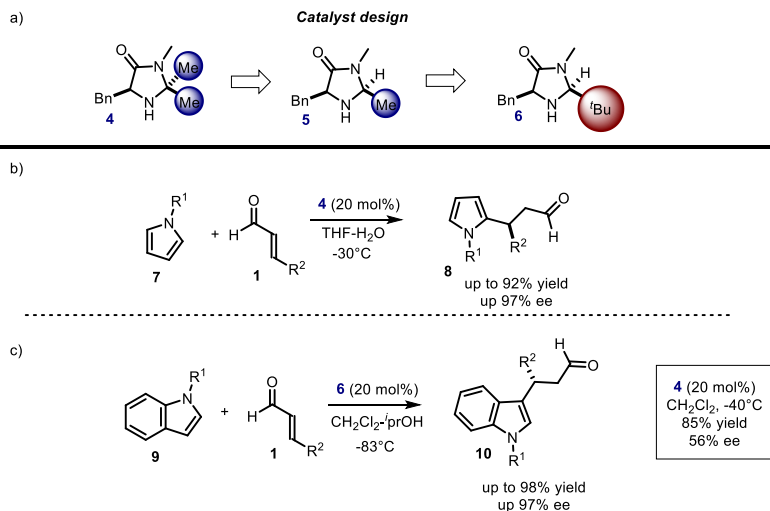
⁶ N. A. Paras, D. W. C. MacMillan, New Strategies in Organic Catalysis: The First Enantioselective Organocatalytic Friedel-Crafts Alkylation, *J. Am. Chem. Soc.*, **2001**, *123*, 4370.

⁷ J. F. Austin, D. W. C. MacMillan, Enantioselective Organocatalytic Indole Alkylations. Design of a New and Highly Effective Chiral Amine for Iminium Catalysis, *J. Am. Chem. Soc.*, **2002**, *124*, 7, 1172.

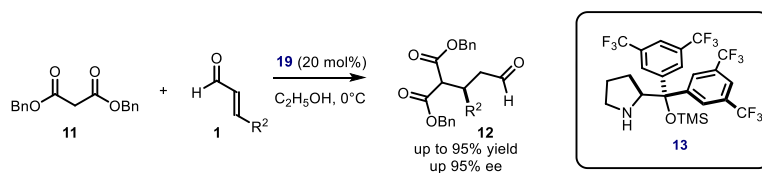
⁸ S. P. Brown, N. C. Goodwin, D. W. C. MacMillan, The First Enantioselective Organocatalytic Mukaiyama-Michael Reaction: A Direct Method for the Synthesis of Enantioenriched γ -Butenolide Architecture, *J. Am. Chem. Soc.*, **2003**, *125*, 1192.

⁹ Y. K. Chen, M. Yoshida, D. W. C. MacMillan, Enantioselective Organocatalytic Amine Conjugate Addition, *J. Am. Chem. Soc.*, **2006**, *128*, 9328.

¹⁰ S. G. Ouellet, J. B. Tuttle, D. W. C. MacMillan, Enantioselective Organocatalytic Hydride Reduction, *J. Am. Chem. Soc.*, **2005**, *127*, 32.



The prolinol-based catalyst **13**, developed independently by Jørgensen¹¹ and Hayashi,¹² also provided efficient stereocontrol in a variety of iminium ion-mediated conjugate addition reactions.¹³ A representative example of addition of malonates **11** to enals **1** is shown in Scheme 4.3.^{13a}



¹¹ M. Marigo, T. C. Wabnitz, D. Fielenbach, K. A. Jørgensen, Enantioselective Organocatalyzed Sulfenylation of Aldehydes, *Angew. Chem. Int. Ed.*, **2005**, *44*, 794.

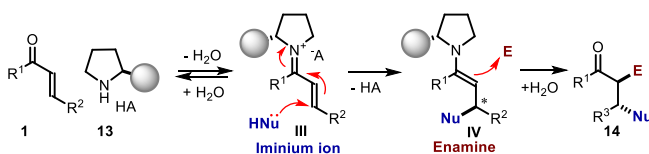
¹² Y. Hayashi, H. Gotoh, T. Hayashi, M. Shoji, Diphenylprolinol Silyl Ethers as Efficient Organocatalysts for the Asymmetric Michael Reaction of Aldehydes and Nitroalkenes, *Angew. Chem. Int. Ed.*, **2005**, *44*, 4212.

¹³ a) S. Brandau, A. Landa, J. Franzen, M. Marigo, K. A. Jørgensen, Organocatalytic Conjugate Addition of Malonates to α,β -Unsaturated Aldehydes: Asymmetric Formal Synthesis of (-)-Paroxetine, Chiral Lactams, and Lactones, *Angew. Chem. Int. Ed.*, **2006**, *45*, 4305, b) L. Zu, a H. Xie, H. Li, J. Wang, W. Wang, Highly Enantioselective Organocatalytic Conjugate Addition of Nitromethane to α,β -Unsaturated Aldehydes: Three-Step Synthesis of Optically Active Baclofen, *Adv. Synth. Catal.*, **2007**, *349*, 2660, c) A.N. Alba, X. Companyó, A. Moyano, R. Rios, Formal Highly Enantioselective Organocatalytic Addition of Alkyl Anions to α,β -Unsaturated Aldehydes: Application to the Synthesis of Isotope- Enantiomers, *Chem. Eur. J.*, **2009**, *15*, 11095.

Nowadays, iminium ion activation is a well-established strategy for the enantioselective β -functionalization of carbonyls with a great number of soft nucleophiles. The catalyst scaffolds developed by MacMillan, and Jørgensen and Hayashi often provide high levels of enantiocontrol and good reaction efficiency. This makes this subfield of organocatalysis a valuable and predictable tool for the synthesis of chiral molecules.

4.3 Enantioselective Organocascade Catalysis

Essential for the expansion of the field was the realization that the addition of a nucleophile to the chiral iminium ion **III** results in the formation of an enamine **IV**. The latter nucleophilic intermediate, which is generated in situ, can undergo a subsequent reaction with an electrophile. Identification of this iminium ion/enamine activation sequence was crucial to fully harness the synthetic power of aminocatalytic processes. This reaction sequence is now the most applied to design organocatalytic cascade processes.¹⁴

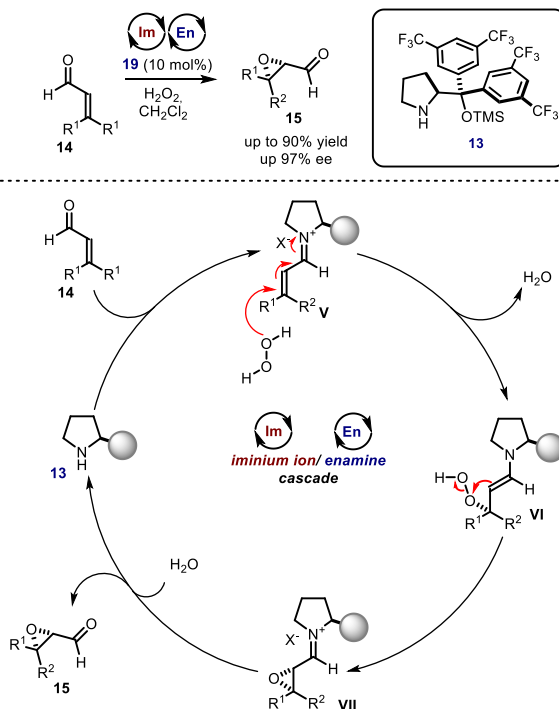


Scheme 4.4 Combining enamine and iminium ion activation modes to implement cascade processes. E: electrophile, Nu: nucleophile, HA: acid.

One of the first achievements in this field was reported by Jørgensen in 2005, who developed the organocatalytic enantioselective epoxidation of α,β -unsaturated aldehydes **14** employing catalyst **13** and hydrogen peroxide (Scheme 4.5).¹⁵ The first step is driven by the formation of the chiral iminium ion **V**, which reacts with hydrogen peroxide in a conjugate addition manifold. The resulting chiral enamine **VI** undergoes intramolecular, nucleophilic attack on the electrophilic oxygen atom to form intermediate **VII** and, after hydrolysis, the final epoxide **15**.

¹⁴ H. Pellissier, Recent Developments in Asymmetric Organocatalytic Domino Reactions, *Adv. Synth. Catal.*, **2012**, 354, 237.

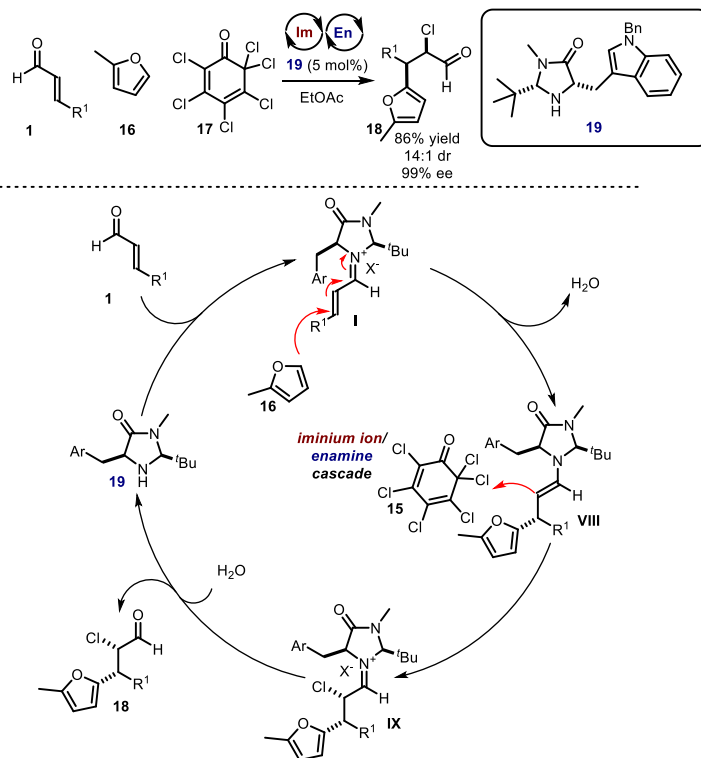
¹⁵ M. Marigo, J. Franzen, T. B. Poulsen, W. Zhuang, K. A. Jørgensen, Asymmetric Organocatalytic Epoxidation of α,β -Unsaturated Aldehydes with Hydrogen Peroxide, *J. Am. Chem. Soc.*, **2005**, 127, 6964.



Scheme 4.5 Enantioselective organocatalytic epoxidation of α,β -unsaturated aldehydes with hydrogen peroxide by means of an iminium ion-enamine tandem sequence, TMS: trimethyl silyl group, Im: iminium ion, En: enamine; the filled grey circle represents a bulky substituent on the chiral amine catalyst.

Soon after, MacMillan reported an organocascade transformation that begins with the conjugate addition of hydride (not shown) or π nucleophiles, such as the furan **16**, to a chiral iminium ion **I** (Scheme 4.6).¹⁶ Next, the 1,4-addition adduct **VIII** participates in the second reaction, wherein enamine activation enables highly diastereoselective additions to the electrophilic chlorine reagent **17**.

¹⁶ Y. Huang, A. M. Walji, C. H. Larsen, D. W. C. MacMillan, Enantioselective Organo-Cascade Catalysis *J. Am. Chem. Soc.*, **2005**, *127*, 15051.



Scheme 4.6 Enantioselective organocascade Friedel-Crafts reaction, chlorination sequence. Im: iminium ion, En: enamine.

These early examples indicated a new direction in asymmetric aminocatalysis, which led to an impressive growth methods, based on organocascade processes, ensuring direct and one-step access to complex molecules from readily available substrates.¹⁴ A variety of benefits arise from cascade process. There is no need for protection/deprotection procedures or isolation of the intermediates, which reduce time and cost of the overall process. The experimentally-simple strategy offers the potential for rapidly increasing structural and stereochemical complexity. Perhaps more importantly, combining multiple asymmetric catalytic transformations in a domino sequence can also impart increased enantiomeric excess to the final product when compared to the corresponding discrete transformations. This happens when a chiral catalyst can effectively drive, in a stereocontrolled fashion, consecutive catalytic reactions. This phenomenon can be rationalized on the basis of the the Horeau principle, which provides the mathematical foundation for rationalizing the enantioenrichment observed along successive cascade

cycles.¹⁷ Indeed, as portrayed in Figure 4.1, simple calculations reveal that cascade sequences can provide the major diastereomer with exquisite levels of enantiocontrol despite combining catalytic cycles that might be only moderately selective (e.g. 80% ee + 80% ee = 98% ee). The cost paid for an increase in enantioselectivity is always material lost, in the form of undesired diastereomers. The lower ee of a single step, the higher this cost becomes. The minor diastereoisomer is generally formed with very low enantiomeric excess.¹⁸

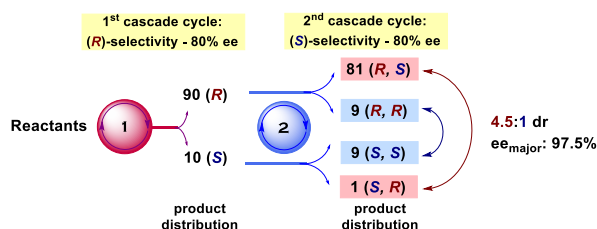


Figure 4.1 Schematic explanation of the Horeau principle and the product enantioenrichment within the cascade. A three-component reaction in which the chiral catalyst promotes two consecutive bond-forming events is considered. It is assumed both of the catalytic steps to infer a 9:1 enantiomeric ratio (80% ee). It is also assumed that no substrate control is operative in the second step of the cascade (no matched/mismatched combination with the chiral catalyst).

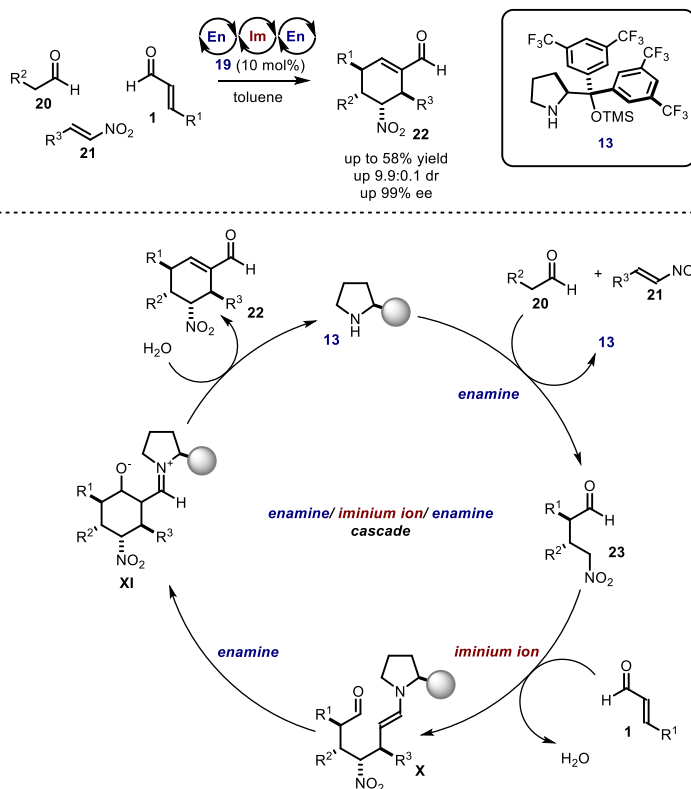
A careful choice of the substrates, and their reactivity, is crucial to accomplish more complex cascade reactions. A remarkable triple cascade process was reported by Enders, who demonstrated the advantages of domino reactions in the synthesis of polyfunctional cyclohexene building blocks **22** (Scheme 4.7).¹⁹ This cascade is a three component reaction of a linear aldehyde **20**, a nitroalkene **21**, an α,β -unsaturated aldehyde **1** and catalyzed by the chiral secondary amine **13**, which is capable of promoting each step of the triple cascade. Mechanistically, the reaction pathway consists of three parts. First, the catalyst **13** activates the aldehyde **20** to form an enamine (not shown), which adds to the nitroalkane **21** in a Michael-type reaction, forming the intermediate **23**, which has now a nucleophilic behavior. Hydrolysis liberates the catalyst **13** that can then condense with the α,β -unsaturated aldehyde **1** to form a chiral iminium ion intermediate, which reacts with nitroalkane **23** in another Michael-type reaction. The last step involves the resulting

¹⁷ F. J. P. Vigneron, M. Dhaenens, A. Horeau, Nouvelle Methode pour Porter au Maximum la Purete Optique d'un Produit Partiellement Dedouble Sans l'Aide d'Acune Substance Chirale, *Tetrahedron*, **1973**, 29, 1055.

¹⁸ J. A. Enquist, Jr, B. M. Stoltz, The Total Synthesis of (2)-Cyanthiwigin F by Means of Double Catalytic Enantioselective Alkylation, *Nature*, **2008**, 453, 1228.

¹⁹ D. Enders, M. R. M. Hüttl, C. Grondal, G. Raabe, Control of Four Stereocentres in a Triple Cascade Organocatalytic Reaction, *Nature*, **2006**, 441, 861.

enamine intermediate **X**, which drives an intramolecular aldol condensation to form the final product **23**. Since the catalyst promotes all the three steps of the cascade, the final adducts, bearing four stereogenic centers, were formed as single enantiomers.

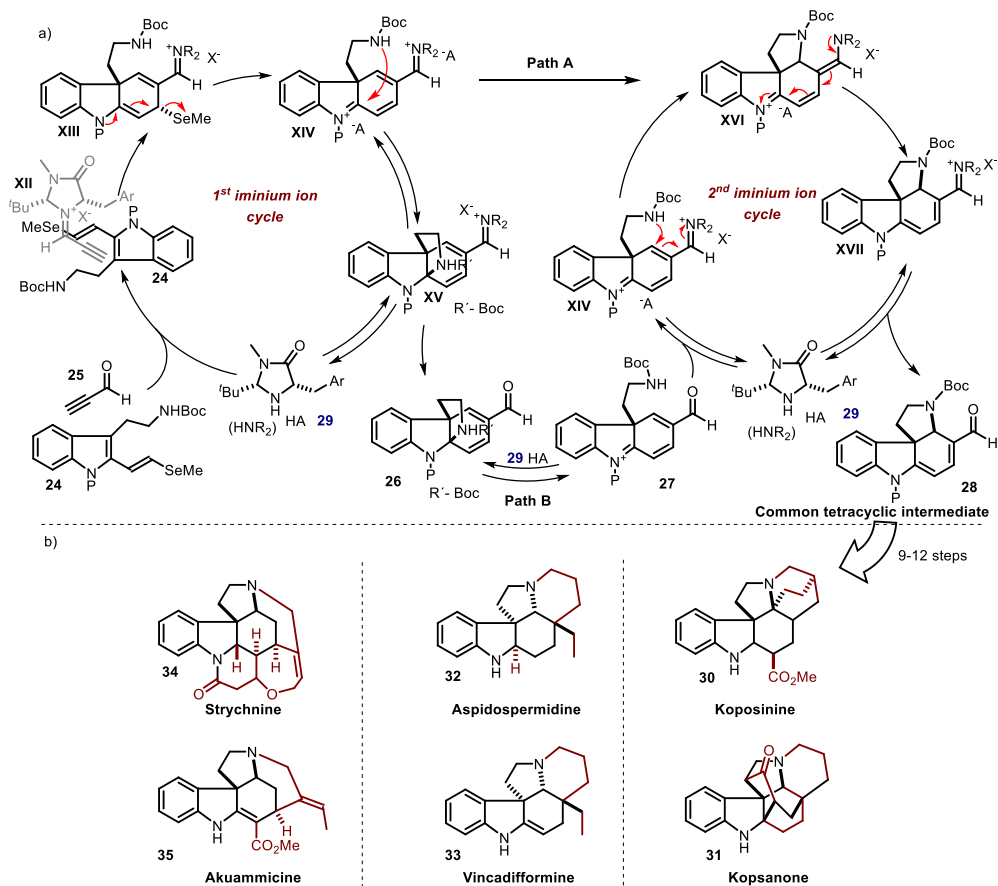


Scheme 4.7 Enantioselective organocatalytic triple cascade reaction. TMS: trimethylsilyl, Im: iminium ion, En: enamine, the filled grey circle represents a bulky substituent on the chiral amine catalyst.

The power of organocascade catalysis has been also demonstrated in the synthesis of many natural products.¹ Due to the rapidly increase of molecular complexity in a single operation, these strategies often open shorter routes for accessing the target molecules. A remarkable collective synthesis of six natural products, by means of organocascade catalysis, was demonstrated by MacMillan in 2011.²⁰ The enantioselective cascade process led to a tetracyclic intermediate **28** endowed with functionalities amenable to the preparation of structurally diverse natural products **30-35** in a few more steps. The

²⁰ S. B. Jones, B. Simmons, A. Mastracchio, D. W. C. MacMillan, Collective synthesis of natural products by means of organo-cascade catalysis, *Nature*, **2011**, 475, 183.

cascade process starts with the enantioselective Diels-Alder reaction of diene **24** with the chiral iminium ion **XII**, generated upon condensation of the chiral secondary amine **29** with propynal **25**. The cycloadduct **XIII** undergoes facile β -elimination of methyl selenide to furnish the unsaturated iminium ion **XIV**. Next, the iminium ion-catalyzed 5-exo-heterocyclization of the carbamate in **XIV** can occur at the δ -position of the indolinium ion (path A) to deliver **XVII** and, after hydrolysis, the enantioenriched spiroindoline core **28**. Alternatively, the intermediate **XIV** can undergo cyclization at the indoline carbon to generate pyrroloindoline **XV**. In this situation, hydrolysis and retro cyclization would afford **27**, which can enter a second catalytic cycle (path B). Next, the intermediate **XIV** can undergo 5-exo-heterocyclization of the pendant carbamate to furnish **28**.



Scheme 4.8 a) Proposed mechanism of organocascade cycles for the generation of a common tetracyclic intermediate **28**. b) Strychnos, Aspidosperma and Kopsia alkaloids prepared by applying enantioselective organocascade strategy. P: protecting group, Boc: tert-butyloxycarbonyl, HA: acid.

This organocascade strategy provides an appealing alternative to the traditional single-target approach. The construction of natural product collections through the assembly of a common intermediate provides researchers with the tools to gain rapid access to large collections of complex molecular architectures.

The field of organocascade catalysis has reached very high level of efficiency and sophistication. The target molecules have become more and more complex, with a trend from simple cascade reactions to triple and even quadruple cascades.²¹ Further expanding the synthetic potential of aminocascade processes would require the introduction of new reactivities, which can go beyond the established boundaries of polar and ionic reaction pathways.

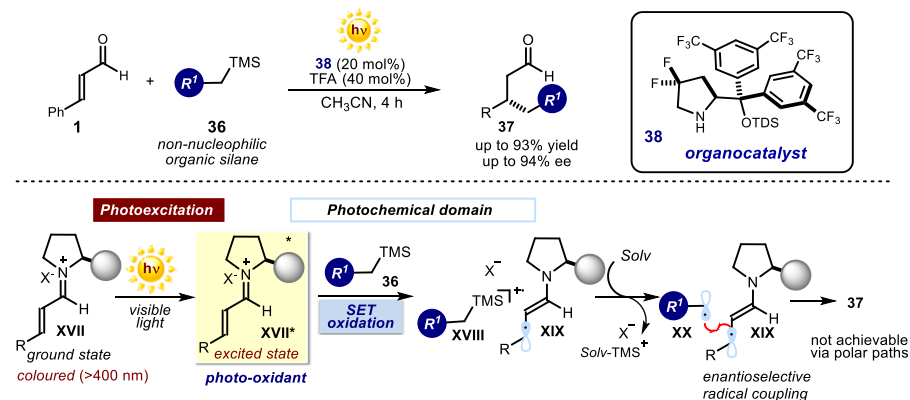
4.4 Enantioselective Iminium Ion Catalysis in the Excited-State

Our research group recently demonstrated that the synthetic potential of enantioselective iminium ion-mediated catalysis can be expanded from the established ground-state domain into the distinct fields of excited-state reactivity²² and enantioselective photochemistry.²³ Visible light excitation brings the electron-poor iminium ion **XVII** to an electronically excited state **XVII***, which can provide further opportunities for reaction invention (Scheme 4.9).² This strategy, where stereoinduction and photoactivation merge in a sole chiral organocatalytic intermediate, enables light-driven enantioselective transformations that cannot be realized using the thermal reactivity of iminium ions. Specifically, it was demonstrated that the photoexcited iminium ion **XVII*** functions as a strong oxidant affording reactive open-shell intermediates **XX** upon single-electron transfer (SET) oxidation of electron-rich substrates. Non-nucleophilic and readily available organic trimethylsilane reagents **36**, which are recalcitrant to classical conjugate addition manifolds, have been successfully used as coupling partners for photochemical functionalization of enals (Scheme 4.9, see also Chapter 2, Scheme 2.17).

²¹ C. Grondal, M. Jeanty, D. Enders, Organocatalytic Cascade Reactions as a New Tool in Total Synthesis, *Nat. Chem.*, **2010**, 2, 167.

²² P. S. Mariano, The Photochemistry of Iminium Salts and Related Heteroaromatic Systems, *Tetrahedron*, **1983**, 39, 3845.

²³ R. Brimiouille, D. Lenhart, M. M. Maturi, T. Bach, Enantioselective Catalysis of Photochemical Reactions, *Angew. Chem. Int. Ed.*, **2015**, 54, 3872.



Scheme 4.9 Light excitation turns chiral iminium ions, which are primarily understood as electrophilic compounds in their ground-state, into strong photo-oxidants. This photochemical strategy allows unconventional β -functionalizations of enals to be realized with high stereocontrol. TDS: thexyldimethylsilyl, TMS: trimethyl silyl, TFA: trifluoroacetic acid, the filled grey circle represents a bulky substituent on the chiral amine catalyst.

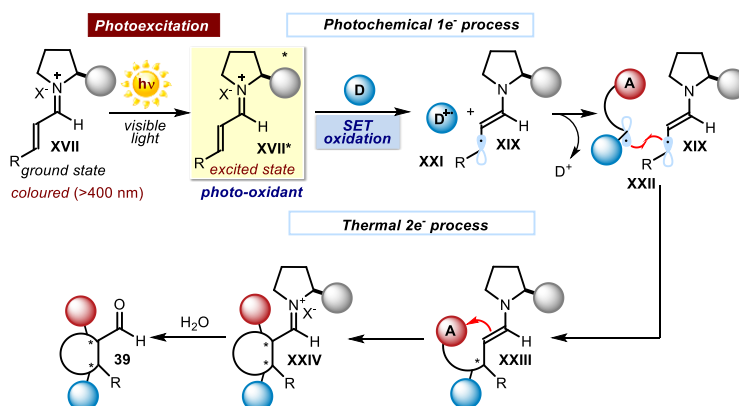
The implication of the iminium ion **XVII** within the photochemical regime was established by investigation of its photophysical behavior. The reduction potential of the excited iminium ion ($E_{\text{red}}^*(\text{XVII}^*/\text{XVII}^-)$), was estimated as +2.3 V (versus Ag/Ag⁺ in CH₃CN) on the basis of electrochemical and spectroscopic measurements.² This established the thermodynamic feasibility of the SET oxidation of **36** (R = phenyl, $E_{\text{ox}}(\text{36}^+/\text{36}) = +1.74$ V). Additional mechanistic studies revealed that substrate **36** (R = phenyl) effectively quenched the excited state of **XVII***, which is consonant with the SET mechanism, triggered by the iminium ion photo-activity, proposed in Scheme 4.9.

The unique reactivity of excited-state chiral iminium ions can uncover previously inaccessible reaction pathways in asymmetric catalysis, while allowing the implementation of novel organocascade reactions.

4.5 Target of the Project

The aim of the research project described in this chapter is to further expand the synthetic applicability of enantioselective organocatalytic cascade reactions. Specifically, our goal is to combine the recently uncovered excited-state reactivity of chiral iminium ions² with the ground-state chemistry of chiral enamines to design cascade processes. This would bring a conceptually new approach to organocascade catalysis, opening new opportunities for the reaction design while combining the fields of enantioselective photochemical radical reactions and classic ground-state organocatalysis. The design plan capitalizes on the generation of photo-excited chiral iminium ions, which can serve as a photo-oxidant

to generate a radical intermediate having two distinct reactive centers. On the one hand, an open-shell center **XXII** that can undergo stereocontrolled radical coupling with the chiral 5π - β -enaminy radical intermediate **XIX**, emerging from the SET reduction of the excited iminium ion. On the other hand, a second electrophilic center, which is unveiled upon the SET oxidation and preserved during the radical coupling step, that can serve as a two-electron acceptor reacting with the ground-state enamine **XXIII**, emerging from the photochemical process (Scheme 4.10). Overall, our design requires a substrate that would be a single-electron donor (D), to participate in the photo-redox process with the excited iminium ion **XVII***, to then unveil an electrophilic position (acceptor A) primed to conventional polar manifolds.



Scheme 4.10 Design plan for an enantioselective photo-organocatalytic cascade process that combines excited-state and ground-state organocatalysis. D: single-electron donor, A: two electron acceptor, SET: single-electron transfer, the filled grey circle represents a bulky substituent on the chiral amine catalyst.

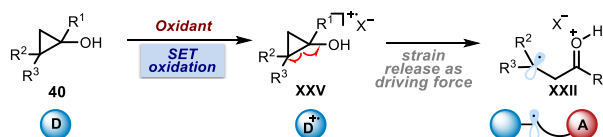
4.6 Results and Discussion

4.6.1 Design Plan

We envisioned that cyclopropanols **40** could serve as suitable substrates for the proposed cascade sequence (Scheme 4.11). Cyclopropanols can undergo a single-electron oxidation processes,²⁴ thus acting as single-electron donors (D) in the reaction with the excited-state iminium ion **XVII***. Removal of one electron from the lone electron pair of

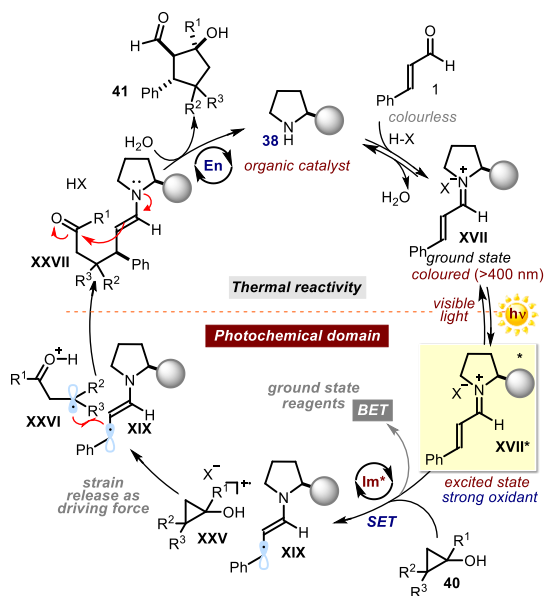
²⁴ For selected reports on the single-electron oxidation of cyclopropanols, see: a) P. S. Mariano, J. Stavinoha, E. Bay, Photochemistry of iminium salts: Electron Transfer Mechanisms for Singlet Quenching and Photoaddition of n-electron Donating Alcohols and Ethers, *Tetrahedron*, **1981**, 37, 19, 3385, b) S. Chiba, Z. Cao, S. A. A. E. Bialy, K. Narasaka, Generation of β -Keto Radicals from Cyclopropanols Catalyzed by AgNO₃, *Chem. Lett.*, **2006**, 35, 18, c) S. Ren, C. Feng, T.-P. Loh, Iron- or silver-catalyzed oxidative fluorination of cyclopropanols for the synthesis of β -fluoroketones, *Org. Biomol. Chem.*, **2015**, 13, 5105.

the oxygen results in the formation of an unstable oxycyclopropyl radical cation **XXV**. Driven by the release of strain energy, this oxycyclopropyl radical cation **XXV** has a strong tendency to undergo rapid ring-opening to form the β -keto radical cation **XXII**. This is a distonic radical species that possesses two distinct reactivity behavior: a radical character, and an electrophilic character (A).



Scheme 4.11 Single-electron oxidation and ring opening of cyclopropanols. SET: single-electron transfer, D: single-electron donor, A: two electron acceptor.

We hypothesized that the intermediate of type **XXII** can serve our purpose to implement a photochemical organocatalytic cascade process. Specifically, we surmised that SET from the electron-rich cyclopropanols **40** to the photo-excited iminium ion **XVII**^{*} would occur to furnish the chiral 5π -electron β -enaminy radical intermediate **XIX**, along with the oxycyclopropyl radical cation **XXV** (Scheme 4.12). Rapid carbon-carbon bond fragmentation would generate the reactive β -keto radical cation **XXVI**. This step plays a decisive role in the redox manifold for it hampers a possible, unproductive back-electron transfer (BET), which would regenerate the starting materials. At this point, a stereocontrolled intermolecular coupling of the chiral β -enaminy radical **XIX** with the distonic radical **XXVI** would form a new carbon-carbon bond while forging the stereogenic center. Next, the resulting ground-state enamine **XXVII** would react with the newly formed ketone in a classical intramolecular aldol reaction, to afford a stereochemically dense cyclopentanol **41**.



Scheme 4.12 Design plan and mechanistic proposal for the enantioselective photo-organocatalytic cascade reaction employing cyclopropanols **40**. SET: single-electron transfer, BET: back electron transfer, Im^* : excited-state iminium ion, En: enamine (ground-state), the filled grey circle represents a bulky substituent on the chiral amine catalyst.

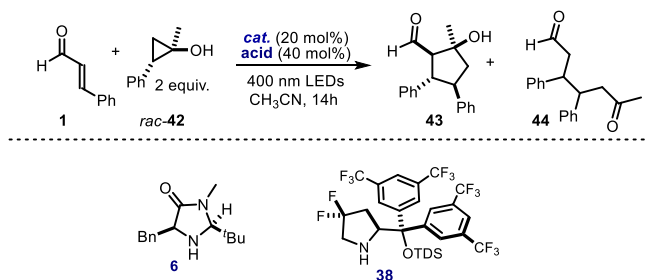
4.6.2 Initial Results

We tested the feasibility of this photochemical cascade strategy by exploring the reaction between cinnamaldehyde **1** and cyclopropanol **42** with the imidazolidinone catalyst **6** in the presence of TFA (trifluoroacetic acid) or diphenyl phosphate. The experiments were conducted under irradiation from a strip containing multiple light emitting diodes (LEDs) with a maximum emission at 400 nm. Pleasingly, the desired product **43**²⁵ was obtained as a single diastereoisomer, albeit with low yield and enantioselectivity, along with the non-cyclized product **44** (Table 4.1).²⁶ No reaction was observed without light irradiation or in the absence of the catalyst, suggesting that the reaction is promoted by the photo-excitation of the iminium ion chromophore (Table 4.1, entries 2 and 3).

²⁵ The relative configuration of **43** was tentatively assigned by comparison of the ¹H NMR spectra and coupling constants with a ketone analogue of **43**, which has been described in the literature. N. Kise, Y. Kitagishi, N. Ueda, Diastereoselective di-Hydrocoupling of Benzalacetones by Electroreduction, *J. Org. Chem.*, **2004**, 69, 959.

²⁶ An assignment of the relative configuration of **44** by NMR spectroscopy was hampered by an overlap of an informative signals on NMR spectra. It was also not possible to determine the ee of **44**.

Table 4.1 Initial experiments.



entry	catalyst	acid	yield 43	ee 43	yield 44
1	6	TFA	18%	0%	27%
2*	6	TFA	0%	0%	0%
3	-	TFA	0%	0%	0%
4	6	Ph ₂ PO ₄ H	7%	9%	11%
5	38	Ph ₂ PO ₄ H	traces	-	6%

Yields determined by ¹H NMR analysis of crude reaction mixtures employing trichloroethylene as a standard, * Performed in the dark. TFA: trifluoroacetic acid, TDS: hexyldimethylsilyl.

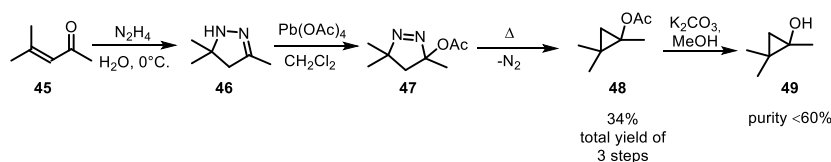
The initial results, presented in Table 4.1, demonstrated the feasibility of our proposal and indicated some limitations related to the use of substrate **42**, since the open adduct **44** was formed as the major product. To account for this product distribution, we hypothesized that the first step of the cascade process (the radical coupling step) results in the formation of two diastereoisomers of **44**, and probably only one of them could undergo the subsequent catalyst-controlled aldol cyclization. Additionally, only traces of the product **43** were observed employing catalyst **38**, which has been previously demonstrated to be the catalyst of choice to promote the photochemical β -alkylation of enals upon iminium ion excitation.²

Based on this, we decided to investigate the reactivity of a different substrate, which could be more suitable for the optimization studies. We decided to use a substrate that would generate only one stereogenic center in the first reaction of the cascade process, since this could greatly simplify the reaction analysis. Additionally, we hoped that the presence of two geminal substituents in the cyclopropanol structure would facilitate the cyclization step favoring formation of the final cyclopentanol.²⁷ This analysis prompted us to select 1,1,2,2-tetra-substituted cyclopropanols of type **49** as potential substrates (Scheme 4.13) for further investigations.

²⁷ M. E. Jung, G. Piizzi, gem-Disubstituent Effect: Theoretical Basis and Synthetic Applications, *Chem. Rev.*, **2005**, *105*, 1735.

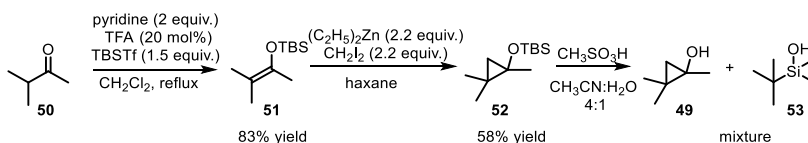
4.6.3 Synthesis of Cyclopropanol **49**

We hypothesized that cyclopropanol **49** could be a suitable substrate for further optimization studies. The synthesis of **49** has been described by DePuy in 1968 (Scheme 4.13).²⁸ The procedure involves the reaction of mesityl oxide **45** with hydrazine to form 3,5,5-trimethyl-2-pyrazoline **46**, which after oxidation with $\text{Pb}(\text{OAc})_4$ and ring contraction, leads to 1,2,2-trimethylcyclopropyl acetate **48** upon extrusion of N_2 . A deprotection of **48** afforded the desired compound **49**. Because of its low boiling point, the isolation of pure **49** was difficult. We did not succeed to isolate compound **49** with satisfactory purity using DePuy's strategy and we decide to develop an alternative synthesis.



Scheme 4.13 Synthesis of cyclopropanol **49** following reported strategy.

Our approach started from the synthesis of silyl enol ether **51** followed by the Simons-Smith cyclopropanation to afford TBS (*tert*-butyldimethylsilyl) protected cyclopropanol **52**²⁹ (Scheme 4.14). Further deprotection of the TBS group afforded the desired cyclopropanol **49**. Unfortunately, a difficult purification step hampered again the isolation of pure **49**. In this case, the difficulty stemmed from the formation of *tert*-butyldimethylsilanol **53**, a side product which was not possible to completely remove from **49**.

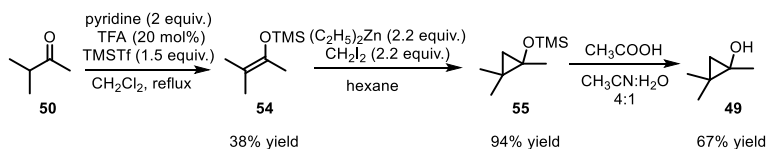


Scheme 4.14 Development of a new strategy to access **49**. TFA: trifluoroacetic acid, TBSTf: *tert*-butyldimethylsilyl trifluoromethanesulfonate, TBAF: tetrabutylammonium fluoride.

²⁸ C. H. DePuy, W. C. Arney, Jr., D. H. Gibson, Chemistry of Cyclopropanols. VI. Cleavage by Electrophilic Halogen, *J. Am. Chem. Soc.*, **1968**, *90*, 1830.

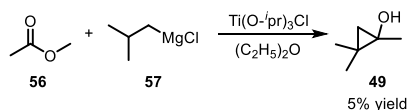
²⁹ We subsequently found that **50** is also a suitable substrate for our photo-organocatalytic cascade reaction and has been employed for most of the optimization studies.

In order to avoid a difficult separation of **49** and **53**, we repeated the reaction sequence using TMS (trimethylsilyl) as the protective group (Scheme 4.15). The trimethylsilanol side product is significantly more volatile than **49** and was easily removed together with the solvent. Another advantage of this synthetic route is that there is no need for any special purification of the last two steps. The cyclopropanation provides a clean reaction so the crude product **55** could be directly used in the next step. The final product **49** was obtained in a pure form by simple extraction with dichloromethane, after treating **55** with acetic acid in an acetonitrile and water mixture (4:1). Additionally, the small amount of solvent needed for the extraction diminishes the loss of highly volatile **49** during the removal of dichloromethane.



Scheme 4.15 A new strategy to access **49**. TFA: trifluoroacetic acid, TMSTf: trimethylsilyl trifluoromethanesulfonate, TMS: trimethylsilyl.

Alternatively, compound **49** can be also accessed using a one-step procedure using a Kulinkovich reaction,³⁰ albeit with very low yield (Scheme 4.16, this method was developed by Giandomenco Magagnano, who joined the project in a later stage of the optimization studies). In general, tetra-substituted cyclopropanols are difficult to obtain through the Kulinkovich reaction, which is a limitation of this reaction.³¹



Scheme 4.16 One step procedure to access **49**.

³⁰ O. L. Epstein, A. I. Savchenko, O. G. Kulinkovich, Titanium(IV) Isopropoxide-catalyzed Reaction of Alkylmagnesium Halides with Ethyl Acetate in the Presence of Styrene. Non-hydride Mechanism of Ligand Exchange in the Titanacyclopropanes, *Tetrahedron Lett.*, **1999**, *40*, 5935.

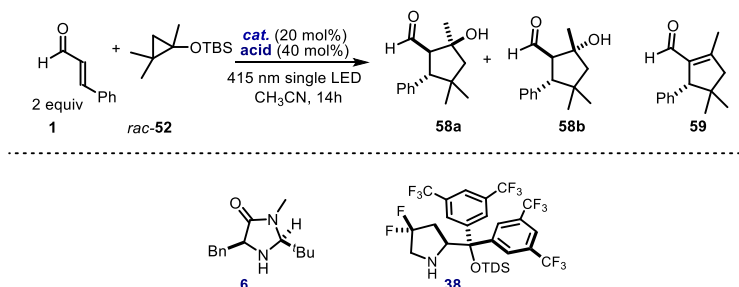
³¹ N. Narsimha Rao, J. K. Cha, Alkoxy-directed Cyclopropanation of 1,1-disubstituted Alkenes with Esters: New Approach to Quaternary Carbon Centers, *Tetrahedron Lett.*, **2015**, *56*, 3298.

4.6.4 Optimization Studies of the Photochemical Organocascade

Since the preparation of the cyclopropanol **49** required many efforts and a long time, optimization studies were started using the O-TBS protected substrate **52**, prepared according to the synthetic route detailed in Scheme 4.13. Silyl protected cyclopropanols often provide a similar reactivity in SET oxidation processes to unprotected cyclopropanols.³² The experiments, detailed in Table 4.2, were conducted under irradiation by a single-LED with maximum emission at 415 nm. The intensity of the single-LED was tuned by using an external power supply (see experimental section for details), which provided better control of the irradiance compared to the previously used LED strip containing multiple LEDs (maximum emission at 400 nm). The reaction catalyzed by the imidazolidinone **6** and using diphenyl phosphate as the acid, which helps iminium ion formation, led to the exclusive formation of the cyclized product **56** as a mixture of two diastereoisomers, with a moderate yield and low enantiomeric excesses. Gratifyingly, when using catalyst **38**, which was purposely designed for photo-iminium ion chemistry, the desired product **58** was obtained with low yield (16% yield), moderate diastereoselectivity (4,1-1 dr) but with a high enantiomeric excess of the major diastereoisomer (90% ee, Table 4.2).

Additionally, a significant amount of aldol condensation side product **59** was generated. The reaction required the presence of a strong acid, like TFA or diphenyl phosphate. Weaker acids such as trichloroacetic acid or benzoic acid derivative were not effective to promote the reaction, probably because of a difficult iminium ion formation.

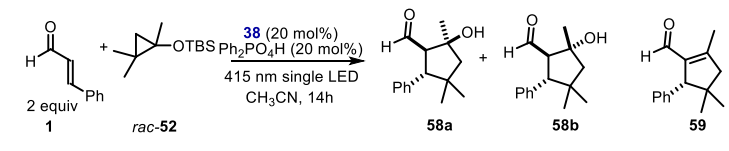
³² H. Rinderhagen, P. A. Waske J. Mattay, Facile Ring Opening of Siloxy Cyclopropanes by Photoinduced Electron Transfer. A New Way to β -keto Radicals, *Tetrahedron*, **2006**, 62, 6589.

Table 4.2 Optimization studies: initial experiments employing substrate **50**.

entry	cat.	acid	yield 58	<i>dr</i> 58a:b	<i>ee</i> 58a:b	yield 59	<i>ee</i> 59
1	6	Ph ₂ PO ₄ H	43%	1.4 : 1	7% : 2%	traces	-
2	38	Ph ₂ PO ₄ H	16%	4.2 : 1	90% : 57%	7%	79%
3	38	TFA	15%	8.0 : 1	90% : 61%	10%	73%
4	38	Cl ₃ CCOOH	traces	-	-	traces	-
6	38	4-CF ₃ C ₆ H ₄ COOH	0%	-	-	0%	-

Yields determined by ¹H NMR analysis of crude reaction mixtures employing trichloroethylene as a standard, TFA: trifluoroacetic acid, TDS: thexyldimethylsilyl, TBS: tert-butyldimethylsilyl.

We observed that, along with the formation of the cyclized product **58**, the adduct **59** was generated, arising from water elimination of the target compound. No open adduct was observed instead. In order to suppress water elimination from **58**, we simply added a small amount of water to the reaction mixture. This almost doubled the yield of product **58**, by preventing the formation of **59** (Table 4.3).

Table 4.3 Optimization studies: influence of water additive.

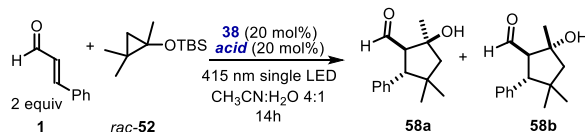
entry	additive	yield 58	<i>dr</i> 58a:b	<i>ee</i> 58a:b	yield 59	<i>ee</i> 59
1	none	16%	4.2 : 1	90% : 57%	7%	79%
2	water	30%	2.3 : 1	90% : 57%	0%	-

Yields determined by ¹H NMR analysis of crude reaction mixtures employing trichloroethylene as a standard. TBS: tert-butyldimethylsilyl.

We then tested again the influence of different acids (Table 4.4). We observed a positive correlation between the strength of the acid and the product yield, but at the expense of the diastereoselectivity. We rationalized this behavior considering that the presence of strong acids somehow facilitates the formation of the second diastereoisomer **58b**. The best result, in terms of yield, was obtained employing trifluoromethanesulfonic acid.

Although a 1 to 1 mixture of diastereoisomers **58a** and **58b** was formed, these stereoisomers could be easily separated by simple column chromatography, and we continued further optimization employing this acid.

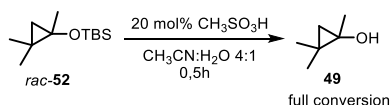
Table 4.4 Optimization studies: influence of the acid.



entry	acid	yield 58	dr 58a:b	ee 58a:b
1	TFA	27%	4.1 : 1	90% : 42%
2	Ph ₂ PO ₄ H	30%	2.3 : 1	90% : 57%
3	CH ₃ SO ₃ H	37%	1.6 : 1	90% : 61%
4	CF ₃ SO ₃ H	46%	1 : 1	90% : 58%

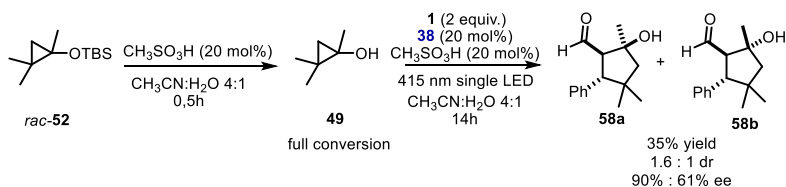
Yields determined by ¹H NMR analysis of crude reaction mixtures employing trichloroethylene as a standard. TBS: tert-butyldimethylsilyl, TFA: trifluoroacetic acid.

Since our reaction conditions (polar solvent and a catalytic amount of a strong acid) should facilitate the deprotection of silyl ethers, we tested whether the unprotected cyclopropanol **49** was generated *in situ* during the reaction. Using NMR spectroscopy, we established that the protected substrate **52** is indeed fully converted into **49** after 30 minutes. The resulting free cyclopropanol **49** was stable in this conditions (Scheme 4.17).



Scheme 4.17 *In situ* generation of **47** under the reaction conditions. TBS: tert-butyldimethylsilyl.

Next, we tested a sequential reaction where the substrate **52** was first mixed in the dark with methyl sulfonic acid for 30 minutes, to afford cyclopropanol **49**, followed by the addition of the other reaction components and light irradiation (Scheme 4.18). This sequential reaction provided almost the same results as the single operation procedure (Table 4.4, entry 3).

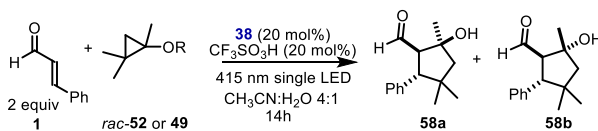


Scheme 4.18 Sequential reaction procedure. TBS: tert-butyldimethylsilyl.

The optimization studies allowed us to obtain product **58** in 46% yield and high enantioselectivity (Table 4.4, entry 4). However, further improvement of the chemical yield under these conditions would be hampered by the full conversion of starting substrate **52**, as inferred by H NMR analysis of the crude reaction mixture. We were not able to detect side products, probably because of their low quantity or very low boiling points, but we hoped that lowering the temperature would slow down any possible side reactions, thus channeling the substrates exclusively through a productive pathway. For this reason, we assembled a reliable single-LED illumination system amenable to temperature control of the reaction (see experimental section for full details). Reactions performed at 0 °C under light irradiation provided higher yields and enantiomeric excesses (Table 4.5). Additionally, higher amounts of the remaining **49** (the deprotected substrate) were observed at the end of the reaction.

At this point of the optimization, we could test the reactivity of unprotected cyclopropanol **49**, since our synthetic endeavors, briefly discussed in a preceding section, to prepare it finally met with success. Substrate **49** was synthesized using the route detailed in Scheme 4.15. The unprotected cyclopropanol provided the same results as substrate **52** (Table 4.5, entries 2 and 3).

Table 4.5 Optimization studies: influence of the temperature and the protecting group.



entry	solvent	R	temp	yield 58	dr 58a:b	ee 58a:b	49 *
1	MeCN:H ₂ O 4:1	TBS	rt	46%	1 : 1	90% : 58%	8%
2	MeCN:H ₂ O 4:1	TBS	0°C	54%	1 : 1.1	95% : 87%	31%
3	MeCN:H ₂ O 4:1	H	0°C	56%	1 : 1.1	95% : 87%	30%
4	MeCN:H ₂ O 6:1	TBS	0°C	61%	1 : 1.1	95% : 87%	31%

Yields determined by ¹H NMR analysis of crude reaction mixtures employing trichloroethylene as a standard. *Unreacted substrate **49** detected at the end of the reaction by ¹H NMR analysis of the crude mixture; TBS: tert-butyldimethylsilyl.

Despite the significant amount of the remaining substrate **49**, the yield of the process could not be further improved by simply increasing the reaction time. This was attributed to the degradation of another important reaction component, the catalyst **38**. We found that only 4 mol% of catalyst **38** was present at the end of the cascade reaction. The catalyst degradation is likely dependent on the SET oxidation of the amine catalyst **38** (not condensed with the cinamaldehyde **1**) by the photo-excited iminium ion **XVII***.³³ This was the main reason that motivated the introduction of the geminal fluorine atoms within the prolinol catalyst scaffold **38** in the original studies on photoexcited iminium ion chemistry.² Indeed, the incorporation of electron-withdrawing fluorine atoms is known to enhance stability towards oxidation, a strategy which is widely used in medicinal chemistry to lower the susceptibility of nearby moieties to enzymatic oxidation.³⁴

Our simple idea for further optimizing the process was to increase the reaction rate in order to generate a higher amount of product **58** before of catalyst **38** decomposition. One possible way to increase the rate of a photo-redox process is to use a co-sensitizer, which can act as a redox mediator.³⁵ The redox mediator is a particular type of compound that can facilitate redox processes with both the photocatalyst and the substrate in separate electron-transfer events, thus positively influencing the reaction rates (Figure 4.2). Many SET processes that are thermodynamically favorable might be kinetically too slow to be useful. A common strategy to address this situation is bypassing one slow SET process with two kinetically more favorable ones by employing redox mediators (Figure 4.2).³⁶ In the oxidative transformation, an excited photocatalyst [PC^n]* would undergo a facile SET process with the redox mediator (RM) to form RM^{+} , which next participates in another rapid SET event with the substrate (sub) to form the sub^{+} reactive species.

³³ The catalyst oxidation from the photoexcited iminium ion triggers the formation of an unstable and highly reactive amine radical cation, resulting in an undesired catalyst degradation path. The nature of the degradation product is still under investigation.

³⁴ B. K. Park, N. R. Kitteringham, P. M. O'Neill, Metabolism of Fluorine-containing Drugs, *Annu. Rev. Pharmacol. Toxicol.*, **2001**, *41*, 443.

³⁵ D. Mangion, D. R. Arnold Photochemical Nucleophile–Olefin Combination, Aromatic Substitution Reaction. Its Synthetic Development and Mechanistic Exploration, *Acc. Chem. Res.*, **2002**, *35*, 297.

³⁶ For selected examples: K. Mizuno, K. Kamiyama, N. Ichinose, N. Otsuji, Photo-oxygenation of 1,2-diarylcyclopropanes via electron transfer, *Y. Tetrahedron*, **1985**, *41*, 2207, M. Riener, D. A. Nicewicz, Synthesis of Cyclobutane Lignans via an Organic Single-Electron Oxidant–Electron Relay System, *Chem. Sci.*, **2013**, *4*, 2625.

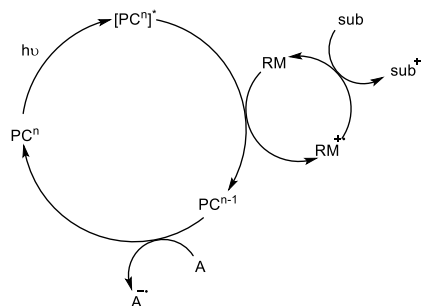


Figure 4.2 Redox mediation of an oxidative transformation. PC: photocatalyst, RM: redox mediator, sub: substrate, A: reductant.

Translating this concept in our system, we wondered if a redox mediator could assist the catalysis by passing the electron between the photo-excited iminium **XVII**^{*} ($[\text{PC}^{\text{II}}]^*$) and cyclopropanol **49** (sub), thus increasing the reaction rate. The addition of biphenyl, a common redox mediator for an oxidative transformations, led to significant increase in yield (product **58** formed in 85% of yield, entry 3 of Table 4.6). Moreover, we observed a higher amount of the remaining catalyst **38** at the end of the reaction. Possible roles of biphenyl in our photochemical reaction will be discussed later in more details.

Table 4.6 Optimization studies: influence of redox mediator.



entry	Additive	yield 58	dr 58a:b	ee 58a:b	38 [*]
1	none	62%	1 : 1.1	95% : 87%	4 mol%
2	0,5 equiv. BP	72%	1 : 1	95% : 86%	6 mol%
3	1 equiv. BP	85%	1 : 1.1	95% : 87%	8 mol%
4	2 equiv. BP	85%	1 : 1.1	95% : 87%	9 mol%

Yields determined by ¹H NMR analysis of crude reaction mixtures employing trichloroethylene as a standard

^{*} catalyst **38** detected at the end of the reaction by H NMR analysis of the crude mixture. TBS: tert-butyldimethylsilyl, BP: biphenyl.

All the reactions presented above were conducted with rigorous exclusion of oxygen. The experiments were performed in Schlenk tubes applying a time-consuming, freeze pump thaw deoxygenation procedure (see experimental sections) to ensure that no traces of oxygen are present in the reaction mixture. When the reaction was performed under air, a diminished yield (41% instead of 85%) was observed. However, a rigorous

deoxygenation procedure (freeze pump thaw) was not necessary and the same reaction efficiency could be obtained performing the experiment in a simple vial using a degassed solvent, which made the reaction set up operationally simpler (see experimental section for full details).

With the optimal conditions in hand, we performed again a control experiment with careful exclusion of light. In this reaction, we could observe only the deprotection of **52** to the cyclopropanol **49**, while neither substrate/reagent consumption nor product formation was detected (Table 4.7, entry 2).

Table 4.7 Optimization studies: reaction set up.

Reaction scheme showing the conversion of 2 equiv of **1** and *rac*-**52** to products **58a** and **58b**. Reagents: **38** (20 mol%), CF₃SO₃H (30 mol%), BP (1 equiv.), 415 nm single LED, CH₃CN:H₂O 6:1, 0°C, 14h.

entry	Set up	yield 58	dr 58a:b	ee 58a:b
1	Shlenk tube	85%	1 : 1.1	95% : 87%
2	Shlenk tube*	0%	-	-
3	Vial	85% (84)**	1 : 1.1	95% : 87%

Yields determined by ¹H NMR analysis of crude reaction mixtures employing trichloroethylene as a standard; * in dark; ** yield of isolated **58**. TBS: tert-butyldimethylsilyl.

We also tested again the reactivity of the unprotected cyclopropanol **49** under the optimal conditions, which yielded product **58** with slightly lower efficiency (81% yield) and similar diastereoselectivity (1:1.4 dr) Table 4.8 entry 2). Exchanging trifluoromethyl sulfonic acid with trifluoroacetic acid, a weaker acid, provided similar yield (80% yield) but a better diastereoselectivity (2.4:1 dr, Table 4.8 entry 3). A final modification was made in the solvent composition. Removal of water resulted in the formation of product **58** with high yield (88% yield) and enantioselectivity (97% ee) and synthetically useful diastereoselectivity (8.4:1 dr, entry 4), and without generation of aldol condensation side product **59** (entries 2-4 in Table 4.8 were performed by Giandomenico Magagnano).

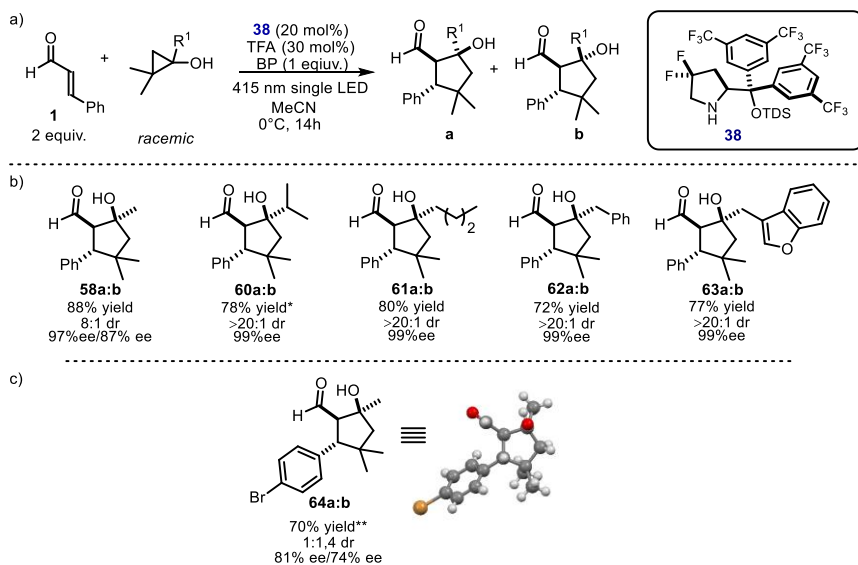
Table 4.8 Optimization studies: influence of the protective group.

entry	solvent	R	Acid	yield 58	dr 58a:b	ee 58a:b
1	MeCN:H ₂ O 6:1	TBS	CF ₃ SO ₃ H	85%	1 : 1.1	95% : 87%
2	MeCN:H ₂ O 6:1	H	CF ₃ SO ₃ H	81%	1 : 1.4	nd
3	MeCN:H ₂ O 6:1	H	TFA	80%	2.4 : 1	nd
4	MeCN	H	TFA	88%	8.4 : 1	97% : 85%

Yields determined by ¹H NMR analysis of crude reaction mixtures employing trichloroethylene as a standard; nd: not determined, TBS: tert-butyldimethylsilyl, TFA: trifluoroacetic acid.

4.6.5 Reaction Scope

With the optimized conditions in hand, we evaluated the synthetic potential of the enantioselective photo-organocatalytic cascade reaction. We tested differently substituted cyclopropanols with cinamaldehyde **1** employing catalyst **38**. A variety of substituents were well tolerated, giving products **58a:b** and **60-63a** with good yield and perfect diastereoselectivity and enantioselectivity (compounds **58a:b**, **61a**, **62a** and **63a** were obtained by Giandomenico Magagnano). Further studies to fully evaluate the scope and limitations of our photochemical cascade reaction is still ongoing in our laboratories. Crystals of compound **64a** were suitable for X-ray crystallographic analysis, which established the stereochemical outcome of the photochemical cascade process.



Scheme 4.19 Photochemical enantioselective photo-organocatalytic cascade reaction of cyclopropanols and cinamaldehyde **1**. a) Reactions performed using the optimized conditions. (b) The scope of the cyclopropanols using cinamaldehyde **1**. Yields are of isolated products; *reaction time: 36h c) The X-ray structure of **64a** is shown, **reaction conditions: Table 4.4 entry 2. TFA: trifluoroacetic acid, BP: biphenyl, TDS: thexyldimethylsilyl.

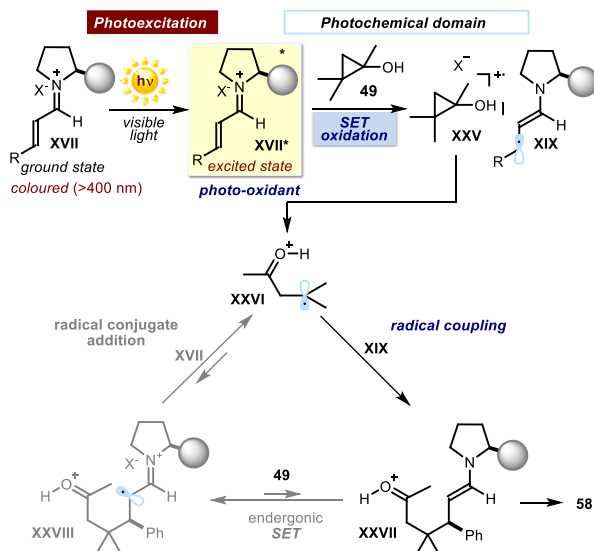
4.6.6 Reaction Mechanism

The Photochemical Step.

Control experiments revealed that the exclusion of light or the absence of the secondary amine catalyst completely suppressed the process. This indicated that the photo-excitation of chiral iminium ion is essential to promote the reaction. The estimated reduction potential of the excited iminium ion (E_{red}^* ($\text{XVII}^*/\text{XVII}^{\cdot-}$)) is +2.30 V (versus Ag/Ag^+ in CH_3CN),² while the reduction potentials of substrates **49** and **52** (E_{ox} ($49^+/\text{49}$) and E_{ox} ($52^+/\text{52}$) are 1.66 V (versus Ag/Ag^+ in CH_3CN), as measured by cyclic voltammetry studies. This indicates that the SET oxidations of **49** and **52** by XVII^* are both thermodynamically feasible. Based on this experimental data and our group's previous studies,² we propose that the condensation of the chiral secondary amine catalyst **38** with enal **1** converts an achromatic substrate into a colored iminium ion XVII . Selective visible-light excitation (>400 nm) provides the electronically excited-state XVII^* through a $\pi-\pi^*$ transition, which functions as a strong SET oxidant (Scheme 4.20). SET from the electron-rich cyclopropanol **49** to photo-excited iminium ion XVII^* occurs to furnish the 5π -electron β -enaminy radical intermediate **XIX** along with the radical cation **XXV**. A

rapid ring-opening of **XXVI** generates the β -keto radical cation intermediate **XXVI**. At this juncture, we propose a stereocontrolled radical coupling of **XXVI** and the chiral 5π - β -enaminy radical intermediate **XIX** to form the new carbon-carbon bond while forging the first stereogenic center.

Alternatively, the β -keto radical cation intermediate **XXVI** could undergo radical conjugate addition to a ground-state chiral iminium ion **XVII**, but this scenario is unlikely. The radical conjugate addition would result in the formation of the unstable intermediate **XXVIII** that tends to undergo reverse reaction to regenerate the more stable iminium ion precursor **XVII**.³⁷ In addition, a fast subsequent SET reduction of the intermediate **XXVIII** would be necessary to generate the enamine **XXVII**, but this process is not feasible because of the endergonic SET from substrate **49** to **XXVIII** (E_{red}^* (**XXVIII**/**XXVII**) $\sim +0.90$ V,² (E_{ox} (**49**⁺/**49**) $+1.66$ V versus Ag/Ag⁺ in CH₃CN).



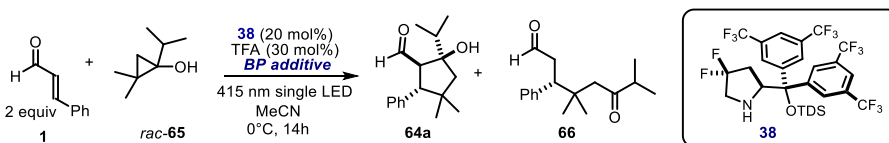
Scheme 4.20 Proposed mechanism of the first step of the cascade reaction. SET: single-electron transfer; the filled grey circle represents a bulky substituent on the chiral amine catalyst.

We were also intrigued by the effect of the biphenyl on the efficiency of our cascade process. The addition of biphenyl was motivated by its established ability to act as a redox

³⁷ a) J. J. Murphy, D. Bastida, S. Paria, M. Fagnoni, P. Melchiorre, Asymmetric Catalytic Formation of Quaternary Carbons by Iminium Ion Trapping of Radicals, *Nature*, **2016**, 532, 218, b) H. J. Jakobsen, S. O. Lawesson, J. T. B. Marshall, G. Schroll, D. H. Williams, Mass spectrometry. XII. Mass spectra of enamines, *J. Chem. Soc. B*, **1966**, 940.

mediator, which can increase reactions rates of the redox processes.³⁶ In this situation, the reaction time necessary to obtain high yield should be significantly shorter. We compared the evolution of the reactions of substrate **65** after 3, 7, and 14 hours, in the presence and in the absence of biphenyl. In this process, we observed the formation of both the cyclized and open products (**64a** and **66**, respectively), as detailed in Table 4.9. Yields refer to the total yields of both products (**64a** + **66**). The same yields (about 53%, entry 1) were obtained after 3 hours, regardless of the presence of biphenyl, which indicated that the additive did not increase the initial rate of the reaction. However, the reaction without biphenyl stopped at the level of 58% yield whilst further reaction progress was observed in the presence of the additive (entries 2 and 3). Additionally, we observed enhanced decomposition of the catalyst **38** in the absence of biphenyl. These results suggest that the biphenyl likely does not act as a redox mediator but might function as a “catalyst protector”. The reduction potential of biphenyl $E_{ox}(\text{BP}^+/\text{BP})$ is +1.90 V (versus Ag/Ag^+ in CH_3CN), a value which is between the redox potentials of substrate **49** ($E_{ox}(\text{49}^+/\text{49}) = +1.66$ V versus Ag/Ag^+ in CH_3CN) and the catalyst **38** ($E_{ox}(\text{38}^+/\text{38}) = +2.20$ V versus Ag/Ag^+ in CH_3CN). This suggests that SET from biphenyl to the excited-state iminium ion **XVII*** can compete with the single-electron oxidation of the catalyst **38**, slowing down catalyst decomposition. The “catalyst protection” seems to be especially important when the process reaches higher conversions of the cyclopropanol **65**, when the substrate/catalyst ratio **65/38** becomes low and the catalyst **38** is more exposed to SET oxidation.

Table 4.9 Reactions with and without biphenyl additive.



entry	time	yield (BP)	38* (BP)	yield (No BP)	38* (No BP)
1	3	54%	19 mol%	53%	17 mol%
2	7	67%	17 mol%	58%	10 mol%
3	14	90%	14 mol%	55%	6 mol%

Total yields of **64a** + **66** determined by ^1H NMR analysis of crude reaction mixtures employing trichloroethylene as a standard, * remaining catalyst **38**, BP: biphenyl, TFA trifluoroacetic acid, TDS: hexyldimethylsilyl. For dr and ee values see table 4.10.

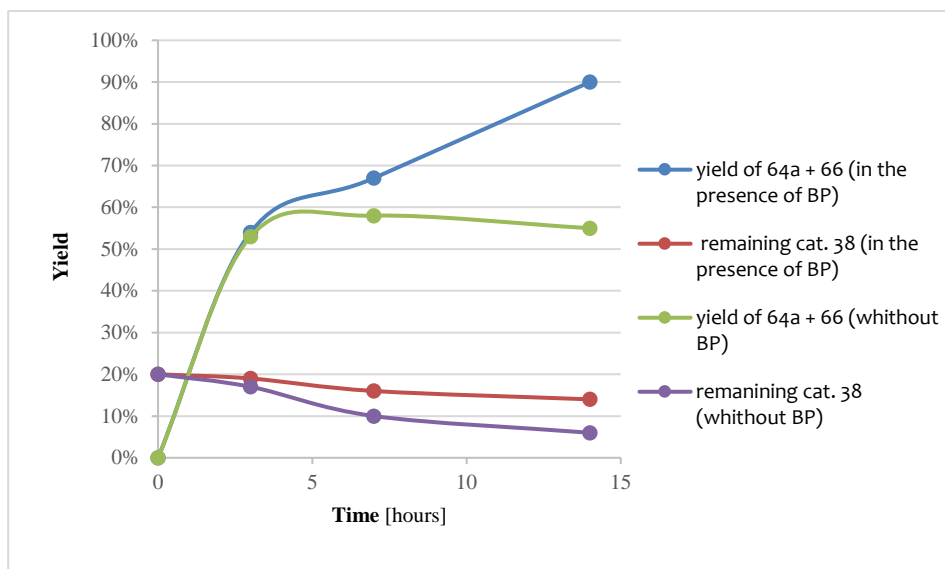


Figure 4.3 Graphic representation of the reaction progress with and without biphenyl additive. BP: biphenyl.

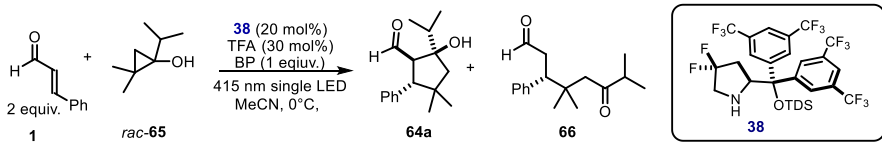
The Ground-state Enamine Step

We were also intrigued by the perfect selectivity observed in the reactions, which led to a single isomer products **60-63a** (single diastereoisomers and single enantiomers, Scheme 4.19). The high enantioselectivity could be explained by statistical product distribution (the Haureau principle), as discussed earlier in this chapter (Figure 4.1).^{17,18} But, according to this model, the generation of a second diastereoisomer of the product with low enantiomeric excess should be observed, which is not consistent with our experimental results. We hypothesized that the generation of a single diastereoisomer of the products **60-63a** could be the result of a kinetic resolution taking place in the enamine-mediated aldol cyclization of the cascade process. This step, which follows the radical coupling event setting the first stereocenter, is responsible for the generation of the additional two stereogenic centers.

We tested this hypothesis employing substrate **65**. In this case, the second step is relatively slow, which allowed us to isolate the non-cyclized adduct **66** and measure its enantiomeric excess. In a first set of experiments, we followed the evolution of the overall light-triggered cascade process using the racemic substrate **65** (Table 4.10). We evaluated the yield and the enantiomeric excess of both the cyclopentanol adduct **64a** and the non-cyclized intermediate **66**. The decreasing optical purity of **66** with the progression of **64a** formation is in line with a kinetic resolution regime governing the enamine-mediated

cyclization event. The catalyst is able to select the major enantiomer of **66**, resulting from the first photochemical step, for selective cyclisation to afford **64a** as a single isomer, while the minor enantiomer of **66** almost does not react.

Table 4.10 Asymmetric amplification by a kinetic resolution of **58b**.



entry	time	yield 64a	ee 64a	yield 66	ee 66
1	3	16%	99%	40%	92%
2	7	30%	99%	37%	90%
3	14	61%	99%	29%	85%
4	36	78%	99%	8%	39%

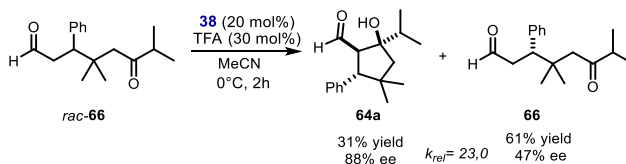
Yields determined by ^1H NMR analysis of crude reaction mixtures employing trichloroethylene as a standard, BP: biphenyl, TFA: trifluoroacetic acid, TDS: thexyldimethylsilyl.

Only a small decrease of the enantiomeric excess of **66** was observed during the first 14 hours (from >92% ee to 85% ee, Table 4.10, entries 1-3). This can be explained by the coexistence of the two enantioselective steps of the cascade process (photo-iminium ion reactivity generating **66** and ground-state enamine chemistry leading to **64a**) and the continuous generation of highly enantioenriched product **66**, of which one enantiomer is slowly consumed in the next step. Later, when most of the substrate **65** was converted into **66**, the resolution of two enantiomers became more apparent (39% ee of the remaining **66**, Table 4.10, entry 4)³⁸.

In a second experiment, detailed in Scheme 4.20, the racemic non-cyclized adduct **66** (synthesized using the racemic imidazolidionone catalyst **4** was mixed with the enantiopure catalyst **38** and trifluoroacetic acid for 2 hours and without light irradiation. The formation of a single diastereoisomer of cyclopentanol **64a** was observed in 31% yield and 88% ee, while the starting material **66** was enantioenriched. As expected, the unreacted intermediate **66** had the opposite absolute configuration than the same adduct **66** generated in the experiment depicted in Table 4.10. Overall, this experiment confirmed that also the enamine-mediated cyclization step is under the control of the chiral catalyst. The two stereocontrolled steps of the reaction sequentially combine to drive the formation

³⁸ Notably, the enantiomeric composition of the racemic cyclopropanol substrate remained racemic during the reaction, indicating that a kinetic resolution of cyclopropanol was not operative and that the SET oxidation was unselective.

of the final product essentially as a single stereoisomer. The second step “corrects” the original stereoselectivity of the photochemical step (about 92% ee, as inferred by entry 1 in Table 4.10), selecting exclusively the major enantiomer of the open product for the cyclization. This fortunate and synergistic combination eventually induces an effective kinetic resolution. The selectivity factor (k_{rel}) was estimated as 23.0 using Eq.1³⁹ where c is yield of the product **64a** (31% yield) and ee is the enantiomeric excess of **64a** (88% ee).

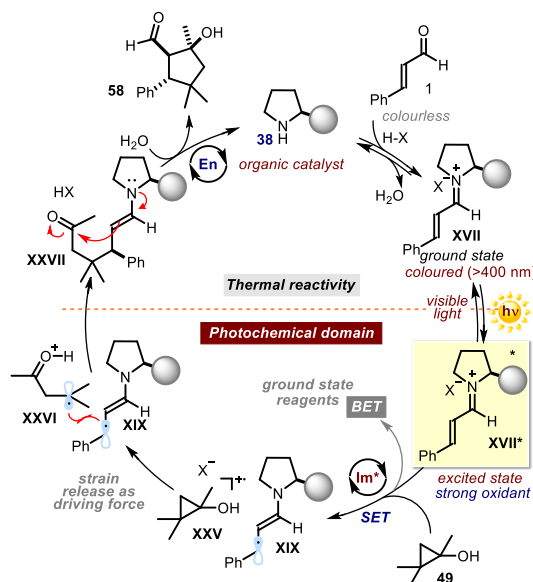


Scheme 4.21 Kinetic resolution of racemic **66**. TFA: trifluoroacetic acid.

$$k_{rel} = \frac{\ln[1-c(1+ee)]}{\ln[1-c(1-ee)]} \quad (1)$$

The overall proposed mechanism is shown in Scheme 4.22, where the two processes of the cascade reaction are presented together.

³⁹ J. M. Keith, J. F. Larrow, E. N. Jacobsen, Practical Considerations in Kinetic Resolution Reactions, *Adv. Synth. Catal.*, **2001**, *343*, 5



Scheme 4.22 Proposed mechanism of the photo-organocatalytic cascade reaction. SET: single-electron transfer, BET: back electron transfer, Im^* : excited-state iminium ion, En: enamine (ground-state), the filled grey circle represents a bulky substituent on the chiral amine catalyst.

4.7 Conclusions and Remarks

In conclusion, we developed an enantioselective photo-organocatalytic cascade reaction by combining the photochemical excited-state reactivity of chiral iminium ions with the ground-state reactivity of enamines. This study demonstrates a novel approach in the design of cascade sequences indicating a new avenue for the development of domino processes. Mechanistic investigations revealed the origin of the asymmetric amplification and provided mechanistic information that could be pertinent for the development of new cascade processes. Moreover, the photo-organocatalytic cascade reaction leads to stereochemically complex cyclopentanol, with high yield and excellent selectivity that cannot be accessed by any other method.

4.8 Experimental Section

The NMR spectra were recorded at 400 MHz and 500 MHz for ^1H , 101 or 126 MHz for ^{13}C and 376 MHz for ^{19}F . The chemical shift (δ) for ^1H and ^{13}C are given in ppm relative to residual signals of the solvents (CHCl_3 @ 7.26 ppm ^1H NMR and 77.16 ppm ^{13}C NMR, and tetramethylsilane @ 0 ppm). Coupling constants are given in Hertz. The following abbreviations are used to indicate the multiplicity: s, singlet; d, doublet; q, quartet; p, pentet; sept, septet; m, multiplet; br, broad signal. High-resolution mass spectra (HRMS) were obtained from the ICIQ High Resolution Mass Spectrometry Unit on MicroTOF Focus and Maxis Impact (Bruker Daltonics) with electrospray ionization. X-ray data were obtained from the ICIQ X-Ray unit using a Bruker-Nonius diffractometer equipped with an APPEX 2 4K CCD area detector. Optical rotations are reported as follows: $[\alpha]_{\text{D}}^{\text{T}}$ (c in g per 100 mL, solvent). Cyclic voltammetry studies were carried out on a Princeton Applied Research PARSTAT 2273 potentiostat offering compliance voltage up to ± 100 V (available at the counter electrode), ± 10 V scan range and ± 2 A current range.

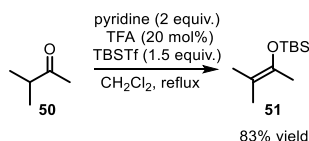
General Procedures. All reactions were performed under an argon atmosphere in oven-dried glassware using standard Schlenk techniques, unless otherwise stated. Synthesis grade solvents were used as purchased, anhydrous solvents were obtained using a commercial SPS (solvent purification system). Chromatographic purification of products was accomplished using force-flow chromatography (FC) on silica gel (35-70 mesh). For thin layer chromatography (TLC) analysis throughout this work, Merck pre-coated TLC plates (silica gel 60 GF254, 0.25 mm) were employed, using UV light as the visualizing agent and Hanessian's stain solution, ethanol solution of phosphomolybdic acid or basic aqueous potassium permanganate (KMnO_4) stain solutions and heat as developing agents. Organic solutions were concentrated under reduced pressure on a Büchi rotary evaporator (*in vacuo* at 40 °C, ~5 mbar).

Determination of Enantiomeric Purity. HPLC analysis on chiral stationary phase was performed on an Agilent 1200-series instrument, employing Daicel Chiralpak IC-3 chiral column, or a Waters ACQUITY® UPC² instrument, using a Daicel Chiralpak IC-3, ID-3, IA, CEL1 chiral columns. The exact conditions for the analyses are specified within the characterization section. HPLC/UPC² traces were compared to racemic samples prepared performing the reaction in the presence of racemic catalyst **6**.

Materials. Commercial grade reagents and solvents were purchased from Sigma-Aldrich, Fluka, Alfa Aesar, Fluorochem, SynQuest and used as received, without further purifications. Cyclopropanol **42** was prepared according to the procedure described in

literature.⁴⁰ Catalyst **38** was synthesized according to the procedure described in literature.²

Synthesis of Starting Materials



Scheme 4.23 Synthesis of **51**.

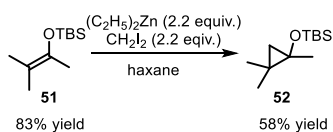
Ketone **50** (16 mmol, 1.378 g, 1.71 mL) was placed in an oven dried 2 neck 250 mL flask equipped with reflux condenser and dissolved in anhydrous DCM (40 mL). Next, pyridine 32 mmol, 2.530 g, 2.59 mL) and trifluoroacetic acid (3.2 mmol, 0.365 g, 0.25 mL) were added to this mixture, which was then heated to reflux. *Tert*-butyldimethylsilyl trifluoromethanesulfonate (24.00 mmol, 6.34 g 5.51 mL) was added to this mixture over 1h using syringe pump, while refluxing. After complete addition the reaction mixture was stirred at reflux for 2h. The reaction mixture was cooled down to room temperature and carefully concentrated. The crude mixture was dissolved in pentane and washed with saturated NaHCO₃ and brine. The organic phase was dried over sodium sulfate and carefully concentrated. The crude mixture was purified on deactivated silica gel (silica gel treated with 2.5% of Et₃N) using pentane to give **51** as a colorless oil (2.65 g, 83% yield).

¹H NMR (400 MHz, CDCl₃) δ 1.82 – 1.78 (m, 3H), 1.63 – 1.58 (m, 6H), 0.97 (s, 9H), 0.13 (s, 6H).

¹³C NMR (75 MHz, CDCl₃) δ 140.2, 109.2, 25.9, 25.7, 19.0, 18.5, 18.2, 17.6, -3.8.

HRMS calculated for C₁₁H₂₅OSi (M+H): 201.1669, found: 201.1666.

⁴⁰ O. L. Epstein, A. I. Savchenko, O. G. Kulinkovich, Titanium(IV) Isopropoxide-catalysed Reaction of Alkylmagnesium Halides with Ethyl Acetate in the Presence of Styrene. Non-Hydride Mechanism of Ligand Exchange in the Titanacyclopentanes, *Tetrahedron Lett.*, **1999**, *40*, 5935.

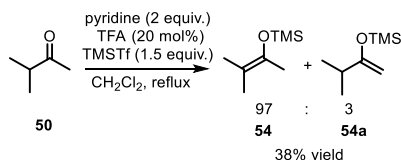
**Scheme 4.24** Synthesis of **52**.

Silyl enol ether **51** (7.24 mmol, 1.45 g) was placed in oven dried 100 mL two neck flask followed by addition Et_2Zn (15.9 mmol, 15.9 mL, 1M, hexanes). The mixture was cooled down to 0°C and diiodomethane (15.9 mmol, 4.26 g, 1.28 mL) was slowly added. The mixture was stirred at 0°C for 15 min and warm to rt and stirred for 2h. After that time reaction mixture was quenched by saturated NH_4Cl and washed with saturated $NaHCO_3$. The aqueous phase was washed with pentane and combined organic layers were dried over sodium sulfate. The solvent was evaporated to give **52** as a colorless oil (900 mg, 58% yield).

1H NMR (400 MHz, $CDCl_3$) δ 1.40 (s, 3H), 1.16 (s, 3H), 1.05 (s, 3H), 0.89 (s, 9H), 0.44 (d, $J = 5.2$ Hz, 1H), 0.22 (d, $J = 5.1$ Hz, 1H), 0.15 (s, 3H), 0.12 (s, 3H).

^{13}C NMR (101 MHz, $CDCl_3$) δ 60.3, 27.0, 25.8, 22.2, 21.9, 20.7, 20.7, 20.5, 18.0, -3.2, -3.7.

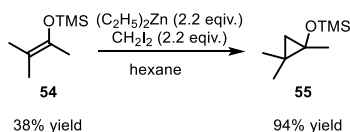
HRMS calculated for $C_{12}H_{27}OSi$ (M+H): 215.1826, found: 215.1825.

**Scheme 4.25** Synthesis of **55**.

Ketone **50** (58 mmol, 5 g, 6.2 mL) was placed in an oven dried 2 neck 500 mL flask equipped with reflux condenser and dissolved in anhydrous DCM (150 mL). Next, pyridine (116 mmol, 9.18 g, 9.39 mL) and trifluoroacetic acid (11.6 mmol, 1.32 g, 0.89 mL) were added to this mixture, which was then heated to reflux. Trimethylsilyl trifluoromethanesulfonate (87 mmol, 19.35g, 15.76 mL) was added to this mixture over 3h using syringe pump, while refluxing. After complete addition the reaction mixture was stirred at reflux for 2h. The reaction mixture was cooled down to room temperature filtrated and carefully concentrated. The crude mixture was dissolved in pentane and washed with saturated sodium bisulfate and brine. The organic phase was dried over

sodium sulfate and carefully concentrated. The crude mixture was purified by vacuum distillation (52–58°C, 70 mBar) to give a mixture of thermodynamic **54** and kinetic products **54a** (**54:54a**, 97:3) as a colorless oil (3.5 g, 38% yield).

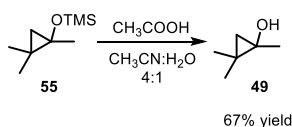
54: $^1\text{H NMR}$ (400 MHz, CDCl_3) δ 1.82 – 1.76 (m, 3H), 1.62 – 1.57 (m, 6H), 0.18 (s, 9H). Spectral data match with the ones reported in literature.⁴¹



Scheme 4.26 Synthesis of **55**.

Silyl enol ether **54** (22.1 mmol, 3.5 g) was placed in oven dried two neck 250 mL two neck flask followed by addition Et_2Zn (48.6 mmol, 48.6 mL, 1M, hexanes). The mixture was cooled down to 0°C and diiodomethane (48.6 mmol, 13.03 g, 3.9 mL) was slowly added. The mixture was stirred at 0°C for 15 min and warm to rt and stirred for 2h. After that time reaction mixture was quenched by saturated NH_4Cl and washed with saturated NaHCO_3 . The aqueous phase was washed with pentane and combined organic layers were dried over sodium sulfate. The solvent was evaporated to give fairly pure **55** as a colorless oil (3.6 g, 94% yield, approximately 90% purity). Compound **55** was used directly in the next step without further purification.

$^1\text{H NMR}$ (400 MHz, CDCl_3) δ 1.42 (s, 3H), 1.15 (s, 3H), 1.06 (s, 3H), 0.48 (d, $J = 5.1$ Hz, 1H), 0.22 (d, $J = 5.2$ Hz, 1H), 0.17 (s, 9H).



Scheme 4.27 Synthesis of **49**.

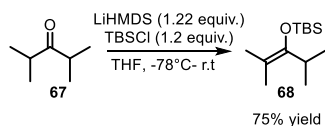
55 (17.4 mmol 3 g) was dissolved in 3,4 mL of MeCN and 0.9 mL of water, followed by addition of acetic acid (8.7 mmol, 523 mg, 1.05 mL). The mixture was stirred for 15 min at room temperature, which lead to full consumption of **55** (indicated by TLC analysis: solvent pentane). The mixture was diluted with DCM and washed with water and brine.

⁴¹ H. P. Beutelman, L. Xie, W. H. Saunders, Jr, Deuterium Isotope Effects and the Mechanism of Kinetic Enolate, *J. Org. Chem.* **1989**, 54, 1703.

The organic layer was dried over sodium sulfate and the solvent was carefully evaporated to give product **49** as a colorless liquid (1.17 g, 37% yield).

$^1\text{H NMR}$ (400 MHz, CHCl_3) δ 1.45 (s, 3H), 1.21 (s, 3H), 1.07 (s, 3H), 0.49 (d, $J = 5.2$ Hz, 1H), 0.27 (d, $J = 5.2$ Hz, 1H).

$^{13}\text{C NMR}$ (101 MHz, CDCl_3) δ 59.0, 26.7, 22.1, 21.5, 21.5, 20.2, 18.3.



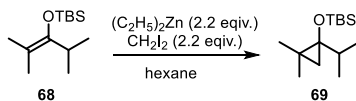
Scheme 4.28 Synthesis of **68**.

The ketone **67** (7.44 mmol, 1.055 mL) was placed in an oven-dried flask sealed with a septum and under argon atmosphere and dissolved in anhydrous THF (30 mL). The solution was cooled to -78°C and a solution of LiHMDS (9.08 mmol, 9.08 mL, 1 M, THF) was added dropwise. The cold bath was removed and the pale yellow solution was stirred for 1 hour at room temperature. The reaction was cooled to -78°C and the *tert*-butylchlorodimethylsilane chloride (8.9 mmol, 1.268 g) dissolved in THF (10 mL) was added dropwise. The reaction mixture was warmed up to room temperature and was stirred for 18h hours. Next, the mixture was diluted with Et_2O and washed with saturated aqueous NH_4Cl . The aqueous phase was washed with E_2O (20 ml x3) and combined organic phases were washed with brine and dried over sodium sulfate. Solvent was evaporated and the resulting orange oil was purified by column chromatography on triethylamine-deactivated silica (silica gel treated with 2.5% Et_3N ; solvent pentane) to give the product **68** (1.268 g, 75% yield).

$^1\text{H NMR}$ (400 MHz, CHCl_3) δ 2.78 (hept, $J = 7.0$ Hz, 1H), 1.63 – 1.60 (m, 3H), 1.59 (s, 3H), 1.02 (s, 3H), 1.00 (s, 3H), 0.98 (s, 9H).

$^{13}\text{C NMR}$ (101 MHz, CDCl_3) δ 148.8, 107.1, 29.8, 26.4, 20.0, 19.0, 19.0, 18.8, -3.1.

HRMS calculated for $\text{C}_{13}\text{H}_{29}\text{OSi}$ (M+H): 229.1982, found: 229.1980



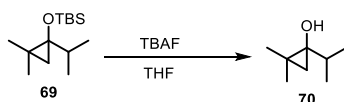
Scheme 4.29 Synthesis of **69**.

Silyl enol ether **68** (14.5 mmol, 3.3 g) was placed in oven dried two neck 250 mL two neck flask followed by addition Et_2Zn (31.8 mmol, 31.8 mL, 1M, hexanes). The mixture was cooled to $0^\circ C$ and diiodomethane (31.8 mmol, 8.51 g, 2.56 mL) was slowly added. The mixture was stirred at $0^\circ C$ for 15 min and warmed to rt and stirred for 2h. After that time reaction mixture was quenched by saturated NH_4Cl and washed with saturated $NaHCO_3$. The aqueous phase was washed with pentane and combined organic layers were dried over sodium sulfate. The solvent was evaporated to give the product **69** as a colorless oil (3.5 g, 86% yield).

1H NMR (400 MHz, $CHCl_3$) δ 1.43 (hept, $J = 6.9$ Hz, 1H), 1.12 (s, 3H), 1.09 (s, 3H), 0.99 (dd, $J = 6.9, 4.0$ Hz, 6H), 0.90 (s, 9H), 0.50 (d, $J = 5.6$ Hz, 1H), 0.20 (d, $J = 5.6$ Hz, 1H), 0.12 (s, 3H), 0.04 (s, 3H).

^{13}C NMR (101 MHz, $CDCl_3$) δ 67.6, 33.2, 26.2, 25.0, 22.7, 20.8, 20.7, 19.5, 18.8, 18.6, -1.8, -2.8.

HRMS calculated for $C_{14}H_{31}OSi$ (M+H): 243.2139, found: 243.2138.

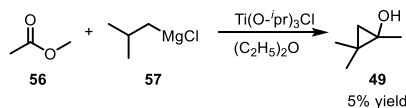


Scheme 4.30 Synthesis of **70**

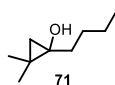
To **69** (12.4 mmol, 3 g.) dissolved in anhydrous THF (10 ml) was added TBAF (tetrabutylammonium fluoride, 24.7 mmol, 24.7 ml, 1M, THF). The mixture was diluted with Et_2O and washed with water. The aqueous layer was washed with Et_2O (3x 20 mL). The combined organic layers were washed with brine, dried over sodium sulfate and the solvent was carefully evaporated. The crude mixture was purified by flash chromatography 2% Et_2O /pentane to give product **70** as a colorless oil (640 mg, 40% yield).

1H NMR (500 MHz, $CDCl_3$) δ 1.56 (s, 1H), 1.57 – 1.46 (m, 1H), 1.23 (s, 3H), 1.13 (s, 3H), 1.09 (d, $J = 6.9$ Hz, 3H), 1.03 (d, $J = 6.8$ Hz, 3H), 0.44 (d, $J = 5.1$ Hz, 1H), 0.24 (d, $J = 5.2$ Hz, 1H).

^{13}C NMR (126 MHz, $CDCl_3$) δ 65.9, 32.2, 26.1, 22.8, 21.6, 20.8, 18.4, 18.1.

General Procedure A for Synthesis of Cyclopropanols**Scheme 4.31** Synthesis of **49** in Kulinkovich reaction.

To a stirred solution of methyl acetate **56** (60 mmol, 4,77 mL) and triisopropoxytitanium chloride (24,00 mmol, 5,74 mL, in Et_2O 80 ml) was added a solution of isobutylmagnesium chloride **57** (180 mmol, 90 mL, 2M, Et_2O) in the same solvent using syringe pump over a period of 4 h at 18-20 °C (water bath). After complete addition, the mixture was stirring for another 2 hours. The mixture was then poured into cooled (5°C) 10% H_2SO_4 and extracted with Et_2O . The combined Et_2O extracts were washed with water, dried over sodium sulfate and the solvent was carefully evaporated. The crude mixture was purified by flash chromatography 2% Et_2O /pentane to give product **49** a colorless oil (300 mg, 5% yield).



1-butyl-2,2-dimethylcyclopropan-1-ol (71). Prepared according to general procedure A using methyl pentanoate (22 mmol, 2.556 g, 2.92 ml), triisopropoxytitanium chloride (5,5 mmol, 1314 mL, in Et_2O 20 ml) and isobutylmagnesium chloride **57** (55 mmol, 27.5 mL, 2M, Et_2O). The crude mixture was purified by flash chromatography 2% Et_2O /pentane to give product **71** a colorless oil (577 mg, 18% yield).

$^1\text{H NMR}$ (400 MHz, CHCl_3) δ 1.79 – 1.33 (m, 6H), 1.21 (s, 3H), 1.08 (d, $J = 0.8$ Hz, 3H), 0.98 – 0.89 (m, 3H), 0.45 (d, $J = 5.2$ Hz, 1H), 0.26 (dd, $J = 5.2, 1.0$ Hz, 1H).

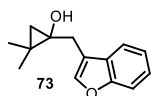
$^{13}\text{C NMR}$ (101 MHz, CDCl_3) δ 62.3, 34.9, 28.3, 26.1, 22.9, 22.1, 21.8, 20.5, 14.1.



1-benzyl-2,2-dimethylcyclopropan-1-ol (72) Prepared according to general procedure A using ethyl-2-phenylacetate (10 mmol, 1.642 g, 1.59 mL), tetraisopropoxytitanium (2.5 mmol, 0.711g, 0.740 mL, in 12 ml of Et_2O) and isobutylmagnesium chloride **57** (24 mmol, 12 mL, 2M, Et_2O). The crude mixture was purified by flash chromatography 2% Et_2O /pentane to give product **72** a colorless oil (254 mg, 14% yield).

$^1\text{H NMR}$ (400 MHz, CHCl_3) δ 7.39 – 7.24 (m, 5H), 3.02 (s, 2H), 1.27 (s, 3H), 1.24 (s, 3H), 0.58 (d, $J = 5.3$ Hz, 1H), 0.53 (d, $J = 5.3$ Hz, 1H).

$^{13}\text{C NMR}$ (126 MHz, CDCl_3) δ 138.9, 129.2, 128.6, 126.4, 62.1, 40.7, 25.9, 22.83, 22.1, 20.4.



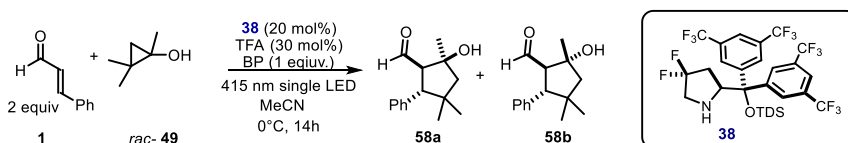
1-(benzofuran-3-ylmethyl)-2,2-dimethylcyclopropan-1-ol (73).

Prepared according to general procedure A using methyl 2-(benzofuran-3-yl)acetate (7.89 mmol, 1.5g), tetraisopropoxytitanium (2.37 mmol, 0.617g, 0.57 mL, in 8 ml of Et₂O) and isobutylmagnesium chloride **57** (23.7 mmol, 11.8 mL, 2M, Et₂O). The crude mixture was purified by flash chromatography 3% Et₂O/pentane to give product **72** a colorless oil (427 mg, 25% yield).

¹H NMR (400 MHz, CHCl₃) δ 7.64 (ddd, *J* = 7.6, 1.4, 0.7 Hz, 1H), 7.58 (t, *J* = 1.2 Hz, 1H), 7.52 (dt, *J* = 8.2, 0.9 Hz, 1H), 7.34 (ddd, *J* = 8.3, 7.2, 1.4 Hz, 1H), 7.31 – 7.25 (m, 1H), 3.10 – 3.01 (m, 2H), 1.29 (s, 3H), 1.24 (s, 3H), 0.62 (dd, *J* = 5.3, 0.7 Hz, 1H), 0.55 (d, *J* = 5.3 Hz, 1H).

¹³C NMR (126 MHz, CDCl₃) δ 155.4, 142.4, 128.5, 124.3, 122.5, 120.0, 117.5, 111.5, 61.4, 29.4, 26.5, 22.4, 22.6, 20.4.

General Procedure B for the Enantioselective Photochemical Organocascade Reaction



Scheme 4.32 General procedure B for the enantioselective photochemical organocascade reaction.

To a 5 mL argon-purged glass vial, containing the amine catalyst **38** (0.02 mmol, 14 mg), and the biphenyl (BP) (0.1 mmol, 15 mg) was added 350 μL of an argon-sparged acetonitrile solution of TFA (trifluoroacetic acid, 0.03 mmol). Cinnamaldehyde **1** (0.2 mmol, 26 mg, 0.025 mL) and cyclopropanol **49** (0.1 mmol, 10 mg) were added at the end. The vial was sealed with Parafilm, and then placed into a platform (0°C), mounted on an aluminium block fitted with a 415 nm high-power single LED ($\lambda = 415$ nm, irradiance = 26 mW/cm², as controlled by an external power supply; the set-up is detailed in Figure 4.4). This set-up secured a reliable irradiation while keeping a constant distance between the reaction vessel and the light source at 0°C. The reaction was stirred under visible light irradiation at 0°C for the indicated time (generally 14 hours). Then the reaction mixture was diluted with CHCl₃ and washed with saturated NaHCO₃. The aqueous layer was washed twice with CHCl₃ and the combined organic layers were washed with brine and dried over sodium sulfate. Solvent was evaporated and the crude mixture was purified by column chromatography on silica gel to furnish the product in the stated yield and enantiomeric purity.

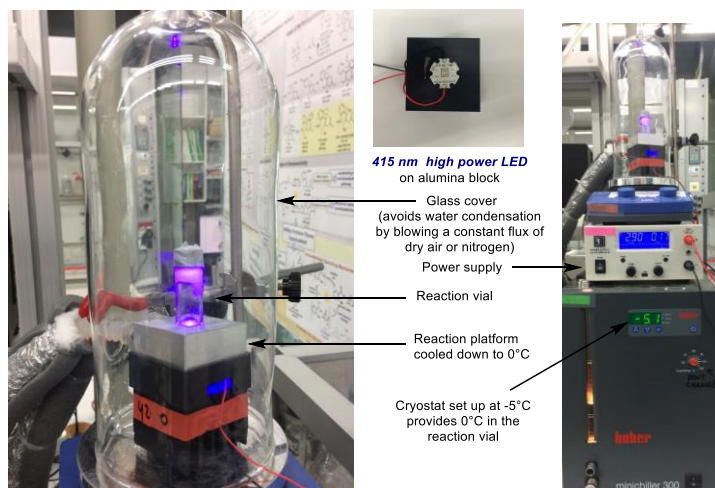
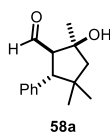


Figure 4.4 Reaction set up photochemical organo-cascade process

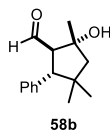


(1R,2S,5R)-2-hydroxy-2,4,4-trimethyl-5-phenylcyclopentane-1-carbaldehyde (58a). Prepared according to general procedure B. Time of irradiation: 14 hours. The crude mixture was purified by flash column chromatography (AcOEt: hexane 5-30%) to afford the product **58a** (19 mg, 80% yield, 97% ee, average of two runs). The enantiomeric excess was determined to be 97% by HPLC analysis on a Daicel Chiralpak IC-3 column: 92:8 hexane/IPA, flow rate 0.8 mL/min, $\lambda = 215$ nm: $\tau_{\text{Minor}} = 12.5$ min, $\tau_{\text{Major}} = 16.1$ min.. Absolute configuration determined in comparison to compound **64a**.

$^1\text{H NMR}$ (300 MHz, CDCl_3) δ 9.66 (d, $J = 2.2$ Hz, 1H), 7.37 – 7.28 (m, 2H), 7.27 – 7.19 (m, 3H), 3.63 (d, $J = 13.3$ Hz, 1H), 3.14 (dd, $J = 13.3, 2.2$ Hz, 1H), 2.34 (s, 1H), 1.97 (d, $J = 14.2$ Hz, 1H), 1.86 (d, $J = 14.1$ Hz, 1H), 1.55 (s, 3H), 1.19 (s, 3H), 0.67 (s, 3H).

$^{13}\text{C NMR}$ (101 MHz, CDCl_3) δ 205.6, 137.6, 128.7, 128.2, 126.9, 79.2, 63.1, 57.5, 55.7, 40.69, 29.7, 29.6, 26.0.

HRMS calculated for $\text{C}_{15}\text{H}_{20}\text{NaO}_2$ ($\text{M}+\text{Na}$): 255.1356, found: 255.1352.



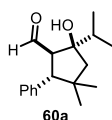
(1R,2R,5R)-2-hydroxy-2,4,4-trimethyl-5-phenylcyclopentane-1-carbaldehyde (58b). Prepared according to general procedure B. Time of irradiation: 14 hours. The crude mixture was purified by flash column chromatography (AcOEt: hexane 5-30%) to afford the product **58b** as a yellow oi (2 mg, 8% yield, 85% ee, average of two runs). The enantiomeric excess was determined to be 85% UPC² analysis on a Daicel Chiralpak IC-3 column with a gradient (100% CO_2 to 60:40 CO_2 /IPA over 4 minutes, curve 6), flow rate 3 mL/min, $\lambda = 215$

nm: $\tau_{\text{Major}} = 2.68$ min, $\tau_{\text{Minor}} = 2.85$ min. Absolute configuration determined in comparison to compound **64a**.

$^1\text{H NMR}$ (300 MHz, CDCl_3) δ 9.74 (d, $J = 2.9$ Hz, 1H), 7.36 – 7.28 (m, 2H), 7.25 – 7.13 (m, 3H), 3.57 (dd, $J = 13.0, 2.9$ Hz, 1H), 3.23 (d, $J = 13.0$ Hz, 1H), 1.98 (d, $J = 13.8$ Hz, 1H), 1.88 (d, $J = 13.8$ Hz, 1H), 1.44 (s, 3H), 1.06 (s, 3H), 0.85 (s, 3H).

$^{13}\text{C NMR}$ (126 MHz, CDCl_3) δ 204.0, 137.4, 128.7, 128.1, 126.9, 79.0, 65.8, 57.9, 55.6, 40.4, 29.0, 28.0, 24.8.

HRMS calculated for $\text{C}_{15}\text{H}_{20}\text{NaO}_2$ ($\text{M}+\text{Na}$): 255.1356, found: 255.1361.



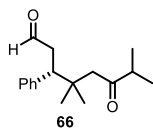
(1R,2R,5R)-2-hydroxy-2-isopropyl-4,4-dimethyl-5-phenylcyclopentane-1-carbaldehyde (60a). Prepared according to general procedure B using corresponding cyclopropanol **70** (0.1 mmol, 13 mg).

Time of irradiation: 36 hours. The crude mixture was purified by flash column chromatography (AcOEt: hexane 2-10%) to afford the product **60a** (20.5 mg, 78% yield, 99% ee, average of two runs). The enantiomeric excess was determined to be 99% by HPLC analysis on a Daicel Chiralpak IC-3 column: 95:5 hexane/IPA, flow rate 0.8 mL/min, $\lambda = 215$ nm: $\tau_{\text{Minor}} = 11.1$ min, $\tau_{\text{Major}} = 15.2$ min. $[\alpha]_{\text{D}}^{25} = +88.6$ ($c = 0.35$, CHCl_3 , 99% ee). Absolute configuration determined in comparison to compound **64a**.

$^1\text{H NMR}$ (400 MHz, CDCl_3) δ 9.70 (d, $J = 2.8$ Hz, 1H), 7.34 – 7.28 (m, 2H), 7.26 – 7.18 (m, 3H), 3.65 (d, $J = 13.0$ Hz, 1H), 3.31 (dd, $J = 13.1, 2.8$ Hz, 1H), 2.44 (s, 1H), 1.97 – 1.85 (m, 2H), 1.75 (d, $J = 14.3$ Hz, 1H), 1.17 (s, 3H), 1.00 (dd, $J = 11.9, 6.8$ Hz, 6H), 0.63 (s, 3H).

$^{13}\text{C NMR}$ (101 MHz, CDCl_3) δ 206.1, 137.6, 128.8, 128.2, 126.9, 85.1, 60.1, 56.3, 53.1, 40.2, 37.5, 29.9, 26.1, 18.0, 17.8.

HRMS calculated for $\text{C}_{17}\text{H}_{24}\text{NaO}_2$ ($\text{M}+\text{Na}$): 283.1669, found: 283.1668.



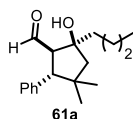
(R)-4,4,7-trimethyl-6-oxo-3-phenyloctanal (66). Prepared according to general procedure B using corresponding cyclopropanol **70** (0.1 mmol, 13 mg). Time of irradiation: 14 hours. The crude mixture was purified by flash column chromatography (AcOEt: hexane 2-10%) to afford the product **60a** (8 mg, 30% yield, 85% ee). The enantiomeric excess was determined to be 85% by HPLC analysis on a Daicel Chiralpak IC-3 column: 92:8 hexane/IPA, flow rate 0.8 mL/min, $\lambda = 215$ nm: $\tau_{\text{Minor}} = 16.0$ min, $\tau_{\text{Major}} = 20.0$ min.

$[\alpha]_{\text{D}}^{25} = -39.3$ ($c = 0.15$, CHCl_3 , 85% ee). Absolute configuration determined in comparison to compound **60a**.

¹H NMR (400 MHz, CDCl₃) δ 9.51 (dd, *J* = 3.1, 1.6 Hz, 1H), 7.32 – 7.27 (m, 2H), 7.26 – 7.15 (m, 3H), 3.70 (dd, *J* = 10.9, 4.8 Hz, 1H), 2.91 – 2.74 (m, 2H), 2.48 (hept, *J* = 6.9 Hz, 1H), 2.30 (d, *J* = 1.3 Hz, 2H), 1.12 (s, 3H), 1.05 (dd, *J* = 6.9, 3.9 Hz, 7H), 0.97 (s, 3H).

¹³C NMR (101 MHz, CDCl₃) δ 214.4, 202.6, 140.5, 129.6, 128.1, 126.9, 49.7, 47.0, 44.2, 42.1, 36.4, 25.4, 24.7, 18.2, 18.2.

HRMS calculated for C₁₇H₂₄NaO₂ (M+Na): 283.1669, found: 283.1667.



(1R,2S,5R)-2-hydroxy-4,4-dimethyl-5-phenyl-2-propylcyclopentane-

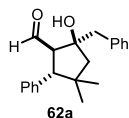
1-carbaldehyde (61a). Prepared according to general procedure B using corresponding cyclopropanol **71** (0.1 mmol, 14 mg). Time of irradiation:

14 hours. The crude mixture was purified by flash column chromatography

(AcOEt: hexane 5-10%) to afford the product **61a** (22 mg, 80% yield, 99% ee, average of two runs). The enantiomeric excess was determined to be 99% by UPC² analysis on a Daicel Chiralpak IA column with a gradient (100% CO₂ to 60:40 CO₂/IPA over 4 minutes, curve 6), flow rate 3 mL/min, λ = 215 nm: τ_{Major} = 3.2 min, τ_{Minor} = 3.61 min. Absolute configuration determined in comparison to compound **64a**.

¹H NMR (400 MHz, CDCl₃) δ 9.65 (d, *J* = 2.4 Hz, 1H), 7.34 – 7.27 (m, 2H), 7.25 – 7.17 (m, 3H), 3.63 (d, *J* = 13.2 Hz, 1H), 3.16 (dd, *J* = 13.2, 2.5 Hz, 1H), 2.34 (s, 1H), 1.92 – 1.78 (m, 3H), 1.69 – 1.59 (m, 1H), 1.49 – 1.33 (m, 4H), 1.17 (s, 3H), 0.94 (t, *J* = 7.1 Hz, 3H), 0.64 (s, 3H).

¹³C NMR (101 MHz, CDCl₃) δ 206.03, 137.78, 128.86, 128.33, 127.03, 82.03, 62.41, 55.73, 55.57, 42.47, 40.68, 29.90, 26.75, 26.25, 23.28, 14.21.



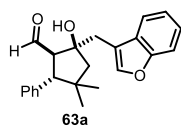
(1R,2R,5R)-2-benzyl-2-hydroxy-4,4-dimethyl-5-phenylcyclopentane-

1-carbaldehyde (62a). Prepared according to general procedure B using corresponding cyclopropanol **72** (0.1 mmol, 18 mg). Time of irradiation:

14 hours. The crude mixture was purified by flash column chromatography (AcOEt: hexane 5-10%) to afford the product **62a** (22 mg, 72% yield, 99% ee, average of two runs). The enantiomeric excess was determined to be 99% by UPC² analysis on a Daicel Chiralpak IA column with a gradient (100% CO₂ to 60:40 CO₂/EtOH over 4 minutes, curve 6), flow rate 3 mL/min, λ = 215 nm: τ_{Major} = 3.38 min, τ_{Minor} = 3.82 min. Absolute configuration determined in comparison to compound **64a**.

¹H NMR (400 MHz, CDCl₃) δ 9.56 (d, *J* = 2.6 Hz, 1H), 7.41 – 7.23 (m, 8H), 7.21 – 7.15 (m, 2H), 3.68 (d, *J* = 13.1 Hz, 1H), 3.28 (dd, *J* = 13.1, 2.6 Hz, 1H), 3.10 (d, *J* = 13.3 Hz, 1H), 3.02 (d, *J* = 13.3 Hz, 1H), 2.51 (s, 1H), 2.06 (d, *J* = 14.2 Hz, 1H), 1.76 (d, *J* = 14.2 Hz, 1H), 1.17 (s, 3H), 0.56 (s, 3H).

^{13}C NMR (101 MHz, CDCl_3) δ 205.4, 137.6, 137.0, 130.3, 128.7, 128.6, 128.2, 127.0, 126.9, 82.1, 61.5, 55.6, 55.2, 47.9, 40.6, 29.8, 26.2.

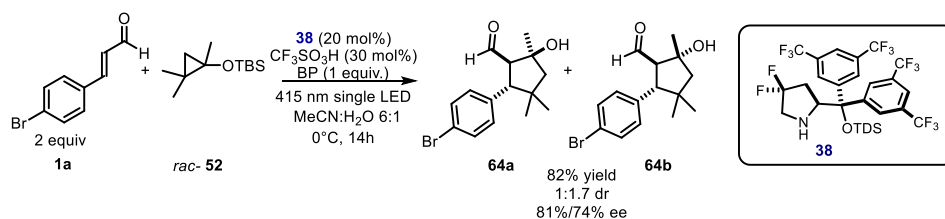


(1R,2R,5R)-2-(benzofuran-3-ylmethyl)-2-hydroxy-4,4-dimethyl-5-phenylcyclopentane-1-carbaldehyde (63a). Prepared according to general procedure B using corresponding cyclopropanol **73** (0.1 mmol, 22 mg). Time of irradiation: 63 hours. The crude mixture was purified by flash column chromatography (AcOEt: hexane 5-10%) to afford the product **61a** (27 mg, 77% yield, 99% ee, average of two runs). The enantiomeric excess was determined to be 99% by UPC² analysis on a Daicel Chiralpak ID-3 column with a gradient (100% CO_2 to 60:40 CO_2/EtOH over 4 minutes, curve 6), flow rate 3 mL/min, $\lambda = 215$ nm: $\tau_{\text{Major}} = 3.27$ min, $\tau_{\text{Minor}} = 3.46$ min. Absolute configuration determined in comparison to compound **64a**.

^1H NMR (500 MHz, CDCl_3) δ 9.62 (d, $J = 2.4$ Hz, 1H), 7.68 – 7.64 (m, 1H), 7.62 (s, 1H), 7.53 (dt, $J = 8.3, 0.8$ Hz, 1H), 7.39 – 7.29 (m, 4H), 7.29 – 7.23 (m, 1H), 7.21 – 7.16 (m, 2H), 3.69 (d, $J = 13.2$ Hz, 1H), 3.33 (dd, $J = 13.2, 2.4$ Hz, 1H), 3.24 (dd, $J = 14.4, 0.9$ Hz, 1H), 3.09 (dd, $J = 14.5, 0.9$ Hz, 1H), 2.73 (s, 1H), 2.07 (d, $J = 14.2$ Hz, 1H), 1.17 (s, 3H), 0.61 (s, 3H).

^{13}C NMR (126 MHz, CDCl_3) δ 205.5, 155.25, 143.3, 137.4, 128.7, 128.5, 128.3, 127.0, 124.5, 122.8, 119.9, 115.8, 111.7, 81.8, 61.6, 55.7, 55.6, 40.7, 35.9, 29.7, 26.1.

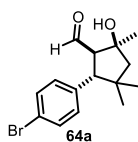
Procedure C for the Enantioselective Photochemical Organo-Cascade Reaction



Scheme 4.33 Procedure C for the enantioselective photochemical organo-cascade reaction.

To a 20 mL Schlenk tube, containing the amine catalyst **38** (0.02 mmol, 14 mg), enal **1a** (0.2 mmol, 42 mg) and the biphenyl (BP) (0.1 mmol, 15 mg) was added 350 μL of an acetonitrile, 50 μL of water and trifluoromethylsulfonic acid (0.03 mmol, 3mg, 1.8 μL) and then TBS protected cyclopropanol **52** (0.1 mmol, 21.5 mg). The reaction mixture was degassed via freeze pump thaw (x3), and the vessel refilled with argon. After the reaction mixture was thoroughly degassed, the Schlenk tube was sealed and positioned in a

platform, cooled down to 0°C, mounted on an aluminium block fitted with a 410 nm high-power single LED ($\lambda = 415$ nm, irradiance = 26 mW/cm², as controlled by an external power supply; the set-up is detailed in Figure 4.4). The reaction was stirred under visible light irradiation at 0°C for 14 hours. Then the reaction mixture was diluted with CHCl₃ and washed with saturated NaHCO₃. The aqueous layer was washed twice with CHCl₃ and the combined organic layers were washed with brine and dried over sodium sulfate. Solvent was evaporated and the crude mixture was purified by column chromatography on silica gel (AcOEt: hexane 10-30%) to furnish the products **64a**:**64b** in the 82% yield, 1:1.7 dr, 81%/74% ee).



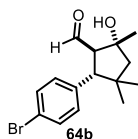
(1R,2S,5R)-5-(4-bromophenyl)-2-hydroxy-2,4,4-trimethylcyclopentane-1-carbaldehyde (64a). (8 mg, 26% yield, 81% ee). The enantiomeric excess was determined to be 81% by HPLC analysis on a Daicel Chiralpak IC-3 column: 92:8 hexane/IPA, flow rate 0.8 mL/min, $\lambda = 215$ nm: $\tau_{\text{Minor}} = 12.6$ min, $\tau_{\text{Major}} = 14.4$ min.

¹H NMR (400 MHz, CDCl₃) δ 9.66 (d, $J = 2.3$ Hz, 1H), 7.49 – 7.44 (m, 2H), 7.11 – 7.06 (m, 2H), 3.61 (d, $J = 13.2$ Hz, 1H), 3.08 (dd, $J = 13.3, 2.3$ Hz, 1H), 2.22 (s, 1H), 1.97 (d, $J = 14.2$ Hz, 1H), 1.87 (d, $J = 14.2$ Hz, 1H), 1.56 (s, 3H), 1.18 (s, 3H), 0.66 (s, 3H).

¹³C NMR (101 MHz, CDCl₃) δ 204.9, 136.8, 131.4, 130.3, 120.9, 79.2, 63.2, 57.6, 55.0, 40.6, 29.6, 29.6, 26.0.

HRMS calculated for C₁₅H₁₉BrNaO₂ (M+Na): 333.0461, found: 333.0456.

The absolute configuration for **64a** was unambiguously inferred by anomalous dispersion X-ray crystallographic analysis, see X-ray Crystallographic Data section.



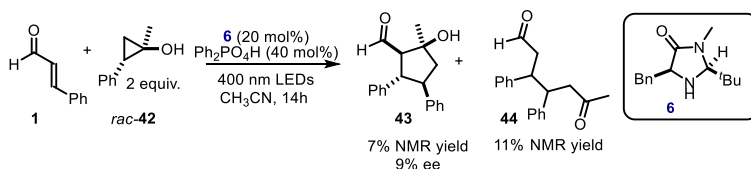
(1R,2R,5R)-5-(4-bromophenyl)-2-hydroxy-2,4,4-trimethylcyclopentane-1-carbaldehyde (64b). (14 mg, 45% yield, 74% ee). The enantiomeric excess was determined to be 74% by UPC² analysis on a Daicel Chiralpak IC-3 column with a gradient (100% CO₂ to 60:40 CO₂/IPA over 4 minutes, curve 6), flow rate 3 mL/min, $\lambda = 215$ nm: $\tau_{\text{Major}} = 2.86$ min, $\tau_{\text{Minor}} = 3.00$ min.

¹H NMR (400 MHz, CDCl₃) δ 9.75 (d, $J = 2.7$ Hz, 1H), 7.47 – 7.40 (m, 2H), 7.11 – 7.02 (m, 2H), 3.53 (dd, $J = 12.9, 2.7$ Hz, 1H), 3.18 (d, $J = 12.9$ Hz, 1H), 2.06 (s, 1H), 1.98 (d, $J = 13.8$ Hz, 1H), 1.87 (d, $J = 13.9$ Hz, 1H), 1.43 (s, 3H), 1.04 (s, 3H), 0.85 (s, 3H).

¹³C NMR (101 MHz, CDCl₃) δ 203.3, 136.7, 131.3, 130.3, 120.8, 79.0, 65.9, 57.9, 54.9, 40.4, 28.8, 28.0, 24.6.

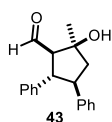
HRMS calculated for C₁₅H₁₉BrNaO₂ (M+Na): 333.0461, found: 333.0456.

Procedure D for the Enantioselective Photochemical Organocascade Reaction



Scheme 4.34 General procedure D for the enantioselective photochemical organocascade reaction.

To a 20 mL Schlenk tube, containing the amine catalyst **6** (0.02 mmol, 5 mg), cyclopropanol **42** (0.2 mmol, 30 mg) and diphenyl phosphate (0.04 mmol, 10 mg) and the was added 200 μL of an acetonitrile. Cinnamaldehyde **1** (0.1 mmol, 13 mg, 0.013 mL) was added at the end. The reaction mixture was degassed via freeze pump thaw (x3), and the vessel refilled with argon. After the reaction mixture was thoroughly degassed, the Schlenk tube was sealed and positioned in the middle of a 250 mL evaporation bath surrounded by a strip containing 400 nm LEDs. A small fan was installed directly above the Schlenk tube so as to keep the temperature constant. Then the reaction mixture was diluted with CHCl_3 and washed with saturated NaHCO_3 . The aqueous layer was washed twice with CHCl_3 and the combined organic layers were washed with brine and dried over sodium sulfate. Solvent was evaporated and the crude mixture was purified by column chromatography on silica gel (AcOEt: hexane 5-20%) to furnish the products **43** and **44b**.



2-hydroxy-2-methyl-4,5-diphenylcyclopentane-1-carbaldehyde (43).

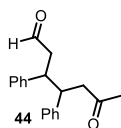
(7% yields determined by ^1H NMR analysis of crude reaction mixtures employing trichloroethylene as a standard, 9% ee). The enantiomeric excess was determined to be 9% by UPC2 analysis on a Daicel Chiralpak CEL-1

column with a gradient (100% CO_2 to 60:40 CO_2/MeCN over 4 minutes, curve 6), flow rate 3 mL/min, $\lambda = 215$ nm: $\tau_{\text{Major}} = 4.47$ $\tau_{\text{Minor}} = 4.87$ min.

^1H NMR (400 MHz, CDCl_3) δ 9.72 (d, $J = 2.0$ Hz, 1H), 7.45 – 6.95 (m, 10H), 3.90 – 3.75 (m, 1H), 3.35 – 3.21 (m, 1H), 3.01 (dd, $J = 12.0, 2.0$ Hz, 1H), 2.58 – 2.38 (m, 2H), 2.19 (dd, $J = 14.2, 8.0$ Hz, 1H), 1.64 (s, 3H).

^{13}C NMR (126 MHz, CDCl_3) δ 204.6, 142.9, 140.0, 128.6, 128.4, 127.7, 127.6, 127.0, 126.4, 80.0, 67.4, 54.9, 51.9, 49.8, 29.7, 29.0.

MS (ES^+) 303, $\text{C}_{19}\text{H}_{20}\text{O}_2\text{Na}$ ($\text{M} + \text{Na}$) $^+$



6-oxo-3,4-diphenylheptanal (44). (11% yields determined by ^1H NMR analysis of crude reaction mixtures employing trichloroethylene as a standard).

^1H NMR (400 MHz, CDCl_3) δ 9.34 (dd, $J = 2.3, 1.4$ Hz, 1H), 7.41 – 7.20 (m, 10H), 3.49 – 3.35 (m, 2H), 2.77 – 2.53 (m, 2H), 2.52 – 2.34 (m, 2H), 1.78 (s, 3H).
 ^{13}C NMR (101 MHz, CDCl_3) δ 207.4, 207.1, 200.9, 142.6, 142.2, 141.9, 128.9, 128.9, 128.7, 128.3, 128.2, 128.2, 127.2, 127.2, 127.0, 48.8, 48.8, 48.5, 46.8, 46.8, 45.9, 30.64, 30.6.

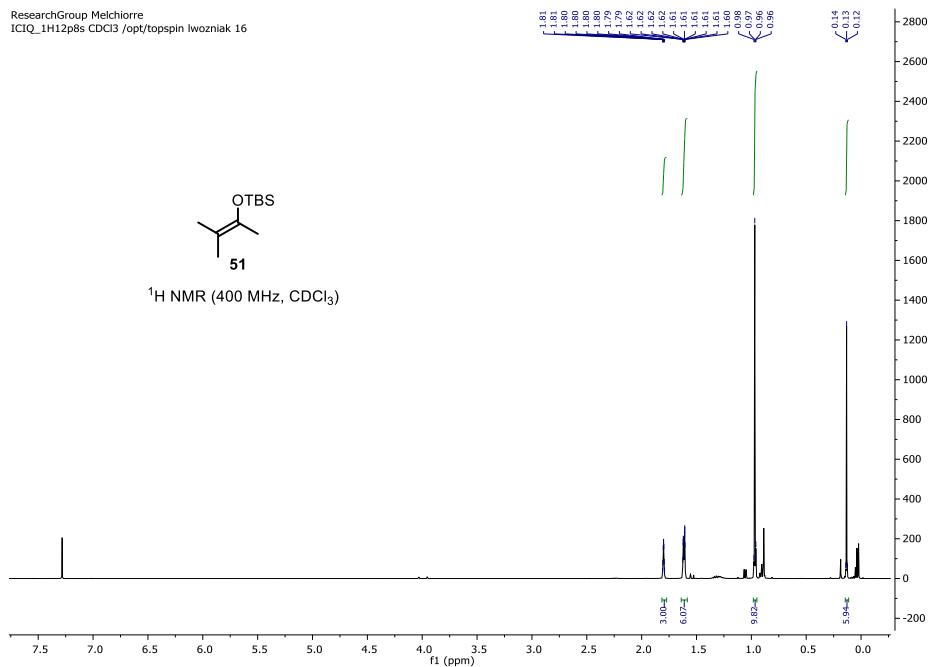
MS (ES $^+$) 335, $\text{C}_{12}\text{H}_{24}\text{O}_2\text{Na}$ (M + Na + MeOH) $^+$

NMR Spectra.

ResearchGroup Melchiorre
ICIQ_1H12p8s CDCl3 /opt/topspin Iwozniak 16



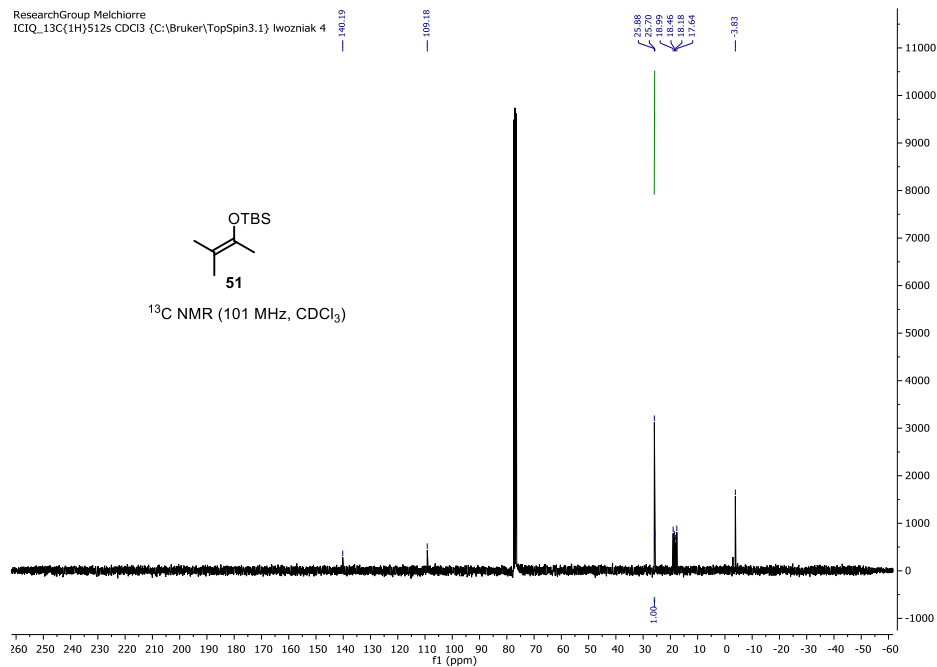
¹H NMR (400 MHz, CDCl₃)



ResearchGroup Melchiorre
ICIQ_13C(1H)512s CDCl3 (C:\Bruker\TopSpin3.1) Iwozniak 4



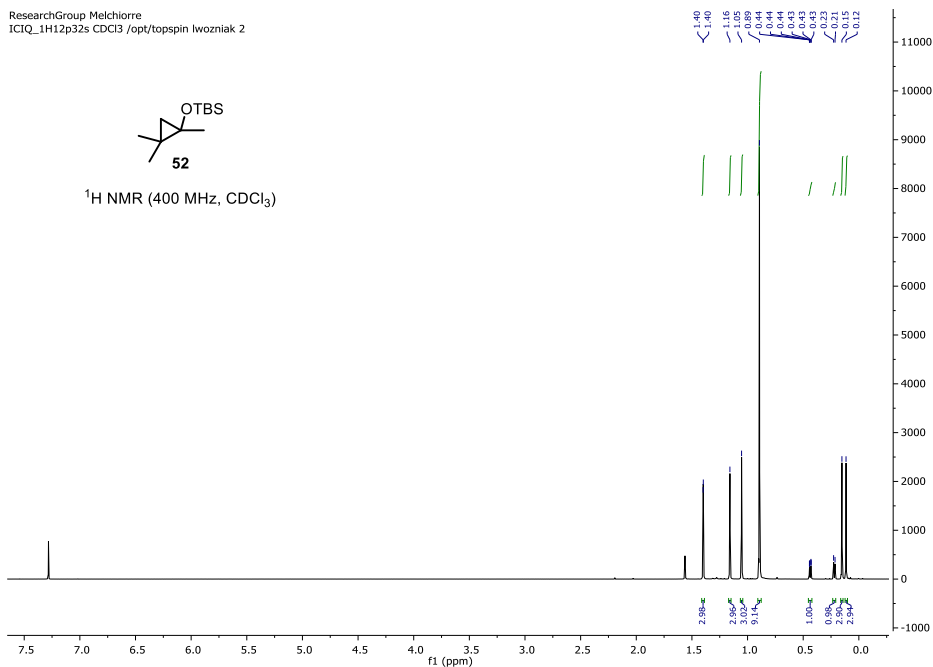
¹³C NMR (101 MHz, CDCl₃)



ResearchGroup Melchiorre
 ICIQ_1H12p32s CDCl3 /opt/topspin Iwozniak 2



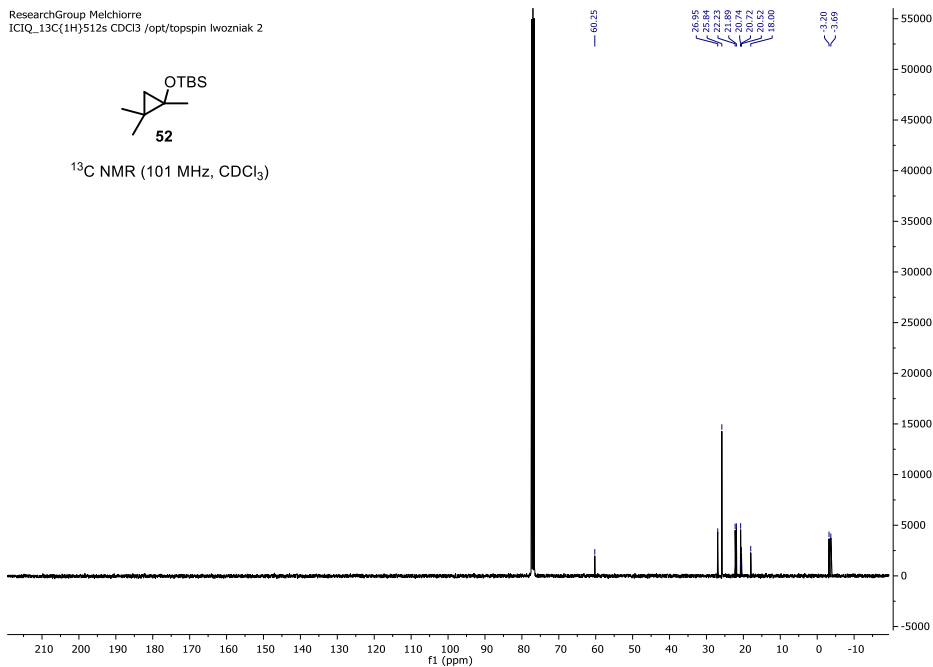
^1H NMR (400 MHz, CDCl_3)

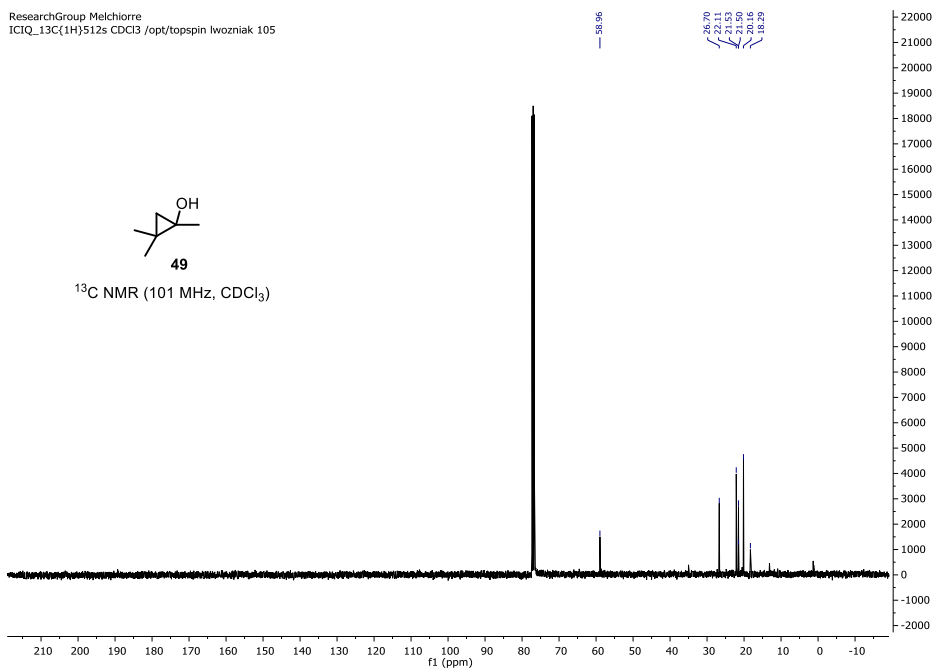
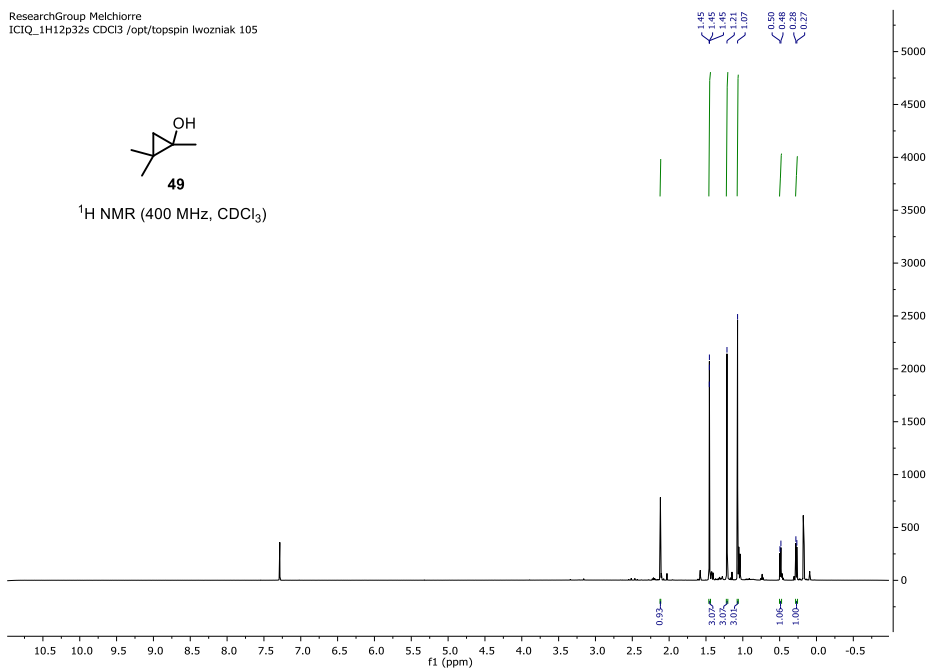


ResearchGroup Melchiorre
 ICIQ_13C(1H)512s CDCl3 /opt/topspin Iwozniak 2



^{13}C NMR (101 MHz, CDCl_3)



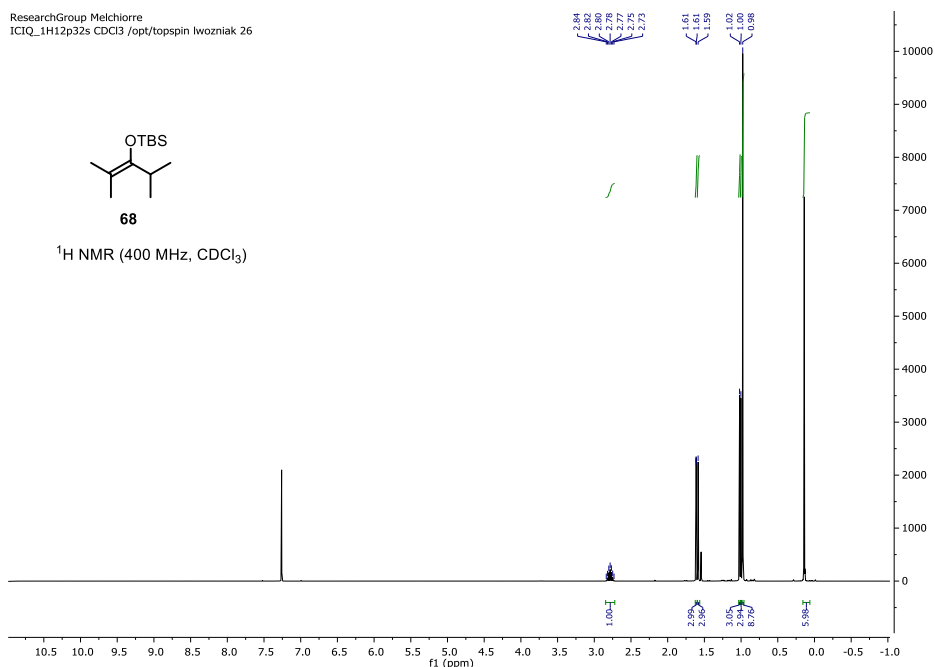


ResearchGroup Melchiorre
 ICIQ_1H12p32s CDCI3 /opt/topspin Iwozniak 26



68

¹H NMR (400 MHz, CDCl₃)

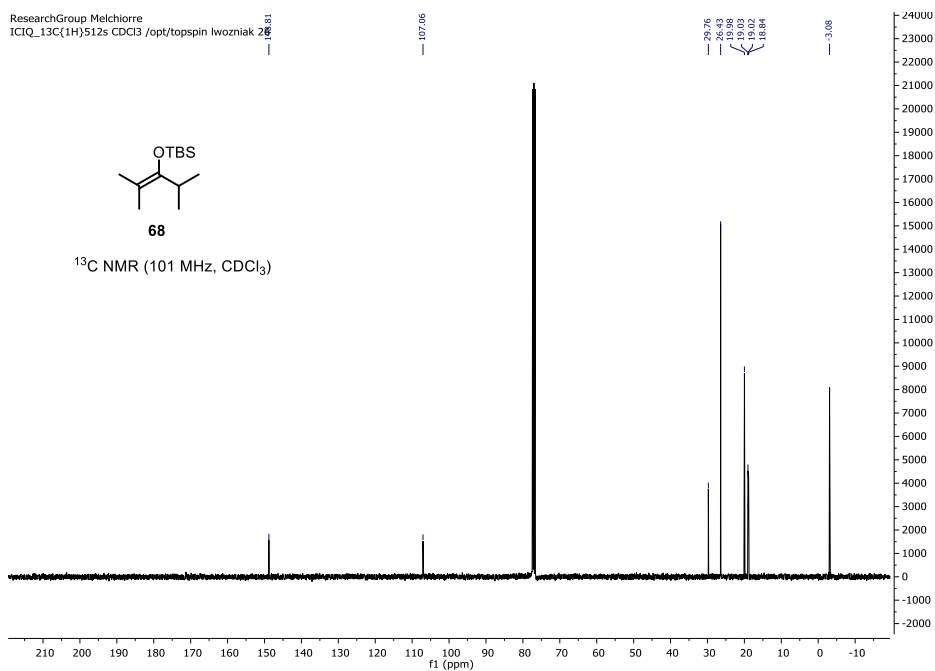


ResearchGroup Melchiorre
 ICIQ_13C(1H)512s CDCI3 /opt/topspin Iwozniak 26



68

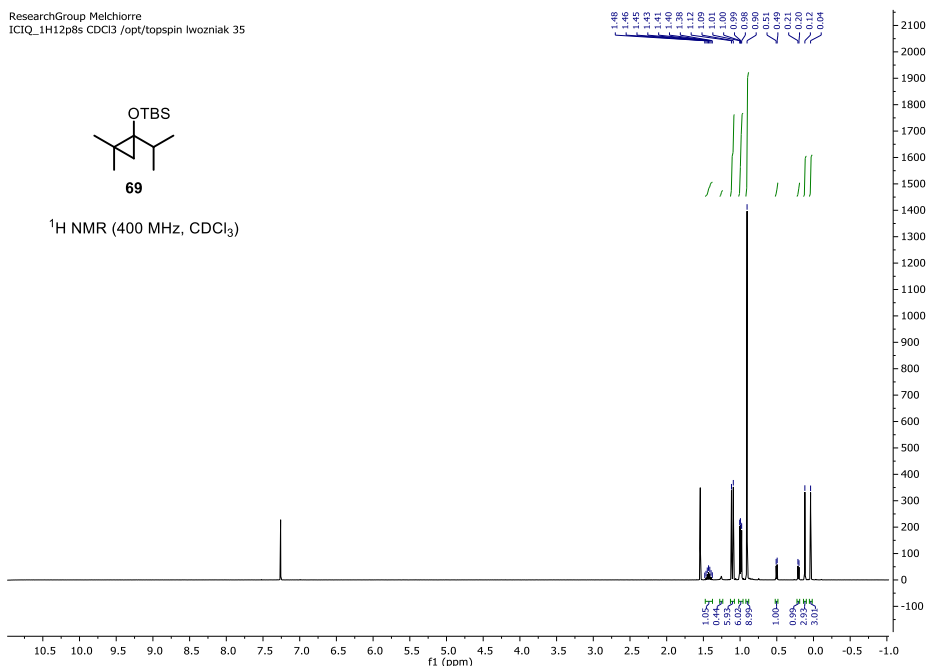
¹³C NMR (101 MHz, CDCl₃)



ResearchGroup Melchiorre
ICIQ_1H12p8s CDCl3 /opt/topspin lwozniak 35



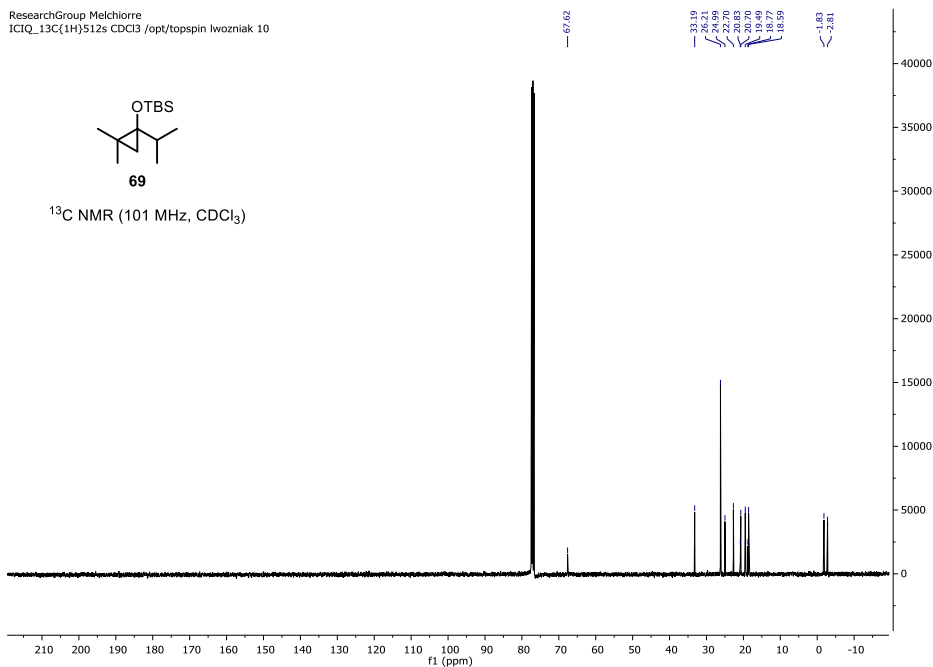
¹H NMR (400 MHz, CDCl₃)



ResearchGroup Melchiorre
ICIQ_13C(1H)512s CDCl3 /opt/topspin lwozniak 10



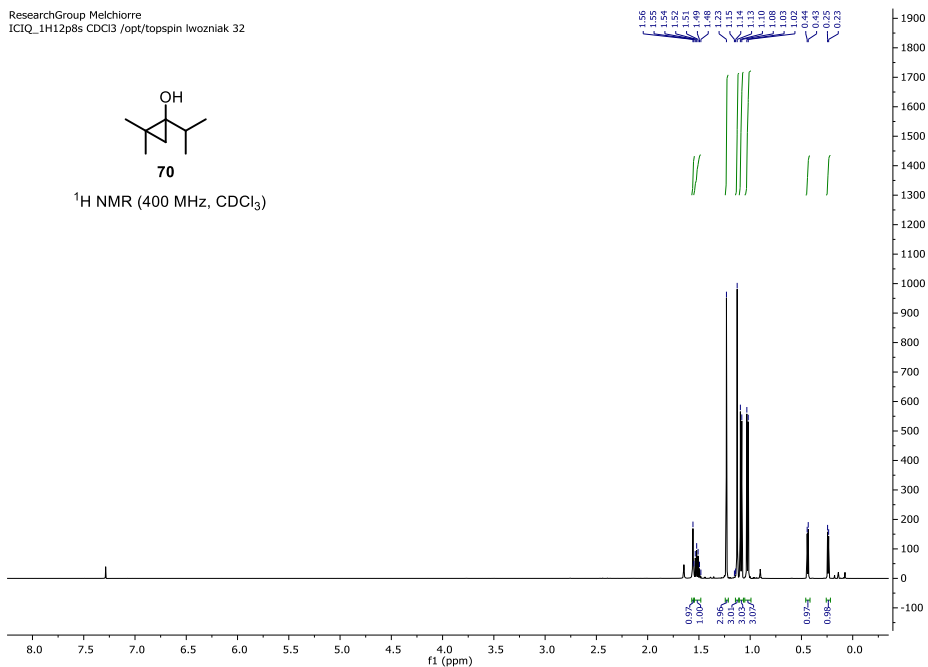
¹³C NMR (101 MHz, CDCl₃)



ResearchGroup Melchiorre
 ICIQ_1H12p8s CDCl3 /opt/topspin lwozniak 32



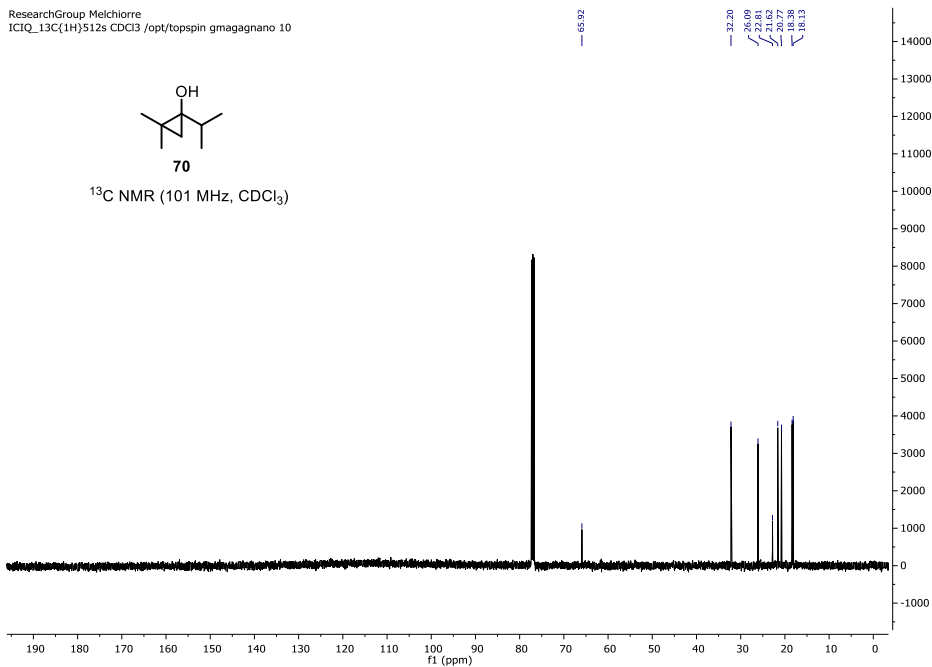
¹H NMR (400 MHz, CDCl₃)



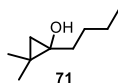
ResearchGroup Melchiorre
 ICIQ_13C(1H)512s CDCl3 /opt/topspin gmagagnano 10



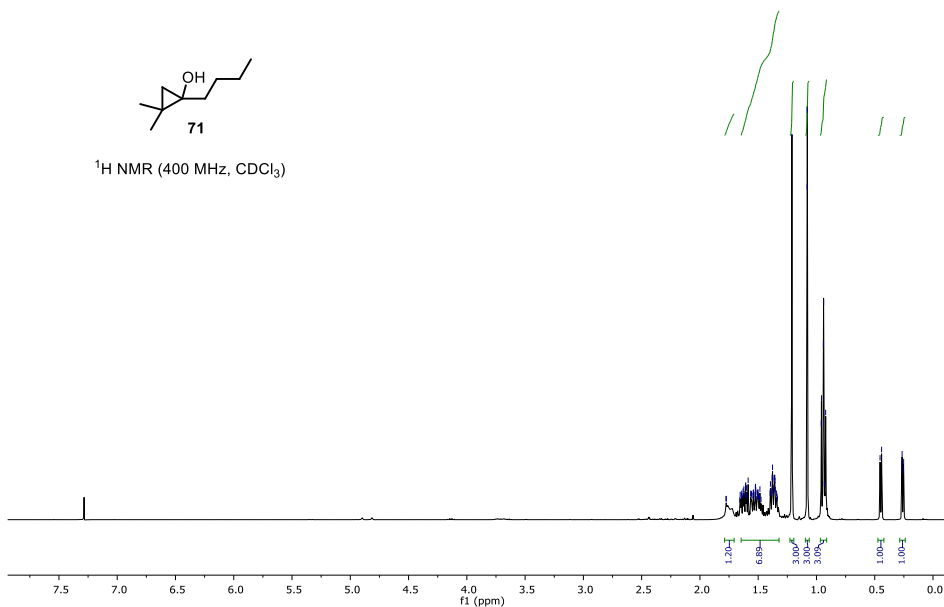
¹³C NMR (101 MHz, CDCl₃)



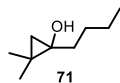
ResearchGroup Melchiorre
 ICIQ_1H12p8s CDCI3 /opt/topspin gmgagnano 46



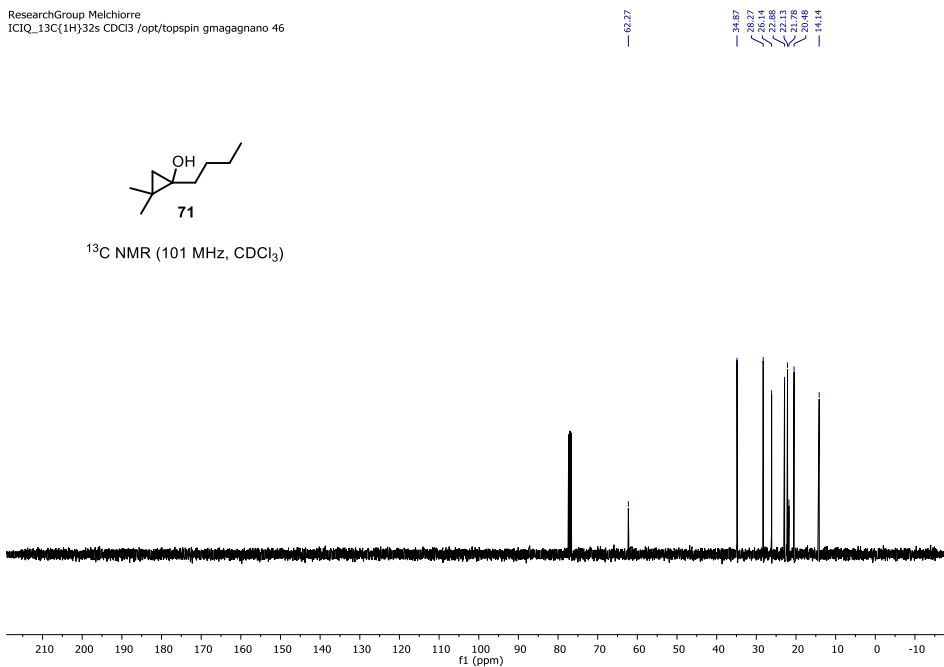
¹H NMR (400 MHz, CDCl₃)

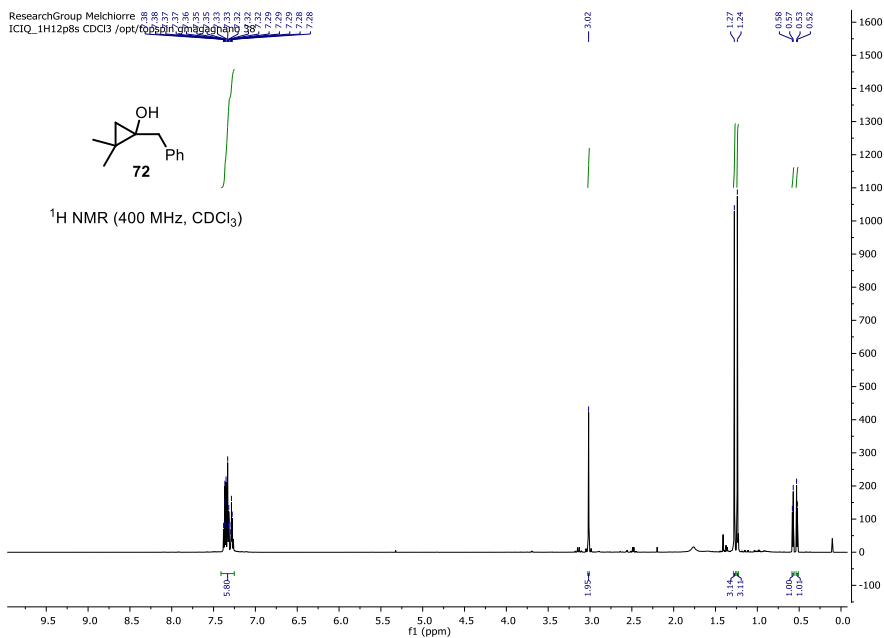


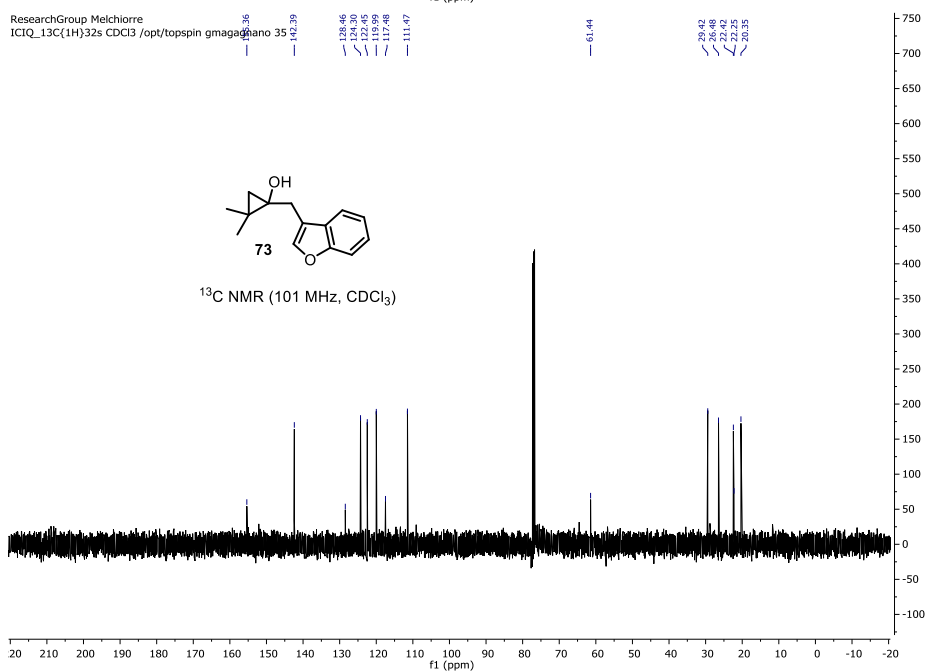
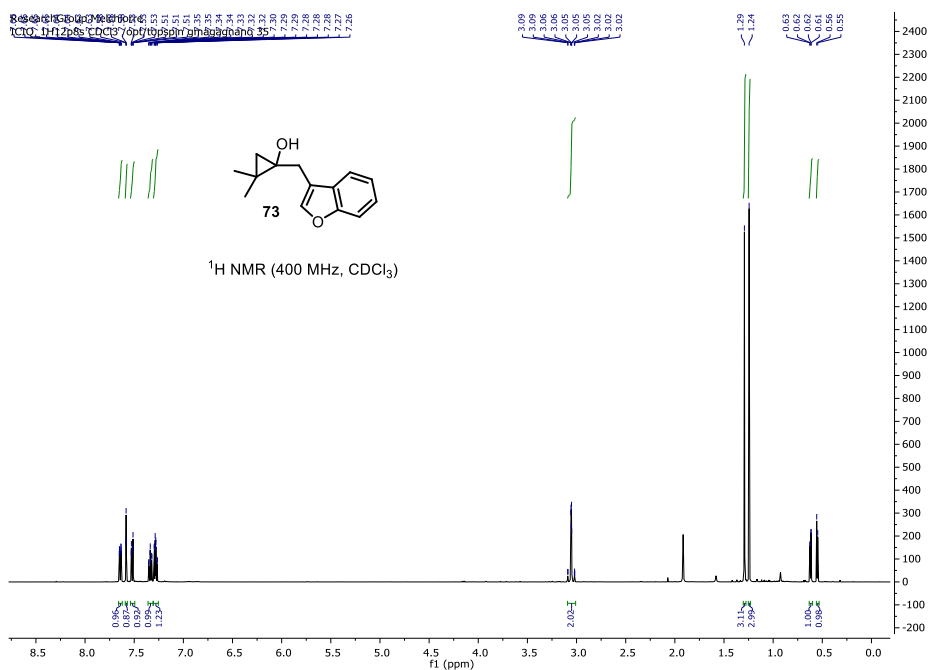
ResearchGroup Melchiorre
 ICIQ_13C(1H)32s CDCI3 /opt/topspin gmgagnano 46

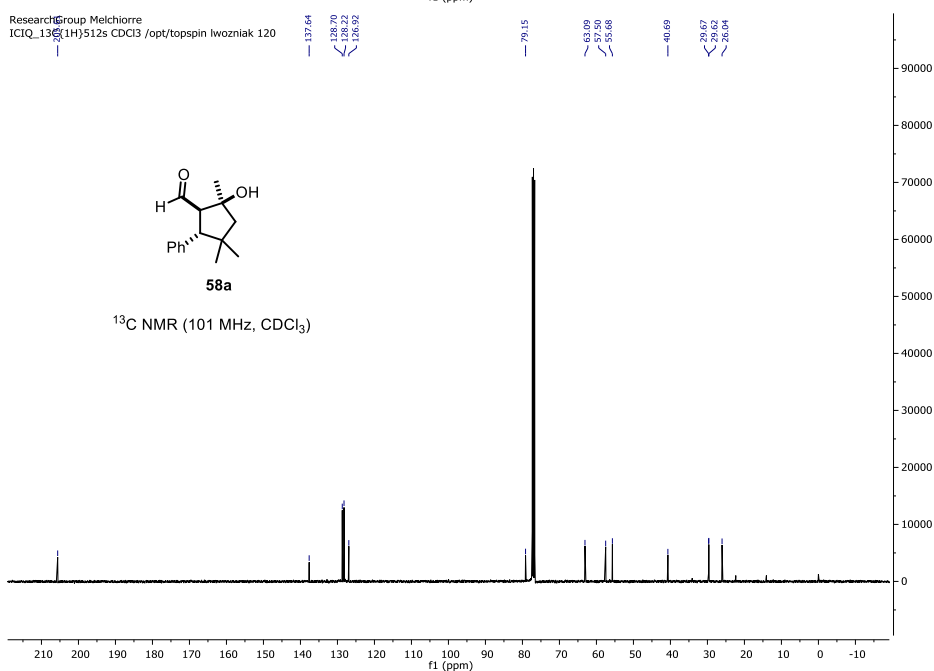
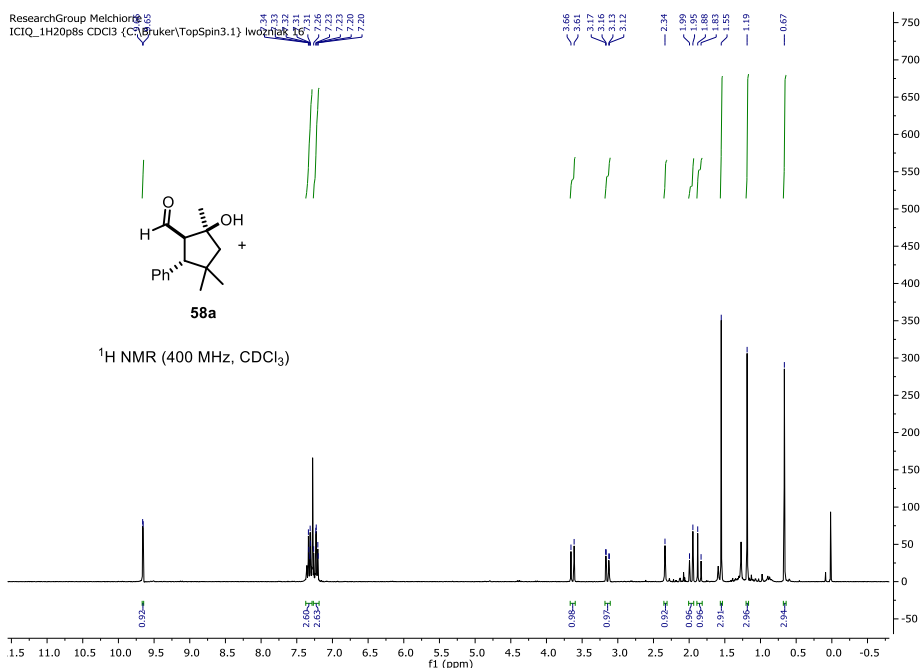


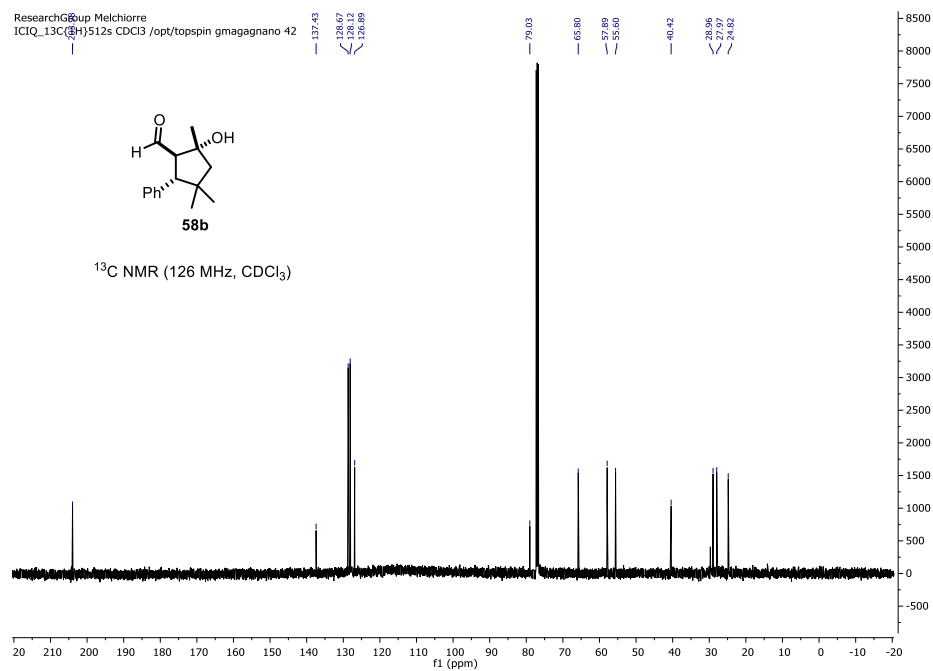
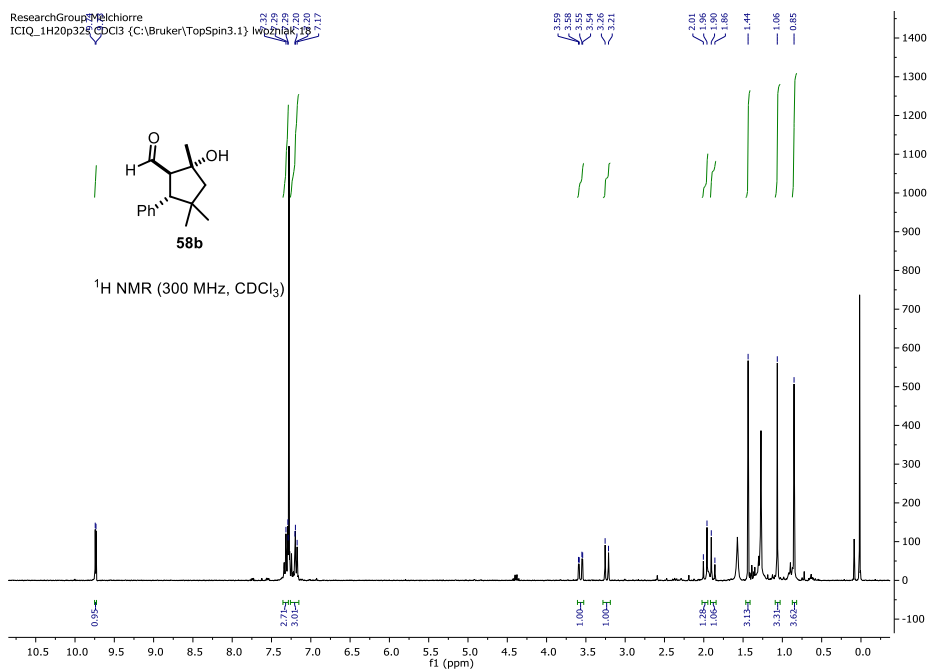
¹³C NMR (101 MHz, CDCl₃)

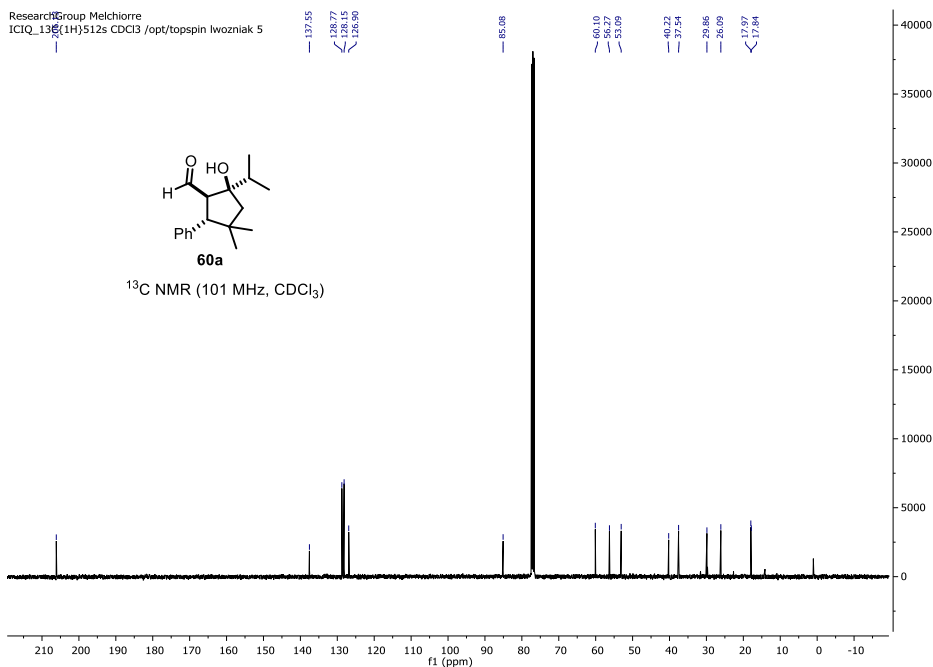
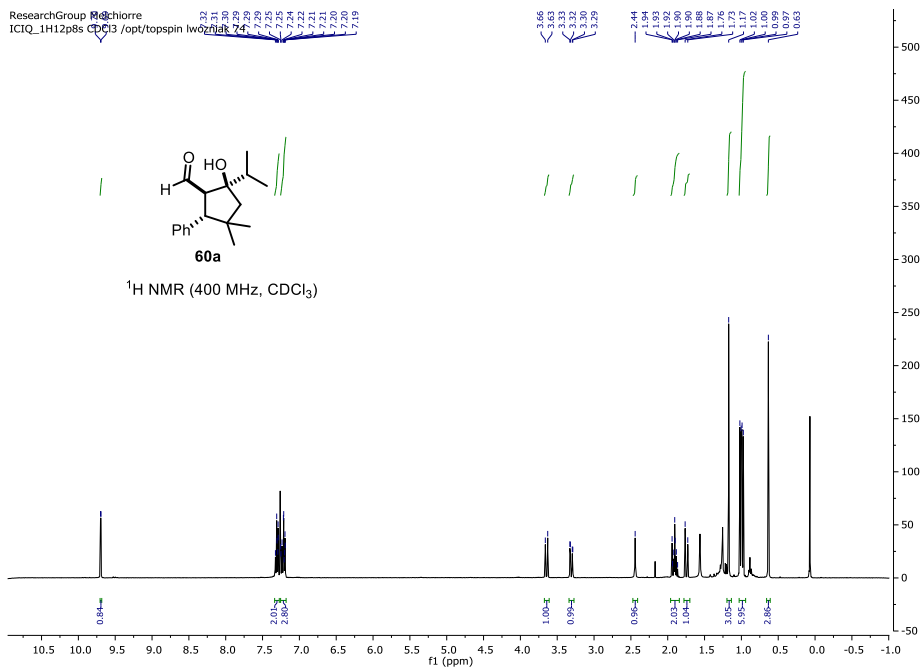


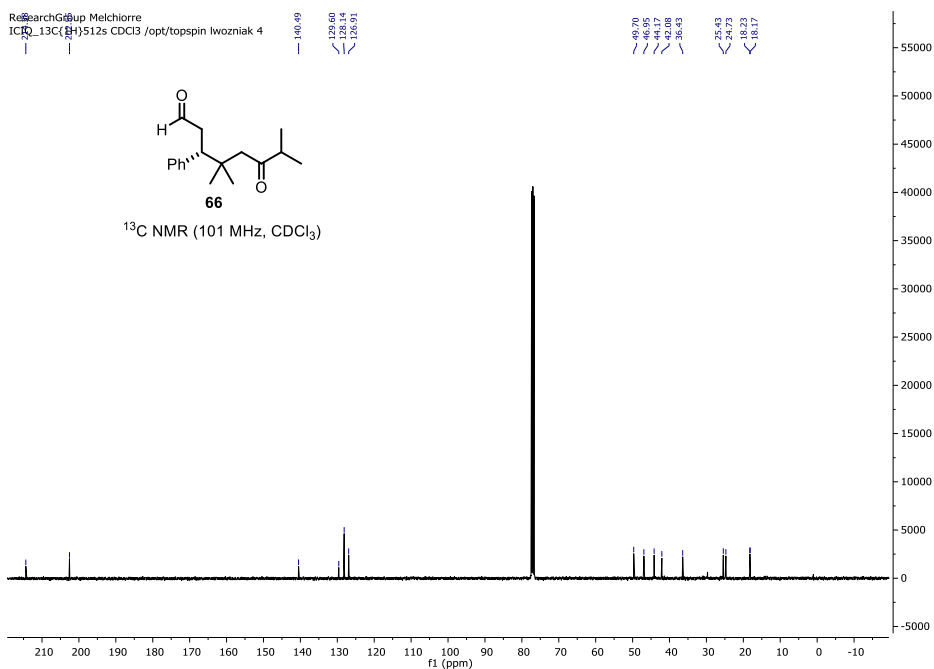
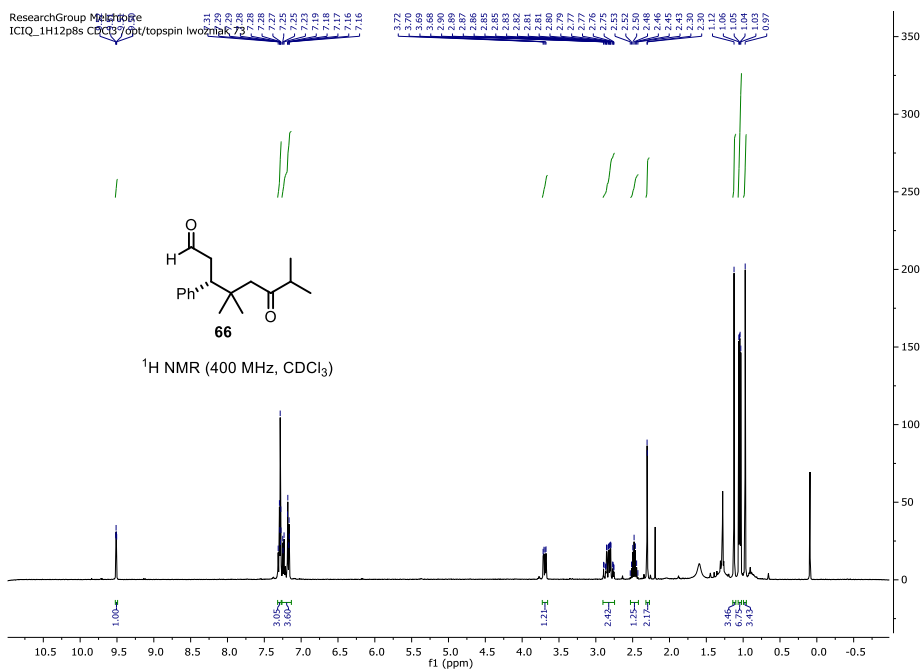


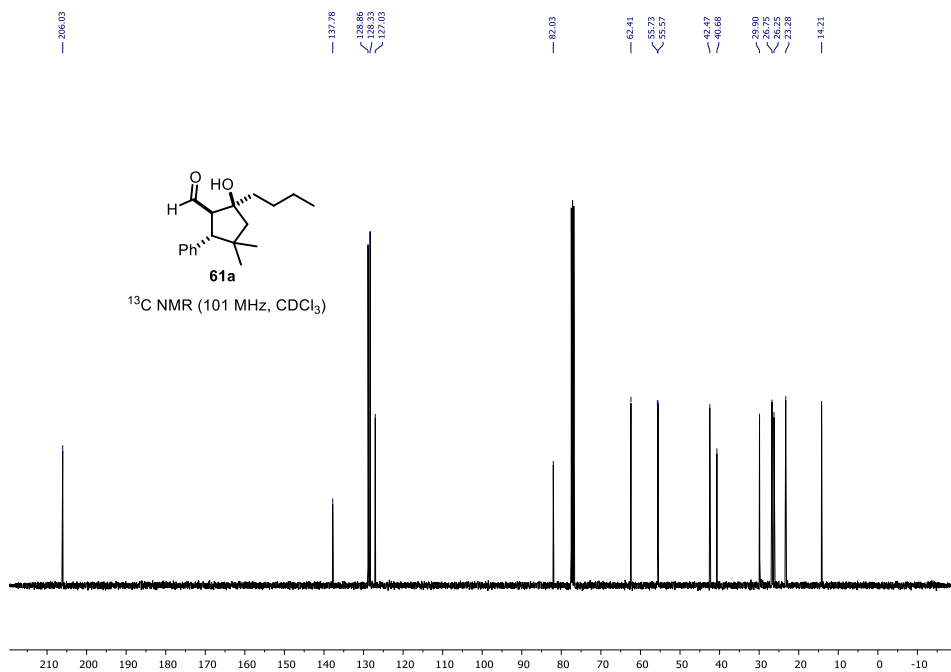
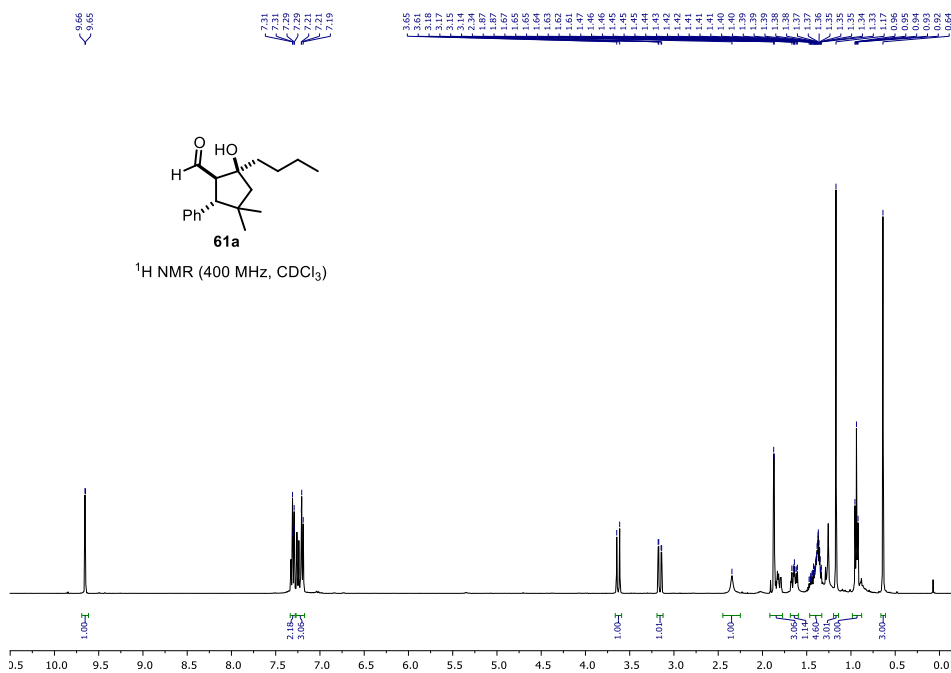


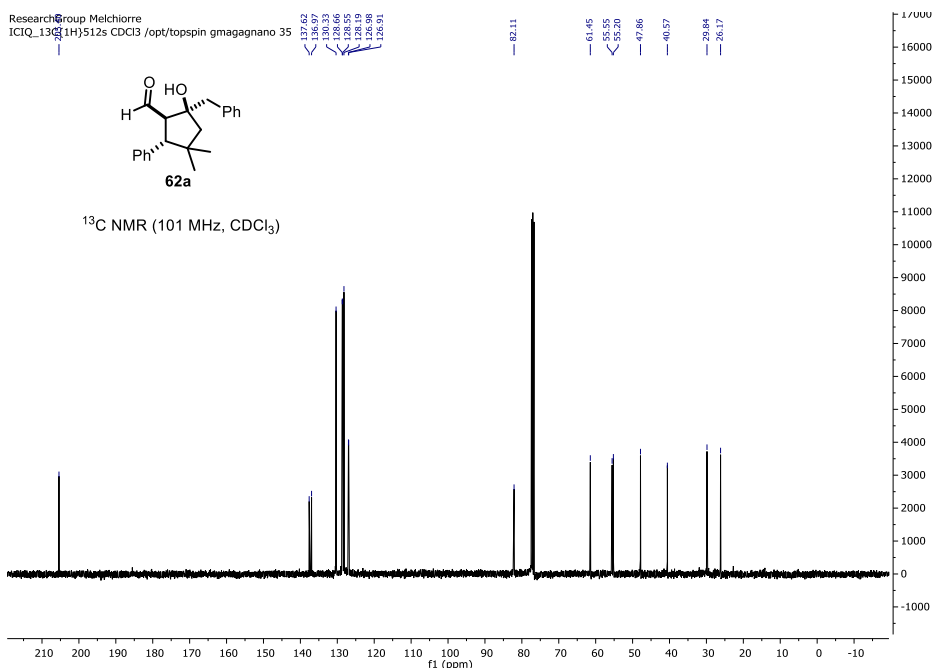
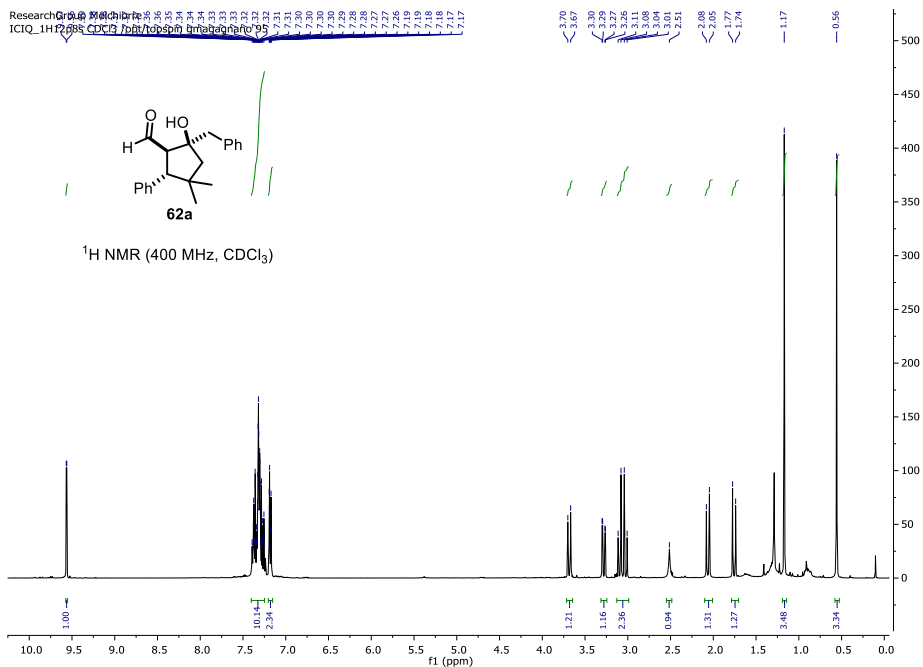


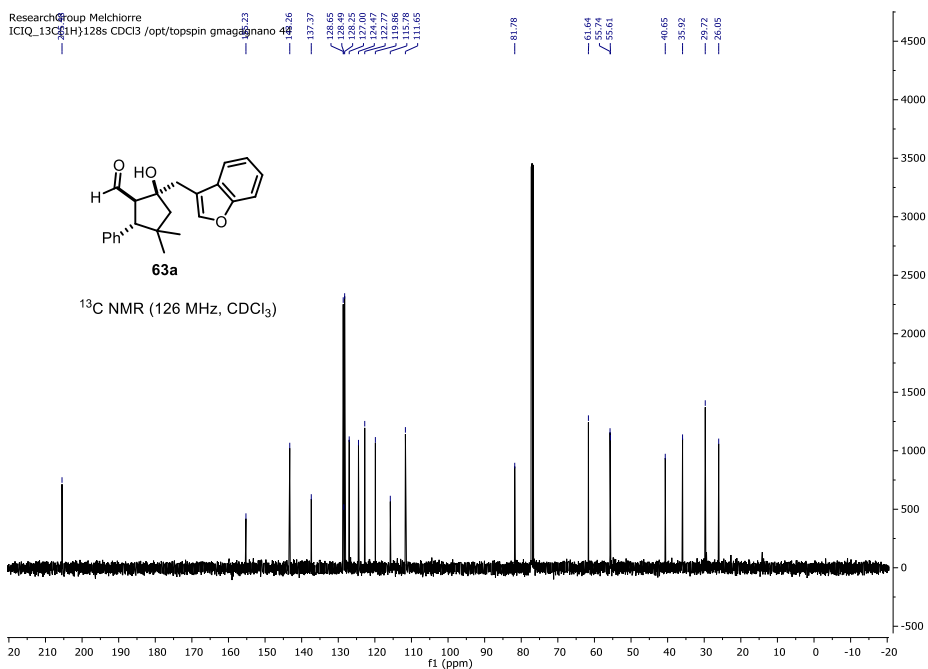
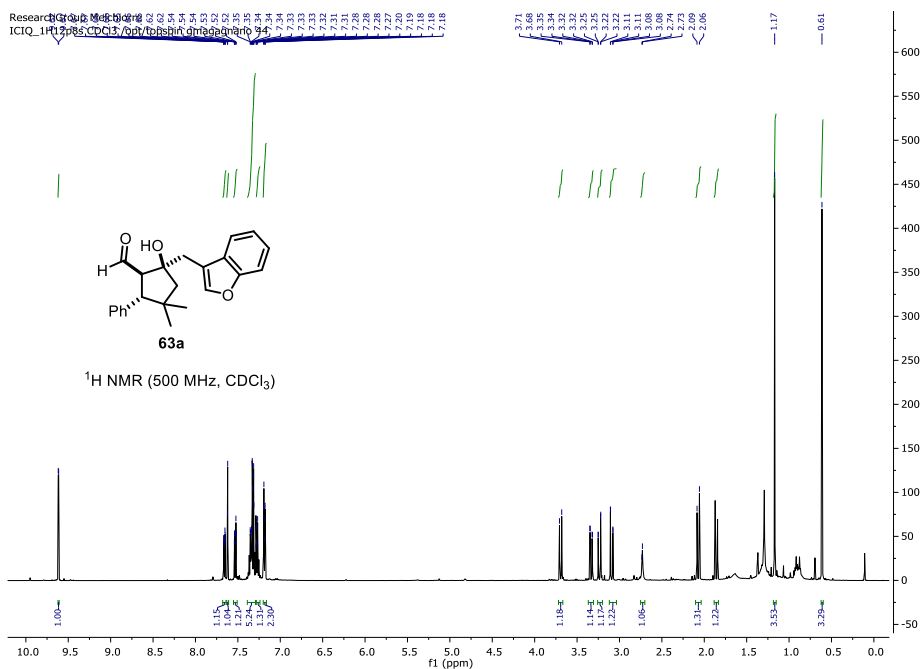


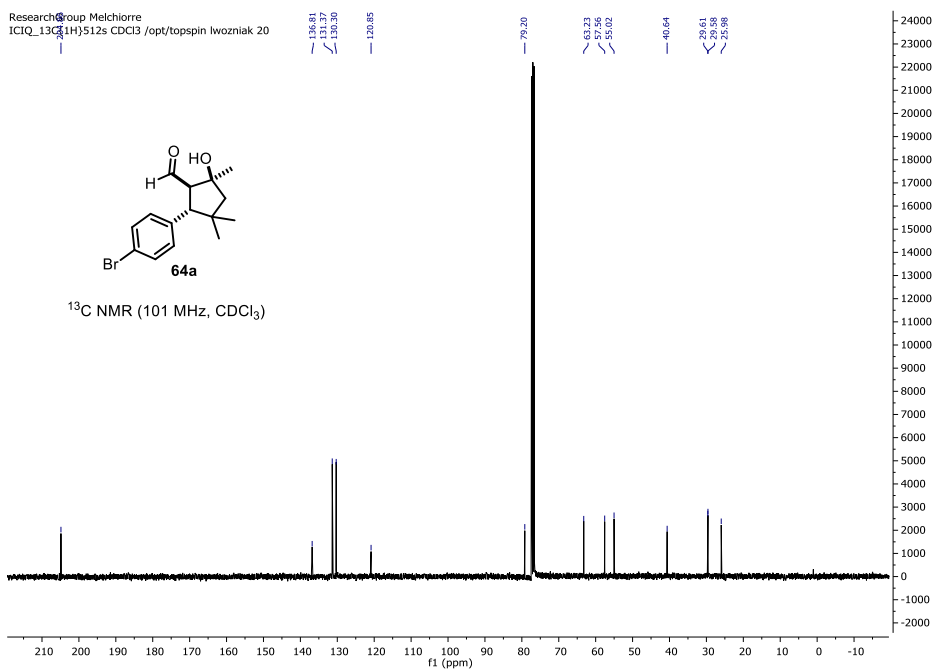
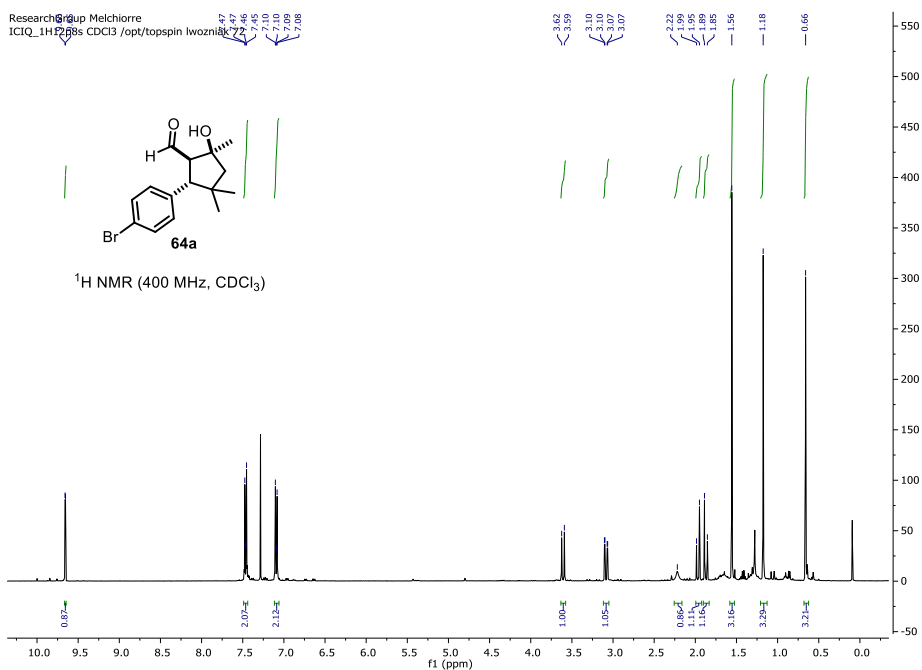


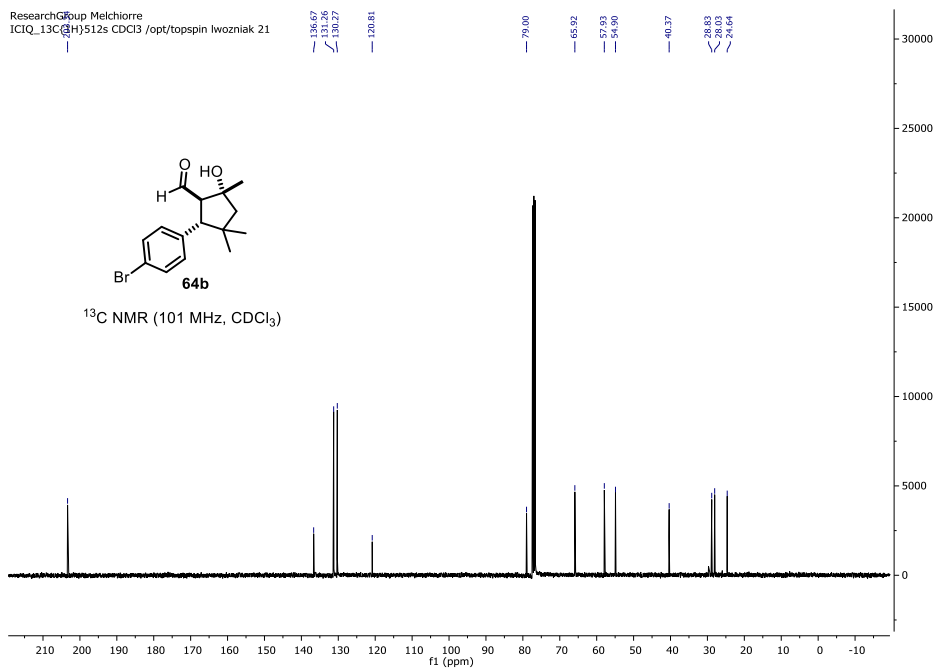
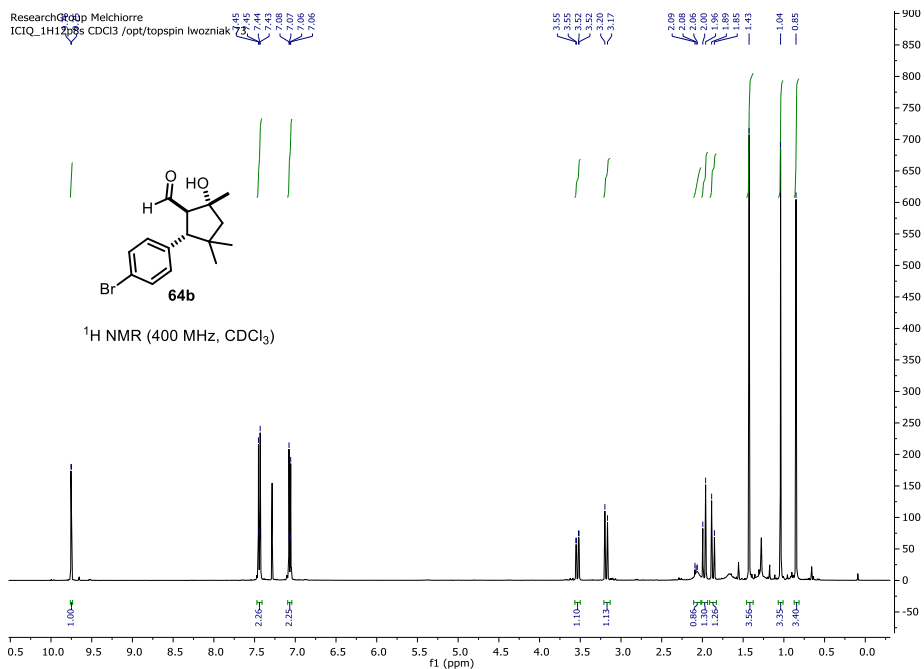


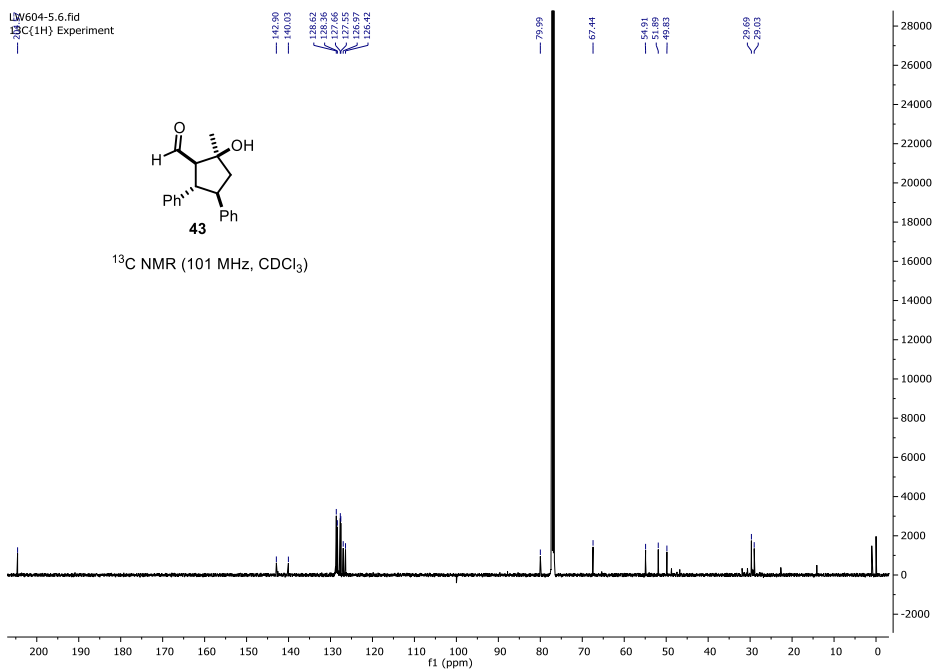
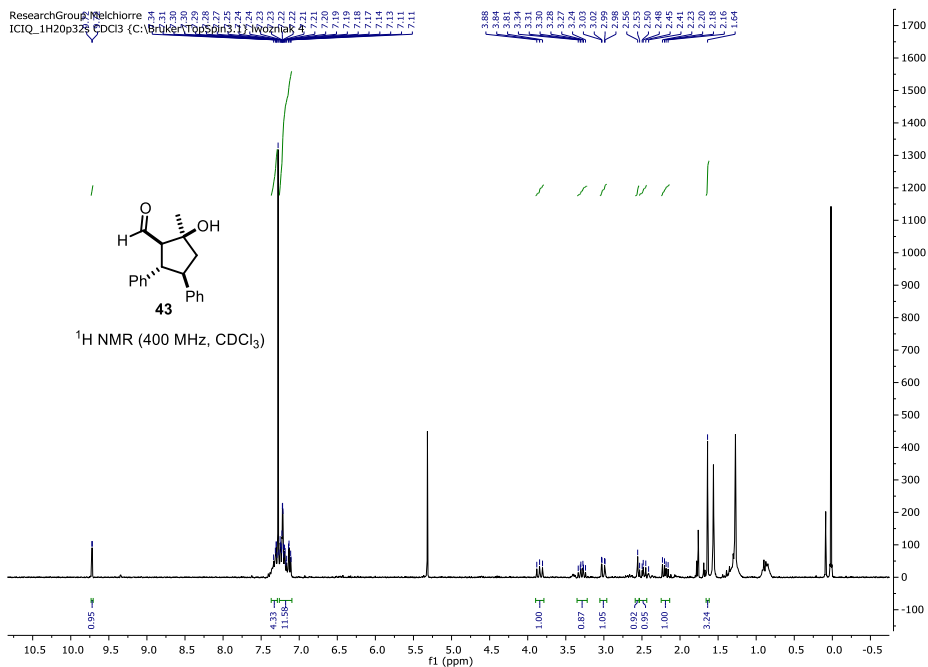




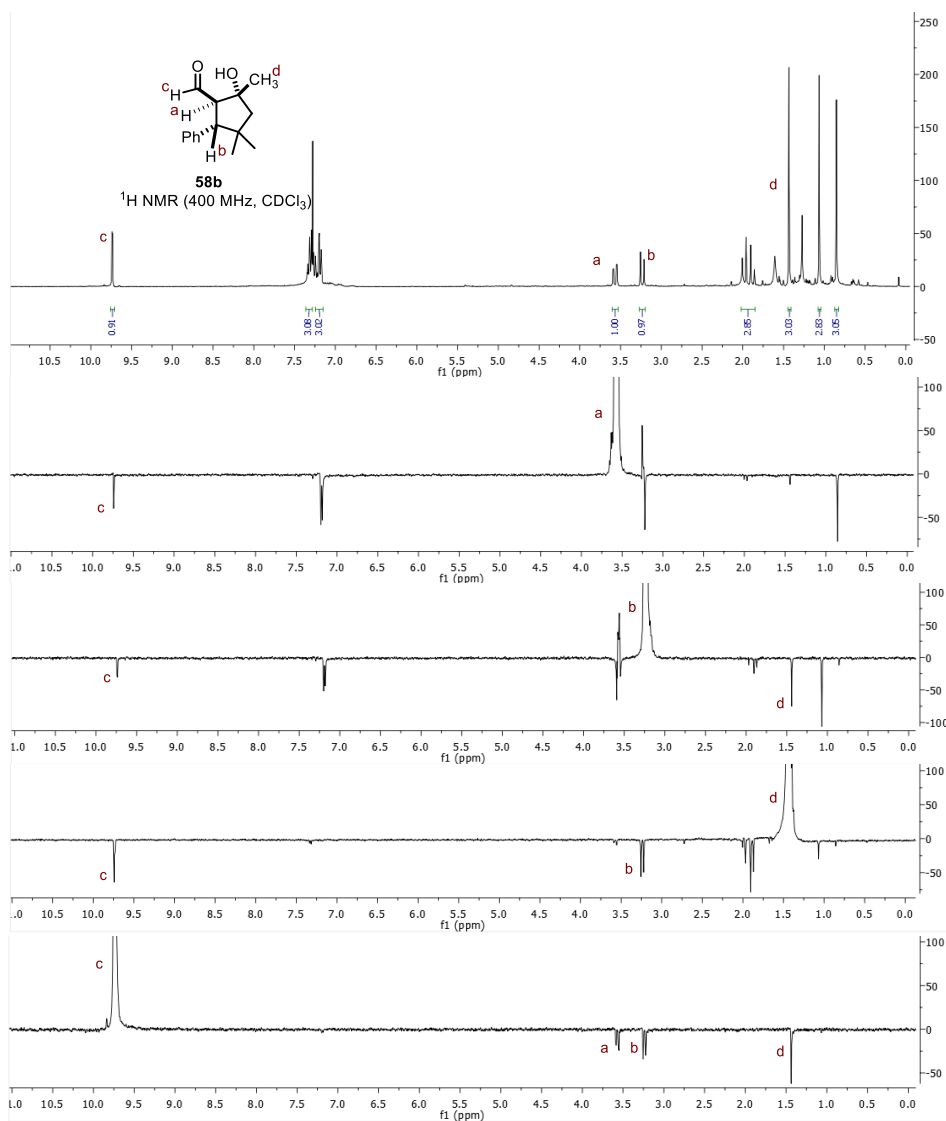






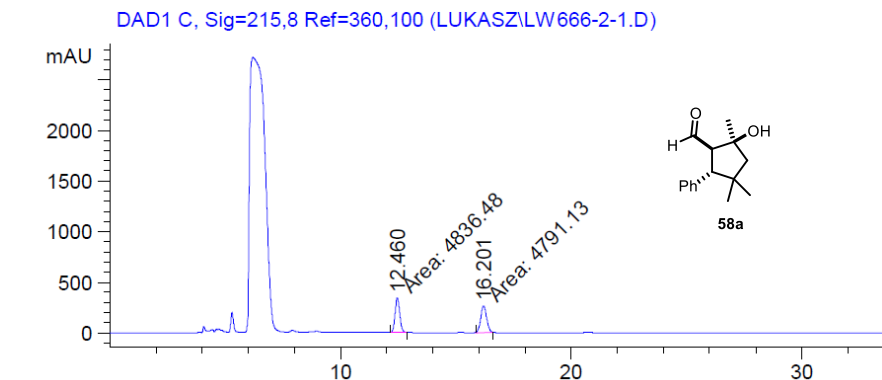


Determination of the relative the configuration of 58b by monodimensional nOe experiments.

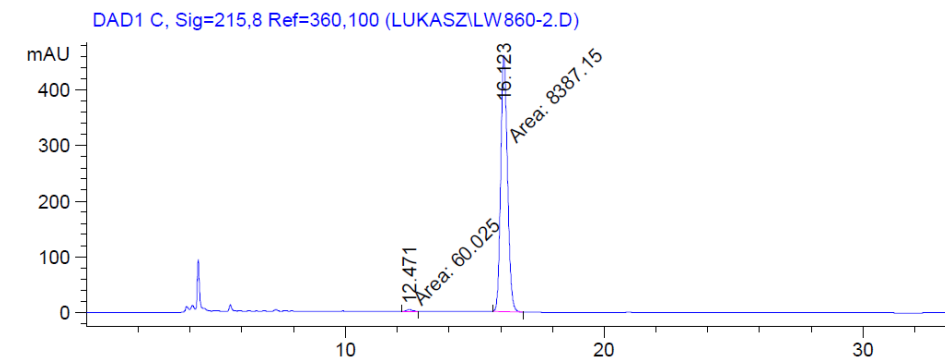


HPLC and UPC² traces

Conditions: HPLC (Daicel Chiralpak IC column, 20 °C, 92:8 hexane/*i*PrOH, flow rate: 0.80 mL/min, $\lambda = 215$ nm) **58a**

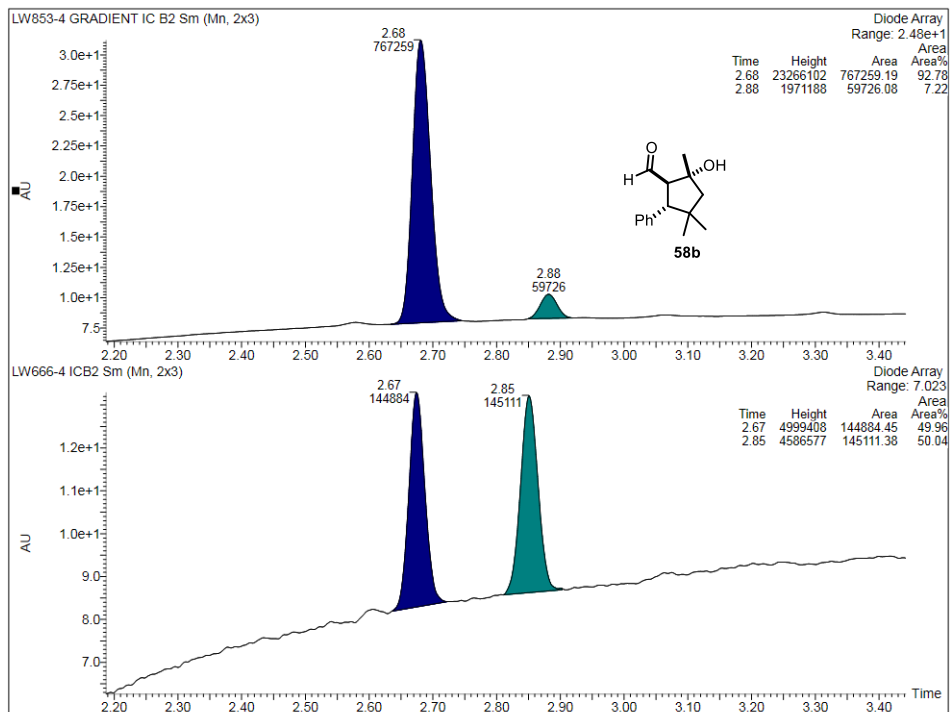


Peak #	RetTime [min]	Type	Width [min]	Area [mAU*s]	Height [mAU]	Area %
1	12.460	MM	0.2338	4836.47656	344.71234	50.2355
2	16.201	MM	0.3029	4791.12891	263.65213	49.7645

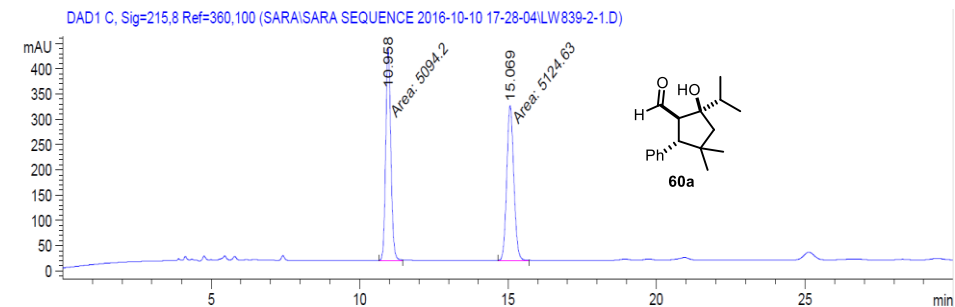


Peak #	RetTime [min]	Type	Width [min]	Area [mAU*s]	Height [mAU]	Area %
1	12.471	MM	0.2674	60.02501	3.74108	0.7106
2	16.123	MM	0.3031	8387.14844	461.16675	99.2894

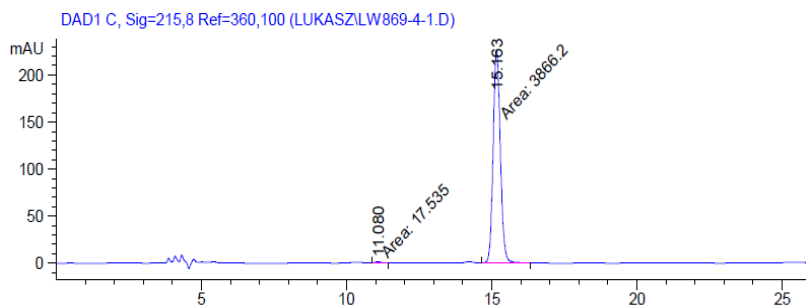
Conditions: UPC² analysis on a Daicel Chiralpak IC-3 column with a gradient (100% CO₂ to 60:40 CO₂/IPA over 4 minutes, curve 6) **58b**



Conditions: HPLC (Daicel Chiralpak IC column, 20 °C, 95:5 hexane/*i*PrOH, flow rate: 0.80 mL/min, $\lambda = 215$ nm) **60a**

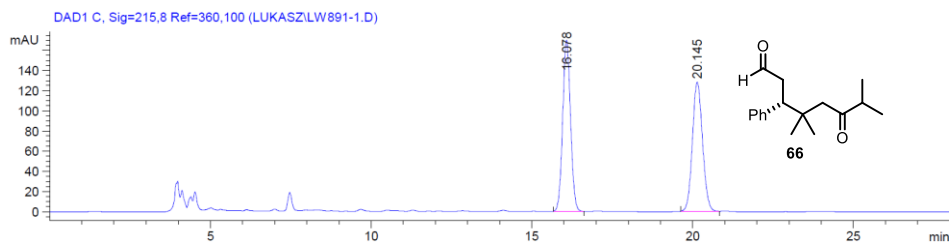


Peak #	RetTime [min]	Type	Width [min]	Area [mAU*s]	Height [mAU]	Area %
1	10.958	MM	0.2011	5094.20166	422.22049	49.8511
2	15.069	MM	0.2785	5124.63379	306.72507	50.1489

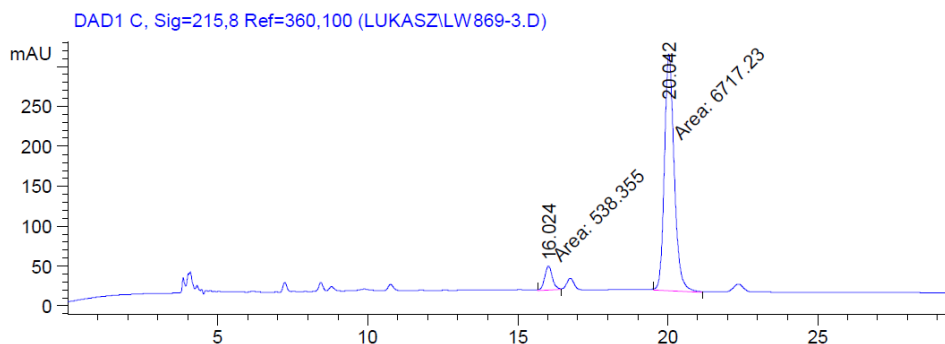


Peak #	RetTime [min]	Type	Width [min]	Area [mAU*s]	Height [mAU]	Area %
1	11.080	MM	0.2269	17.53496	1.28803	0.4515
2	15.163	MM	0.2849	3866.19556	226.14935	99.5485

Conditions: HPLC (Daicel Chiralpak IC column, 20 °C, 95:5 hexane/*i*PrOH, flow rate: 0.80 mL/min, $\lambda = 215$ nm) **66**

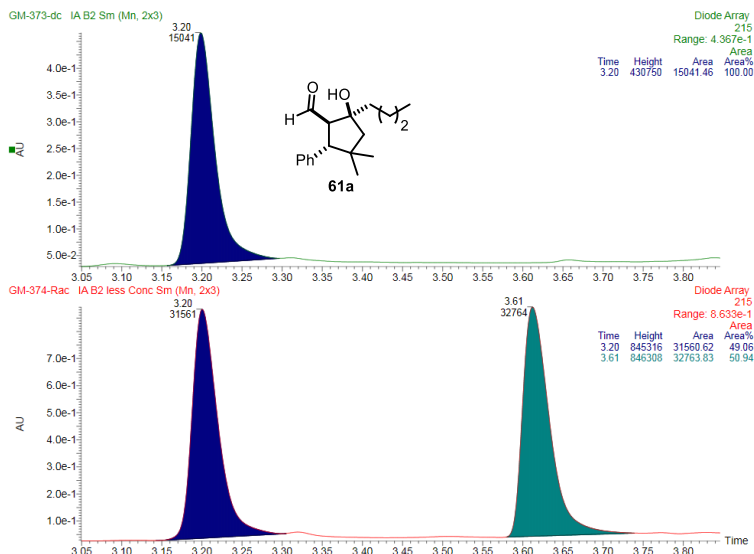


Peak #	RetTime [min]	Type	Width [min]	Area [mAU*s]	Height [mAU]	Area %
1	16.078	BB	0.2625	2888.44971	169.80843	50.6971
2	20.145	BB	0.3398	2809.01123	128.11705	49.3029

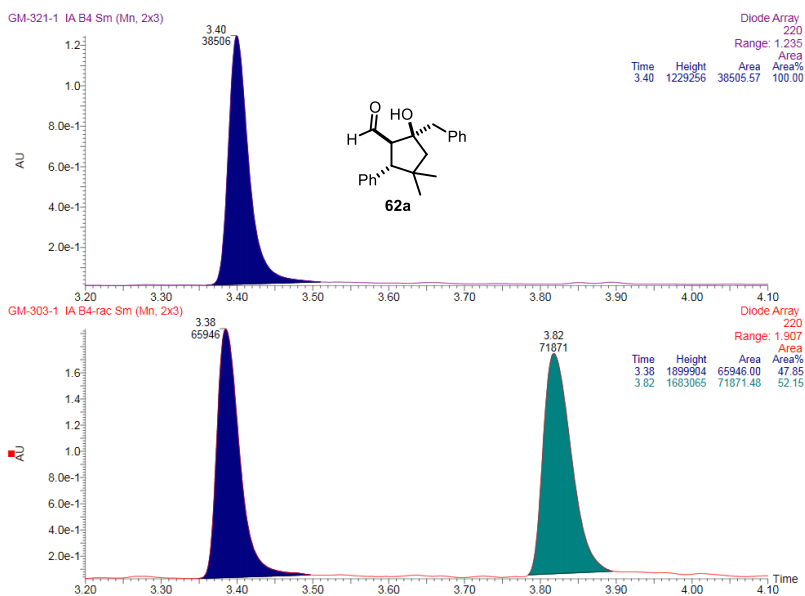


Peak #	RetTime [min]	Type	Width [min]	Area [mAU*s]	Height [mAU]	Area %
1	16.024	MM	0.2970	538.35492	30.21196	7.4199
2	20.042	MM	0.3773	6717.23242	296.70389	92.5801

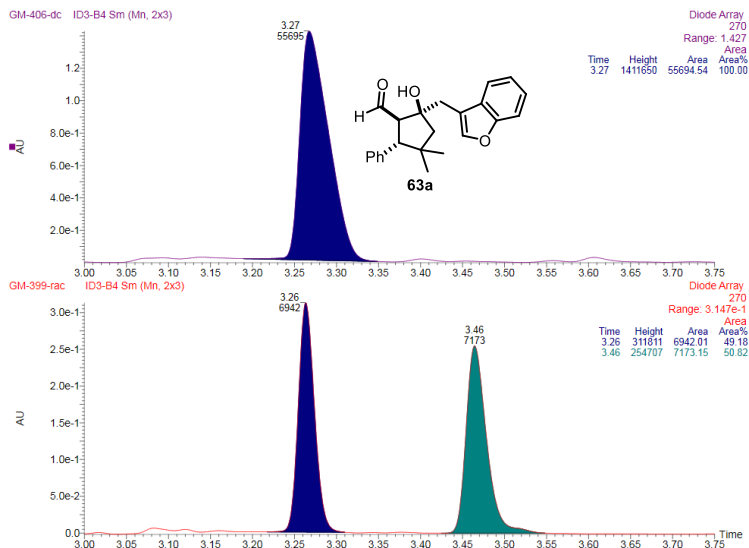
Conditions: Conditions: UPC² analysis on a Daicel Chiralpak IA column with a gradient (100% CO₂ to 60:40 CO₂/IPA over 4 minutes, curve 6). **61a**



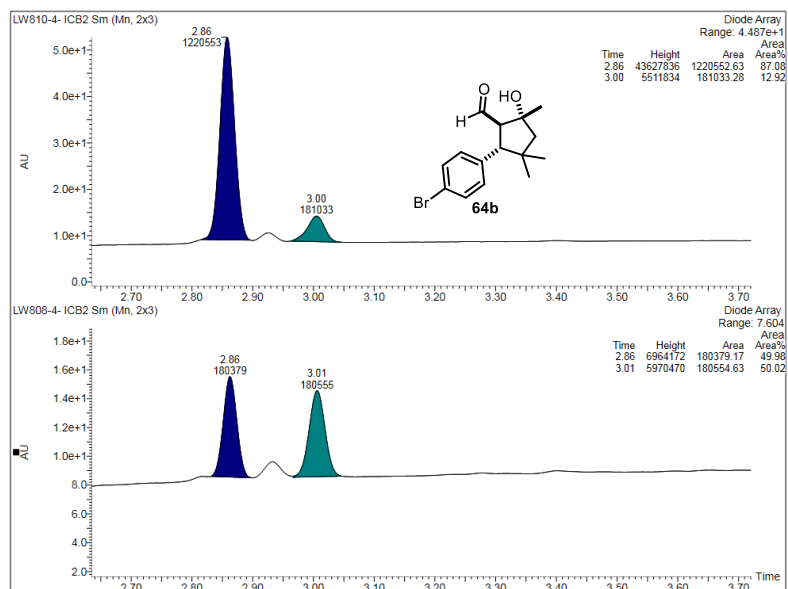
Conditions: Conditions: UPC² analysis on a Daicel Chiralpak IA column with a gradient (100% CO₂ to 60:40 CO₂/EtOH over 4 minutes, curve 6). **62a**



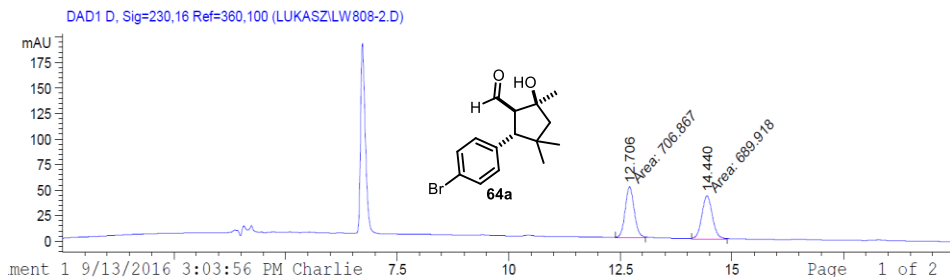
Conditions: Conditions: UPC² analysis on a Daicel Chiralpak ID-3 column with a gradient (100% CO₂ to 60:40 CO₂/EtOH over 4 minutes, curve 6) **63a**



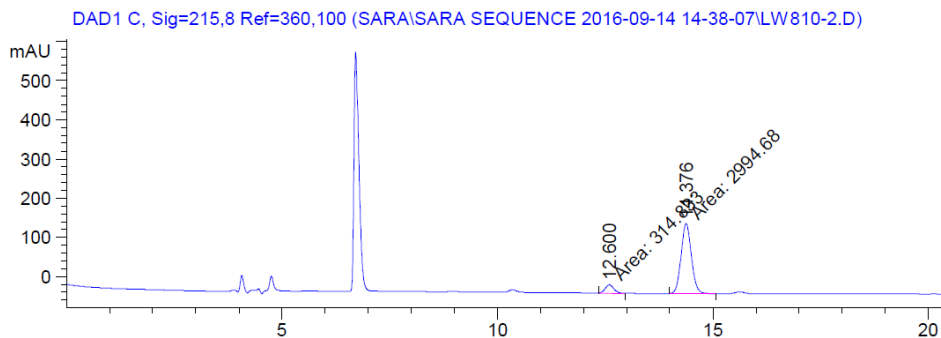
Conditions: Conditions: UPC² analysis on a Daicel Chiralpak IC-3 column with a gradient (100% CO₂ to 60:40 CO₂/IPA over 4 minutes, curve 6) **64b**



Conditions: HPLC (Daicel Chiralpak IC column, 20 °C, 92:8 hexane/*i*PrOH, flow rate: 0.80 mL/min, $\lambda = 215$ nm) **64a**

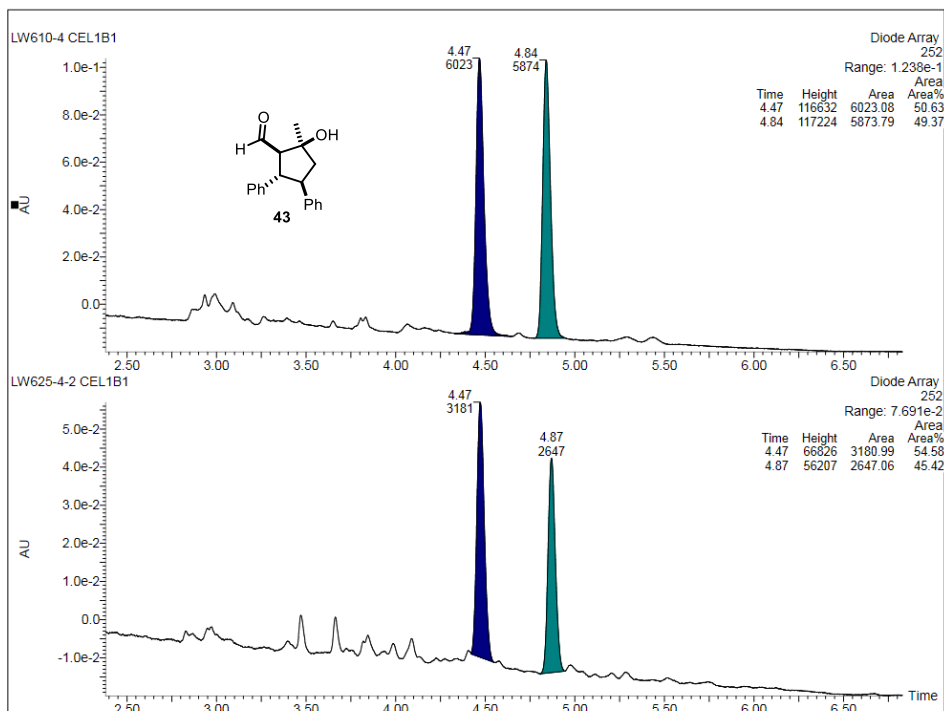


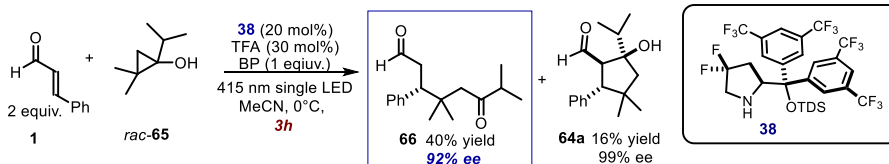
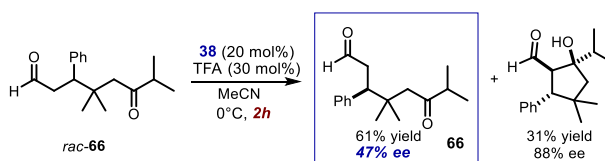
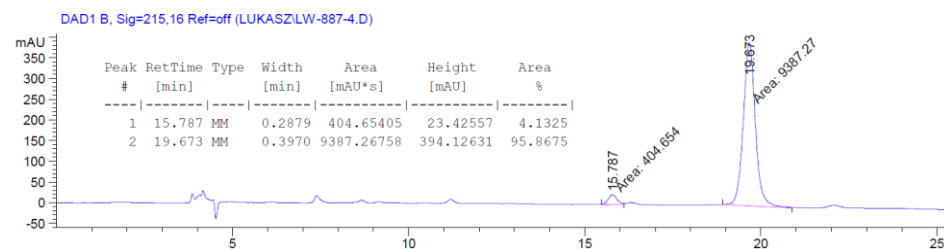
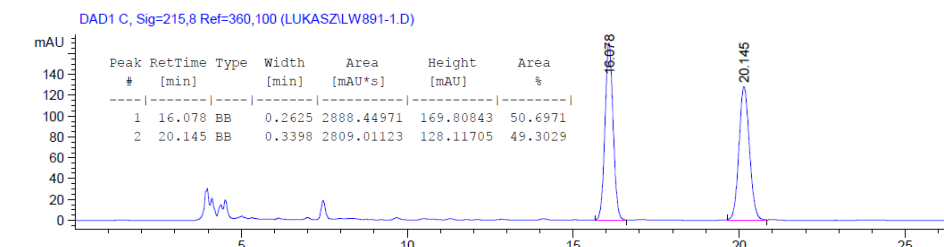
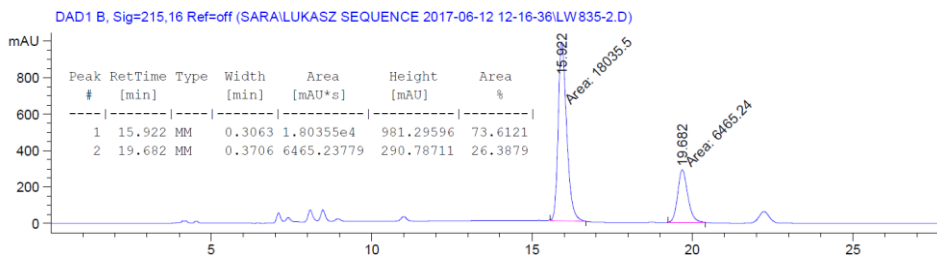
Peak #	RetTime [min]	Type	Width [min]	Area [mAU*s]	Height [mAU]	Area %
1	12.706	MM	0.2365	706.86664	49.81049	50.6067
2	14.440	MM	0.2720	689.91815	42.27217	49.3933



Peak #	RetTime [min]	Type	Width [min]	Area [mAU*s]	Height [mAU]	Area %
1	12.600	MM	0.2405	314.83255	21.81644	9.5130
2	14.376	MM	0.2782	2994.68237	179.38528	90.4870

Conditions: UPC² analysis on a Daicel Chiralpak CEL column with a gradient (100% CO₂ to 60:40 CO₂/MeCN over 4 minutes, curve 6) **43**



Kinetic resolution of 66

Scheme 4. 35 General procedure B for the enantioselective photochemical organo-cascade reaction.

Scheme 4. 36 Kinetic resolution of racemic **66**


Cyclic Voltammograms

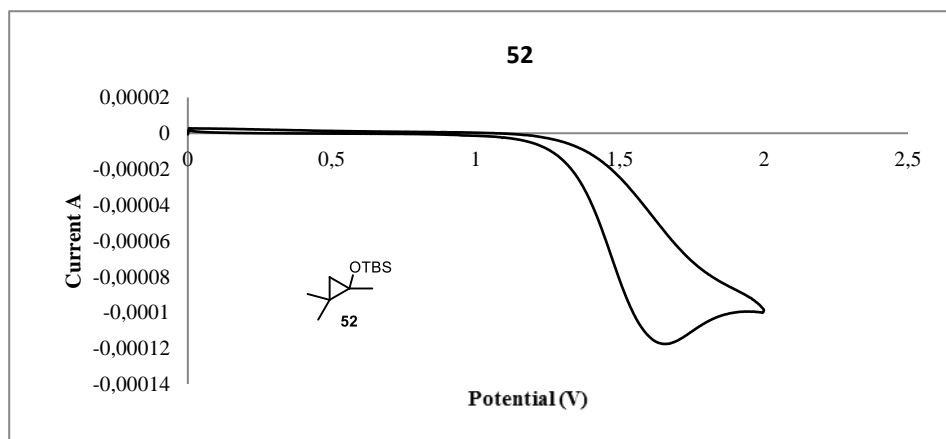


Figure 4.5 Cyclic voltammogram of tert-butyl dimethyl(1,2,2-trimethylcyclopropoxy)silane **52** [0.01 M] in [0.1 M] TBAPF₆ in ACN. Sweep rate: 50 mV/s. Pt electrode working electrode, Ag/AgCl (KCl 3M) reference electrode, Pt wire auxiliary electrode. $E_{ox}(52^{+}/52) = (+1.66 \text{ V})$.

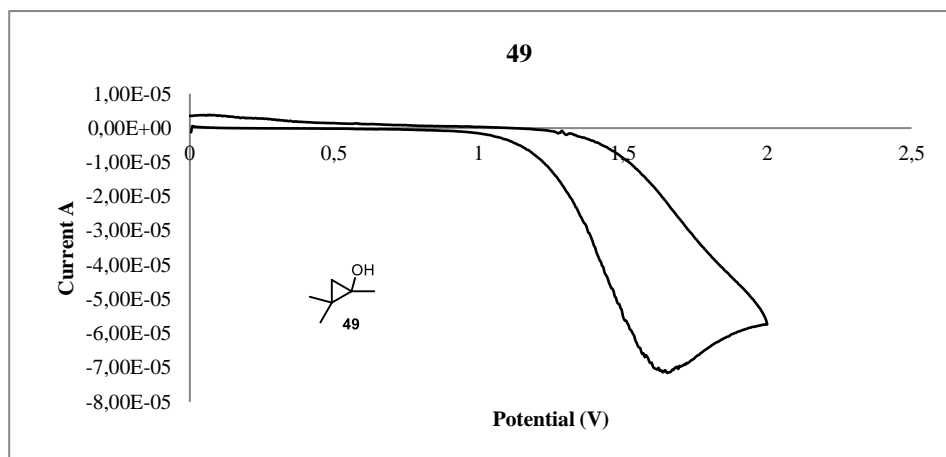
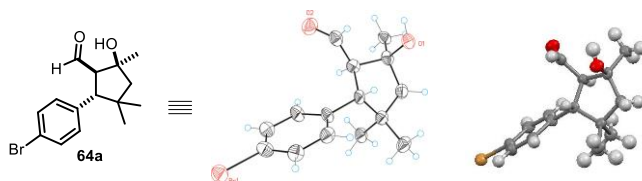


Figure 4.6 Cyclic voltammogram of tert-butyl dimethyl(1,2,2-trimethylcyclopropoxy)silane [0.01 M] in [0.1 M] TBAPF₆ in ACN. Sweep rate: 50 mV/s. Pt electrode working electrode, Ag/AgCl (KCl 3M) reference electrode, Pt wire auxiliary electrode. $E_{ox}(49^{+}/49) = (+1.65 \text{ V})$.

Single Crystal X-ray Diffraction Data for Compound 64a.

X-ray structure determinations: Crystals of compound **64f** were obtained by slow diffusion of hexane into a saturated dichloromethane solution. *Data Collection.* Measurements were made on a Bruker-Nonius diffractometer equipped with an APPEX 2 4K CCD area detector, a FR591 rotating anode with MoK α radiation, Montel mirrors and a Cryostream Plus low temperature device ($T = 100\text{K}$). Full-sphere data collection was used with ω and φ scans.

**Table 4.11** Crystal data and structure refinement for **64a**.

Identification code	LW810-2-1
Empirical formula	C ₁₅ H ₁₉ Br O ₂
Formula weight	311.21
Temperature	100(2) K
Wavelength	0.71073 Å
Crystal system	Orthorhombic
Space group	P2(1)2(1)2(1)
Unit cell dimensions	a = 5.8486(3)Å, $\alpha = 90^\circ$. b = 11.2191(7)Å, $\beta = 90^\circ$. c = 21.2978(12)Å, $\gamma = 90^\circ$.
Volume	1397.47(13) Å ³
Z	4
Density (calculated)	1.479 Mg/m ³
Absorption coefficient	2.934 mm ⁻¹
F(000)	640
Crystal size	0.15 x 0.06 x 0.03 mm ³
Theta range for data collection	2.637 to 30.669°.
Index ranges	-8 <= h <= 8, -16 <= k <= 13, -
Reflections collected	20330
Independent reflections	3991 [R(int) = 0.1090]

Completeness to theta =30.669°	93.9%
Absorption correction	Multi-scan
Max. and min. transmission	0.917 and 0.705
Refinement method	Full-matrix least-squares on F ²
Data / restraints / parameters	3991/ 0/ 166
Goodness-of-fit on F ²	1.098
Final R indices [I>2sigma(I)]	R1 = 0.0767, wR2 = 0.1647
R indices (all data)	R1 = 0.1187, wR2 = 0.1861
Flack parameter	x =0.025(13)
Largest diff. peak and hole	1.427 and -1.486 e.Å ⁻³

General Conclusions

This doctoral thesis presents novel strategies to carry out enantioselective transformations driven by visible light.

The first part (Chapter 3) describes a photochemical enantioselective perfluoroalkylation of cyclic β -ketoesters. The chemistry uses readily available substrates and proceeds at ambient temperature under visible light illumination. This study establishes the ability of chiral enolates, generated under PTC conditions, to serve as suitable donors in the formation of photoactive EDA complexes while providing effective asymmetric induction in the trapping of the resulting radical species.

The second part (Chapter 4) describes a new strategy to design an organocatalytic cascade process. This study demonstrates that reactivities of excited-state and ground-state chiral organocatalytic intermediates can be combined in one enantioselective photochemical cascade process. Specifically, the reactivity of excited chiral iminium ions was merged with the traditional ground-state chemistry of enamines.

Overall, the studies undertaken during this doctoral thesis indicate that the combination with light can create new opportunities for expanding the synthetic applicability of organocatalysis beyond conventional two-electron-pair reactivity patterns.